



Developing a novel antifungal strategy by targeting an epigenetic reader domain

Kaiyao Wei

► To cite this version:

Kaiyao Wei. Developing a novel antifungal strategy by targeting an epigenetic reader domain. Microbiology and Parasitology. Université Grenoble Alpes [2020-..], 2020. English. NNT : 2020GRALV013 . tel-03951404

HAL Id: tel-03951404

<https://theses.hal.science/tel-03951404>

Submitted on 23 Jan 2023

HAL is a multi-disciplinary open access archive for the deposit and dissemination of scientific research documents, whether they are published or not. The documents may come from teaching and research institutions in France or abroad, or from public or private research centers.

L'archive ouverte pluridisciplinaire **HAL**, est destinée au dépôt et à la diffusion de documents scientifiques de niveau recherche, publiés ou non, émanant des établissements d'enseignement et de recherche français ou étrangers, des laboratoires publics ou privés.

THÈSE

Pour obtenir le grade de

DOCTEUR DE L'UNIVERSITÉ GRENOBLE ALPES

Spécialité : Virologie - Microbiologie - Immunologie

Arrêté ministériel : 25 mai 2016

Présentée par

Kaiyao WEI

Thèse dirigée par **Carlo PETOSA**, responsable d'équipe
et codirigée par **Jérôme GOVIN**, inserm

préparée au sein du **Laboratoire Institut de Biologie Structurale**
dans l'**École Doctorale Chimie et Sciences du Vivant**

Développement d'une nouvelle stratégie antifongique ciblant un domaine de lecture épigénétique

Developing a novel antifungal strategy by targeting an epigenetic reader domain

Thèse soutenue publiquement le **8 octobre 2020**,
devant le jury composé de :

Monsieur CARLO PETOSA

DIRECTEUR DE RECHERCHE, CNRS DELEGATION ALPES, Directeur
de thèse

Madame ALIX COSTE

DOCTEUR-INGENIEUR, UNIVERSITE DE LAUSANNE - SUISSE,
Rapporteuse

Monsieur PANAGIS FILIPPAKOPOULOS

PROFESSEUR ASSOCIE, UNIVERSITE D'OXFORD - GRANDE-
BRETAGNE, Rapporteur

Monsieur NICOLAS PAPON

PROFESSEUR DES UNIVERSITES, UNIVERSITE D'ANGERS,
Examineur

Monsieur GWENAEL RABUT

CHARGE DE RECHERCHE HDR, Institut de Génétique et
Développement de Rennes, Examineur

Madame ANDREA DESSEN

DIRECTRICE DE RECHERCHE, CNRS DELEGATION ALPES,
Présidente



REMERCIEMENTS

Je souhaite tout d'abord remercier Mme Alix Coste et M. Panagis Filippakopoulos d'avoir accepté d'être les rapporteurs de mes travaux de thèse, ainsi que Mme Andréa Dessen, M. Nicolas Papon et M. Gwenaël Rabut pour avoir accepté d'évaluer ce travail.

Je remercie mes codirecteurs de cette thèse, Carlo Petosa et Jérôme Govin, sans qui elle n'aurait pas eu lieu. Je vous remercie pour votre intérêt, votre enthousiasme, votre soutien et vos conseils durant ma thèse. Je vous remercie également pour votre disponibilité pour répondre à mes questionnements et votre appui dans la construction de ma carrière professionnelle.

Je remercie Flore Mietton et Morgane Champleboux pour toute votre aide pour démarrer cette thèse, ainsi que pour m'avoir passé le relais. Je vous remercie sincèrement pour la confiance que vous m'avez accordée et pour tout ce que vous m'avez enseigné.

Je remercie également le CEA, le CNRS et le LabEx GRAL qui ont financé ces travaux ; j'espère avoir été à la hauteur de leurs espérances.

Je remercie tous nos collaborateurs : Charles E. McKenna et Muriel Cornet. Mes remerciements spécifiques à Nathan Dupper, Yingsheng Zhou et Justin Overhulse pour la réalisation du criblage et les composés que vous avez optimisés.

J'adresse aussi mes sincères remerciements à mon comité de suivi de thèse pour les conseils avisés apportés lors des entrevues annuelles : Darren Hart et Guillem Jambon ; votre aide et votre gentillesse m'ont été précieuses lorsque j'en avais le plus besoin.

Mes remerciements à Corinne Mercier, vous m'avez accepté et avez suivi mon parcours universitaire pendant les deux ans de Master. Vous avez toujours été disponible pour vos étudiants et avez contribué à leur réussite ; pour cela, je vous adresse mes sincères remerciements.

À l'IBS ...

Fabienne Hans, Marjolaine Noirclerc-Savoye et Dimitrios Skoufias, je vous exprime toute ma reconnaissance pour l'aide que vous m'avez apportée durant cette thèse et pour la suite.

Je salue les anciens, Mizar Oliva, Muge Senarisoy et Kevin Floc'h, ainsi que ceux qui poursuivent leurs travaux, Anna Seck et Anne-Sophie Banneville : vous avez été bien plus que des collègues.

Je remercie Isabel Garcia-Saez, Joanna Timmins, Elisabetta Boeri Erba, Rose-Laure Indorato et toutes celles et ceux qui sont et qui étaient dans le groupe VIC ou d'autre groupe de l'IBS. Merci pour les bons moments que nous avons passés ensemble.

À l'IAB et à EDyP ...

Marie Arlotto et Camille Sayou, merci pour toute votre aide et votre soutien durant ma thèse. Je remercie chaleureusement Sara El Kennani et Julie Marais, pour tous les moments qu'on a partagé ! Merci pour votre aide, votre bonne humeur...

Mes remerciements à Sandrine Fremy, Marie Courçon et Encar Garcia-Oliver, pour la vie du laboratoire vous m'avez apporté.

Je salue Loris Delrieu et Raphaël Dupeyron. Je vous souhaite une belle continuation couronnée de succès et d'épanouissement scientifique. Je remercie Sieme Hemadia, Anouk Emadali, Patricia Betton et Thierry Gautier pour nos fous rires.

Merci à tous ceux que j'aurai oubliés qui ont contribué de loin ou de près au déroulement de cette thèse.

WEI Kaiyao

韦凯尧

愿，生，可如夏花之绚烂
终，亦如秋叶之寂美

Je souhaite vivre comme les fleurs d'été, éclatantes et brillantes

Je souhaite partir comme les feuilles d'automne, belles et tranquilles

(Adapted from Stray Birds, Rabindranath Tagore)

TABLE OF CONTENTS

LIST OF MAIN ABBREVIATIONS.....	10
LIST OF FIGURES.....	12
LIST OF TABLES.....	15
CHAPTER I – INTRODUCTION	17
1. THE URGENT NEED FOR NOVEL ANTIFUNGAL AGENTS.....	18
1.1. PATHOGENIC FUNGI AND <i>CANDIDA</i> SPECIES	18
1.1.1. <i>Fungi and fungal infection</i>	18
1.1.2. <i>Yeasts and pathogenic yeasts</i>	18
1.1.3. <i>Candida species and invasive candidiasis</i>	19
1.2. <i>CANDIDA GLABRATA</i> : PREVALENT PATHOGENIC YEAST IN THE HOSPITAL	21
1.2.1. <i>Candida glabrata epidemiology</i>	21
1.2.2. <i>Candida glabrata biology</i>	23
1.2.3. <i>Host defense interactions of Candida glabrata</i>	27
1.2.4. <i>Virulence factors of Candida glabrata</i>	30
1.3. LIMITED PHARMACOLOGY TO TREAT <i>CANDIDA GLABRATA</i> INFECTIONS	35
1.3.1. <i>Development of antifungal agents</i>	35
1.3.2. <i>Amphotericin B: ergosterol binder</i>	38
1.3.3. <i>Azoles: ergosterol biosynthesis inhibitors</i>	39
1.3.4. <i>Echinocandins: glucan biosynthesis inhibitors</i>	42
1.3.5. <i>Flucytosine: DNA biosynthesis inhibitors</i>	44
1.3.6. <i>Antifungal resistance and Candida glabrata</i>	44
1.3.7. <i>Novel potential antifungal agents in development</i>	47
1.4. CONCLUSION.....	50
2. TARGETING AN ESSENTIAL CHROMATIN PROTEIN AS A NOVEL ANTIFUNGAL STRATEGY.....	51
2.1. CHROMATIN STRUCTURE AND POST-TRANSLATIONAL MODIFICATION OF HISTONES	51
2.1.1. <i>Chromatin structure and epigenetics</i>	51
2.1.2. <i>Post-translational modifications of histones</i>	54
2.2.3. <i>Bromodomain: reader of histone acetylation</i>	57
2.2. BROMODOMAIN AND EXTRA-TERMINAL PROTEINS	60
2.2.1. <i>Overview of BET proteins</i>	60
2.2.2. <i>Functions of BET proteins</i>	62
2.2.3. <i>BET proteins as a therapeutic target in human disease</i>	66

2.2.4. Specific BET bromodomains inhibitors	69
2.3. Bdf1: DRUGGABLE FUNGAL BET PROTEIN	75
2.3.1. Overview and functions of Bdf1	75
2.3.2. Bdf1 bromodomains as an antifungal target in <i>Candida albicans</i>	78
2.4. CONCLUSION	79
3. PH.D. PROJECT: INVESTIGATION OF BDF1 BROMODOMAIN INHIBITION AS A POTENTIAL ANTIFUNGAL THERAPEUTIC STRATEGY AGAINST <i>CANDIDA GLABRATA</i>	81
3.1. OBJECTIVE	81
3.2. WORK PLAN	81
3.2.1. Verification of the role of Bdf1 bromodomain function in <i>C. glabrata</i>	81
3.2.2. Structural studies of <i>C. glabrata</i> Bdf1 bromodomains.	82
3.2.3. Identification and characterization of CgBdf1 inhibitors.	83
CHAPTER II – RESULTS	84
1. BDF1 AND ITS BROMODOMAINS ARE ESSENTIAL IN <i>CANDIDA GLABRATA</i>	85
1.1. BDF1 PROTEIN IS ESSENTIAL IN <i>C. GLABRATA</i>	85
1.1.1. Construction of BDF1 conditional knockdown and rescue strains	85
1.1.2. Bdf1 is essential for the viability of <i>C. glabrata</i>	87
1.2. BDF1 BROMODOMAINS ARE ESSENTIAL IN <i>C. GLABRATA</i> GROWTH.	89
1.2.1. Deletion of Bdf1 bromodomains inhibit the growth of <i>C. glabrata</i>	89
1.2.2. Point mutations in Bdf1 bromodomains inhibit the growth of <i>C. glabrata</i>	90
1.3. CONCLUSION	91
2. STRUCTURE STUDIES ON <i>CANDIDA GLABRATA</i> BDF1 BROMODOMAINS	91
2.1. LIGAND BINDING SPECIFICITY OF <i>C. GLABRATA</i> Bdf1 BROMODOMAINS	91
2.2. PURIFICATION OF RECOMBINANT <i>C. GLABRATA</i> Bdf1 BROMODOMAINS	93
2.3. CRYSTAL STRUCTURE ANALYSIS OF <i>C. GLABRATA</i> Bdf1 BROMODOMAINS	97
2.4. PURIFICATION OF <i>C. GLABRATA</i> Bdf1 CONSTRUCT CONTAINING BOTH BROMODOMAINS AND THE FULL LENGTH Bdf1	100
2.5. CONCLUSION	102
3. HIGH-THROUGHPUT CHEMICAL SCREENING <i>IN VITRO</i> FOR INHIBITORS OF <i>CANDIDA GLABRATA</i> BDF1 BROMODOMAINS	103
3.1. OPTIMIZATION OF THE HOMOGENEOUS TIME-RESOLVED FLUORESCENCE (HTRF) ASSAY	103
3.1.1. Signal/Background Ratio	104
3.1.2. Z' factor and final optimized HTRF conditions	113
3.2. <i>IN VITRO</i> EFFECT OF FOUR HUMAN BET BROMODOMAIN INHIBITORS ON <i>C. GLABRATA</i> Bdf1 BROMODOMAINS	118
3.3. DISCOVERY OF <i>C. GLABRATA</i> Bdf1 BROMODOMAIN 1 INHIBITORS	121
3.4. CONCLUSION	123

4. IN VITRO CHARACTERIZATION OF SCREENING HITS	124
4.1. IN VITRO HIT VALIDATION	124
4.1.1. High-throughput adaption for in bench HTRF assay	124
4.1.2. Hit confirmation and IC ₅₀ determination	126
4.2. STRUCTURAL BASIS OF CgBD INHIBITION	129
4.2.1. Structural basis of I-BET151 and JQ1 resistance by CgBDs	129
4.2.2. Binding features of CgBD1 inhibitors	136
4.3. CHEMICAL OPTIMIZATION OF DUAL CgBDs INHIBITOR ICG-29	144
4.4. CONCLUSION	146
5. CHARACTERIZATION OF BIOACTIVE INHIBITORS	147
5.1. DISCOVERY OF A BIOACTIVE DUAL <i>C. GLABRATA</i> Bdf1 BROMODOMAIN INHIBITOR	147
5.1.1. iCG-24: an inhibitor active against <i>C. glabrata</i> mutant strains	147
5.1.2. Analogue compounds of iCG-24	149
5.1.3. iCG-24-409: a dual Bdf1 BD inhibitor active against <i>C. glabrata</i>	154
5.2. TARGET VERIFICATION OF ICG-24-409	156
5.2.1. Cellular Thermal Shift Assay	156
5.2.2. Bromodomain replacement	160
5.3. FURTHER CHARACTERIZATION OF ICG-24-409	163
5.3.1. Characterization of CgBdf1 bromodomain binding activity of iCG-24-409	163
5.3.2. Binding mode of iCG-24-409 by co-crystallography	170
5.3.3. Cytotoxicity of iCG-24-409 towards human cell lines	173
5.3.4. Yeast growth inhibitory activity of iCG-24-409 against other pathogenic <i>Candida</i> species	175
5.4. CONCLUSION	179
CHAPTER III – DISCUSSION	180
1. PROJECT SUMMARY	181
2. EFFECT OF ICG-24-409 ON THE EXPRESSION OF GENES REGULATED BY CGBDF1	182
3. VALIDATION OF THE BDF1 INHIBITION STRATEGY IN VIVO	184
3.1. pTET PROMOTER STRATEGY	184
3.2. <i>C. GLABRATA</i> STRAIN CONSTITUTIVELY EXPRESSING HUMANIZED Bdf1	185
4. INHIBITOR OPTIMIZATION	187
4.1. DEVELOPMENT OF MORE POTENT AND SELECTIVE CgBD INHIBITORS	187
4.2. DEVELOPMENT OF DRUG CARRIERS	187
4.3. DEVELOPMENT OF PRODRUGS AND PROTEOLYSIS-TARGETED CHIMERA SYSTEM	190
4.3.1. Prodrugs	190
4.3.2. Proteolysis-targeted chimeras (PROTACs)	191

5. TOWARD A BROADER ANTIFUNGAL SPECTRUM	193
5.1. Bdf1 BROMODOMAINS INHIBITION IN <i>C. ALBICANS</i> AND <i>C. GLABRATA</i>	193
5.2. ADAPTATION ON POTENTIAL THERAPY AGAINST <i>CANDIDA AURIS</i>	194
5.3. Bdf1 BROMODOMAIN INHIBITION, NARROW OR BROAD SPECTRUM	196
6. POSSIBLE RESISTANCE DEVELOPED AGAINST BDF1 INHIBITION	198
6.1. BET INHIBITION RESISTANCE IN CANCERS	199
6.2. STUDIES TO INVESTIGATED POSSIBLE Bdf1 INHIBITION RESISTANCE IN ANTIFUNGAL THERAPIES.....	200
7. PROJECT CONCLUSION	202
CHAPTER IV – METHODS	205
1. CHEMICALS	205
2. PROTEIN EXPRESSION AND PURIFICATION	205
2.1. PROTEINS USED FOR CRYSTALLIZATION, TSA AND ITC.....	205
2.2. PROTEINS USED FOR HTRF, PULL-DOWN AND HISTONE PEPTIDE ARRAY	206
3. PULL-DOWN AND HISTONE PEPTIDE ARRAY ASSAY	208
3.1. PULL-DOWN ASSAY.....	208
3.2. HISTONE PEPTIDE ARRAY ASSAY	208
4. ITC AND TSA.....	208
5. HTRF ASSAY	209
6. HIGH-THROUGHPUT CHEMICAL SCREENING	210
7. GENERATION OF <i>C. GLABRATA</i> MUTANT STRAINS	211
7.1. STRAINS AND PLASMIDS.....	211
7.2. MEDIA AND GROWTH CONDITION.....	212
7.3. PLASMIDS CONSTRUCTION	212
7.4. <i>C. GLABRATA</i> GENOMIC DNA EXTRACTION	213
7.5. <i>C. GLABRATA</i> TRANSFORMATION	214
8. YEAST GROWTH ASSAYS.....	214
8.1. GROWTH ON SOLID MEDIA	214
8.2. GROWTH ON LIQUID MEDIA.....	215
9. ANALYSIS OF WHOLE-CELL EXTRACTS AND ANTIBODIES	215
10. CELLULAR THERMAL SHIFT ASSAYS (CETSAS)	216
11. CYTOTOXICITY ASSAYS ON HUMAN CELLS	217

CHAPTER V - REFERENCES	218
APPENDICES.....	240
APPENDIX I. CRYSTALLIZATION CONDITIONS AT THE EMBL HTX FACILITY	240
APPENDIX II. CRYSTALLOGRAPHIC STATISTICS.....	258
APPENDIX III. IC ₅₀ OF HITS TO BE VALIDATED	260
APPENDIX IV. GENES SELECTED TO PERFORM CHIP EXPERIMENTS.....	262
APPENDIX V. RESUME EN FRANÇAIS.....	263
<i>Introduction et objectif</i>	263
<i>Résultats</i>	265
<i>Conclusion</i>	267

LIST OF MAIN ABBREVIATIONS

ABC	ATP-Binding Cassette	GPI-CWP	GlycosylPhosphatidylInositol-anchored Cell Wall Protein
ATP	Adenosine TriPhosphate	GSH	Glutathion
BD1	BromoDomain 1 of BET protein	GSK	GlaxoSmith Kline
BD2	BromoDomain 2 of BET protein	GST	Glutathion S-Transferase
Bdf1	Bromodomain factor 1	hBD	human Brd4 BromoDomain
Bdf2	Bromodomain factor 2	HDAC	Histone DeACtylase
BET	Bromodomain and Extra-Terminal	HMT	Histone MethylTransferase
BETi	BET protein inhibitor	Hsp90	Heat shock protein 90
BI	Blood Infection	HTRF	Homogeneous Time Resolved Fluorescence
CaBD	CaBdf1 BromoDomain	HTX	High-Throughput crystallization
CaBdf1	Candida albicans Bdf1	IAB	Institute for Advanced Bioscience
Calibr	California institute for biomedical research	IBS	Institut de Biologie Structurale
CC₅₀	Half-maximal Cytotoxicity Concentration	IC₅₀	Half-maximal Inhibitory Concentration
CETSA	CELLular Thermal Shift Assay	ICU	Intense Care Unit
CgBD	CgBdf1 BromoDomain	ITC	Isothermal Titration Calorimetry
CgBdf1	Candida glabrata Bdf1	K_d	Binding constant
CTD	C-Terminal Domain	kDa	kiloDalton
CYP450	CYtochrome P450	LR	Lectin Receptor
DHODH	DiHydroOrotate DeHydrogenase	MIC₉₀	90% Minimum Inhibitory Concentration
DMSO	DiMethyl SulfOxide	MPD	2-Methyl-2,4-PenDanediol
DNA	DeoxyriboNucleic Acid	NA	Nicotinic Acid
DNMT	DNA Methyl Transferase	NF-κB	Nuclear Factor-κB
Dox	Doxycycline	NFAT	Nuclear Factor of Active T cell
EC₅₀	Half-maximal Effective Concentration	NMR	Nuclear Magnetic Resonance
EMBL	European Molecular Biology Laboratory	NRC	NUT-Rearranged Carcinoma
Epa	Epithelial adhesin	NUT	NUclear protein in Testis
ET	Extra-Terminal domain of BET protein	OD	Optical Density
FDA	Food and Drug Administration	p-TEFb	positive Transcription Elongation Factor b
FL	Full-Length		
5-FU	5-FluoroUracil	PCAF	P300/CBP-Associated Factor
GC	Guanine-Cytosine	PDB	Protein Data Bank

pMET	promoter MET3	snRNA	small nuclear RNA
PROTAC	PRO teolysis- T argeted Chimera	TAF	TBP -Associated Factor
PTM	Post - T ranslational M odification	TBP	TATA - B inding P rotein
RNA	Ribo Nucleic Acid	Th	T - h elper cell
RNA pol II	RNA polymerase II	TLR	Toll - L ike R eceptor
ROS	Reactive Oxygen Species	Tm	Melting Temperature
S/B	Signal/Background	TSA	Thermal Shift Assay
SC	Synthetic Complete medium	TSS	Transcription Start Site
SC₅₀	Half-maximal Stimulatory Concentration	USC	University of Southern California
ScBD	ScBdf1 BromoDomain	V-ATPase	Vacuolar proton-translocating ATPase
ScBdf1	Saccharomyces cerevisiae Bdf1	WCE	Whole Cell Extract
SEC	Size-Exclusion Chromatography	WT	Wild-Type

LIST OF FIGURES

FIGURE 1. SIZE COMPARISON OF <i>C. ALBICANS</i> IN DIFFERENT MORPHOLOGIES (A) AND <i>C. GLABRATA</i> (B)	25
FIGURE 2. PHYLOGENY OF SEQUENCED <i>CANDIDA</i> AND <i>SACCHAROMYCES</i> CLADE SPECIES	26
FIGURE 3. SCHEMATIC REPRESENTATION OF <i>C. ALBICANS</i> AND <i>C. GLABRATA</i> IMMUNE RESPONSE EVASION	29
FIGURE 4. MECHANISMS OF <i>C. ALBICANS</i> AND <i>C. GLABRATA</i> HOST DAMAGE AND INVASION	32
FIGURE 5. BIOFILMS FORMED BY <i>C. ALBICANS</i> AND <i>C. GLABRATA</i>	33
FIGURE 6. CHRONOLOGY OF ANTIFUNGAL DRUG DEVELOPMENT.	36
FIGURE 7. MECHANISM AND STRUCTURE OF SOME CURRENTLY AVAILABLE SYSTEMIC ANTIFUNGAL AGENTS..	37
FIGURE 8. SOME POTENTIAL ANTIFUNGAL AGENTS CURRENTLY IN CLINICAL TRIALS	47
FIGURE 9. LEVELS OF DNA PACKAGING	52
FIGURE 10. CHROMATIN PLASTICITY BY DNA OR HISTONES MODIFICATIONS.....	53
FIGURE 11. SOME POST-TRANSLATIONAL MODIFICATIONS (PTMS) OF HISTONES.....	55
FIGURE 12. BROMODOMAINS ARE THE SPECIFIC READERS OF HISTONE ACETYLATION	58
FIGURE 13. PHYLOGENETIC TREE OF HUMAN BROMODOMAINS	59
FIGURE 14. DOMAIN ARCHITECTURE OF BET PROTEINS AND DIACETYLLYSINE BINDING MODE OF THE BET BROMODOMAIN.....	61
FIGURE 15. FUNCTIONS OF BRD4 IN TRANSCRIPTION.....	64
FIGURE 16. SOME SPECIFIC BET BROMODOMAIN INHIBITORS.....	70
FIGURE 17. REPRESENTATIVE BIVALENT BET INHIBITORS (A) AND PROTEOLYSIS-TARGETED CHIMERAS (PROTACS) (B)	74
FIGURE 18. TRANSCRIPTIONAL FUNCTIONS OF BDF1 IN <i>S. CEREVISIAE</i>	76
FIGURE 19. BDF1 BROMODOMAINS MAY BE AN ANTIFUNGAL THERAPEUTIC TARGET FOR <i>C. ALBICANS</i> INFECTIONS	80
FIGURE 20. CONSTRUCTION OF <i>BDF1</i> CONDITIONAL KNOCKDOWN AND RESCUE STRAINS	86
FIGURE 21. BDF1 AND ITS BROMODOMAINS ARE ESSENTIAL FOR <i>C. GLABRATA</i> GROWTH	88
FIGURE 22. HISTONE PEPTIDE BINDING FUNCTION OF CGBDF1 BROMODOMAINS. A. PHYLOGENETIC GUIDE TREE OF HUMAN AND YEAST BET PROTEINS.....	92
FIGURE 23. NICKEL PURIFICATION OF THE HIS TAGGED CGBDF1 BROMODOMAINS (HIS-BDS)	94
FIGURE 24. SIZE-EXCLUSION CHROMATOGRAPHY (SEC) PURIFICATION OF THE CGBDF1 BROMODOMAINS (CGBDS)	95
FIGURE 25. SOME CRYSTALS OBTAINED OF CGBD1 (A) AND CGBD2 (B) AND THEIR CORRESPONDING CRYSTALLIZATION CONDITIONS	98
FIGURE 26. STRUCTURE OF BROMODOMAINS FROM CGBDF1	99
FIGURE 27. NICKEL AND SEC PURIFICATION OF THE HIS TAGGED CGBDF1 CONSTRUCT CONTAINING BOTH BROMODOMAINS (CGBDF1 128-418) AND THE FULL LENGTH BDF1	101
FIGURE 28. HOMOGENEOUS TIME-RESOLVED FLUORESCENCE (HTRF) ASSAY	105
FIGURE 29. PURIFICATION OF THE GST TAGGED CGBDF1 BROMODOMAINS (GST-BDS) FROM 50 ML OF CULTURE	106
FIGURE 30. COMPARISON OF SEVEN CGBDF1 BD1 CONSTRUCTS AND HUMAN BRD4 BD1 IN AN HTRF ASSAY.	108

FIGURE 31. COMPARISON OF SEVEN CGBDF1 BD2 CONSTRUCTS AND HUMAN BRD4 BD2 IN AN HTRF ASSAY.	110
FIGURE 32. EFFECT OF DMSO ON HTRF ASSAY PERFORMANCE.....	111
FIGURE 33. HTRF ASSAYS OF GST-CGBDS EXHIBIT AN IMPROVED S/B RATIO FOLLOWING SIZE-EXCLUSION CHROMATOGRAPHY (SEC).....	112
FIGURE 34. FINAL S/B RATIOS OBSERVED FOR GST-CGBD1 AND CGBD2	113
FIGURE 35. THE USE OF Z' FACTOR TO EVALUATE A SCREENING ASSAY.....	114
FIGURE 36. CHARACTERIZATION OF GST-CGBDS BY HTRF	115
FIGURE 37. FOUR HUMAN BET INHIBITORS INHIBIT BDF1 BROMODOMAINS IN HTRF ASSAYS BUT NOT YEAST VIABILITY.....	120
FIGURE 38. SCREENING WORKFLOW TO IDENTIFY SELECTIVE CGBD1 (A), CABD1 (B) AND CABD2 (C) INHIBITORS	122
FIGURE 39. Z' FACTOR AND S/B RATIO GIVEN BY THE TWO GST-CGBDS IN DIFFERENT CONDITIONS.....	125
FIGURE 40. CONFIRMED HITS AGAINST CGBD1.....	128
FIGURE 41. BINDING FEATURE OF I-BET151 TO CGBD2	134
FIGURE 42. COMPARISON OF THE LIGAND-BINDING POCKETS OF CGBD1 (B) WITH THAT OF BRD4 BD1 (A, PDB CODE 3MXF)	136
FIGURE 43. BINDING OF ICG-63 ONTO DIFFERENT BROMODOMAINS.....	142
FIGURE 44. BINDING OF ICG-29 ONTO DIFFERENT BROMODOMAINS.....	143
FIGURE 45. IDENTIFICATION OF ICG-24 AS ACTIVE <i>C. GLABRATA</i> GROWTH INHIBITOR	148
FIGURE 46. COMPARISON OF TWO ICG-24 DERIVED COMPOUNDS. (A) CHEMICAL STRUCTURES. (B) COMPARISON OF THE CGBD INHIBITION ACTIVITY <i>IN VITRO</i> WITH YEAST GROWTH INHIBITION ACTIVITY.....	152
FIGURE 47. ICG-24-409 IS A SELECTIVE DUAL CGBD INHIBITOR WITH INTERESTING BIOACTIVITY.....	155
FIGURE 48. SCHEMATIC ILLUSTRATION OF THE CETSA PROCEDURE.....	157
FIGURE 49. I-BET151 PROTECTED CGBDF1 FROM HEAT.....	158
FIGURE 50. CETSA ASSAY TO VERIFY THE BINDING OF ICG-24-409 TO CGBDF1.....	159
FIGURE 51. ICG-24-409 DID NOT ENHANCE THE THERMAL STABILITY OF A FLAG TAGGED CGBDF1 PROTEIN IN A CETSA.....	160
FIGURE 52. BROMODOMAIN REPLACEMENT STRATEGY SHOWING THAT ICG-24-409 INHIBITS <i>C. GLABRATA</i> GROWTH BY TARGETING CGBDF1 BDS.....	162
FIGURE 53. ICG-24-409 BINDING TO CGBD2 SHOWN BY TSA.....	165
FIGURE 54. THE PRINCIPLE OF ISOTHERMAL TITRATION CALORIMETRY (ITC)	167
FIGURE 55. PRELIMINARY ITC EXPERIMENTS FOR THE INTERACTION BETWEEN CGBD1 AND ICG-24-409.....	168
FIGURE 56. PRIMARY ITC TESTS FOR THE INTERACTION BETWEEN CGBD2 AND ICG-24-409	169
FIGURE 57. STRUCTURE OF CGBD1 BOUND TO ICG-24-409 AND PREDICTED INTERACTIONS FOR DIFFERENT BROMODOMAINS.....	172
FIGURE 58. ICG-24-409 SHOWS LOW CYTOTOXICITY AGAINST HUMAN CELLS.....	174
FIGURE 59. ICG-24-409 AND OTHER ICG-24 DERIVED INHIBITORS INHIBITED THE GROWTH OF PATHOGENIC <i>CANDIDA</i> SPECIES OTHER THAN <i>C. GLABRATA</i>	176
FIGURE 60. ALIGNMENT MODEL OF ICG-24-409 ONTO CABDF1 BROMODOMAINS.....	178
FIGURE 61. PROPOSED CHIP EXPERIMENT TO VERIFY EFFECTS OF ICG-24-409 ON THE FUNCTION OF CGBDF1.	183
FIGURE 62. CONSTRUCTION OF STRAINS TO VALIDATE THE ROLE OF BDF1 IN <i>C. GLABRATA</i> VIRULENCE.	186

FIGURE 63. EXAMPLES OF DRUG CARRIER SYSTEMS.....	189
FIGURE 64. USE OF PRODRUG AND PROTEOLYSIS-TARGETED CHIMERA (PROTAC) STRATEGIES WITH BDF1 INHIBITORS AS A POTENTIAL ANTIFUNGAL THERAPY	192
FIGURE 65. POSSIBLE USE OF A BDF1 INHIBITOR IN ANTIFUNGAL THERAPIES	198
FIGURE 66. GENERAL TASKS OF THE PROJECT.....	203

LIST OF TABLES

TABLE 1. RISK FACTORS FOR INVASIVE CANDIDIASIS	19
TABLE 2. SOME COMPARISONS AMONG <i>C. GLABRATA</i> , <i>C. ALBICANS</i> AND <i>S. CEREVISIAE</i>	27
TABLE 3. MANAGEMENT OF INVASIVE CANDIDIASIS. (ADAPTED FROM PAPPAS ET AL., 2018)	37
TABLE 4. SOME OF THE SPECIFIC BET BROMODOMAIN INHIBITORS IN CLINICAL TRIAL	71
TABLE 5. KEY PURIFICATION CONDITIONS FOR INITIAL CONSTRUCTS OF CGBDS	96
TABLE 6. KEY PURIFICATION CONDITIONS FOR FINAL CONSTRUCTS OF CGBDS	97
TABLE 7. POSITIONS OF CRYSTALLIZATION PLATE THAT FORM CRYSTALS	97
TABLE 8. HTRF CONDITIONS FOR GST-BD CONSTRUCTS SCREENING	106
TABLE 9. PURIFICATION OF GST-BDS FROM 1 L OF BACTERIA CULTURE	113
TABLE 10. HTRF CONDITIONS FOR INHIBITION TEST	116
TABLE 11. HTRF CONDITIONS FOR CHEMICAL SCREENING	117
TABLE 12. COMPARISON BETWEEN THE HTRF ASSAY DEVELOPED HERE AND THAT DEVELOPED FOR CABD2 PREVIOUSLY	117
TABLE 13. HTRF CONDITIONS FOR HUMAN BET BROMODOMAINS	119
TABLE 14. INHIBITION EFFECTS OF HUMAN BETIS	119
TABLE 15. HTRF CONDITIONS FOR Z' FACTOR DETERMINATION IN CALIBR	121
TABLE 16. HTRF CONDITIONS FOR CHEMICAL SCREENING IN CALIBR	121
TABLE 17. HTRF CONDITIONS FOR Z' FACTOR TEST	126
TABLE 18. HTRF CONDITIONS FOR INHIBITOR VALIDATION	126
TABLE 19. IC50 OF VALIDATED CGBDS INHIBITORS	127
TABLE 20. MIX OF CGBD1 AND I-BET151 (25 MM IN DMSO)	130
TABLE 21. POSITIONS OF CRYSTALLIZATION PLATE THAT FORM CO-CRYSTALS OF CGBD1 WITH I-BET151	130
TABLE 22. CRYSTALLIZATION CONDITIONS FOR MANUAL HANGING DROPS TEST OF CGBD1 WITH I-BET151	131
TABLE 23. MIX OF CGBD2 AND I-BET151 (25 MM IN DMSO)	132
TABLE 24. POSITIONS OF CRYSTALLIZATION PLATE THAT FORM CO-CRYSTALS OF CGBD2 WITH I-BET151	133
TABLE 25. CRYSTALLIZATION CONDITIONS FOR MANUAL HANGING DROPS TEST OF CGBD2 WITH I-BET151	133
TABLE 26. POSITIONS OF CRYSTALLIZATION PLATE THAT YIELDED CO-CRYSTALS OF CGBD1 WITH DIFFERENT INHIBITORS	137
TABLE 27. POSITIONS OF CRYSTALLIZATION PLATE THAT YIELDED CO-CRYSTALS OF CGBD2 WITH DIFFERENT INHIBITORS	138
TABLE 28. CRYSTALLIZATION CONDITIONS FOR MANUAL HANGING DROPS TEST OF CGBD1 WITH ICG-24	139
TABLE 29. CRYSTALLIZATION CONDITIONS FOR MANUAL HANGING DROPS TEST OF CGBD1 WITH ICG-56	139
TABLE 30. CRYSTALLIZATION CONDITIONS FOR MANUAL HANGING DROPS TEST OF CGBD1 WITH ICG-63	140
TABLE 31. CRYSTALLIZATION CONDITIONS FOR MANUAL HANGING DROPS TEST OF CGBD2 WITH ICG-24	140
TABLE 32. CRYSTALLIZATION CONDITIONS FOR MANUAL HANGING DROPS TEST OF CGBD2 WITH ICG-29	141

TABLE 33. CRYSTALLIZATION CONDITIONS AND DIFFRACTION DATA ANALYSIS OF CO-CRYSTALS OF CGBD1 WITH ICG-63 AND CO-CRYSTALS OF CGBD2 WITH ICG-29	141
TABLE 34. STRUCTURE AND IC ₅₀ VALUES OF COMPOUNDS ICG-16, ICG-29 AND THEIR DERIVED COMPOUNDS	145
TABLE 35. STRUCTURE AND IC ₅₀ OF ICG-24 AND ITS DERIVED COMPOUNDS	151
TABLE 36. EC ₅₀ AGAINST <i>C. GLABRATA</i> GROWTH OF ICG-24 AND ITS DERIVED COMPOUNDS	153
SUPPLEMENTARY TABLE 1. PLASMIDS USED IN THIS STUDY.....	211
SUPPLEMENTARY TABLE 2. STRAINS USED IN THIS STUDY.....	212
SUPPLEMENTARY TABLE 3. PRIMERS USED TO GENERATE <i>C. GLABRATA</i> MUTANT STRAINS	213

Chapter I – Introduction

1. The urgent need for novel antifungal agents

1.1. Pathogenic fungi and *Candida* species

1.1.1. Fungi and fungal infection

Fungi constitute an independent eukaryotic kingdom, distinct from plants and animals, that began to appear on Earth about 1.6 million years ago. This kingdom is estimated to have between 1.5 and 3.8 million species, with about 120 000 currently accepted (Garcia-Solache and Casadevall, 2010; Hawksworth and Lücking, 2017). Among all these species, about 300 are human pathogens. Most of the others are non-pathogenic since they cannot grow at mammalian body temperature, which is generally higher than the environmental temperature (Robert and Casadevall, 2009; Garcia-Solache and Casadevall, 2010). In fact, only after the second half of the 20th century did fungal infections begin to become a major clinical problem and even now, compared to bacterial, viral or even parasitic infections, they are generally still not recognized as posing a big threat to human health. However, the fact is that fungal infections cause more than 1.6 million deaths every year and over 300 million patients suffer from serious fungal-related diseases (Editorial, 2017; Casadevall, 2018). Among pathogenic fungi, *Candida*, *Aspergillus*, *Pneumocystis* and *Cryptococcus* spp. are considered to be the most common species linked to human fungal infections (Editorial, 2017).

1.1.2. Yeasts and pathogenic yeasts

Yeasts are members of the fungal kingdom that mainly live as a unicellular form. Today, about 1500 yeast species have been identified (Kurtzman and Piškur, 2006). Yeasts are tightly linked with human activities. The use of *Saccharomyces cerevisiae* yeast species as the main fermenting agent in beverage and food fermentation has played a very important role in the history of most societies. A subgroup of this species is widely used to make bread, beer and wine (Legras *et al.*, 2007). *S. cerevisiae* also plays an important role in modern biological research as a model organism, and is one of the most studied eukaryotic microorganisms (Ostergaard, Olsson and Nielsen, 2000). Other yeast species, like *Cryptococcus neoformans*

and *Cryptococcus gattii*, are considered human opportunistic pathogens. These two species can cause cryptococcosis which annually affects more than one million people in the world and leads to over 600 000 deaths per year (Cogliati, 2013). Another group of human opportunistic pathogenic yeasts are the *Candida* species.

1.1.3. *Candida* species and invasive candidiasis

Candida is a genus containing over 150 different yeast species, but only a few of them are human pathogens since most cannot grow at 37 °C (Rodrigues, Silva and Henriques, 2014). Most pathogenic *Candida* species are opportunistic pathogens. They are normal components of the human microbiota. In immunocompetent individuals, they can cause local infections such as oral or vaginal infections, which generally can be easily and effectively treated. However, in immunocompromised patients with various high risk factors (Table 1), *Candida* species can cause invasive infections (Arendrup, 2010).

Table 1. Risk factors for invasive candidiasis (Table from Kullberg and Arendrup, 2016).

Critical illness, with particular risk among patients with long-term intensive care unit (ICU) stay
Abdominal surgery, with particular risk among patients having anastomotic leakage or who have had repeat laparotomies
Acute necrotizing pancreatitis
Hematologic malignant disease
Solid-organ transplantation
Solid-organ tumors
Neonates, particularly those with low birth weight, and preterm infants
Use of broad-spectrum antibiotics
Presence of central vascular catheter, total parenteral nutrition
Hemodialysis
Glucocorticoid use or cancer chemotherapy
<i>Candida</i> colonization, particularly if multifocal

Invasive candidiasis is estimated to affect between 250 000 and 700 000 people per year around the world and is responsible for over 50 000 deaths annually (Kullberg and Arendrup, 2016; Bongomin *et al.*, 2017). One study based on 14 414 patients from 1265 intensive care units (ICUs) in 75 countries showed that in 2006 and 2007, *Candida* species ranked as the third most common infectious organism worldwide infecting 17% of patients, just after *Staphylococcus aureus* (20.5%) and *Pseudomonas* species (19.9%). In North America and western Europe *Candida* species rank in second place, following only *Staphylococcus aureus* (Vincent *et al.*, 2009).

Invasive candidiasis, an invasive infection caused by *Candida* species, often presents as a bloodstream infection named candidemia. Candidemia can also be accompanied by secondary dissemination to various structures and organs, including the central nervous system (Arendrup, 2010). Candidemia ranks in fourth place in hospitals in the United States among nosocomial bloodstream infections and in third place for ICU patients (Wisplinghoff *et al.*, 2004). The mortality (30 days after diagnosis) of candidemia patients was generally from 20 to 40%, according to different studies between 2002 and 2011 (Wisplinghoff *et al.*, 2004; Hassan *et al.*, 2009; Lockhart *et al.*, 2012; Puig-Asensio *et al.*, 2014). However, a study in South Africa showed mortality as high as 60% and another in Spain showed a mortality as high as 66.6% for *Candida* infected ICU patients (Olaechea *et al.*, 2004; Kreusch and Karstaedt, 2013). One study in Brazil even had a total mortality of 72.2% and up to 85% among ICU patients (Doi *et al.*, 2016). Besides, *Candida* infections cause an additional cost per patient of at least £8252 in the United Kingdom in 2007 and more than 8000 € in Spain in 2004 (Olaechea *et al.*, 2004; Hassan *et al.*, 2009).

Among *Candida* species, *C. albicans*, *C. glabrata*, *C. parapsilosis*, *C. tropicalis* and *C. krusei* account for 92% of candidemia cases (Guinea, 2014). *C. albicans* is still the most frequent, but is significantly less prevalent compared to a few decades ago (Kullberg and Arendrup, 2016). Studies in the US showed that the proportion of candidemia due to *C. albicans* was about 50% or even lower and similar results were obtained in Australia and Spain (Lockhart *et al.*, 2012; Matsumoto *et al.*, 2014; Pfaller, Jones and Castanheira, 2014; Puig-Asensio *et al.*, 2014; Wisplinghoff *et al.*, 2014; Chapman *et al.*, 2017). Non-*albicans Candida* have emerged as increasingly important pathogens, especially *C. glabrata* in northern Europe

and North America and *C. parapsilosis* in southern Europe, Asia and South America (Kullberg and Arendrup, 2016).

1.2. *Candida glabrata*: prevalent pathogenic yeast in the hospital

1.2.1. *Candida glabrata* epidemiology

For a long time, *C. glabrata* was considered as commensal flora and relatively nonpathogenic. During the early 1990s, *C. glabrata* infections were responsible for only about 5% of candidiasis in the US (Fidel Jr, Vazquez and Sobel, 1999). However, infections caused by this yeast increased significantly and it has become a very important pathogenic yeast (Fidel Jr, Vazquez and Sobel, 1999). The proportion of candidemia caused by *C. glabrata* is high in developed countries, especially in North America and northern Europe.

1.2.1.a. Geographic epidemiology

A study in the US showed that from 1998 to 2006, the proportion of *C. glabrata* blood infection (BI) was 16.7%, which ranked in third place after *C. albicans* and *C. parapsilosis* (Wisplinghoff *et al.*, 2014). However, two studies showed that from 2006 to 2012, *C. glabrata* BI became the major non-*albicans* candidemia in the US, with the proportion increasing to 24.6-29% (Lockhart *et al.*, 2012; Pfaller, Jones and Castanheira, 2014). Another study based on 14 Iowa hospitals even showed a proportion of 36% for *C. glabrata* candidemia from 2011 to 2012 (Matsumoto *et al.*, 2014). A similar situation was observed in Australia, where the proportion of *C. glabrata* candidemia rose from 16.5% in 2004 to 26.7% in 2015 (Chapman *et al.*, 2017).

In northern and western Europe, *C. glabrata* is ranked as the second most common *Candida* species in patients just after *C. albicans*. In Nordic countries, the proportion of *C. glabrata* candidemia varies, with the lowest in Norway (11.7%) and the highest in Denmark (29%) (Hesstvedt *et al.*, 2017; Lindberg *et al.*, 2019). Ireland (28%) and Belgium (27.3%) have a similar rate compared to Denmark and the US, while France has a lower rate of 18.6% in the ICU setting (Lortholary *et al.*, 2014; Trouvé *et al.*, 2017; Ryan *et al.*, 2019). In southern and

eastern Europe countries like Italy, Spain and Romania, the proportion is lower (12.9-14.8%) and *C. glabrata* ranks in third or fourth place (Puig-Asensio *et al.*, 2014; Mencarini *et al.*, 2018; Scapaticci *et al.*, 2018).

The epidemiology of *C. glabrata* in Asia varies among different countries. China and Japan have a similar proportion of *C. glabrata* candidemia (10.8-14.5%, ranking in third or fourth place) while in South Korea, the rate is higher at 24.2% (ranking in the third place) (Lin *et al.*, 2018; Xiao *et al.*, 2018; Ko *et al.*, 2019; Sakagami *et al.*, 2019). For southeastern Asian countries, the rate of *C. glabrata* candidemia is relatively low except in Singapore (26.5%) where the epidemiology is similar to the US and northern Europe (Tan *et al.*, 2016). In South America, the proportion of candidemia due to *C. glabrata* is low, similar to that in southeastern Asia. The highest rate is in Brazil, which is between 10.2% and 19%. However, it links often with the highest antifungal resistance rate (Nucci *et al.*, 2013; Doi *et al.*, 2016; Canela *et al.*, 2018). In South Africa, *C. glabrata* ranks the third after *C. albicans* and *C. parapsilosis* but with a high proportion of 23% (Kreusch and Karstaedt, 2013). A study in Israel showed that *C. glabrata* was the second cause of candidemia from 2005 to 2016, however, the percentage kept increasing and reach about 25% in 2016 (Israel *et al.*, 2019).

1.2.1.b. Epidemiology in different clinical settings

The epidemiology of invasive candidiasis caused by *C. glabrata* can vary in different settings. Studies have shown that *C. glabrata* affects elder more than younger patients (Lamoth *et al.*, 2018). The mean age of patients with *C. glabrata* BI can be 10 years older than those with candidemia caused by other *Candida* species (Wisplinghoff *et al.*, 2014). For patients that receive solid organ transplants, the proportion of *C. glabrata* invasive infections (24.4%) matches the average level in the US (Andes *et al.*, 2016). However, for cancer patients, the rate of *C. glabrata* infection can be very high and the therapeutic response is poorer than for *C. albicans* infection. It should be pointed out that for leukemia patients and those with neutropenia, *C. glabrata* can represent 44-47% of fungemia cases, which is significantly higher compared to *C. albicans* (10-22%) (Bodey *et al.*, 1999). An Iranian study even showed that *C. glabrata* was the first cause of invasive candidiasis in the ICU setting, being responsible for 47.8% of the cases. This study proposed that the reason for the high *C. glabrata* rate was its

high antifungal resistance (Alimehr *et al.*, 2015). Another study performed in France showed that prior exposure to antifungal agents like fluconazole or caspofungin can significantly increase the rate of *C. glabrata*, from 18% to 25% or 35%, respectively (Lortholary *et al.*, 2011).

1.2.1.c. Diagnosis and mortality

The diagnosis of invasive *C. glabrata* infections is difficult. There is no unique clinical picture for such infections, which can vary from low-grade fever to fulminant septic shock just like other invasive candidiases. Indeed, for invasive candidiasis in general, there are no characteristic signs or symptoms. A generally persistent fever without antimicrobial response is the one of the very few symptoms before blood culturing permits a definitive diagnosis, which can take a long time (Fidel Jr, Vazquez and Sobel, 1999; Ksiezopolska and Gabaldón, 2018). Today, blood PCR is developed as a new diagnostic test. This test is more rapid compared to fungal culturing. However, it cannot detect all species and the cost is high (Pappas *et al.*, 2018).

The mortality of *C. glabrata* infections varies according to different studies. In Ireland and South Africa, the mortality of *C. glabrata* BI was higher at about 57% (Kreusch and Karstaedt, 2013; Ryan *et al.*, 2019) while another study in the USA showed a lower mortality (90 days) for solid organ transplant recipients, which was 27.7%, but still higher than *C. albicans* (22.6%) (Andes *et al.*, 2016). The highest mortality (83%) was observed in a study in 1989 in the USA. However, their data were based on only 12 patients (Komshian *et al.*, 1989). Besides, Bodey *et al.* showed that *C. glabrata* candidemia has a significant poorer antifungal response rate than that caused by *C. albicans* (Bodey *et al.*, 1999).

1.2.2. *Candida glabrata* biology

Like other *Candida* species, *C. glabrata* belongs to the Saccharomycetes class, the Saccharomycetales order, the Saccharomycetaceae family and the *Candida* genus. Compared to *C. albicans* (4 to 6 μm), *C. glabrata* has smaller cells (1 to 4 μm) (Figure 1). However, these two (as well as other *Candida*) species, cannot be distinguished on Sabouraud Dextrose Agar (SDA) medium, a type of agar growth medium containing peptones used to

diagnose fungal infections, because both form similar cream-colored colonies (Fidel Jr, Vazquez and Sobel, 1999). As a nosocomial pathogen, *C. glabrata* seems to be the most robust among pathogenic yeast for persisting on inanimate surfaces. It can survive in that condition up to 5 months, while the survival time for *C. albicans* is 4 months and only 14 days for *C. parapsilosis* (Kramer, Schwebke and Kampf, 2006).

1.2.2.a. *Candida glabrata* and pseudohypha formation

C. albicans can adopt different morphologies under different growth conditions, including the round yeast form and elongated forms like hyphae and pseudohyphae (**Figure 1A**) (Sudbery, 2011). Unlike *C. albicans*, *C. glabrata* was considered for a long time not to have a filamentous form (**Figure 1B**) (Fidel Jr, Vazquez and Sobel, 1999). Because of the lack of pseudohypha formation, *C. glabrata* was first classified in the genus *Torulopsis* until the definition of the *Candida* genus was changed in 1978, which reclassified *C. glabrata* within this genus (Fidel Jr, Vazquez and Sobel, 1999). While it is true that *C. glabrata* is generally observed only in blastoconidial form, a filamentous form can also be observed under special conditions. In 2000 Csank found that *C. glabrata* could form pseudohypha in solid nitrogen starvation media and invaded the media like diploid *S. cerevisiae* did. However, *C. glabrata* was unable to invade rich media like YPD whereas haploid *S. cerevisiae* could (Csank and Haynes, 2000). In 2016 Sasani *et al.* demonstrated that, besides nitrogen starvation, high CO₂ pressure could also induce *C. glabrata* pseudohypha formation (Sasani *et al.*, 2016). It was reported that *S. cerevisiae* forms pseudohypha to seek nutrients (Csank and Haynes, 2000) but the role of *C. glabrata* pseudohypha formation in the infection process is still unknown.

1.2.2.b. *Candida glabrata*, *Candida albicans* and *Saccharomyces cerevisiae*

Even though *C. glabrata* share the same genus name with *C. albicans* and other major *Candida* human pathogens, this species is phylogenetically closer to *S. cerevisiae* than other major *Candida* pathogens. Almost all major *Candida* human pathogens (except *C. glabrata* and *C. krusei*) belong to *Candida* clade in which the CUG codon is translated into a serine instead of leucine (also named CTG clade). *C. glabrata*, on the other hand, has a common

ancestor with *S. cerevisiae* and both of them belong to *Saccharomyces* clade (Figure 2) (Butler *et al.*, 2009; Rodrigues, Silva and Henriques, 2014).

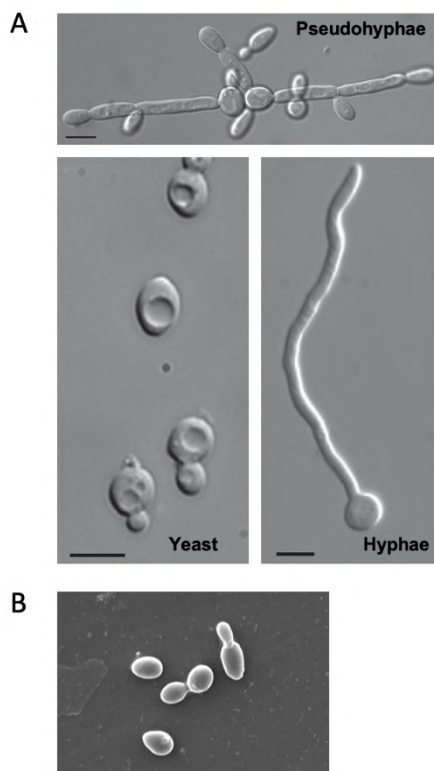


Figure 1. Size comparison of *C. albicans* in different morphologies (A) and *C. glabrata* (B). Scale bars in the main panels represent 5 μm. (Figures from K. M. Ahmad *et al.*, 2014; Sudbery, 2011)

Furthermore, *C. glabrata* shares a high degree of genetic similarity with *S. cerevisiae*. According to the genome sequencing of the strain CBS138 in 2004, *C. glabrata* proteins showed an average of 65% amino acid identity with their *S. cerevisiae* orthologues. The genome size and the guanine-cytosine (GC) content in *C. glabrata* (12.3 Mb and 38.8%, respectively) are also similar to those in *S. cerevisiae* (12.1 Mb and 38.3%, respectively). Only 8.6% of *C. glabrata* genes lack an orthologue in *S. cerevisiae* while 29.5% lack an orthologue in *C. albicans*. However, *C. glabrata* has lost 29 genes compared to *S. cerevisiae*. These include genes involved in galactose, phosphate, nitrogen and sulphur metabolism and in thiamine, pyridoxine and nicotinic acid biosynthesis (Dujon *et al.*, 2004; Kaur *et al.*, 2005; Gabaldón and Carreté, 2016). These losses of function might be explained by the evolution of *C. glabrata* as a human pathogen because the relevant auxotrophies can be compensated by the mammalian host environment.

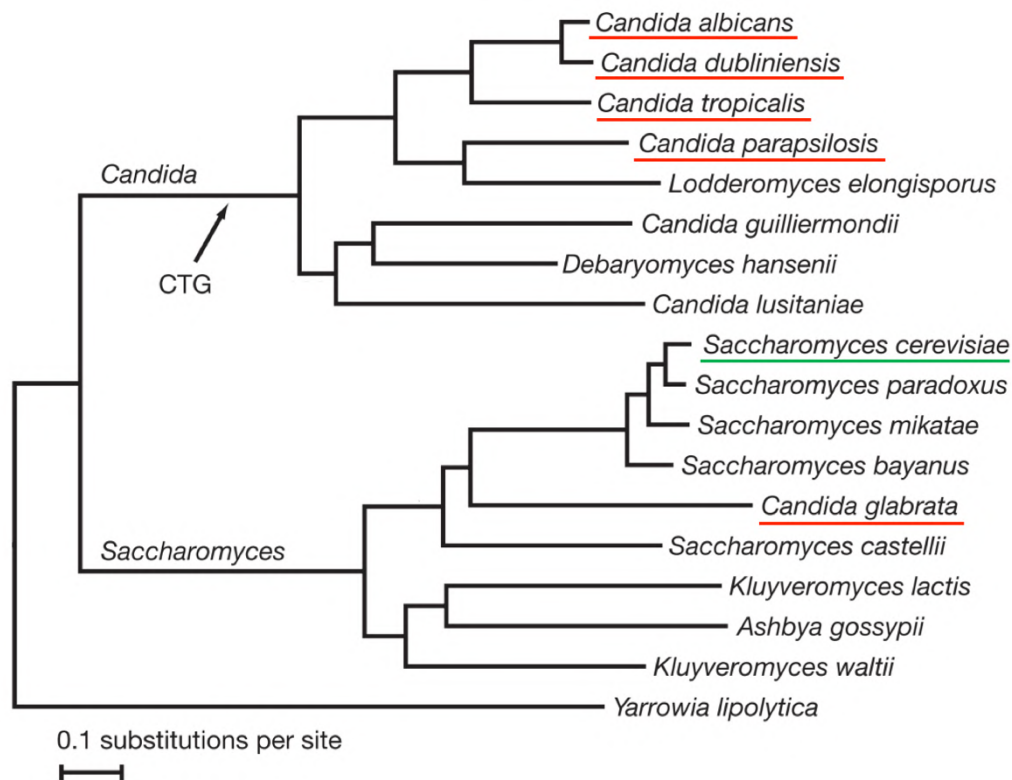


Figure 2. Phylogeny of sequenced *Candida* and *Saccharomyces* clade species. Major human pathogens are underlined in red while *S. cerevisiae* is underlined in green. (Figure from Butler *et al.*, 2009)

1.2.2.c. Life cycle of *Candida glabrata*

Another significant difference between *C. glabrata* and *C. albicans* is that the former has a haploid genome while the latter has a diploid one (Kaur *et al.*, 2005; Rodrigues, Silva and Henriques, 2014). A sexual cycle with mating activity has been observed in *C. albicans* and *S. cerevisiae*, but not in *C. glabrata*. However, in 2002 Srikantha *et al.* showed that *C. glabrata* had three mating type-like loci (*MTL1*, *MTL2* and *MTL3*) just like *S. cerevisiae* (*MAT*, *HML* and *HMR*) and their configurations were also similar to those in *S. cerevisiae*. They also demonstrated that *C. glabrata* had two distinct haploid mating types (**a** and α) just like in *S. cerevisiae* (Srikantha, Lachke and Soll, 2003). Five years later Muller *et al.* tried to mate *C. glabrata* but without success. Yet they still found that *C. glabrata* kept many genes for the mating pathway in their genome compared to *S. cerevisiae*. They proposed that mating activity might exist in *C. glabrata* but the special conditions required were unknown (Muller *et al.*, 2008). Another study by Dodgson *et al.* in 2005 suggested that genetic exchanges occurred in *C. glabrata* but at a very limited rate and that the primary mode of reproduction

for this species was clonal. They proposed another hypothesis that *C. glabrata* initially had a sex cycle which was lost during evolution (Dodgson *et al.*, 2005).

Table 2. Some comparisons among *C. glabrata*, *C. albicans* and *S. cerevisiae*. (Adapted from Kaur *et al.*, 2005)

	<i>C. glabrata</i>	<i>C. albicans</i>	<i>S. cerevisiae</i>
Genotype	Haploid	Diploid/Tetraploid	Haploid/Diploid
Virulence	Opportunistic pathogen	Opportunistic pathogen	Non-pathogenic
CTG clade	No	Yes	No
Mating genes	Present	Present	Present
Mating activity	Not observed	Present	Present
True hyphae	Absent	Present	Absent
Pseudo hyphae	Special conditions	Present	Present
Biofilm formation	Present	Present	Present
Auxotrophy	Niacin, thiamine, pyridoxine	None	None

1.2.3. Host defense interactions of *Candida glabrata*

1.2.3.a. Host defense against *Candida glabrata*

The interaction between the host defense system and *C. glabrata* is not very clear. Phagocytic cells (neutrophils, macrophage and dendritic cells) of the host innate immune system are considered to be the first response against fungal infections. Fungal surface structures like β -1,3-glucans and chitin are detected as non-self by the immune system. These non-self features are recognized by various immune receptors, especially toll-like receptors (TLRs) and lectin receptors (LR), which lead to phagocytosis and other immune responses. Following phagocytosis and formation of the phagolysosome (fusion of phagosome and lysosome), fungicidal molecules and conditions (low pH, reactive oxygen and nitrogen species like H₂O₂ and NO, antifungal peptides and enzymes) are produced inside the phagolysosome. In addition to phagocytosis, the immune system also has extracellular killing mechanisms involving the release of large amounts of reactive oxygen species (ROS). Neutrophils are mainly associated with this mechanism (Nicola, Casadevall and Goldman, 2008; Rodrigues, Silva and Henriques, 2014). Patients with neutropenia are associated with a poorer recovery

rate from candida infections (both *C. glabrata* and *C. albicans*), reflecting the important role of neutrophils in candidemia host defense (Bodey *et al.*, 1999).

For healthy immunocompetent people, following phagocytosis, dendritic cells present *Candida*-specific antigens to naïve T cells and activate them. The activation of the adaptive immune response generally leads to the elimination of the fungal pathogen. That is the reason why invasive candidiasis, like candidemia, occurs mostly in immunocompromised people, especially hospitalized patients (Galocha *et al.*, 2019). It was also suggested that in the adaptive immune response, T-cells are more critical than B-cells for host defense against *C. glabrata* (Fidel Jr, Vazquez and Sobel, 1999).

1.2.3.b. *Candida glabrata* immune evasion and macrophages

Microorganisms generally have various strategies to overcome the stress produced by the immune system. *C. albicans* can mask β -1,3-glucans exposed on the cell surface through cell wall remodeling to reduce phagocytosis and neutrophil recruitment (Galocha *et al.*, 2019). Unlike *C. albicans*, *C. glabrata* seems to use phagocytosis by host macrophages as an immune system evasion strategy. Studies have shown that after being phagocytosed, *C. glabrata* survives and replicates inside the macrophage (Kaur, Ma and Cormack, 2007; Seider *et al.*, 2011; Rai *et al.*, 2012). In fact, this yeast causes very little macrophage damage and does not induce macrophage apoptosis in contrast to *C. albicans*, which forms hyphae and kills the phagocytotic cell (Seider *et al.*, 2011) (**Figure 3**). Seider *et al.* also proposed two ways that *C. glabrata* may use to escape the macrophage: the pathogen may rupture the macrophage when too many fungal cells are generated in the host cell or, they may just wait for the age-related death of the macrophage.

Several mechanisms may be involved in the intracellular survival of *C. glabrata* in the macrophage. The environment inside the macrophage lacks glucose as a carbon source. *C. glabrata* has been shown to be able to remodel its chromatin in order to upregulate genes participating in gluconeogenesis, the glyoxylate and methylcitrate cycles, β -oxidation of fatty acids and ammonium transport, and to downregulate genes involved in glycolysis (Kaur, Ma and Cormack, 2007; Rai *et al.*, 2012). Chew *et al.* recently discovered an essential gene, *ICL1*, which participates in the uptake of acetate, ethanol and oleic acid as carbon sources. The

disruption of this gene abolished the survival ability of *C. glabrata* in response to macrophage engulfment (Chew *et al.*, 2019).

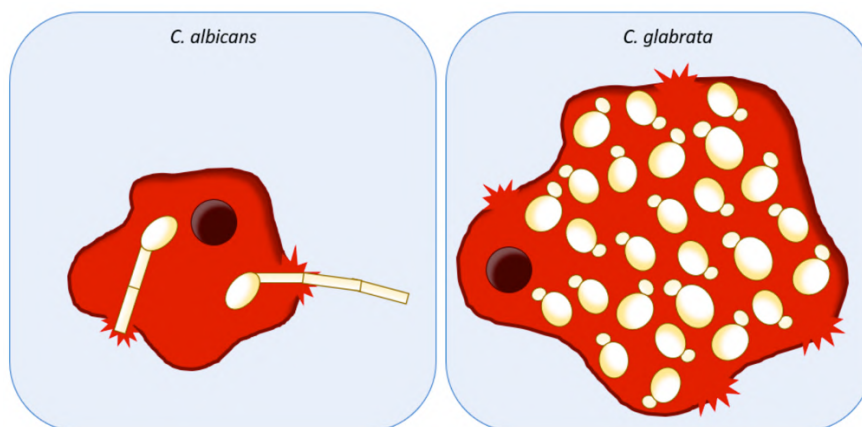


Figure 3. Schematic representation of *C. albicans* and *C. glabrata* immune response evasion. *C. albicans* (left) actively escape from the phagocytosis of macrophages (red) through hyphal formation and phagocyte piercing leading to immune cell death. *C. glabrata* (right) survive and duplicate inside the macrophages and may lead to immune cell lysis due to fungal load. (Figure from Galocha *et al.*, 2019)

Reactive nitrogen and oxygen species are often used by macrophages as fungicidal molecules. It was shown that *C. glabrata* does not stimulate murine macrophages to produce NO and, like *C. albicans*, can also actively repress ROS production by macrophages (Kaur, Ma and Cormack, 2007; Seider *et al.*, 2011). The tolerance of *C. glabrata* to ROS is associated mostly with the activities of catalase and of the superoxide dismutases Sod1/Sod2 and with the glutathione and thioredoxin pathways (Galocha *et al.*, 2019). With its sole catalase coding gene *CAT1*, *C. glabrata* was still shown to be more resistance to H₂O₂ than *S. cerevisiae* and *C. albicans*. Resistance is significantly higher when the yeast is in stationary phase, when as much as 1 M H₂O₂ can be tolerated (Cuéllar-Cruz *et al.*, 2008). However, ROS may not play an important role in *C. glabrata* growth. In fact, experimental inhibition of ROS production cannot rescue the viability of ROS sensitive *C. glabrata* strains *in vitro* and the lack of the *CAT1* gene does not influence the virulence in a murine model of disseminated infection (Cuéllar-Cruz *et al.*, 2008; Seider *et al.*, 2014).

Low pH within the mature phagosomes (phagolysosome) also contributes to the antimicrobial environment. The pH of phagolysosomes can reach 4.5-5.5 while the value is 6.0 for the early phagosome. However, the fact that *C. glabrata* does not colocalize with acidic

phagosomes indicates that it is not exposed to the low pH environment within the macrophage (Seider *et al.*, 2011; Rai *et al.*, 2012). Seider *et al.* also showed that *C. glabrata* blocked only the end process of phagosome maturation: fusion with lysosomes. In fact, the average pH of *C. glabrata* containing endosomes is about 6.1, just like that in early phagosomes (Seider *et al.*, 2011).

1.2.3.c. Cytokines and *Candida glabrata*

C. glabrata was also shown to reduce cytokine production of the infected macrophage, including proinflammatory cytokines (IL-1 β , IL-6, IL-8, IFN- γ and TNF- α) and anti-inflammatory cytokine IL-10 (Seider *et al.*, 2011). Another study showed that this yeast increased the release of another anti-inflammatory cytokine, IL-4, by the infected macrophage (Rai *et al.*, 2012). Interestingly, the proinflammatory cytokine GM-CSF (granulocyte-monocyte colony stimulating factor) was shown to be strongly produced by *C. glabrata* infected macrophages (Seider *et al.*, 2011). Another study also showed that endocytosis of *C. glabrata* by oral epithelial cells could stimulate the latter to produce GM-CSF (Li and Dongari-Bagtzoglou, 2009). This cytokine participates in the recruitment of macrophages to the infection site and may explain the enhancement of mononuclear tissue infiltration observed *in vivo* following *C. glabrata* infection (Jacobsen *et al.*, 2010). Together, these observations suggest that macrophages provide a favorable environment for *C. glabrata* and support the idea that this yeast may utilize macrophages as a safe place to evade the immune system.

1.2.4. Virulence factors of *Candida glabrata*

1.2.4.a. Host damage and invasion

The ability of opportunistic pathogens to cause infections relies on two abilities, the induction of host damage and host immune evasion. Microorganisms usually first have to pass through the epithelial tissue. Epithelial cells are generally the first cell line of defense since their “tight junctions” prevent the entrance of the microorganisms. However, human pathogens are generally capable to cross these barriers (Galocha *et al.*, 2019). *C. albicans* can

invade the host cells by two major mechanisms: hyphal formation with lytic enzyme activity and endocytosis by host cells (**Figure 4A**, left) (Goyer *et al.*, 2016).

The mechanisms that *C. glabrata* uses to invade the host are not very clear (Galocha *et al.*, 2019) and it appears to be less able to induce cell or tissue damage to get into the host compared to *C. albicans*. *C. glabrata* can form pseudohyphae under particular conditions, but this formation has never been reported *in vivo* and its role in the infection process is still unknown (Csank and Haynes, 2000; Sasani *et al.*, 2016; Galocha *et al.*, 2019). *C. albicans* can secrete hydrolytic enzymes, proteinases and phospholipases to damage the host cell and to facilitate invasion while *C. glabrata* has very low hydrolytic enzyme activity and does not secrete proteases (Galocha *et al.*, 2019). Interestingly, *C. glabrata* can secrete phospholipases which can destroy the host cell membrane (Ghannoum, 2000; Rodrigues, Silva and Henriques, 2014), and a strong correspondence between phospholipase activity and persistent candidemia in *C. glabrata* has been suggested (Ghannoum, 2000). However, not all clinically isolated *C. glabrata* strains produce detectable phospholipase activity and even for those that do, the secreted amount is significantly lower than that of *C. albicans* (Ghannoum, 2000; Rossoni *et al.*, 2013; Canela *et al.*, 2018).

It was also suggested that the most common route for this yeast to enter the bloodstream is through nosocomial conditions such as surgery, catheter and burn injuries (Galocha *et al.*, 2019). However, without using any of these conditions, a mouse model of *C. glabrata* hematogenous disseminated infection was achieved (Atanasova *et al.*, 2013). That indicates the existence of other invasion routes for this pathogen. A study by Silva *et al.* demonstrated that a single *C. glabrata* infection rarely caused oral epithelial cell invasion while coinfection with *C. albicans* significantly enhanced invasion by *C. glabrata* (Silva *et al.*, 2011). In 2016, Tati *et al.* verified these results and further showed that *C. glabrata* bound to *C. albicans* hyphae (**Figure 4B**) (Tati *et al.*, 2016). They also demonstrated that 2 adhesins (Als1 and Als2) of the *C. albicans* hyphal wall and 5 cell wall protein genes of *C. glabrata* (*EPA8*, *EPA9*, *AWP2*, *AWP7* and *CAGLOF00181*) participated in the adhesion of *C. glabrata* to *C. albicans* hyphae. These results, together with the fact that *C. glabrata* often colocalizes with *C. albicans* in the infected sites, indicated that the former might exploit the tissue damage caused by the later to invade tissues (Coco *et al.*, 2008; Galocha *et al.*, 2019). On the other hand, a study by Li and Dongari-Bagtzoglou proposed that endocytosis might also be a pathway for *C. glabrata*

invasion (**Figure 4A**, right). They found that once the oral epithelial cells were treated with an endocytosis inhibitor (cytochalasin D), *C. glabrata* internalization was no longer observed (Li and Dongari-Bagtzoglou, 2009).

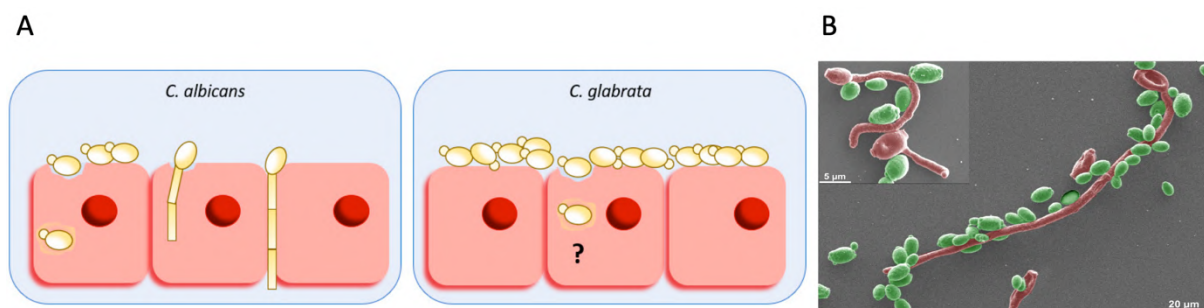


Figure 4. Mechanisms of *C. albicans* and *C. glabrata* host damage and invasion. A. *C. albicans* (left) enter host cells by endocytosis or hyphal formation. *C. glabrata* (right) host invasion mechanisms are not very clear. Endocytosis is considered to be one of the entrance mechanisms used by *C. glabrata* besides nosocomial injuries. (Figure from Galocha et al., 2019) B. *C. glabrata* (green) binds to *C. albicans* (cherry) hyphae by scanning electron microscopy. Magnifications, $\times 500$. (Figure from Tati et al., 2016)

1.2.4.b. Biofilm formation

Like other *Candida* species, *C. glabrata* can form a multilayered biofilm structure to colonize the host or abiotic surface (Rodrigues, Silva and Henriques, 2014). The formation of biofilms can give the yeast advantages during infection, including host immune evasion. It has been found that *C. albicans* biofilms are more resistant to the killing activity of neutrophils because of their architecture and their ability to impair the release of extracellular traps by neutrophils (Xie et al., 2012; Johnson et al., 2016). Moreover, the biofilms seem to increase the resistance against antifungal agents. Choi et al. showed that fluconazole was ineffective against both *C. albicans* and *C. glabrata* biofilms compared to planktonic cells (Choi et al., 2007). In fact, biofilms were shown to be more virulent than planktonic cells in a *C. albicans* candidemia murine model (Uppuluri et al., 2010) and *Candida* biofilms corresponded with a higher mortality in candidemia patients (Vitális et al., 2020).

The biofilm structures of *C. glabrata* and *C. albicans* are different. The biofilms of *C. albicans* are thick with a complex structure comprising yeast cells, pseudohyphae, hyphae and extracellular matrix. *C. glabrata* biofilms are thinner than those of *C. albicans*. The average thickness of *C. glabrata* biofilms is about 5 μm *in vitro* and it can be thicker and reach around 75

to 90 μm in an *in vivo* model (Seneviratne *et al.*, 2009; Kucharíková *et al.*, 2015). Among major pathogenic *Candida*, *C. glabrata* is the only one with a biofilm structure composed only of yeast cells and extracellular matrix (**Figure 5**) (Seneviratne *et al.*, 2009; Silva *et al.*, 2009). *C. glabrata* biofilms have a relatively high quantity of protein and carbohydrate in their extracellular matrix, five times higher than those of *C. parapsilosis* and *C. tropicalis* in some cases (Silva *et al.*, 2009). It has also been shown that compared to *C. parapsilosis* and *C. tropicalis*, *C. glabrata* biofilms have a significant lower metabolic activity and a higher number of cultivable cells (Silva *et al.*, 2010).

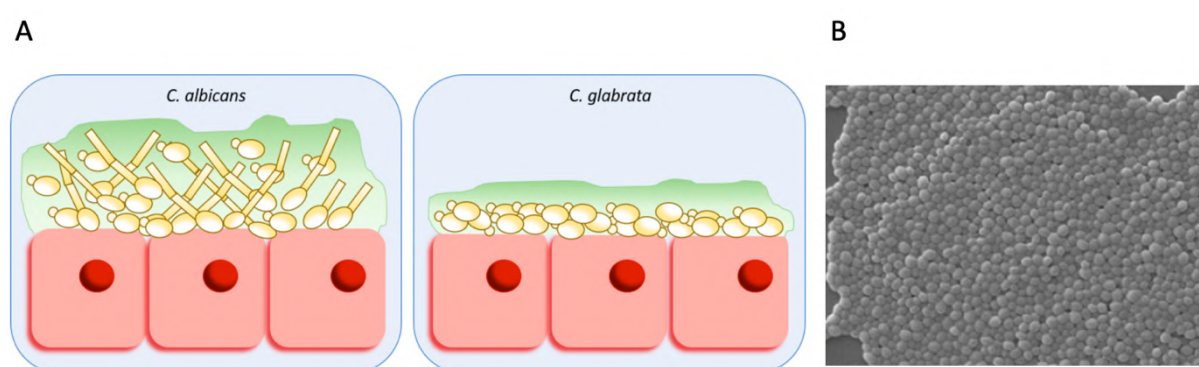


Figure 5. Biofilms formed by *C. albicans* and *C. glabrata*. A. Schematic representation of the structure of *C. albicans* (left) and *C. glabrata* (right) biofilms. *C. albicans* biofilms are thicker and have more extracellular matrix (green). *C. glabrata* biofilms are composed of only compact yeast cells while *C. albicans* biofilms have yeast cells, pseudohyphae and hyphae. (Figure from Galocha *et al.*, 2019) B. *C. glabrata* biofilm formation in Sabouraud Dextrose Broth. Magnification, $\times 1000$. (Figure from Rodrigues *et al.*, 2014)

1.2.4.c. Adhesion

Biofilm formation, as well as the binding to host tissues, requires *Candida* cells to have adhesive capabilities. The proteins responsible are called adhesins in *Candida* species. The adhesion of *C. glabrata* is mediated by the family of epithelial adhesins (Epa) which contains 17 to 23 genes depending on the strain (Rodrigues *et al.*, 2017). Among these genes, *EPA1*, *EPA6* and *EPA7* are considered the most important.

In *C. glabrata*, adhesion is largely mediated by a Ca^{2+} -dependent lectin, which is encoded by the *EPA1* gene and whose host ligands are N-acetyl lactosamine-containing glycoconjugates. The deletion of this gene can lead to a 95% reduction in adherence to epithelial cells *in vitro* (Cormack *et al.*, 2016). It has also been shown that *S. cerevisiae* strains

expressing *EPA1*, but not *EPA2-5*, gained the ability to adhere to epithelial cells (Castaño *et al.*, 2005). The expression of *EPA1* varies greatly (up to over 100-fold) between individual cells, which make this gene one of the most heterogeneously expressed among a yeast population. The ability to adhere to epithelial cells and the *EPA1* expression level is strongly correlated (Halliwell *et al.*, 2012). The transcription of *EPA1* is weak during stationary phase (Castaño *et al.*, 2005). *EPA1* is located in a locus adjacent to a telomere that comprises four genes named *HYR1*, *EPA1*, *EPA2* and *EPA3*, all encoding glycosylphosphatidylinositol-anchored cell wall proteins (GPI-CWPs). Interestingly, deletion of the *EPA1* gene (*epa1Δ*) alone does not lead to decreased virulence and the deletion of all four genes in the locus (*hyr1 epa1 epa2 epa3* strain) has only a modest influence on colonization, especially in the kidney (De Las Peñas *et al.*, 2003). Another two *EPA* genes, *EPA4* and *EPA5*, are also located close to the telomere. However, among these 6 genes (*HYP1*, *EPA1-5*), only *HYP1* and *EPA1* are transcriptionally active (De Las Peñas *et al.*, 2003).

Castaño *et al.* found that in some strains with an *epa1Δ* background, *C. glabrata* could still be hyperadherent, indicating that adhesins other than Epa1 also play an important role in adherence. They then proposed Epa6 and Epa7 as two other important adhesins for *C. glabrata* adherence (Castaño *et al.*, 2005). Like Epa1, Epa6 is a GPI-anchored cell wall protein with an N-terminal domain close to Epa1. The expression of *EPA6* can be strongly activated when *RIF1*, a gene involved in cell cycle regulation, is deleted. Like *EPA1-5*, *EPA6* is also close to the telomere (Castaño *et al.*, 2005). During infection, the expression of *EPA6* is only active during urine infection in a murine model, but not bloodstream infection (Domergue *et al.*, 2005). Domergue *et al.* also showed that nicotinic acid (NA) limitation induced the expression of *EPA6* and an excess of NA led to the repression of this gene. *EPA7* is another subtelomeric gene very similar to *EPA6*. These two genes differ by only 6% over their whole length, and by only 2.1% and 2.6% in their ~4 kb upstream sequence and in the region between the gene and the telomere, respectively. Also, *S. cerevisiae* strains containing one or both genes gained the ability to adhere to epithelial cells (Castaño *et al.*, 2005).

EPA1-7 genes are subtelomeric and this localization is important for the regulation of their expression. *SIR3* and *RIF1* are two important genes that regulate telomere length and repress the expression of *EPA* genes. The deletion of these genes led to a hyperadherent phenotype and increased the virulence of *C. glabrata*, especially for kidney colonization

(Castaño *et al.*, 2005). Castaño *et al.* also showed that *EPA1* and *EPA6* contributed importantly to adhesion in a *rif1Δ* background while in a *sir3Δ* background, *EPA1*, *EPA6* and *EPA7* were all important.

Besides the Epa family, another protein family that contributes to adhesion was discovered in 2008. These proteins, which are all GPI proteins and have adhesin-like characteristics, were named adhesin-like wall proteins (Awp). De Groot *et al.* identified four such proteins (Awp1-4) and showed that they could be phase specific or strain specific (De Groot *et al.*, 2008).

1.3. Limited pharmacology to treat *Candida glabrata* infections

In this part, I will introduce the currently available treatments for invasive fungal infections, including the available antifungal families, the resistance developed by *C. glabrata* and new agents under development. The objective is to give a general idea of what arsenal we have at our disposal and what we can improve to fight invasive fungal infections.

1.3.1. Development of antifungal agents

The introduction of amphotericin B in 1958 by Squibb Laboratories opened the door to the era of systemic antifungal chemotherapy. After that, development in this field was very slow. The next big step forward had to wait till 1990 with the introduction of fluconazole. The characteristics of this molecule made it fulfill the needs of safety (lower toxicity and risk of drug interaction), efficiency (wide distribution) and practice (oral bioavailability) all together for the first time in antifungal therapy. The azole family became a first-line choice for invasive fungal infection treatment during that time. Less than ten years later, echinocandins were introduced as a new class of antifungal. Almost at the same time, voriconazole and posaconazole were introduced as broad-spectrum triazole agents, which were shown to be more efficient than amphotericin B for certain fungi. Developments seemed to accelerate in this era. However, just when it seemed like the dawn for antifungal therapy had finally arrived, developments in this field came to a halt. Over the nearly twenty years that have passed since the first echinocandin was approved, no new major advance in systemic antifungal treatment

has been made and no new antifungal family has been discovered (**Figure 6**) (Lewis, 2011; Perfect, 2017).

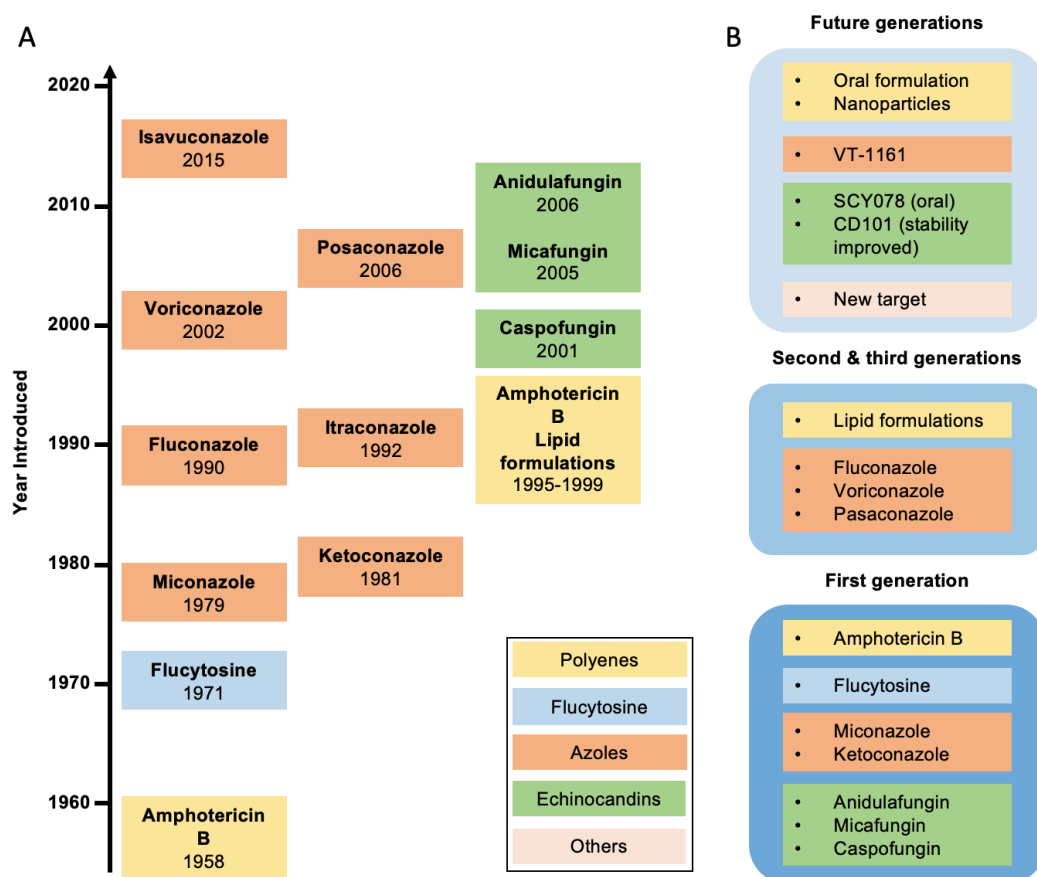


Figure 6. Chronology of antifungal drug development. **A.** Timeline of currently available systemic antifungal drugs. **B.** Summary of the different generations of drugs currently available and under development. Polyenes, flucytosine, azoles and echinocandins are the only four currently available classes of systemic antifungal agents. Based on the first generation, improvements have been made to increase their activity, safety, pharmacokinetics (for azoles) and to reduce the toxicity (for amphotericin B). Future generations of compounds and new classes of drugs are in development. Today, flucytosine is no longer considered as a major systemic antifungal agent since it is rarely used alone. (Adapted from Lewis, 2011; Perfect, 2017)

Therapy against many superficial mycoses is well developed with a series of drugs that can successfully control the fungal infections. However, when we turn to invasive fungal infection therapy, the number of major drug families is still fixed at three: polyenes (amphotericin B), azoles and echinocandins (**Figure 7**) (Perfect, 2017).

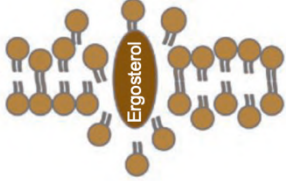
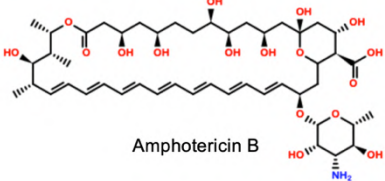
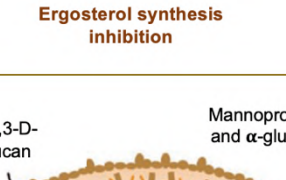

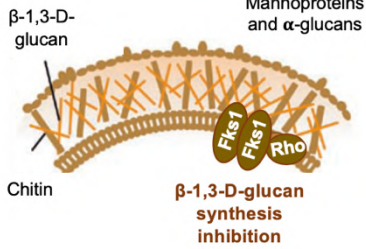

	Mechanism	Drug class	Drugs
Cell membrane	Ergosterol binding 	Polyenes	 Amphotericin B
	Ergosterol synthesis inhibition 	Azoles	 Fluconazole Itraconazole Voriconazole Posaconazole Isavuconazole Miconazole Ketoconazole
Cell wall	 β-1,3-D-glucan Mannoproteins and α-glucans Chitin Fks1 Fks2 Rho β-1,3-D-glucan synthesis inhibition	Echinocandins	 Caspofungin Anidulafungin Micafungin

Figure 7. Mechanism and structure of some currently available systemic antifungal agents. Ergosterol is the essential sterol of the fungal cell membrane. The fungal cell wall is primarily composed of chitin, β-1,3-D-glucan, mannoproteins and α-glucans. Catalytic subunits Fks1 and Fks2 of the glucan synthase complex are the putative target binding site of echinocandins. Rho is a cell wall-regulating protein. (Adapted from Lewis, 2011)

Table 3. Management of invasive candidiasis. (Adapted from Pappas et al., 2018)

	Preferred initial therapy	Alternative initial therapy	Sep-down therapy
Unidentified	Echinocandin	-	-
<i>C. albicans</i>	" "	Fluconazole	Fluconazole
<i>C. glabrata</i>	" "	Amphotericin B	Voriconazole
<i>C. parapsilosis</i>	" "	Fluconazole	Fluconazole
<i>C. tropicalis</i>	" "	Fluconazole	Fluconazole
<i>C. krusei</i>	" "	Amphotericin B	Voriconazole
<i>C. auris</i>	" "	Amphotericin B	Susceptibility dependent

1.3.2. Amphotericin B: ergosterol binder

After first being isolated in the 1950s from *Streptomyces nodosus*, amphotericin B (**Figure 7**) quickly became the standard treatment for fungal infections over the following 40 more years. Until today, with the broadest antifungal spectrum among all systemic antifungals, this drug remains the most potent fungicide in clinical use (Lewis, 2011; Perfect, 2017).

1.3.2.a. Mode of action of amphotericin B

Amphotericin B interacts hydrophobically directly with ergosterol, an essential component of the fungal cell membrane. This interaction leads to the formation of complexes that intercalate into the cell membrane. Pores and channels are then formed, which disrupt the function of the membrane and lead to the leakage of intracellular contents and ultimately to cell death (Brajtburg *et al.*, 1990). Another proposed antifungal mechanism is that amphotericin B can also stimulate phagocytic cells of the host immune system with an oxidation dependent menace (Groll, Piscitelli and Walsh, 1998). This compound has also been reported to induce the expression of IL-1 β and TNF- α in human monocytes and the release of those cytokines (Rogers *et al.*, 1998). Since ergosterol is the principal sterol of the fungal cell membrane, most human pathogenic fungi are sensitive to amphotericin B and the development of resistance is still rare (Lewis, 2011).

1.3.2.b. Spectrum and pharmacokinetics of amphotericin B

Amphotericin B is active against almost all pathogenic fungi, including yeasts, molds and dimorphic fungi (Lewis, 2011). Intravenous administration is the only route available for amphotericin B. The distribution of the compound is mainly in the blood stream and highly bound to serum proteins. Penetration into the central nervous system (CNS), bone and eyes is poor. Amphotericin B can also be used for prophylaxis and as a therapy for orointestinal mucosa infections thanks to its negligible absorption from the gastrointestinal tract (Groll, Piscitelli and Walsh, 1998).

1.3.2.c. Toxicities of amphotericin B

Amphotericin B has both acute and delayed toxicity. Acute toxicity includes fever, chills, rigor, anorexia, nausea, vomiting, myalgias (muscle pain), arthralgias (joint pain) and headache. This type of toxicity is related to drug infusion and decreases over time with continued drug administration. The use of anti-inflammatory agents can also reduce those acute reactions. The delayed toxicity of amphotericin B is related to its biochemical characteristics. Generally, amphotericin B has a greater affinity toward fungal ergosterol compared to cholesterol in the mammalian cell membrane. However, this specificity may be lost when a high concentration of compound accumulates in some sites, for example, the kidney. Nephrotoxicity is the most important delayed toxic effect of amphotericin B, which includes a decrease in glomerular filtration rate and renal blood flow, eventual azotemia, distal tubular degeneration and nephrocalcinosis. Other delayed side effects include renal concentration defects, magnesium wasting, etc. (Groll, Piscitelli and Walsh, 1998; Lewis, 2011).

1.3.2.d. Lipid formulations of amphotericin B

The delayed side effects of amphotericin B need a high concentration of the drug, meaning that those toxicities are dose dependent. Increasing the selectivity for the fungal cell membrane relative to the human cell membrane may reduce those effects, especially nephrotoxicity. Based on this theory, different lipid formulations of amphotericin B, such as amphotericin B lipid complex and AmBisome, were developed during the 1990s. Those lipid formulations were considered to reduce interactions between the molecule and the human cell membrane. Early clinical studies verified indeed a significant decrease in toxicity with these formulations compared to conventional amphotericin B even when a higher dose was administered. However, dose related renal toxicity cannot be totally avoided and may still occur with lipid formulations (Groll, Piscitelli and Walsh, 1998; Perfect, 2017).

1.3.3. Azoles: ergosterol biosynthesis inhibitors

In the late 1970s, azoles were developed as a new family of systemic antifungal agents in order to decrease the side effects of systemic antifungal treatment by amphotericin B.

Unlike the latter, azoles are synthetic, with one or more five-memberedazole rings. This family can still be classified into two groups depending on the number of nitrogen atoms in their ring structure: compounds with two nitrogen atoms are called imidazoles while those containing three nitrogen atoms are named triazoles (Groll, Piscitelli and Walsh, 1998; Allen *et al.*, 2015; Perfect, 2017).

Imidazoles are the firstly developedazole agents, including the early introduced miconazole and ketoconazole. These compounds are still used for the treatment of superficial mycoses. As for invasive fungal infections, imidazoles are of limited use because of their chemical and pharmacokinetic characteristics and toxicity. The introduction of fluconazole and itraconazole as triazoles in the early 1990s marked a big step in the management of fungal infections (Allen *et al.*, 2015). With their broad spectrum activity and safety, triazole antifungal agents became the first-line choice for systemic fungal infections during that time (Perfect, 2017). Even in 2011, 21 years after its introduction, fluconazole was still the most used systemic antifungal agents in Nordic countries (Hesstvedt *et al.*, 2017).

1.3.3.a. Mode of action of azoles

The azoles primarily inhibit the fungal cytochrome P450 (CYP450)-dependent lanosterol 14- α -demethylase Erg11, thereby blocking the demethylation of lanosterol to ergosterol. This inhibition leads to the accumulation of toxic precursors and to the lack of ergosterol in the cell membrane, resulting in impaired membrane fluidity followed by growth arrest and cell death (**Figure 7**) (Groll, Piscitelli and Walsh, 1998; Lewis, 2011; Perfect, 2017). It was also shown that ketoconazole inhibited the activity of NADH oxidase of the mitochondria from *C. albicans* and impaired the function of the respiratory chain (Uno, Shigematsu and Arai, 1982).

1.3.3.b. Spectrum and pharmacokinetics of azoles

Theazole family of agents are principally active against pathogenic yeast (e.g., *C. albicans* and *C. neoformans*) and dimorphic fungi (e.g., *Coccidioides immitis* and *Histoplasma capsulatum*). The activity is weaker against some non-*albicans* *Candida* species, especially *C.*

glabrata. Fluconazole is inactive against mold (e.g, *Aspergillus fumigatus* and *Aspergillus terreus*), but new-generation drugs like voriconazole and posaconazole have strong activity against some pathogenic molds (Groll, Piscitelli and Walsh, 1998; Lewis, 2011).

Among azole agents, fluconazole has very good pharmacokinetic properties. This low molecular weight, hydrosoluble bis-triazole can be administrated by both oral and intravenous routes, providing almost the same pharmacokinetic properties. The bioavailability can be over 90% after oral administration, which is independent of food and intragastric pH. Peak blood concentration arrives only one to two hours after being administered. Unlike amphotericin B, fluconazole is mostly present as the free drug in the blood stream and only 12% binds to serum proteins. The distribution of fluconazole is also better than that of amphotericin B since it presents an excellent penetration into the eyes and the CNS. Fluconazole is relatively stable during metabolism: almost 80% of the drug excreted in the urine is unchanged and active. Most of the pharmacokinetic properties of other azoles are similar to those of fluconazole. Ketoconazole and itraconazole can only be well absorbed at low pH. The serum protein binding rate of itraconazole is very high (95%) but it is still widely distributed throughout the body. The liver metabolizes most itraconazole to an inactive form before its exclusion (Groll, Piscitelli and Walsh, 1998).

1.3.3.c. Toxicities of azoles

Some major toxicities of azoles are due to their interactions with mammalian CYP450 dependent enzymes. As the most used systemic antifungal azoles, fluconazole is much less toxic compared to amphotericin B. Administration with very high dose is needed to induce hepatotoxicity (1600 mg/day) and neurotoxicity (2000 mg/day). Other side effects, such as skin rash, headache, transaminase increase, nausea, vomiting and other gastrointestinal responses are reported at a very low rate (less than 5%) and are often reversible. The side effects of itraconazole and other azoles are similar to those of fluconazole (Groll, Piscitelli and Walsh, 1998).

1.3.3.d. Isavuconazole: the newest azoles

Isavuconazole is the newest generation of azoles that was approved by the U.S. Food and Drug Administration (FDA) in 2015. This extended-spectrum triazole is active against pathogenic yeasts and molds. Its 90% minimum inhibitory concentration (MIC₉₀) *in vitro* for *A. fumigatus* is higher than voriconazole, posaconazole and amphotericin B but still low (about 1-2 µg/mL). This drug is still more active against *Candida* spp with a MIC₉₀ lower than 0.1 µg/mL. However, *C. glabrata* is less susceptible to isavuconazole, and antagonistic activity was observed between this drug and amphotericin B against *C. glabrata* (Denis *et al.*, 2018). A pre-clinical study also showed that isavuconazole was more efficient against *C. krusei* brain infections compared to fluconazole and voriconazole in mouse models (Majithiya *et al.*, 2009).

1.3.4. Echinocandins: glucan biosynthesis inhibitors

Echinocandins are large lipopeptide molecules and the newest antifungal family introduced in the beginning of 2000s. Caspofungin, micafungin and anidulafungin are the only three drugs approved in this family today. With their broad-spectrum fungicidal activity and their safety in clinical use, this drug family has had a great success over the past decade. It is today considered to be the first line of treatment for invasive candidiasis (Table 3) (Denning, 2003; Pappas *et al.*, 2015; Perfect, 2017).

1.3.3.a. Mode of action of echinocandins

The structure of the fungal cell wall is maintained largely by β-1,3-glucan. In *S. cerevisiae*, the genes encoding β-1,3-glucan synthase are *FKS1* and closely related *FKS2*. Orthologues of *FKS1* or *FKS2* are present in all fungi studied to date. Echinocandins interact and block the function of the *FKS1* protein and lead to the lack of β-1,3-glucan in the fungal cell wall (Figure 7). That makes fungi susceptible to osmotic lysis, especially during the rapid growth phase (Douglas *et al.*, 1997; Denning, 2003; Lewis, 2011).

1.3.3.b. Spectrum and pharmacokinetics of echinocandins

Echinocandins are active strictly against only *Candida* spp and *Aspergillus* spp, with very few exceptions, due to the differences of the β -1,3-glucan polymerization in the cell wall and the expression of glucan synthase. The activity of the three echinocandins is fungicidal against *Candida* spp and fungistatic against *Aspergillus* spp (Denning, 2003).

Echinocandins are administrated intravenously, their oral bioavailability being insufficient for a consistent antifungal effect. The distribution of anidulafungin is better than micafungin with a greater distribution volume. Also, the administration of two doses is enough for anidulafungin to achieve the blood steady-state whereas treatment for four days or 2 weeks are needed for micafungin and caspofungin, respectively. All three drugs have a high serum protein binding activity (>80%) and poor penetration to the CNS. Echinocandins are mainly degraded in the liver, but micafungin has two metabolites that remain active for antifungal activity (Denning, 2003).

1.3.3.c. Toxicities of echinocandins

The most studied side effects among echinocandins are those for caspofungin. Fever, thrombophlebitis (an inflammatory process causing a blood clot to form in and block a vein) at the infusion site, headache, and elevation of liver enzyme levels are the most common side effects. Histamine-like reactions may occur when infusion is rapid. Anaphylaxis has also been reported but rarely. Even worse toxicities like hepatic dysfunction, hepatitis and even hepatic failure are also reported in isolated cases, but it is not clear if they are drug-related (Bennett, 2006).

1.3.3.d. New generation of echinocandins in development

Rezafungin (CD101) is the newest echinocandin in development that is currently in phase III clinical trials. This molecule was shown to have excellent activity against *Candida* spp and *Aspergillus* spp (Castanheira *et al.*, 2014). The preclinical evaluation of rezafungin indicated that this molecule was chemically and metabolically stable and has a high percentage of serum protein binding (98%) which is similar to anidulafungin. However, the

former showed a better tolerance compared to the latter in rat models without effects on body weight, hematology, coagulation or urinalysis. Also, the half-life of rezafungin was longer than that of any other available echinocandins in animal models (Ong *et al.*, 2016). A phase I clinical trial also verified its tolerance by demonstrating that administration with a dose up to 400 mg per week for 3 weeks was well tolerated and safe. Other advantages in pharmacokinetic properties included long plasma half-life, low apparent clearance and minimal accumulation over several weeks. These advantages made a weekly administration possible (Sandison *et al.*, 2017). In 2018, a phase II clinical test was still ongoing (Sofjan *et al.*, 2018).

1.3.5. Flucytosine: DNA biosynthesis inhibitors

Flucytosine was originally developed in the 1950s as an antineoplastic agent before its antifungal activity was discovered in the 1960s. This molecule is a pyrimidine analogue and can be converted into 5-fluorouracil (5-FU) by cytosine deaminase in the fungal cytoplasm. After being phosphorylated, 5-FU can on the one hand incorporate into RNA and cause miscoding and on the other hand, convert to the deoxynucleotide form and inhibit thymidylate and DNA synthesis. 5-FU cannot be used directly as an antifungal agent because it is not taken up by fungal cells. Flucytosine has low toxicity since the activity of cytosine deaminase is absent or very low in human cells. Moreover, this drug can be administered by both oral and intravenous routes. However, flucytosine is rarely used alone because resistance is easily and quickly developed by fungi during monotherapy. On the other hand, flucytosine has been shown to have a synergistic effect with amphotericin B or azoles, which has led to its combination use with these two drug families for systemic fungal infection treatment (Groll, Piscitelli and Walsh, 1998; Perfect, 2017).

1.3.6. Antifungal resistance and *Candida glabrata*

C. glabrata has a naturally low susceptibility to azoles and is associated with a lower susceptibility to all antifungals including amphotericin B (Fidel Jr, Vazquez and Sobel, 1999;

Sanguinetti, Posteraro and Lass-Flörl, 2015). Furthermore, acquired resistance can also be developed (Fidel Jr, Vazquez and Sobel, 1999). *C. glabrata* has one of the highest antifungal resistance rates against all azole agents among almost all *Candida* species and can show 100% resistance against fluconazole and 67.3% against parconazole (Wisplinghoff *et al.*, 2014). At the same time, a study by Pfaller *et al.* showed that among the major non-*albicans* isolates (*C. glabrata*, *C. parapsilosis*, and *C. tropicalis*), *C. glabrata* was the only one that showed simultaneous resistance against both azole and echinocandin agents (Pfaller, Jones and Castanheira, 2014). Similar results were obtained by Lockhart and Matsumoto who showed that *C. glabrata* developed the highest resistance rate against azoles and echinocandins among major *Candida* pathogens in Atlanta, Baltimore and Iowa (Lockhart *et al.*, 2012; Matsumoto *et al.*, 2014).

For many fungi, including *C. glabrata*, genomic plasticity plays an important role to allow adaptation to environmental changes, such as host response and antifungal pressure (Rodrigues, Silva and Henriques, 2014). The haploid genome of this yeast allows it to express and spread beneficial mutations easily and adapt itself faster to selection pressures (Otto and Gerstein, 2008). In 2012, Rai *et al.* showed that *C. glabrata* modified its chromatin structure to survive inside the macrophage after infection (Rai *et al.*, 2012). Later the same year, using the same CBS138/ATCC2001 strain in different laboratories, Bader *et al.* discovered that *C. glabrata* showed different karyotypes even under laboratory conditions without any extreme selective pressure. They also showed that the observed chromosomal aberrations correlated with different cell wall phenotypes (Bader *et al.*, 2012).

1.3.6.a. Amphotericin B resistance

Molecular mechanisms leading to amphotericin B resistance in *C. glabrata* are poorly documented. In 2012 Hull *et al.* showed that mutations in *ERG2* led to a reduced sensitivity to amphotericin B. This group also found that an azole and amphotericin B cross-resistant strain contained *ERG11* mutations. Another study in Kuwait showed similar results that *C. glabrata* strains with reduced susceptibility to amphotericin B contained mutations in *EGR2* and *EGR6*. Since these genes participate in ergosterol biosynthesis, the mutants had no detectable ergosterol level in their cell membrane, which instead showed the accumulation of other

intermediate sterols, in contrast with the wild-type susceptible strain for which 90% of the total cell sterol was ergosterol (Hull, Bader, *et al.*, 2012; Hull, Parker, *et al.*, 2012; Ahmad *et al.*, 2019).

1.3.6.b. Azoles resistance

C. glabrata is believed to have natural resistance to azoles and this is one of the reasons why infections by this yeast have recently increased. In fact, the introduction of triazoles in the early 1990s also marked the time point that *C. glabrata* infections began to arise (Rodrigues, Silva and Henriques, 2014). The mechanisms by which *C. glabrata* develops azole resistance are complex. First, *ERG11*, which participates in ergosterol biosynthesis, is upregulated (Henry, Nickels and Edlind, 2000). Secondly, genes encoding drug efflux transporters, such as *CDR1* and *PDH1*, are also greatly upregulated under azole pressure. The proteins Cdr1p and Pdh1p are ATP-binding cassette (ABC) transporters that can pump the drug out of the yeast cell (Bennett, Izumikawa and Marr, 2004). Finally, mitochondrial dysfunction is also believed to play a role in the development of azole resistance (Miyazaki *et al.*, 2010).

1.3.6.c. Echinocandins resistance

Echinocandins are the newest antifungals but resistance to these drugs has already begun to appear. One study from Duke University Hospital showed that the resistance rate for *C. glabrata* had increased from 4.9 % in 2001 to 12.3 % in 2010. Compared to other *Candida* species, *C. glabrata* seems to have a higher potential to develop resistance against echinocandins for some unknown reason. Besides drug efflux transporters, *C. glabrata* echinocandin resistance and clinical failure primarily correlates with mutations of *KFS* genes, including *KFS1* and *KFS2*, which encode the targets of echinocandins. In fact, among *Candida* species, *C. glabrata* is the only one to have two redundant and differently regulated *KFS* subunits (Alexander *et al.*, 2013; Rodrigues, Silva and Henriques, 2014; Healey and Perlin, 2018).

1.3.7. Novel potential antifungal agents in development

Considerable effort is ongoing around the world to identify new and more efficient antifungals. Here are just a few examples of the new antifungal agents and targets under development.

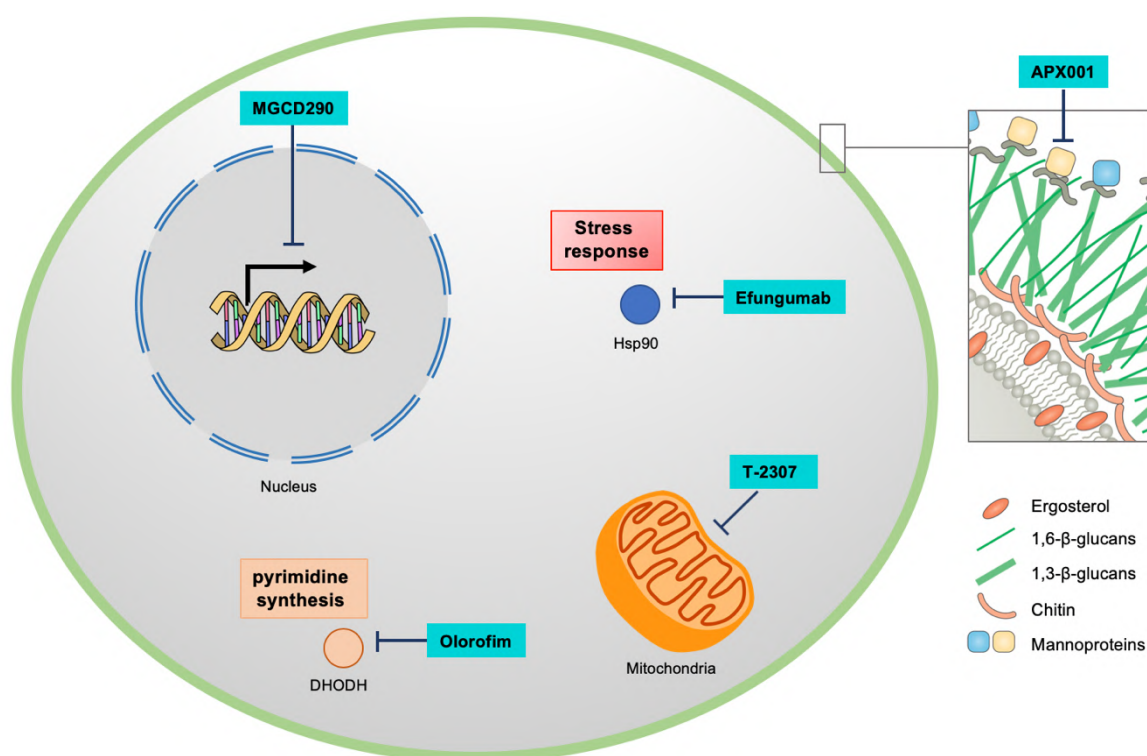


Figure 8. Some potential antifungal agents currently in clinical trials. Dihydroorotate dehydrogenase (DHODH) plays an essential role in pyrimidine biosynthesis. Heat shock protein 90 (Hsp90) is a protein chaperone and plays a key role in cell stress response. (Adapted from Perfect, 2017)

1.3.7.a. Some agents in clinical trail

APX001 was discovered by Tsukuba Research Laboratories in Japan. It targets fungal cell wall components like echinocandins, inhibits the biosynthesis of glycosyl phosphatidylinositol and then blocks the binding of essential mannoproteins to the fungal cell wall (Hata *et al.*, 2011; Perfect, 2017). *In vitro* tests showed that this molecule was efficient against almost all *Candida* species, including *Candida auris* (*C. auris*) and other azole or echinocandin resistant strains, but not *C. krusei*. It was also active against mold like *Aspergillus* species. The toxicity shown *in vitro* was as low as fluconazole (Miyazaki *et al.*, 2011; Hager *et*

al., 2018; Zhao *et al.*, 2018). Preclinical tests in a mouse model showed that APX001 was efficient against infections caused by *Candida*, *Aspergillus* and *Fusariosis* species (Hata *et al.*, 2011). APX001 completed phase I clinical trials for intravenous administration in August 2017 and for oral administration in January 2019 (data from clinicaltrials.gov, Ref. NCT02957929 and NCT02956499).

T-2307 is an arylamidine synthesized by Tokuyama Corporation. This molecule enters the fungal cell through a specific spermine and spermidine carrier (Nishikawa *et al.*, 2016). Once concentrated inside the cell, T-2307 can selectively inhibit fungal respiratory chain complexes III and IV, resulting in a disruption of mitochondrial membrane potential and a decrease of the intracellular ATP level (Shibata *et al.*, 2012; Yamashita *et al.*, 2019). The *in vitro* activity of T-2307 showed broad-spectrum activity against *Candida* and *Aspergillus* species. Mouse models showed that this molecule was efficient against systemic candidiasis, aspergillosis and cryptococcosis and even more active compared to micafungin and amphotericin B against candidiasis. It also exhibited the ability to significantly reduce the fungal burden in mice infected with *C. auris* and with echinocandin resistant *C. glabrata* (Mitsuyama *et al.*, 2008; Wiederhold *et al.*, 2016, 2020). T-2307 was reported to be in a phase I clinical trial in 2017 (Perfect, 2017).

Efungumab, also called mycograb, is a human recombinant monoclonal antibody created by NeuTec Pharma. This antibody targets a chaperone protein, heat shock protein 90 (Hsp90), in the fungal cell wall and extracellular material (Pachil *et al.*, 2006). Preclinical data showed that Efungumab improved the effect of caspofungin and amphotericin B in invasive candidiasis (Hodgetts *et al.*, 2008; Pachil *et al.*, 2006). However, one study reported that the synergistic effect of amphotericin B and Efungumab seemed to be a nonspecific effect since other unrelated proteins also had the same effect (Richie *et al.*, 2012). Efungumab completed a phase I clinical trial in February 2009 and is currently in a phase II clinical trial against cryptococcal meningitis in patients with AIDS (data from clinicaltrials.gov, Ref. NCT00324025 and NCT00847678).

MGCD290, developed by MethylGene, Inc. in Canada, is an inhibitor of histone deacetylase 2 (Hos2). Hos2 belongs to a family of enzymes that remove the acetyl group from lysine residues of histones named histone deacetylases (HDACs). Proteins of this family regulate the expression of genes and other cellular functions like cell proliferation and cell

death (Pfaller *et al.*, 2009; Perfect, 2017). An *in vitro* study showed that MGCD290 had a modest effect alone. However, synergy between this molecule and azoles or echinocandins against *Candida* and *Aspergillus* species was shown. More importantly, synergistic effects could be obtained with azoles or echinocandins against azole- or echinocandin-resistant strains, respectively (Pfaller *et al.*, 2009, 2015). A phase I clinical trial finished in April 2013 and phase II is currently ongoing against severe vulvovaginal candidiasis (data from clinicaltrials.gov, Ref NCT01497223).

Olorofim (also called F901318) specifically inhibits fungal dihydroorotate dehydrogenase (DHODH), which plays an essential role in the pyrimidine biosynthesis pathway (Oliver *et al.*, 2016). *In vitro* and *in vivo* studies have all shown that this molecule efficiently inhibits *Aspergillus* species (Oliver *et al.*, 2016; Buil *et al.*, 2017). Another study also showed the activity of Olorofim against *Coccidioides* *in vitro* and *in vivo* (Wiederhold *et al.*, 2018). Currently in a phase II clinical trial, the effects of olorofim against *Candida* have not yet been reported (Perfect, 2017).

1.3.7.b. Some other agents and targets

AmBMU and AmBAU are two amphotericin B derived compounds synthesized by Davis *et al* in 2015 (Davis *et al.*, 2015). These two molecules showed a highly improved antifungal effect in a systemic candidiasis mouse model with lower toxicity compared to the original amphotericin B. As for amphotericin B, little resistance arose against either compound. With these improved characteristics, AmBMU and AmBAU could be the best candidate to replace amphotericin B in antifungal therapy. However, no further report has been published since 2015.

Icofungipen (PLD-118, formerly named BAY 10-8888) is a cyclic β -amino acid. It is a specific inhibitor of isoleucyl-tRNA synthetase and can result in protein synthesis and cell growth inhibition (Ziegelbauer, Babczinski and Schönfeld, 1998). The antifungal effect of icofungipen has already been validated *in vitro* and *in vivo*, by using oropharyngeal and esophageal or systemic *C. albicans* infection animal models. It was also shown that this compound was nearly completely orally bioavailable (Petraitis *et al.*, 2004; Hasenoehrl *et al.*, 2006).

Several potential antifungal targets were also proposed. Wurtele *et al* proposed that histone H3 lysine 56 acetylation (H3K56ac) could be a potential antifungal target (Wurtele *et al.*, 2010). They found that genetic and pharmaceutical changes of H3K56ac levels, induced by targeting Hst3, a histone deacetylase (HDAC), reduced the virulence of *C. albicans* in mouse models. Hammad *et al* indicated that mannan, a fungal cell wall polysaccharide component, might also be an antifungal target and showed that a mannose-binding lectin could significantly reduce *C. albicans* cell proliferation *in vitro* (Hammad *et al.*, 2018). Another target proposed was Vacuolar proton-translocating ATPase (V-ATPase), which is located in the fungal cell membrane. Minematsu *et al* showed that a V-ATPase inhibitor had a synergistic effect with azoles against *C. glabrata*. They also found that cells lacking the *VPH2* gene which encodes a subunit of V-ATPase led to the reduced virulence by *C. glabrata* (Minematsu *et al.*, 2019).

1.4. Conclusion

Candida is a genus of yeasts that represents one of the human commensal microbial flora of the mucosal surface. In immunocompromised individuals, *Candida* may cause invasive diseases. Invasive candidiasis is the most common fungal disease among hospitalized patients. According to conservative estimates, invasive candidiasis affects more than 250,000 people worldwide per year. Among *Candida* species, *C. albicans* is still the most frequently detected species in invasive candidiasis. However, non-*albicans Candida* plays an increasingly significant role, with *C. glabrata* being the most important of these species. *C. glabrata* is the second most common cause of *Candida* infections. This species associates generally with a higher overall mortality, which may be due to its drug resistance.

The number of available antifungal drugs to treat *C. glabrata* invasive infections is limited. There are three major drug classes currently available to treat *C. glabrata* and other systemic fungal infections: polyenes (amphotericin B), azoles and echinocandins. Amphotericin B targets the essential component ergosterol in the fungal cell membrane and efficiently kills fungi. However, its high toxicity limits its use. Another antifungal class, the azoles, also targets the ergosterol in the fungal cell membrane by inhibiting its synthesis. However, *C. glabrata* has intrinsically low susceptibility to azoles and can acquire drug

resistance very easily. Echinocandins represent the newest class of antifungal agents. This antifungal family targets glucan synthesis in the fungal cell wall. Unfortunately, echinocandin resistance can also emerge rapidly after the initiation of therapy.

Even though many studies have already tried to find new antifungal families, the limited number of currently available antifungal drugs and the alarming rise in drug-resistant strains indicates that more novel therapeutic agents against *C. glabrata* are urgently needed. The goal of this project is to investigate a potentially new antifungal strategy which targets an essential chromatin protein.

2. Targeting an essential chromatin protein as a novel antifungal strategy

2.1. Chromatin structure and post-translational modification of histones

2.1.1. Chromatin structure and epigenetics

DNA is well organized to form chromatin in the nucleus. The basic structural unit of chromatin is the nucleosome. Two copies of each of the four histones, H2A, H2B, H3 and H4, form the histone core octamer, around which is wrapped about 146 DNA base pairs to form the ~10 nm nucleosome core particle. Stabilized by the linker histone H1, several nucleosome cores then package into regular solenoid or irregular fibre structures, which are further organized into loops and chromatin domains (**Figure 9**) (Luger *et al.*, 1997).

The DNA fragment connecting two nucleosomes, the linker DNA, is generally 20 to 50 bp long and, compared to the wrapped nucleosomal DNA, is less compact and more accessible to proteins. Depending on the compaction level of DNA, chromatin can be divided into two states: heterochromatin and euchromatin. Heterochromatin represents the regions where DNA is compact and generally transcriptionally inactive. Euchromatin, in contrast, has a more relaxed structure and is transcriptionally active. The chromatin architecture is in fact a highly

dynamic and regulated structure, providing different accessibility in different regions, which allows the regulation of several processes such as transcription, DNA repair and replication (Dawson, Kouzarides and Huntly, 2012). The term “epigenetics” was introduced to explain how stable and heritable phenotypic changes occur without any alteration in the DNA sequence (Berger *et al.*, 2009). This term has been extended and now also describes the control of gene expression.

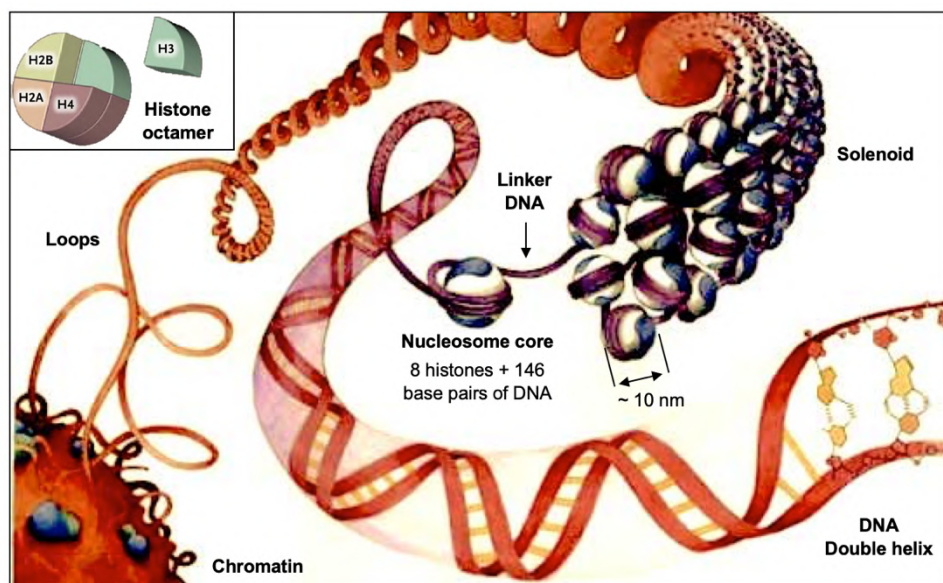


Figure 9. Levels of DNA packaging. The double helix of DNA forms nucleosomes with histones, which in turn are compacted into solenoid or fibre structures, loops and larger chromatin domains. (Adapted from Nicolas Bouvier ArtWork and Dawson, Kouzarides and Huntly, 2012)

In mammals, protein coding genes are transcribed by RNA polymerase II (RNA pol II) with the general transcription factors sharing the common name TFII. Transcription generally begins in the region named TATA box which is about 25 nucleotides upstream of the transcription start site. Transcription factor TFIID is the first one to anchor itself onto the TATA box with its subunit TATA-binding protein (TBP). After the recruitment and assembly of TFIIB, RNA pol II and other transcription factors are then assembled at the promoter to form the transcription pre-initiation complex. RNA pol II then begins to synthesize a short length of RNA but it soon pauses at the promoter. The phosphorylation of the C-terminal domain (CTD) of the RNA pol II changes the conformation of the polymerase, which allows the release of RNA pol II from the initiation complex and its progression along the DNA during the elongation

phase of transcription. All these processes need a relaxed structure of the chromatin allowing the accessibility, assembly and movement of the transcription complex.

Multiple factors influence the chromatin architecture, including the dynamic modifications of histones and DNA. These modifications can modify the interactions between histones or between histones and DNA, or can also recruit other epigenetic regulators (Dawson, Kouzarides and Huntly, 2012). There are four major factors implicated in chromatin plasticity (**Figure 10**): histone variants, DNA modification, chromatin remodeling and histone post-translational modifications.

Histone variants can be found in each histone family except H4 in mammalian cells. Unlike canonical histones, which present multiple copies in the genome, histone variants are usually encoded by single copy genes that are active throughout the cell cycle to play specific roles. There are very few sequence differences between canonical histones and variants. However, these few differences offer the possibility to either activate transcription by destabilizing the nucleosome or repress gene expression by chromatin compaction. For example, histone variant H2A.Z is generally associated with transcriptional activation while the variant macro-H2A associates with transcriptionally silent regions (Bönisch and Hake, 2012; El Kennani *et al.*, 2017, 2018).

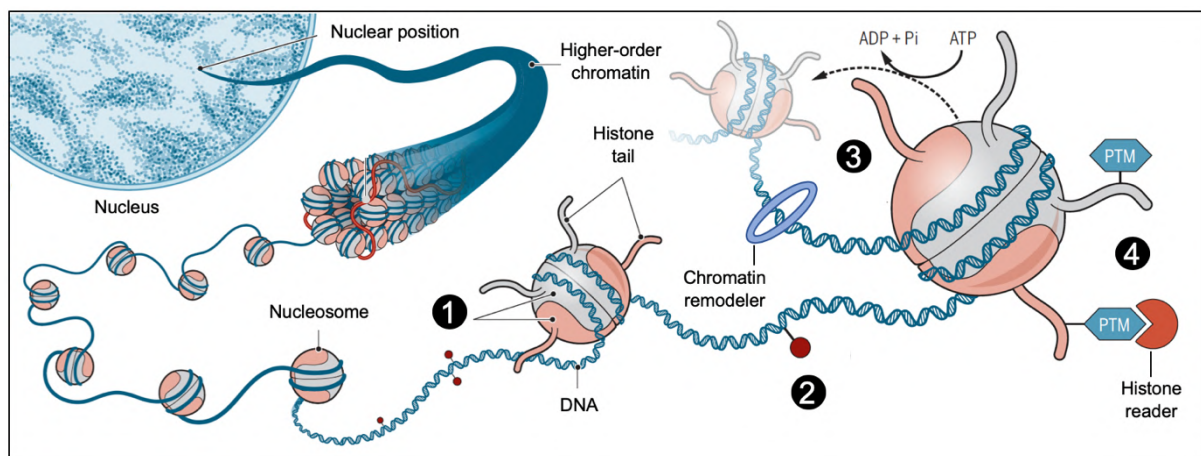


Figure 10. Chromatin plasticity by DNA or histones modifications. The dynamics of chromatin architecture play an important role in many processes like gene expression, DNA repair and replication. Four major mechanisms are implicated in chromatin structure modifications: 1, histone variants; 2, DNA modifications; 3, chromatin remodeling; and 4, histone post-translational modifications (PTMs). (Adapted from Yadav, Quivy and Almouzni, 2018)

DNA methylation is the most common DNA modification in terms of gene expression regulation. DNA methylation is mediated by DNA methyltransferases (DNMTs) and typically occurs on cytosine within CpG dinucleotides. Generally, hypermethylation associates with gene silencing and is found in heterochromatin regions, while hypomethylation is associated with transcriptional activation in euchromatin (Biermann and Steger, 2007; Rajender, Avery and Agarwal, 2011).

Chromatin remodeling involves ATP-dependent chromatin remodeling complexes that modify the location and/or structure of nucleosomes. The primary role of these complexes is to hydrolyze ATP to obtain energy to slide histones along the DNA. The twisting, spooling and bulging of DNA have been observed as their activities. Nucleosome remodeling can lead to both gene activation and silencing. SWI/SNF, ISWI, CHD and INO80 are the four ATPase remodeling complex families (Narlikar, Fan and Kingston, 2002; Fan *et al.*, 2003; Rajender, Avery and Agarwal, 2011; Clapier *et al.*, 2017).

2.1.2. Post-translational modifications of histones

The post-translational modification (PTM) of histones is an essential mechanism for the regulation of cell function. Amino acid residues, mostly in the N-terminal histone tails, provide the sites for these modifications, which include methylation, acetylation, phosphorylation, ubiquitylation, etc. To date, at least 16 different classes of histone PTMs have been identified and they can all play a role in transcriptional activation or repression (**Figure 11**). The total set of histone PTMs together with the information they provide is often referred to as the “histone code”. The enzymatic complexes that add these histone modifications are called “writers” while those that remove them are “erasers”. In addition, protein complexes which can recognize different PTMs and drive further cell processes are called “readers” (Rajender, Avery and Agarwal, 2011; Dawson, Kouzarides and Huntly, 2012).

2.1.2.a. Histone methylation

Histone methylation is one of the most important histone PTMs. The writers of histone methylation are histone methyltransferases (HMTs) and the erasers are histone demethylases.

Many sites on histone tails, generally lysine and arginine residues, can serve as methylation targets. Different methylation levels can also be found on a single amino acid. In mammals, dimethylations represent up to 40-80% of methylation cases on histone H3 lysine residue 9 (H3K9), H3K27, H3K36 and H4K20 (Kooistra and Helin, 2012). The functions of histone methylation include both transcriptional activation and repression depending largely on the site of methylation. Generally, H3K4, H3K36 and H3K79 methylation is associated with gene expression, while H3K9, H3K27 and H4K20 mark gene silencing (**Figure 11**) (Berger, 2002; Kooistra and Helin, 2012). The readers of histone lysine methylation are protein domains called chromodomains. The Polycomb and HP1 (heterochromatin protein 1) are two examples of chromodomain containing proteins that recognize trimethylated H3K27 (H3K27me3) and H3K9me3, respectively (Fischle *et al.*, 2003).

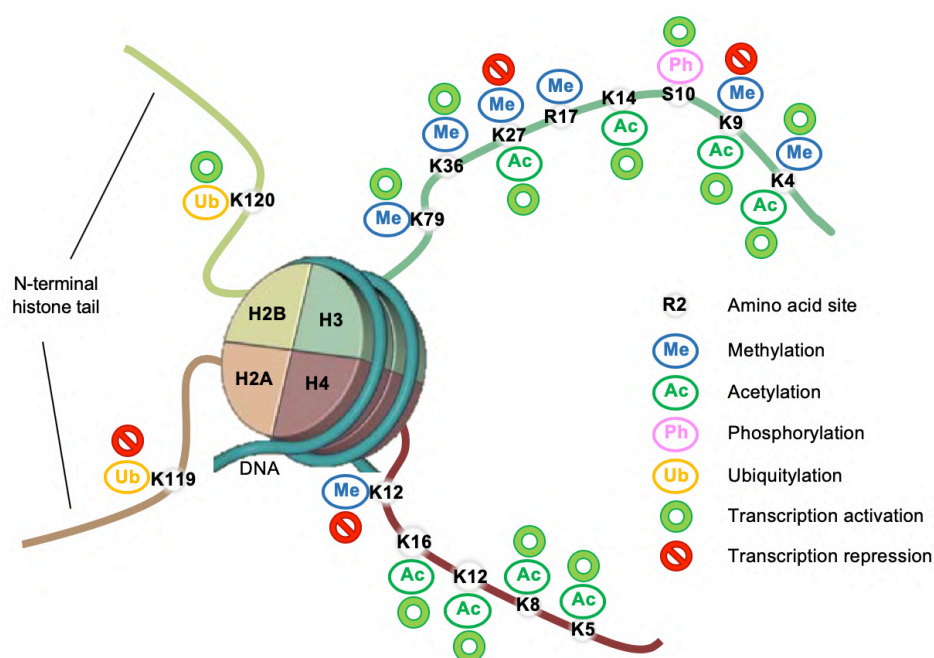


Figure 11. Some post-translational modifications (PTMs) of histones. PTMs of histones can occur in the N-terminal tails of all four core histones. These modifications occur in specific amino acid sites and the same residue can be the subject of different modifications to elicit different outcomes. (Adapted from Dawson *et al.*, 2012).

2.1.2.b. Histone phosphorylation and ubiquitylation

Histone phosphorylation and ubiquitylation are less common compared to methylation. Phosphorylation on Ser10 of histone H3 (H3S10ph) plays an important role in

activation of gene expression. However, phosphorylation of the histone variant H2AX leads to chromosome condensation and transcription repression (Berger, 2002; Fernandez-Capetillo *et al.*, 2003). Histone ubiquitylation, like methylation, can provoke both gene expression and silencing. Additional ubiquitylation of H2A is associated with gene repression while H2B ubiquitylation is linked to transcriptional activation (Baarends *et al.*, 2003; Zhu *et al.*, 2005).

2.1.2.c. Histone acetylation

Histone acetylation is another widespread histone modification besides methylation. It is also the first histone PTM to have been described. This modification generally occurs at lysine residues and neutralizes the positive charge of those residues. The interaction between histones and DNA is charge-dependent, and the neutralization of charges by acetylation makes the interaction weaker and results in chromatin structure relaxing. The accessibility of target DNA to transcription factors is then enhanced, which leads to transcriptional activation (Rajender, Avery and Agarwal, 2011; Zentner and Henikoff, 2013). Besides transcriptional activation, histone acetylation also plays a role in chromatin decompaction, DNA repair, protein stability and the regulation of protein interactions (Filippakopoulos and Knapp, 2014).

Histone acetyltransferases (HATs) are responsible for adding acetyl groups onto histones. HATs are generally considered as transcriptional coactivators. Many of them are subunits of large protein complexes and are recruited to the promoter by other transcription activators. In contrast, histone deacetylases (HDACs) remove acetyl groups from histones. HDAC functions are often linked to gene silencing and chromatin compaction (Utley *et al.*, 1998; Berger, 2002; Haberland, Montgomery and Olson, 2009).

Unlike histone methylation with a measured half-life in days, histone acetylation is a highly dynamic event with a half-life measured in minutes (Barth and Imhof, 2010). Both HATs and HDACs contribute to the rapid cycle of acetylation and deacetylation around transcription sites. The balance between the two activities controls the overall gene expression level for several development processes and disease states (Haberland, Montgomery and Olson, 2009; Zentner and Henikoff, 2013).

2.2.3. Bromodomain: reader of histone acetylation

Similar to chromodomains, which are the readers of histone lysine methylation, bromodomains are the specific protein modules that recognize acetylated lysines ([Figure 12A](#)). The name “bromo” was coined from the chromatin remodeling enzyme called “brahma” that activates transcription in *Drosophila melanogaster*, where it was first identified (Tamkun *et al.*, 1992). Bromodomains are widespread protein modules that can be found in numerous chromatin associated proteins (Zentner and Henikoff, 2013).

2.2.3.a. Structure and classification of bromodomains

Bromodomains are approximately 110 amino acids in length with highly conserved structures (Filippakopoulos *et al.*, 2012; Smith and Zhou, 2016). However, after their initial discovery in 1992, their structure and overall function remained unclear for several years. In 1999, the acetyllysine binding function was identified for the bromodomain of p300/CBP-associated factor (PCAF, also known as KAT2B), a human transcription coactivator, and its structure was solved by nuclear magnetic resonance (NMR) spectroscopy. It was the first time that the unique three-dimensional bromodomain structure was revealed (Dhalluin *et al.*, 1999). This structure revealed that the bromodomain fold comprises four α helices, α_A , α_B , α_C and α_Z . Two loops located at one end of the domain, the ZA loop connecting α_A and α_Z and the BC loop connecting α_B and α_C , form a hydrophobic binding pocket that recognizes the acetylated lysine of histones ([Figure 12B](#)) (Smith and Zhou, 2016).

After elucidation of the first bromodomain structure, studies of the binding mode of bromodomains to acetylated histones were pursued. In 2000, Owen *et al.* elucidated how the bromodomain in the yeast HAT protein GCN5 (also known as KAT2A) recognizes an H4K16Ac peptide (Owen *et al.*, 2000). In this crystal structure, a hydrogen bond is formed between the carbonyl oxygen of the lysine acetyl group and the amide nitrogen of a highly conserved asparagine residue (Asn407 in GCN5p and Asn803 in PCAF). (A few bromodomains have a threonine or tyrosine in place of this conserved asparagine; e.g., ASH1L, MLL). Besides the direct hydrogen bond, a hydrogen bond network is also formed by the acetyl group, specific bromodomain residues and five water molecules in the binding pocket ([Figure 12C](#)). The array of five water molecules is also conserved and has been observed in many ligand-bound

bromodomain structures (Owen *et al.*, 2000; Filippakopoulos *et al.*, 2012; Ferri, Petosa and McKenna, 2016).

Bromodomains occur in many proteins. The human genome encodes 61 bromodomains present in 46 different proteins. These proteins can contain one (e.g., PCAF), two (e.g., Brd4) or several bromodomains. Six bromodomains are found in Polybromo 1 (PB1), a chromatin remodeling factor (Filippakopoulos *et al.*, 2012). Bromodomains have been clustered into eight groups according to sequence similarity (**Figure 13**) (Smith and Zhou, 2016).

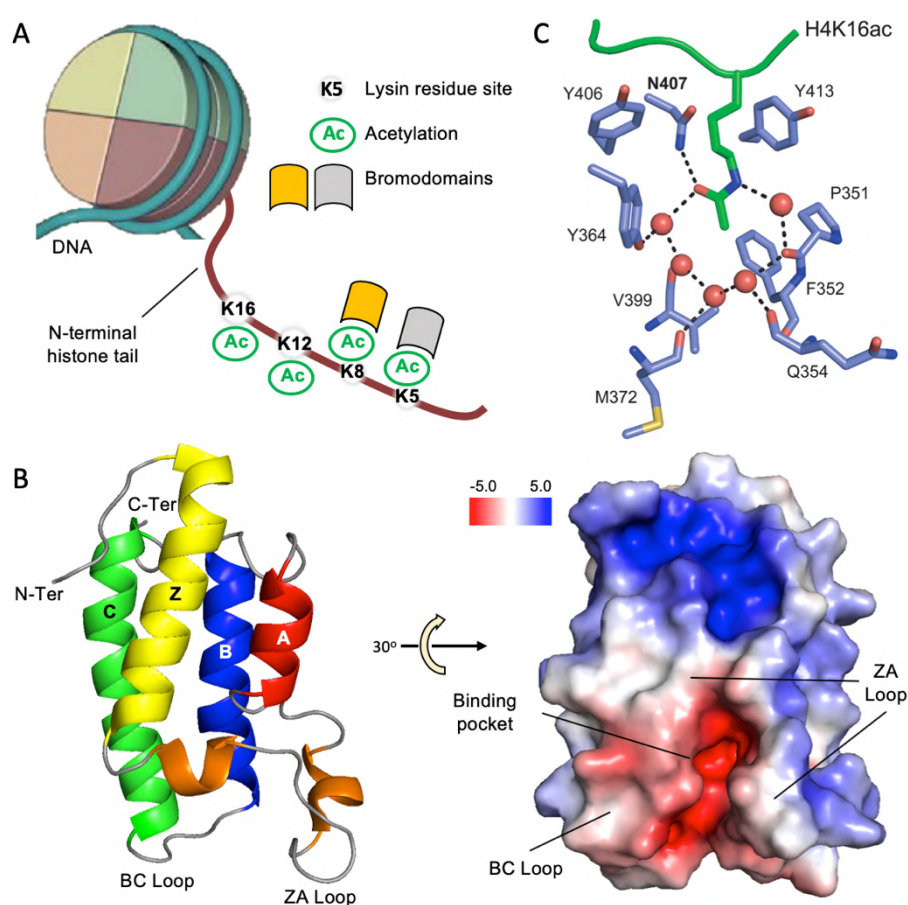


Figure 12. Bromodomains are the specific readers of histone acetylation. **A.** Different bromodomains bind to acetylated lysine residues of histones. **B.** NMR structure of the PCAF bromodomain (PDB: 1N72). The four helices α_A , α_B , α_C and α_Z are shown in red, blue, green and yellow, respectively (left). Electrostatic surface shows the binding pocket formed by the ZA and BC loops (right). **C.** Stick representation showing the hydrogen bond network in the cocrystal structure of GCN5 bromodomain (light blue) bound to the acetylated peptide H4K16ac (green) (PDB: 1E6I). The water molecules in the binding pocket are marked as red spheres. Key residues are labeled and hydrogen bonds are shown as black dashed lines (Smith and Zhou, 2016).

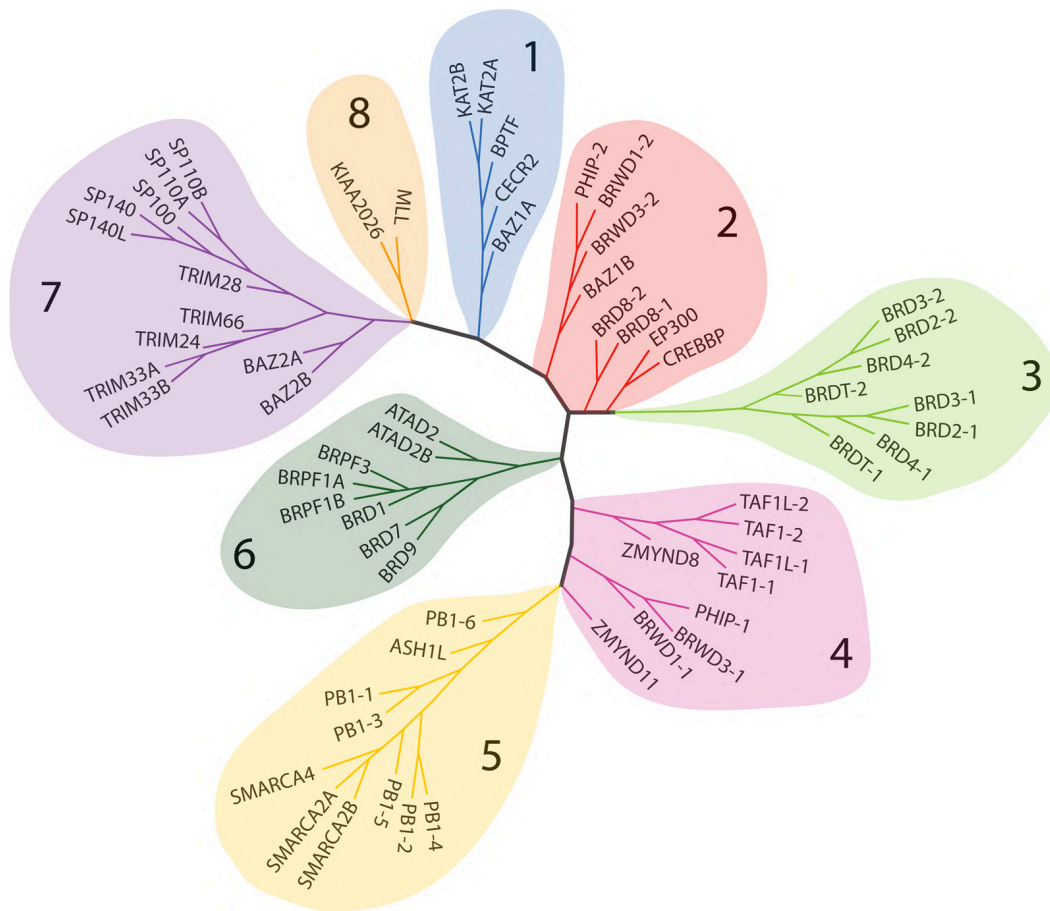


Figure 13. Phylogenetic tree of human bromodomains. Branches are grouped depending on primary sequence identity. (Figure from Smith and Zhou, 2016)

2.2.3.b. Functions of bromodomain proteins

The basic function of bromodomains is to bind to acetyllysine residues within a peptide context. Based on this simple function, however, different multidomain bromodomain-containing proteins can exert different functions in cells. These proteins generally use their bromodomains to anchor themselves to the chromatin and then directly or indirectly recruit other protein complexes to drive or regulate diverse cellular processes (Filippakopoulos *et al.*, 2012; Smith and Zhou, 2016).

Bromodomain proteins are generally large multidomain proteins and play roles in chromatin remodeling, transcription regulation or histone modification. TAF1 (also known as TAF_{II}250) and its testes-specific homologue TAF1L from group 4 are subunits of the transcription factor TFIID and directly drive transcriptional initiation (Wassarman and Sauer,

2001; Wang and Page, 2002). Proteins such as PCAF and GCN5 from the first group are HATs and act as transcriptional coactivators (Filippakopoulos *et al.*, 2012). Some chromatin remodeling regulators, like SMARC2 (also known as BRM), a subunit of the SWI/SNF remodeling complex, anchor themselves via acetylated histones on chromatin to trigger chromatin remodeling processes (Harikrishnan *et al.*, 2005). Other proteins like BAZ2A (also known as TIP5) and ZMYND11 (also known as BS69) are subunits of complexes that repress transcription (Masselink and Bernards, 2000; Zhou *et al.*, 2009). There are also some bromodomain proteins, such as Brd9 and BAZ2B, whose function remains poorly understood. At the same time, the function of bromodomains in some proteins like the methyltransferases ASH1L and MLL is also under investigation (Filippakopoulos *et al.*, 2012; Smith and Zhou, 2016).

2.2. Bromodomain and Extra-Terminal proteins

2.2.1. Overview of BET proteins

Bromodomain and extra-terminal (BET) proteins contain bromodomains belonging to the third group (**Figure 13**) (Smith and Zhou, 2016). The first protein of this family was described as FSH in *Drosophila* in 1985 (Digan *et al.*, 1986). There are four BET proteins in human cells: Brd2, Brd3, Brd4 and BrdT. BET proteins share a common domain organization, consisting of two N-terminal bromodomains (BD1 and BD2) and a C-terminal extra-terminal (ET) domain (**Figure 14A**). The two bromodomains anchor the protein to acetylated sites, while the ET domain mostly plays a role in recruiting other cell function regulation factors. Some proteins like Brd4 and BrdT also have a specific C-terminal domain (CTD) that contributes to the interaction with other proteins (Shi and Vakoc, 2014).

The binding mode of BET bromodomains to the acetylated peptide is a distinct from that of canonical bromodomains. Unlike the GCN5 bromodomain that binds to a single acetyllysine residue, BET bromodomains are able to bind two acetyllysine residues at the same time. In 2009, Morinière *et al.* discovered that at least two adjacent acetylated lysines on histone H4 tails were needed for a strong interaction with murine BrdT and reported the crystal structure BrdT BD1 bound to a diacetylated histone H4 peptide (Morinière *et al.*, 2009). After that, Gamsjaeger *et al.* found by NMR studies that the specific binding mode of BrdT was

also shared by Brd3 (Gamsjaeger *et al.*, 2011). Later, it was confirmed that human BET bromodomains also recognize multi-acetylated histone tails. For example, the two acetylated lysines of histone H4 peptide bind simultaneously to Brd4 BD1 and different diacetylated peptides share a similar conformation (Filippakopoulos *et al.*, 2012). This conformation is shown in **Figure 14B**. Of the two acetyllysine, one goes deep into the binding pocket and hydrogen bonds with the conserved arginine Asn140 and with the hydrogen bond network generated by other key residues (e.g. Tyr97) and water molecules, while the other interacts with water molecules and hydrophobic residues closer to the entrance of the binding pocket.

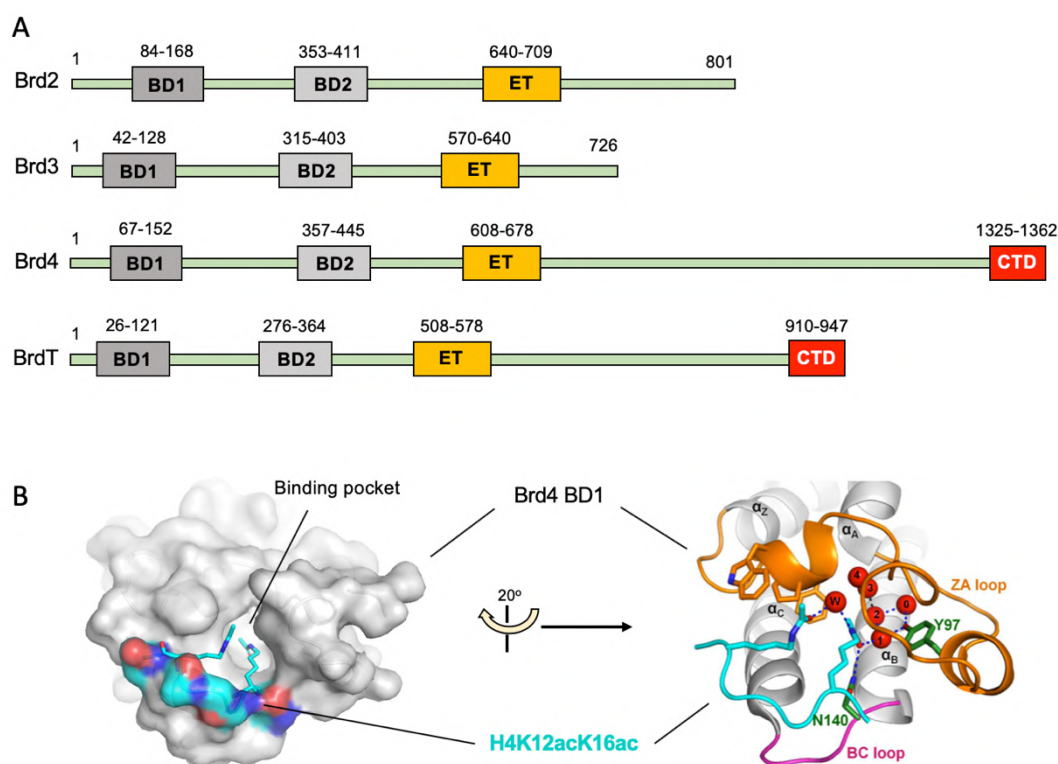


Figure 14. Domain architecture of BET proteins and diacetyllysine binding mode of the BET bromodomain. **A.** Common architecture of human BET proteins. BD1 and BD2 are the two bromodomains, ET and CTD represent extra-terminal and C-terminal domains, respectively. **B.** Crystal structure of Brd4 BD1 bound to the diacetylated histone peptide (H4K12acK16ac) shown as a surface representation (left) and with details of ligand recognition (right) (PDB: 3UVX). The acetylated peptide is in cyan, the four helices in gray, the ZA loop in orange and the BC loop in magenta. Five water molecules are marked as red spheres. Two key residues, N140 and Y97, are labeled in green and their hydrogen bond interactions with the peptide are shown as blue dashed lines. (Figure adapted from Ferri *et al.*, 2016; Lambert *et al.*, 2019)

2.2.2. Functions of BET proteins

2.2.2.a. Functions of Brd4

BET proteins all play roles in transcriptional regulation or chromatin remodeling. Among these proteins, the best studied is Brd4, whose common functions are summarized in [Figure 15](#).

A major role of Brd4 is in the initiation of the transcription elongation phase. As mentioned before, transcription driven by RNA pol II include two phases: initiation and elongation. The initiation phase is driven by the binding of TFIID to the TATA box and the assembly of the transcription pre-initiation complex, including RNA pol II. During this phase, TFIIH phosphorylates serine 5 (S5) of the RNA pol II CTD and triggers a short burst of transcription. However, the polymerase is then held in this complex and transcription is paused by two negative factors, DSIF and NELF. To enter the elongation phase, the polymerase needs to be released from the pre-initiation complex. The complex P-TEFb (Positive Transcription Elongation Factor b), composed of kinase Cdk9 and Cyclin T, then phosphorylates serine 2 of the RNA pol II CTD as well as the two negative factors, allowing the polymerase to be released and the elongation phase to start (Sims, Belotserkovskaya and Reinberg, 2004; Zhou, Li and Price, 2012).

P-TEFb is a nuclear localized kinase complex that plays a key role in the activation of transcriptional elongation. However, most of this complex in the cell is in an inactive state, inhibited by a factor HEXIM and a 7SK small nuclear RNA (snRNA) in cells (Blazek *et al.*, 2005). During transcription, Brd4 specifically recognizes and binds to acetylated histones and recruits P-TEFb to the promoter. Next, Brd4 activates P-TEFb allowing the latter to stimulate the transcription elongation phase ([Figure 15](#)) (Moon *et al.*, 2005; Yang *et al.*, 2005). Brd4 interacts with P-TEFb via its two domains, BD2 and CTD. BD2 binds to the triacetylated Cyclin T subunit of P-TEFb and may play a regulatory role. The CTD is the primary Brd4 domain that interacts with P-TEFb, leading to the dissociation of HEXIM and 7SK snRNA from the latter to activate its kinase activity (Schröder *et al.*, 2012). Besides the common function of Brd4 mentioned above, the ability of Brd4 to directly phosphorylate Ser2 of RNA pol II was observed (Devaiah *et al.*, 2012; Pradhan *et al.*, 2016). Recently, it was shown that Brd4 also phosphorylates CDK9 of P-TEFb to regulate its kinase activity (Donati, Lorenzini and Ciarrocchi, 2018).

The ET domain of Brd4 also plays an important role in transcription, although its function was determined much later compared to the bromodomains and the CTD. The ET domain provides a platform for protein recruitment and interacts with a series of factors involving in transcription, including NSD3. NSD3 (also known as WHSC1L1) is an HMT that catalyzes H3K36 methylation, a transcriptional activation mark (**Figure 11**). Brd4 recruits NSD3 to the target gene, where NSD3 mediates histone methylation to activate gene expression (Li *et al.*, 2009; Rahman *et al.*, 2011; Lambert *et al.*, 2019). The Brd4 ET domain also recruits JMJD6 to demethylate arginine 2 and 3 of histone H3, leading to transcription activation (Rahman *et al.*, 2011; Kwok *et al.*, 2017). Moreover, a Brd4 fragment containing the ET domain was shown to associate with a subunit of SWI/SNF, SMARCA4, indicating that Brd4 may also play a role in chromatin remodeling through its ET domain (Rada-Iglesias *et al.*, 2011; Rahman *et al.*, 2011).

In 2013, Floyd *et al.* discovered a shorter spliced isoform of Brd4, in which there was no CTD, but a unique domain at its C-terminus. Instead of playing a role in transcription regulation, this Brd4 isoform functions in DNA damage response. After binding acetylated histones, this isoform recruits a remodeling complex to compact chromatin, leading to the inhibition of DNA damage repair (Floyd *et al.*, 2013). It was more recently shown that Brd4 also possesses HAT activity that acetylates H3 and H4. The acetylation of H3K122 by Brd4 was shown to be critical for chromatin decompaction, leading to a favorable environment for transcription (Devaiah *et al.*, 2016). Other functions of Brd4 include participation in DNA replication (Brd2 has the same function) (Sansam *et al.*, 2018), heat shock induced splicing (Hussong *et al.*, 2017) and alternative splicing (Uppal *et al.*, 2019).

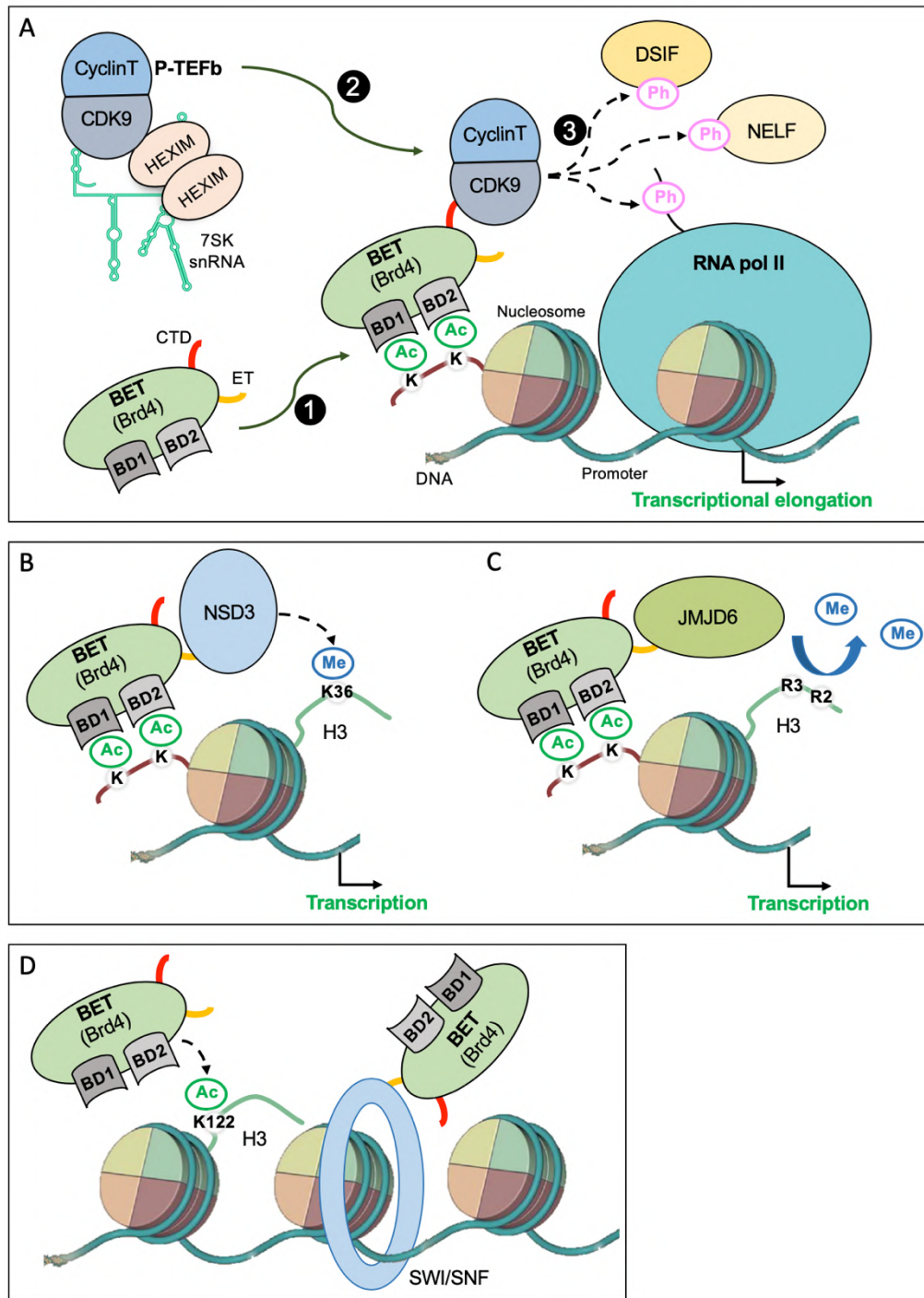


Figure 15. Functions of Brd4 in transcription. **A.** Brd4 in transcriptional elongation. 1, Brd4 binds to acetylated lysines of histones via its two bromodomains (BD1 and BD2); 2, Brd4 recruits P-TEFb to the promoter by its CTD and then activates the later by excluding the negative factors HEXIM and 7SK snRNA; 3, active P-TEFb phosphorylates the CTD of RNA pol II and the negative regulators DSIF and NELF, leading to the end of the pause of RNA pol II to continue transcription (Ferri, Petosa and McKenna, 2016). **B** and **C.** ET domain interactions with NSD3 (**B**) and JMJD6 (**C**). NSD3 methylates H3K36, while JMJD6 demethylates H3R2 and H3R3. Both effects can lead to gene expression (Rahman *et al.*, 2011). **D.** The Brd4 ET domain associates with a subunit of the SWI/SNF complex and may contribute to chromatin remodeling. Brd4 also has the ability to acetylate H3K122 to decompact chromatin structure and favor transcription (Rahman *et al.*, 2011; Devaiah *et al.*, 2016).

2.2.2.b. Functions of Brd2 and Brd3

Brd2 and Brd3 have overlapping functions which are not as well investigated as those of Brd4 (Bechter and Schöffski, 2020). Both BETs associate with hyperacetylated chromatin along the transcribed genes. Their presence facilitates transcription driven by RNA pol II through hyperacetylated nucleosomes and this effect is bromodomain dependent. In addition, Brd2 has acetylated histone dependent and ATP independent histone chaperone activity (LeRoy, Rickards and Flint, 2008). Upon acetylated histone binding, Brd2 can recruit TBP and transcription factors like E2F and can associate with the SWI/SNF remodeler to form a complex during transcription (Sinha, Faller and Denis, 2005; Denis *et al.*, 2006; Peng *et al.*, 2007). Similarly, Brd3 associates with a range of chromatin remodeling complexes via its ET domain (Wai *et al.*, 2018). Given that Brd2 and Brd3 do not have a CTD (**Figure 14A**) and that the ET domain is highly conserved among human BETs (> 80% identity) (Rahman *et al.*, 2011), these two proteins may play a positive transcriptional regulation role via the recruitment mediated by their ET domains like Brd4 does. In 2017, another function of Brd2 was discovered; namely, that this protein also plays a role in transcription boundary maintenance by limiting the spread of enhancer activity (Hsu *et al.*, 2017). Recently, it was shown that Brd3 impacts rRNA production and plays a role in ribosome biogenesis (Lambert *et al.*, 2019). It was also suggested that Brd4 may be the most important BET to maintain steady state gene expression, but that efficient gene expression induction requires the cooperation of all BET proteins including Brd2 and Brd3 (Gilan *et al.*, 2020). Like Brd4 which has different isoforms, in 2016 the short isoform of Brd3 (Brd3R) was also identified with its role as a reprogramming factor (Shao *et al.*, 2016).

2.2.2.c. Functions of BrdT

BrdT is the testis specific BET whose gene is silenced in somatic cells and is active only during meiosis in the testis (Bourova-Flin *et al.*, 2017). The domain arrangement of BrdT is very similar to that of Brd4 (**Figure 14A**), indicating that these proteins likely have similar functionality. Indeed, the BrdT CTD binds to P-TEFb and could share the same mechanism with Brd4. It was also suggested that BrdT was in fact a functional testis specific paralogue of Brd4 (Gaucher *et al.*, 2012). The main role of BrdT is to stimulate the expression of genes specific

for spermatogenesis-related chromatin compaction, as well as to regulate chromatin organization and histone modifications during meiosis. Loss of BrdT function directly results in complete male sterility (Gaucher *et al.*, 2012; Manterola *et al.*, 2018). It should be mentioned that there are some differences in the bromodomain binding behaviour of Brd4 and BrdT. In Brd4, BD1 plays major role in chromatin association while BD2 enhances this binding and both bromodomains are responsible for gene expression regulation (Nguyen *et al.*, 2014; Runcie *et al.*, 2018). In contrast, BD2 of BrdT does not participate in the interaction with acetylated nucleosomes (Miller *et al.*, 2016).

2.2.3. BET proteins as a therapeutic target in human disease

Just like BrdT plays an essential role in spermatogenesis, other BETs also have their major physiological functions based on their basic role as transcriptional regulators: Brd2 functions in cell growth and neuronal cell generation while Brd3 and Brd4 are important for cell proliferation (Taniguchi, 2016; Lambert *et al.*, 2019). These physiological roles of BETs make them ideal targets in several disease settings, and some examples will be given here.

2.2.3.a. BET proteins in cancer

Given that BET proteins play important roles in cell growth and proliferation, it is not surprising that their deregulation occurs in many human cancers. The first and best studied case of abnormal BETs in cancer concerns their genetic fusion with another protein, nuclear protein in testis (NUT). NUT is encoded by a gene on chromosome 15. Tumors presenting the rearrangement of *NUT* genes are called NRCs (*NUT*-rearranged carcinomas), which toward younger patients are rare but highly malignant (French *et al.*, 2004; Bechter and Schöffski, 2020). In 2003, French *et al.* found the first bromodomain-containing oncogene in solid tumors, *BRD4-NUT*, and five years later, the fusion between Brd3 and NUT was discovered. Both fusion proteins contain the two bromodomains and the ET domain of the BET. It was also shown that this type of carcinoma is linked to a high lethality (French *et al.*, 2003, 2008).

Besides forming fusion proteins, BETs can also associate with crucial transcription factors, like MYC, in tumor development. MYC is a transcription factor that normally regulates

the expression of 10-15% of genes in the human genome and its upregulation is found in many cancers (Ott, 2014). It was shown that Brd4 is enriched at the *MYC* gene locus and regulates *MYC* transcription in multiple myeloma cells. The specific inhibition of BETs downregulates the *MYC* transcription program and leads to cell cycle arrest and cellular senescence (Delmore *et al.*, 2011). Later, *MYC* downregulation caused by BET inhibition was observed in many tumor settings as well, including Burkitt's lymphoma, acute myeloid and mixed lineage leukaemia, prostate cancer and lung cancer (Wang and Filippakopoulos, 2015).

Brd3 and Brd4 were also shown to play a role in estrogen receptor alpha (ER α) positive breast tumors by recruiting the transcription factor WHSC1 (also known as NSD2) to facilitate ER α expression. Inhibition of BETs can also arrest breast tumor cell growth in culture (Feng *et al.*, 2014). Besides Brd3 and Brd4, Brd2 was also found to form a complex with RUNX3 and to participate in lung adenocarcinoma development (Lee *et al.*, 2013). Finally, the overexpression of Brd2, Brd4 and BrdT was observed in a series of tumors, but their precise roles in tumorigenesis are still under investigation (Bechter and Schöffski, 2020).

2.2.3.b. BET proteins in inflammation and autoimmune disease

The deregulation of pro-inflammatory cytokines is a key mechanism involved in inflammation and autoimmune diseases. The nuclear factor- κ B (NF- κ B) is the main immune regulator and participates in the pathogenesis of many autoimmune diseases (Pasparakis, 2009). NF- κ B regulates the expression of a series of inflammatory genes and this function is especially regulated by acetylation at lysine 310 (K310) of its subunit RelA. In this case, instead of being recruited by acetylated histones, Brd4 is recruited by the acetylated K310 of NF- κ B to NF- κ B target gene promoters. Brd4 then activates those NF- κ B target genes through the P-TEFb pathway mentioned above (Huang *et al.*, 2009).

Brd2 was also shown to participate in the regulation of inflammatory gene expression in the development of rheumatoid arthritis. It also plays a role in pro-inflammatory cytokine regulation in macrophages (Mahdi *et al.*, 2009; Filippakopoulos and Knapp, 2014). Moreover, the inhibition of BET bromodomains disrupts chromatin complexes essential for inflammatory gene expression in macrophages, preventing the endotoxic shock induced by lipopolysaccharide and the sepsis induced by bacteria in mice (Nicodeme *et al.*, 2010).

Recently, BET bromodomain inhibition was shown to abolish T-helper 17 (Th17) driven neutrophilic inflammation in cockroach allergen extract induced asthma. The combination of dexamethasone and BET inhibitor led to the complete blockage of both Th2 and Th17 driven immune responses in the lung by reducing eosinophils, neutrophils and mucin secretion (Nadeem *et al.*, 2018).

2.2.3.c. BET proteins in other diseases

BETs play critical role in pathogenic cardiac remodeling during heart failure. Brd4 was reported to participate in the activation of the expression of some transcription factors, like NFAT (nuclear factor of active T cells) and GATA4, which control the expression of pathological genes in heart failure. The inhibition of BET bromodomains was also shown to suppress pathogenic cardiac gene expression and to stop pathogenic hypertrophy and heart failure in mice (Anand *et al.*, 2013).

Besides the endogenous diseases above, BET proteins also participate in viral infections. Brd2 was shown to repress the transcription of HIV (human immunodeficiency viruses) (Boehm *et al.*, 2013). Similarly, Brd4 has the ability to block the assembly of the elongation complex mediated by the viral transcriptional protein Tat on HIV promoter. The inhibition of BET, especially Brd2 and Brd4, results in the activation of HIV transcription and increases proviral transcription elongation (Zhu *et al.*, 2012; Boehm *et al.*, 2013; Li *et al.*, 2013). Unlike HIV infection, Brd4 seems to play an active role in HPV (human papillomavirus) infections. During the early stages of infection, Brd4 associates with viral proteins E2 and E3 to facilitate the tethering of the viral genome to the host genome, leading to the formation of foci containing additional factors. The antiviral effect against HPV by BET inhibition has also already been shown (Sakakibara *et al.*, 2013; Morse *et al.*, 2018). Brd2, Brd3 and Brd4 also interact with the integrase of MLV (murine leukemia virus) and bromodomain inhibition of these proteins leads to inhibition of MLV replication at the integration step of this retrovirus (De Rijck *et al.*, 2013).

2.2.4. Specific BET bromodomains inhibitors

Given the importance of the bromodomain in the physiological functions of BET proteins and the implication of BET proteins in several human disease settings, the development of BET bromodomain specific inhibitors has the potential to be of great chemotherapeutic value. For this reason, in recent years there has been enormous interest from academic labs and biopharmaceutical companies to develop such inhibitors. The first small molecule bromodomain inhibitor was reported in 2005, concerning a compound that targets the PCAF bromodomain (Zeng *et al.*, 2005). Five years later, the discovery of the first selective BET bromodomain inhibitors JQ1 and I-BET762 opened the door to the BET bromodomain inhibition field (Filippakopoulos *et al.*, 2010; Nicodeme *et al.*, 2010; Ferri, Petosa and McKenna, 2016). Since then, more and more specific BET bromodomain specific inhibitors ([Figure 16](#)) have been identified. Their applications are found in diverse human diseases and several have already entered clinical trials ([Table 4](#)).

2.2.4.a. Non-selective BET bromodomain specific inhibitors

JQ1 is a thienodiazepine compound which contains two stereoisomers: (+)-JQ1 and (-)-JQ1. (-)-JQ1 has no bromodomain binding activity, and so for the purpose of this thesis the term “JQ1” refers only to (+)-JQ1. JQ1 forms hydrogen bonds with the conserved asparagine in the binding site of BET bromodomains and mimics the binding mode of acetylated lysine, resulting in a direct binding competition with the latter. This molecule has a high selectivity towards BET bromodomains, with a K_d about 50 nM for Brd4 BD1 and less than 200 nM for the other BET bromodomains. Its effect on non-BET bromodomains is not evident (Filippakopoulos *et al.*, 2010). Potential applications of JQ1 in human disease has been reported in many studies, including Brd4-NUT positive carcinomas, inflammation and even neurodegenerative disease (Filippakopoulos *et al.*, 2010; Belkina, Nikolajczyk and Denis, 2013; Kedaigle *et al.*, 2020).

Derived compounds from JQ1, including CPI-203 and OTX-015, were also developed. CPI-203 was reported to enhance antitumor activity in mantle cell lymphoma and pancreatic neuroendocrine tumors (Moros *et al.*, 2014; Wong *et al.*, 2014). OTX-015 is shown to inhibit the proliferation of multiple human cancer cell lines and is currently in clinical trials ([Table 4](#))

(Zaware and Zhou, 2019). I-BET762 (also named GSK525762) is a benzodiazepine molecule with a structure very similar to JQ1 (**Figure 16**). First reported in 2014, I-BET762 has a similar binding mode compared to JQ1 as well, and was initially studied as a compound participating in immune moderation (Nicodeme *et al.*, 2010).

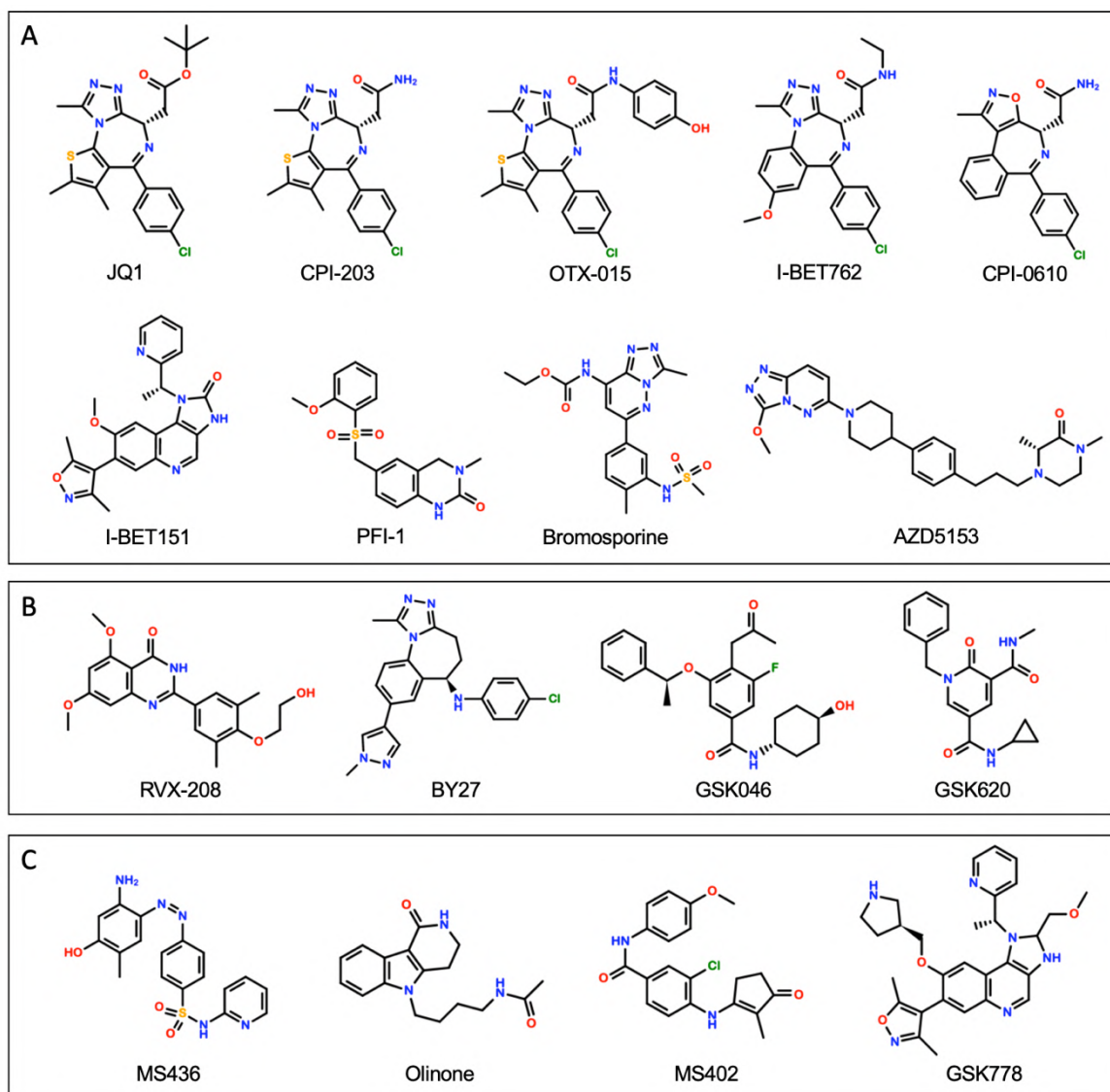


Figure 16. Some specific BET bromodomain inhibitors. **A.** Inhibitors with activity against both BET bromodomains BD1 and BD2. **B** and **C.** BET inhibitors with high selectivity against BD1 (C) or BD2 (B).

Besides the “JQ1 like” molecules, other specific BET inhibitors have been reported. I-BET151 (also named GSK1210151A) developed by GlaxoSmithKline (GSK) in 2011 was the first reported “non-JQ1 like” BET inhibitor and was introduced for the treatment of MLL-fusion leukaemia (Dawson *et al.*, 2011). In 2013 another inhibitor named PFI-1 was reported,

followed three years later by Bromosporine. Both inhibitors were introduced in the context of leukemia. PFI-1 and Bromosporine form direct hydrogen bonds with the conserved asparagine as JQ1 and I-BET151 do. However, Bromosporine is less selective since it can also inhibit non-BET bromodomains (Picaud, Da Costa, *et al.*, 2013; Picaud *et al.*, 2016). Also in 2016, Bradbury *et al.* published compound AZD5153. The unique feature of this compound is that a single AZD5153 molecule can simultaneously interact with two BET bromodomains, in such a way that both sides of the molecule contact the conserved asparagines in both interacting bromodomains (Bradbury *et al.*, 2016).

Table 4. Some of the specific BET bromodomain inhibitors in clinical trial. (Updated and adapted from Ferri *et al.*, 2016)

Inhibitor	Phase	Condition	Status	Clinical trial
RVX-208	I, II	Atherosclerosis, Dyslipidemia, CAD	Completed	NCT00768274
	II	Atherosclerosis, CAD	Completed	NCT01058018
	II	CAD	Completed	NCT01067820
	II	Dyslipidemia, CAD	Completed	NCT01423188
	II	Diabetes	Completed	NCT01728467
	II	Dyslipidemia, CAD	Terminated	NCT01863225
	III	T2DM, CAD	Active	NCT02586155
I-BET762	I	NMC & other solid tumors	Completed	NCT01587703
	II	Hematological Malignancies	Active	NCT01943851
OTX-015	I	AML, DLCL	Completed	NCT01713582
	I	NMC, CRPC & other solid tumors	Completed	NCT02259114
CPI-0610	I	Lymphoma	Completed	NCT01949883
	I	Multiple myeloma	Completed	NCT02157636
	I/II	AML, MDS, MDS/MPN	Recruiting	NCT02158858
TEN-010	I	NMC & other solid tumors	Completed	NCT01987362
	I	AML, MDS	Completed	NCT02308761
BAY 1238097	I	Advanced malignancies	Terminated	NCT02369029
ABBV-075	I	Breast cancer, multiple myeloma, NSCLC, AML	Completed	NCT02391480
INCB 054329	I/II	Advanced malignancies	Terminated	NCT02431260
BMS-986158	I	Pediatric solid cancer, lymphoma, brain tumor	Recruiting	NCT03936365
	I/II	TNBC, ovarian cancer, small-cell lung cancer	Recruiting	NCT02419417
FT-1101	I	AML, MDS	Completed	NCT02543879
RO6870810	I	Multiple myeloma	Completed	NCT03068351

Abbreviations: AML, Adult Myeloid Leukemia; BET, Bromodomain and Extra-Terminal; CAD, coronary artery disease; CRPC, castrate-resistant prostate cancer; DLCL, Diffuse Large B-Cell Lymphoma; GSK, GlaxoSmithKline; MDS, Myelodysplastic syndrome; MDS/MPN, Myelodysplastic/Myeloproliferative Neoplasms; MF, myelofibrosis; MLL, Mixed-Lineage Leukemia; NSCLC, non-small cell lung cancer; NMC, Nut-Midline Carcinoma; TNBC, triple negative breast cancer; T2DM, Type 2 Diabetes Mellitus.

2.2.4.b. Selective BET bromodomain specific inhibitors

Most of the early BET inhibitors had similar activity for both BD1 and BD2 of the same protein. Molecules of this type are named pan-BET inhibitors. However, the two bromodomains have non-identical functions. It was reported that BD1 was sufficient to maintain pre-existing transcription and steady-state gene expression while BD2 is involved in the recruitment of BET proteins to help induce rapid gene expression. Both BD1 and BD2 are needed for the rapid increase in gene expression during inflammation (Gilan *et al.*, 2020). The different functions of the two bromodomains in each BET protein indicate the importance to develop selective BET bromodomain inhibitors.

Selective BET bromodomain inhibition began with that of BET BD2, with the introduction of RVX-208 in 2013, currently in clinical trials (Table 4). RVX-208 showed 20-fold higher affinity for Brd3 BD2 ($\sim 0.194 \mu\text{M}$) compared to BD1 ($\sim 4.06 \mu\text{M}$) and in AlphaScreen inhibition assays, it reached up to 170-fold selectivity for BD2 compared to BD1. The co-crystal structure demonstrated that RVX-208 had few interactions with Brd4 BD1 apart from the direct hydrogen bond with the conserved arginine (N140) and a water-mediated hydrogen bond with the conserved tyrosine (Y97). In contrast, this molecule mimics very well the manner that acetylated lysines bind to Brd4 BD2. In fact, it occupies the entire channel in Brd4 BD2 which is adapted to acetylpeptide binding (Picaud, Wells, *et al.*, 2013). BY27 is another selective BET BD2 inhibitor with a K_d at least 10-fold higher for BD1 compared to BD2. This compound showed tumor growth inhibition with low toxicity at high dose compared to the pan-BET inhibitor I-BET762 (Chen *et al.*, 2019). Recently, Gilan *et al.* reported two selective BET BD2 inhibitors, GSK046 and GSK620, and indicated that BD2 selective inhibitors are primarily involved in inflammation regulation in inflammatory and autoimmune disease (Gilan *et al.*, 2020).

The development of a selective BET BD1 inhibitor began almost at the same time as that of selective BD2 inhibitors. MS436 is the first reported BD1 inhibitor which selectively targets Brd4 BD1 versus Brd4 BD2. However, the selectivity is not very high between the two bromodomains of Brd4 and there is no selectivity between BD1 and BD2 of Brd3 (Zhang *et al.*,

2013). In 2014, Gacias *et al.* published the compound Olinone that targeted only BET BD1 but not BD2 because of a steric clash. They also showed that Olinone triggered the differentiation of mouse primary oligodendrocyte progenitors while a pan-BET inhibitor did not show the same effect (Gacias *et al.*, 2014). Later, another BD1 inhibitor, MS402, was shown to inhibit primarily Th17 cell differentiation with little or almost no effect on other T-helper cells and regulatory T cells. In contrast, pan-BET inhibitors inhibited the differentiation of broad T-helper cell lineages (Cheung *et al.*, 2017). However, Gilan *et al.* recently showed that BD1 inhibition just phenocopied the anti-tumor effect caused by pan-BET inhibitors using GSK778 synthesized by their own (Gilan *et al.*, 2020).

2.2.4.c. Other forms of BET bromodomain inhibitors

Besides monovalent BET inhibitors, bivalent inhibitors that comprise a single molecule capable of simultaneously inhibit two bromodomains have also been developed. The common structure of this type of compound is that of two monovalent inhibitors connected by a linker of variable composition and length, which can determine the functional activity of the inhibitor (**Figure 17A**) (Ren *et al.*, 2018). MT1 is a molecule that contains two JQ1 moieties joined by a long PEG7 linker. This compound showed over 100-fold higher activity against hematopoietic cancer cell growth and significantly delayed the progression of leukemia in mice compared to the original JQ1 (Tanaka *et al.*, 2016). Another bivalent inhibitor is MS645, which connects two JQ1 molecules with an alkyl linker. This compound did not show a high gain in binding affinity for BET proteins compared to monovalent JQ1. However, MS645 can downregulate the expression of proinflammation cytokines that are not affected by either JQ1 or MT1. Moreover, whereas JQ1 affects only Brd4, MS645 blocks Brd4 together with mediator protein MED1 and transcriptional regulator YY1, resulting in the inhibited transcription of genes involved in cell-cycle control and DNA damage repair that are required for the rapid growth of the cancer cell (Ren *et al.*, 2018).

All the compounds mentioned above inhibit BET bromodomains by direct competitive binding to the acetyllysine binding site. This type of inhibition requires a relatively high level of inhibitor to be maintained in cells. In order to circumvent this requirement, target protein degradation strategies have been established. One of these strategies is the use of a

proteolysis-targeted chimera (PROTAC) (**Figure 17B**). Each PROTAC molecule contains three parts: a target protein binding part (in this case, a BET inhibitor targeting the BET protein), a ligand of ubiquitin-protein ligase (E3) and a linker. PROTACs bind at the same time to the target protein and E3, resulting in the ubiquitination of the target protein by E3 followed by target protein degradation by the ubiquitin-proteasome system. The most used E3 ligands are VHL and CRBN recruiting moieties (**Figure 17B**), which target two different E3 complexes: CRL2^{VHL} E3 and CRL4^{CRBN} E3, respectively (Cromm and Crews, 2017). The first PROTAC for a BET protein, MZ1, was published in 2015. This molecule links JQ1 and a VHL ligand and can rapidly induce reversible, long-lasting and selective removal of Brd4 over Brd2 and Brd3. Compared to JQ1, MZ1 leads to the distinct and limited transcriptional responses of cancer-related genes, resulted from selective Brd4 suppression (Zengerle, Chan and Ciulli, 2015). Another example of a BET PROTAC is ARV-825, concerning the combination of OTX-015 and a CRBN recruiting moiety. Like MZ1, ARV-825 selectively degrades Brd4 and more effectively induces cell proliferation inhibition and apoptosis in Burkitt's lymphoma cells (Lu *et al.*, 2015).

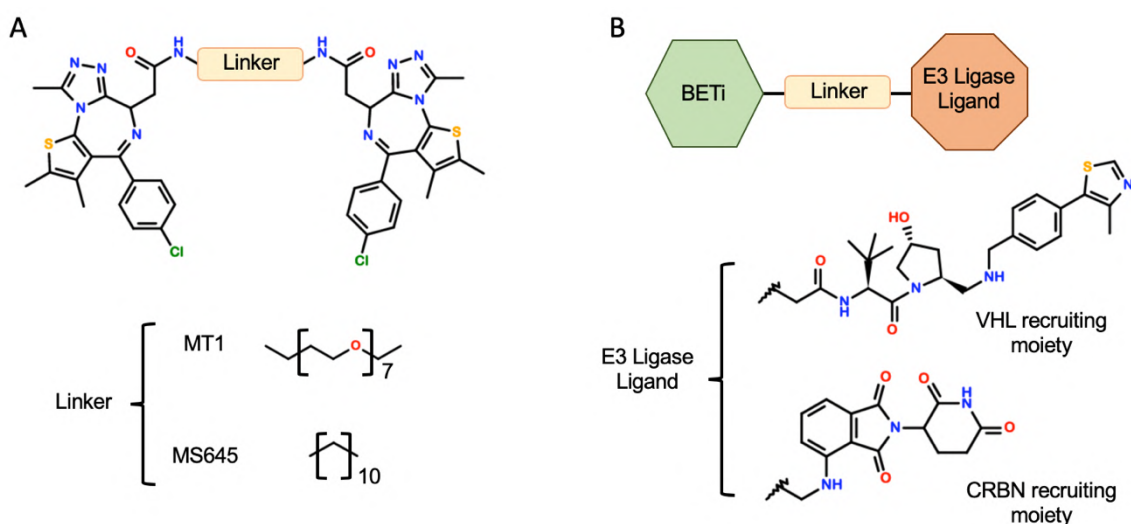


Figure 17. Representative bivalent BET inhibitors (A) and proteolysis-targeted chimeras (PROTACs) (B). BETi: BET bromodomain inhibitor. VHL and CRBN are the recognition subunits of two different E3 complexes (Cromm and Crews, 2017).

2.3. Bdf1: Druggable fungal BET protein

2.3.1. Overview and functions of Bdf1

Bromodomain factor 1 (Bdf1) is the BET protein in fungi. Unlike mammalian cells that contain four BET family members, Bdf1 is the only BET protein in many yeast species (Wapinski *et al.*, 2007). Identified in 1994, Bdf1 was described as a transcription factor encoded by a single copy gene in chromosome 12 in *S. cerevisiae* (Lygerou *et al.*, 1994). Because of the existence in *S. cerevisiae* of the very close homolog Bdf2 that is partly functionally redundant with Bdf1, the deletion of *BDF1* is not lethal in this yeast species. However, Bdf1 is still considered functionally more important than Bdf2 since disrupting *BDF2* leads to less severe phenotypes compared to disrupting *BDF1* (Lygerou *et al.*, 1994; Matangkasombut *et al.*, 2000). Moreover, Bdf1 can reduce the expression of *BDF2* but Bdf2 cannot affect the transcription of *BDF1* (Fu *et al.*, 2013). Since the functional studies of Bdf1 were mainly performed in *S. cerevisiae*, the functions of this protein described below concern only the case in *S. cerevisiae* and are summarized in [Figure 18](#).

2.3.1.a. TFIID associated function of Bdf1.

Although Bdf1 is a member of the BET family, the first function reported for Bdf1 is not shared by any human BET proteins and is associated with TFIID in transcription initiation. As mentioned before, activation of the transcription of protein coding genes in eukaryotic cells is triggered by promoter recognition by TFIID, which consists of TATA-binding protein (TBP) and TBP-associated factors (TAFs). In mammals, the largest subunit of TFIID is TAF1 that can directly activate gene expression. Mammalian TAF1 contains its own two bromodomains and has HAT and kinase activity (Wassarman and Sauer, 2001; Wang and Page, 2002). In yeast, the TAF1 homologue only has HAT activity and lacks bromodomains. In 2000, Matangkasombut *et al.* demonstrated the kinase activity of Bdf1. They also reported that Bdf1 associated with TFIID via the subunit TAF7 to participate in forming the transcription pre-initiation complex in

S. cerevisiae. These results suggested that Bdf1 corresponded to the C-terminal half of mammalian TAF1 and was in fact the missing bromodomain and kinase part of TFIID in yeast (Matangkasombut *et al.*, 2000) (**Figure 18A**).

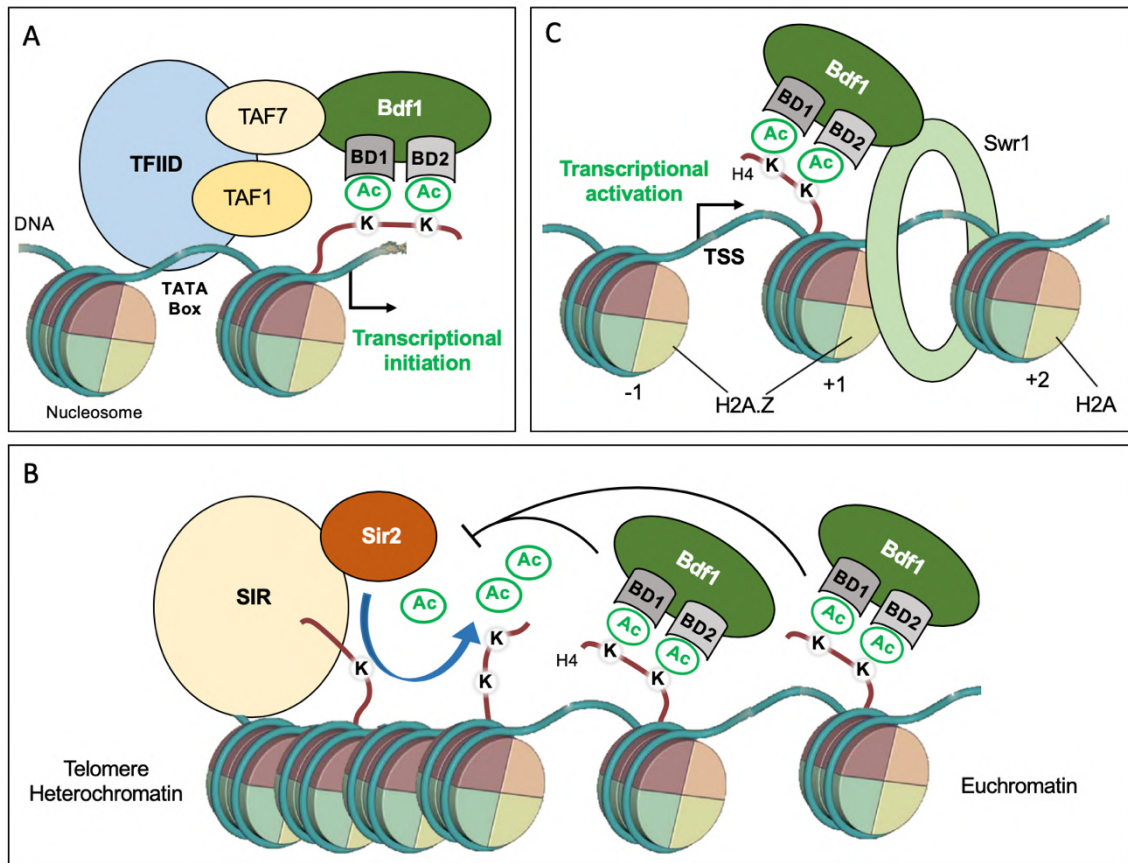


Figure 18. Transcriptional functions of Bdf1 in *S. cerevisiae*. **A.** Bdf1 associates with the TFIID subunit TAF7. TAF1 has histone acetyl transferase activity and Bdf1 has kinase activity. Both contribute to the transcription initiation driven by TFIID (Matangkasombut *et al.*, 2000). **B.** Bdf1 binds to acetylated histone H4 and protects them from the histone deacetylase activity of Sir2, leading to the limitation of spreading of telomere heterochromatin driven by SIR complex (Ladurner *et al.*, 2003). **C.** Bdf1 binds to acetylated histones and accumulates primarily in the first (+1) nucleosome after the transcription start site (TSS), where it recruits the remodeler Swr1 to exchange H2A to H2A.Z, leading to transcription activation (Mizuguchi *et al.*, 2004; Koerber *et al.*, 2009).

2.3.1.b. TFIID independent functions of Bdf1.

Bdf1 also participates in epigenetic regulation just like human BET proteins do. In 2003, Bdf1 was reported to associate with chromatin by acetylated histone binding via its two bromodomains (Matangkasombut and Buratowski, 2003). The same year, Bdf1 was suggested to play a role in maintaining hetero-euchromatin boundaries, especially at telomeres and

mating loci (Ladurner *et al.*, 2003). In yeast, the SIR (silent information regulator) complex silences genes and forms heterochromatin at telomeres and mating loci (Aparicio, Billington and Gottschling, 1991). The SIR subunit Sir2, an NAD-dependent HDAC, recognizes acetylated histones, then localizes SIR to telomeres and deacetylates histones H3 and H4 (Imai *et al.*, 2000; Armstrong *et al.*, 2002). Bdf1, in contrast, protects acetylated H4 from the deacetylation effect by competing with Sir2 to bind to the acetylated H4. This protection effect leads to the limitation of SIR silencing process spreading from the telomeres. Correspondingly, mutations in Bdf1 were shown to result in the downregulation of genes close to telomeres (Ladurner *et al.*, 2003).

Bdf1 also associates with an ATPase of the Swi2/Snf2-family named Swr1, which is a subunit of the remodeling complex SWR-C and is responsible for histone-variant exchange. It was suggested that Bdf1 bound to acetylated chromatin, generally the first (+1) or second (+2) nucleosome after the transcription starting site (TSS), then recruited and formed a complex with Swr1. Swr1 in turn triggered the replacement of H2A by the variant H2A.Z at the -1 and +1 nucleosomes of TSS, resulting in transcription activation and limiting heterochromatin spreading (Krogan *et al.*, 2003; Mizuguchi *et al.*, 2004; Koerber *et al.*, 2009). It was also reported that Bdf1 but not Bdf2 participated in pre-mRNA splicing by regulating the levels of the enzymes responsible for splicing. However, this function does not appear to be mediated by its bromodomains (Albulescu *et al.*, 2012; García-Oliver *et al.*, 2017). More recently, about 35% of Bdf1 in the cell was found to form a complex with Bdf2 whose functions though are still unknown (García-Oliver *et al.*, 2017).

2.3.1.c. Physiological functions of Bdf1.

Bdf1 participates in chromatin remodeling, transcriptional initiation and pre-mRNA splicing, indicating that this protein has an important role in yeast physiology. Indeed, the deletion of only *BDF1* but not *BDF2* leads to a slow growth phenotype as well as temperature sensitivity and DNA damage in *S. cerevisiae* (Matangkasombut *et al.*, 2000).

The first reported physiological function of Bdf1 is its essential role in sporulation, which is similar to the role of BrdT during spermatogenesis concerning chromatin compaction. Dated to 1995, only one year after its identification, Chua and Roeder first demonstrated that

without Bdf1, *S. cerevisiae* failed to maintain meiotic division and had a total defect in spore formation (Chua and Roeder, 1995). Five years later, it was reported that Bdf1 was induced during meiosis, was recruited by hyperacetylated H4 during late sporulation and functioned in post-meiotic chromatin compaction. It was also shown that Bdf1 was enriched in mature spores compared to growing yeast cells (Govin *et al.*, 2010). More recently, Bdf1 was found to be recruited via its bromodomains before meiosis and to enrich on the promoter of NDT80, a gene encoding a key meiotic regulator (Winter, 2012; García-Oliver *et al.*, 2017).

Another revealed physiological function of Bdf1 is its participation in the salt stress response, which was discovered quite late compared to that in sporulation. In 2007, a group in China first reported a salt-sensitive phenotype caused by *BDF1* deletion (Liu *et al.*, 2007). Two years later the same group indicated that the absence of Bdf1 resulted in mitochondrial dysfunction and caused apoptosis under salt stress (Liu *et al.*, 2009). Later, the rescue capacity of Bdf2 was shown in a *BDF1* deletion strain with mitochondrial dysfunction (Fu *et al.*, 2013). Finally, the same laboratory suggested that Bdf1 also regulated the endocytosis system under salt stress (Fu *et al.*, 2015).

2.3.2. Bdf1 bromodomains as an antifungal target in *Candida albicans*

It was shown that the deletion of both *BDF1* and *BDF2* in *S. cerevisiae* was lethal (Ladurner *et al.*, 2003) and that Bdf2 was absent in many pathogenic yeast, including *C. albicans* and *C. glabrata* (Wapinski *et al.*, 2007). These observations, along with the fact that Bdf1 bromodomains bind to hyperacetylated H3 and H4, regulating the expression of more than 500 genes (Ladurner *et al.*, 2003) and that bromodomains are needed for the viability of yeast when Bdf2 is absent (Matangkasombut and Buratowski, 2003), suggested that targeting the Bdf1 bromodomains could be a potential antifungal strategy.

There are significant differences between human BET and yeast Bdf1 bromodomains in primary sequence (**Figure 19B**). Recently, our laboratories determined the high-resolution crystal structures of BD1 and BD2 from *C. albicans* Bdf1 (CaBdf1), showing that the ligand binding pockets of these domains also differ significantly from those of human BET bromodomains (data not shown). By generating strains of *C. albicans* in which the expression

of *BDF1* is controlled by the antibiotic doxycycline (**Figure 19C**), our teams showed that the deletion of *Bdf1*, or the deletion of both *BD1* and *BD2*, resulted in a growth defect in *C. albicans*. Similarly, *C. albicans* strains bearing point mutations that inactivate both bromodomains showed a growth defect as well (**Figure 19D**). An efficient inhibition assay was developed and high-throughput chemical screening led to the identification of several compounds that selectively inhibit *CaBdf1* bromodomains. These compounds are currently undergoing medicinal chemistry optimization (data not shown). Taken together, it was confirmed in our laboratories that *Bdf1* bromodomain inhibition holds promise as a potential antifungal strategy in *C. albicans* (Mietton *et al.*, 2017).

2.4. Conclusion

In the eukaryotic cell nucleus, the basic repeated unit of chromatin is the nucleosome. In each nucleosome, a fragment of DNA is wrapped around a protein octamer, formed by two copies of each core histone (H2A, H2B, H3 and H4). That structure is stabilized by the linker histone H1. In many processes, like gene transcription and DNA repair, the chromatin is modified to adopt a more open structure and many mechanisms are involved in the modification of nucleosome and chromatin structures.

The post-translational modification (PTM) of histones plays a central role in the regulation of gene expression and the determination of chromatin structure. Among the different PTMs, histone acetylation is one of the most important. Recognized by epigenetic reader domains named bromodomains, histone acetylation is generally associated with open chromatin and enhanced transcriptional activity. Many protein families contain bromodomains, including the Bromodomain and Extra-Terminal (BET) protein family. The proteins of this family share a common architecture: they contain two highly conserved N-terminal bromodomains (*BD1* and *BD2*), and an extra-terminal (*ET*) domain. BET proteins are implicated in diverse diseases, such as cancer, inflammatory disease and infectious disease. Many BET bromodomain inhibitors have been identified. The use of these inhibitors has already validated BET bromodomain inhibition as a potential therapeutic strategy in many human diseases.

Bdf1 is the fungal BET protein. In *S. cerevisiae*, Bdf1 interacts with the transcription factor TFIID to initiate transcription and is involved in remodeling chromatin structure. Bdf1 regulates the expression of over 500 genes and is essential in *S. cerevisiae*. Recently, our teams validated small-molecule inhibition of Bdf1 bromodomains as a potential antifungal strategy against the pathogenic fungus *C. albicans*.

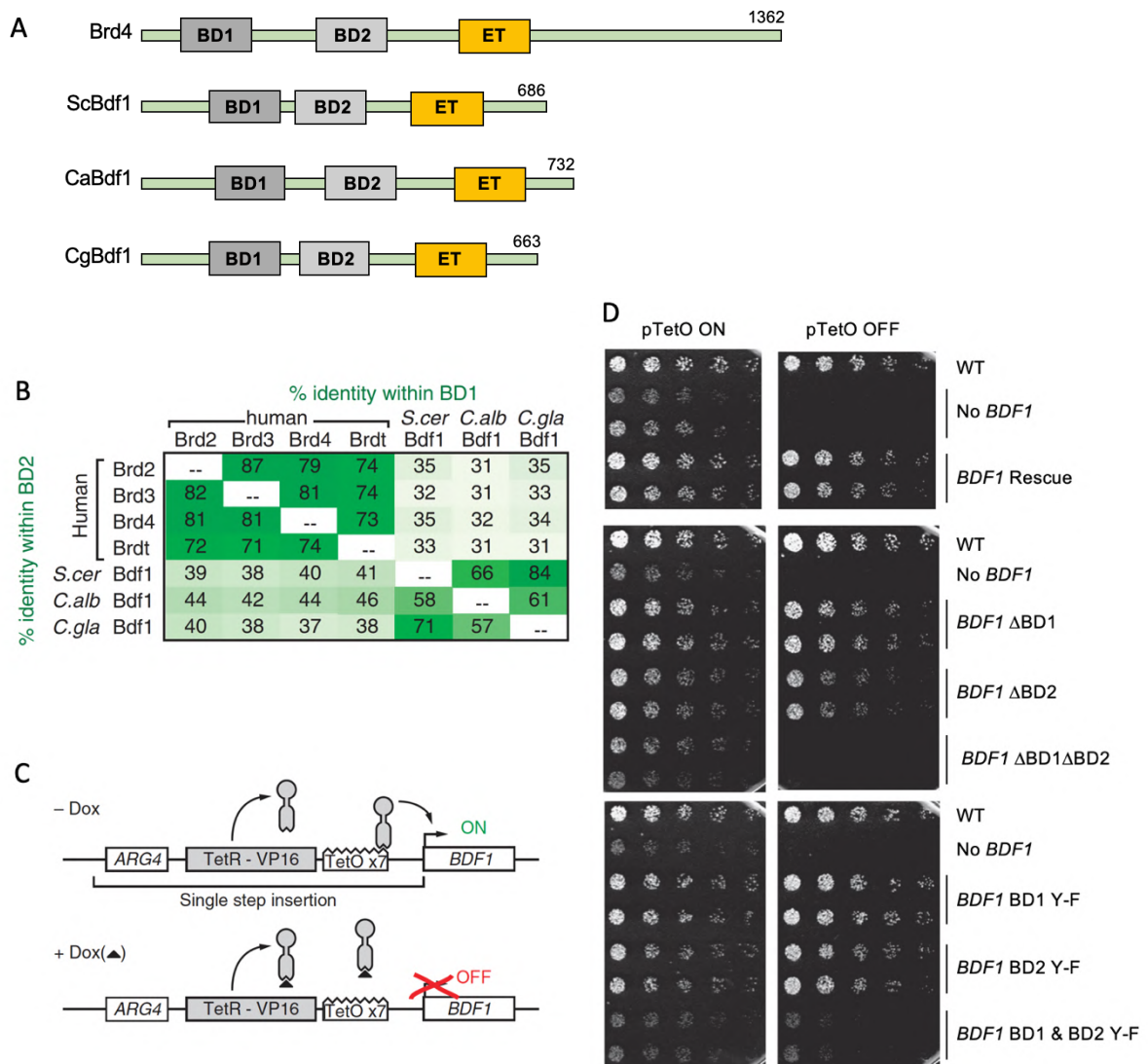


Figure 19. Bdf1 bromodomains may be an antifungal therapeutic target for *C. albicans* infections. **A.** Domain organization of fungal Bdf1 and human Brd4 proteins. **B.** Sequence identity among human and fungal BET BD1 or BD2 bromodomains (upper and lower diagonal entries, respectively). *S. cer*: *S. cerevisiae*; *C. alb*: *C. albicans*; *C. gla*: *C. glabrata*. **C.** Tet-OFF construct to control the expression of *BDF1*. Doxycycline (Dox) inhibits the binding of TetR-VP16 to TetO, preventing *BDF1* transcription. **D.** Bdf1 repression and Bdf1 bromodomain disruption lead to a growth defect in *C. albicans*. “Δ” represents the deletion of bromodomain BD1 or BD2; Y-F represents the mutation Y248F for BD1 and Y425F for BD2. (Adapted from Mietton *et al.*, 2017)

3. Ph.D. project: Investigation of Bdf1 bromodomain inhibition as a potential antifungal therapeutic strategy against *Candida glabrata*.

Given that *C. glabrata* is the second most common cause of *Candida* infections in many countries around the world, that there has been an especially alarming rise in drug-resistant strains and that there are few available antifungal agents, novel therapeutic agents against *C. glabrata* infections are urgently needed.

3.1. Objective

In this Ph.D. project, I set out to adapt the strategies previously developed for *C. albicans* to develop small-molecule inhibitors that target *C. glabrata* Bdf1 bromodomains. The overall goal of this project is to provide a new strategy against *C. glabrata* infections by targeting its Bdf1 bromodomains. Specific objectives are to:

- (i) verify that Bdf1 bromodomain function is essential in *C. glabrata*;
- (ii) investigate the ligand-binding activity and structure of *C. glabrata* Bdf1 bromodomains;
- (iii) identify compounds that selectively inhibit *C. glabrata* Bdf1 bromodomains.

The successful completion of this project is expected to validate *C. glabrata* Bdf1 bromodomains as an antifungal target and to yield inhibitors for potential development into a new class of drugs against *C. glabrata* infection.

3.2. Work plan

3.2.1. Verification of the role of Bdf1 bromodomain function in *C. glabrata*.

This project involved two collaborating laboratories, headed by Carlo Petosa at the IBS and Jérôme Govin at the IAB. The yeast genetics and fungal assays would be carried out in the

Govin lab, while the biochemical and structural work would mainly be performed in the Petosa lab. To verify the essential role of Bdf1 in *C. glabrata* (CgBdf1), the *BDF1* gene coding for this protein should be either knocked out or conditionally knocked down. The Govin lab previously tried to knock out *BDF1* in *C. albicans* without success because there were no colonies formed. That suggested already the essential role of *BDF1* in *C. albicans* growth. The lab then developed a strategy that allowed selective control of *BDF1* expression by putting this gene under the control of an inducible promoter. They tested two promoters, the *MET3* promoter (inhibited by methionine and cysteine) and the Tet-Off promoter (inhibited by doxycycline). The use of both promoters led to the same conclusion that Bdf1 bromodomain function was essential for the growth of *C. albicans*.

The *C. glabrata* genome is haploid, which facilitates genetic manipulation. First, Bdf1 conditional knockdown strains of *C. glabrata* would need to be generated by replacing the endogenous *BDF1* promoter by a *MET3* promoter. These strains would allow me to measure the effect on yeast growth of different Bdf1 expression levels by changing the concentration of methionine and cysteine in the medium. *C. glabrata* strains having point mutations predicted to abolish the ligand binding activity of either BD1, BD2 or both domains would also be generated in order to verify the essential role of these domains for CgBdf1 function and fungal viability. The phenotype of the above mutant strains would then be characterized. Evidence that a decrease in Bdf1 expression level results in growth defects would support the working hypothesis that CgBdf1 is a potential antifungal target.

3.2.2. Structural studies of *C. glabrata* Bdf1 bromodomains.

Besides their essential role for *C. glabrata* growth, it was also important to check whether the bromodomains in *C. glabrata* Bdf1 were sufficiently different from those in human BET proteins to allow small molecules to selectively inhibit the former. Purified BD1 and BD2 from CgBdf1 would need to be screened for crystallization. Crystals would be analyzed at the macromolecular crystallography beamlines of the ESRF synchrotron and structures determined by molecular replacement.

3.2.3. Identification and characterization of CgBdf1 inhibitors.

I would adapt the HTRF assay previously developed in our lab to screen for compounds that disrupt acetylpeptide binding by *C. glabrata* Bdf1 BD1 and BD2. Once the assay was optimized, collaborators at Calibr would use it to perform high-throughput screening of chemical libraries.

Hits identified would then be tested in the HTRF assay to construct dose-response curves and determine half-maximal inhibitory concentration (IC_{50}) values. The best hits would be tested against human BET bromodomains to determine whether compounds are selective for the fungal protein. ITC would be used to confirm results and to obtain precise K_d values. The most promising inhibitors would be used to determine co-crystal structures in order to establish the precise binding mode. Compounds would be tested on *C. glabrata* cultures to determine whether they inhibit growth.

Chapter II – Results

1. Bdf1 and its bromodomains are essential in *Candida glabrata*

1.1. Bdf1 protein is essential in *C. glabrata*

1.1.1. Construction of *BDF1* conditional knockdown and rescue strains

As mentioned before, Bdf1 is essential in *S. cerevisiae* and *C. albicans*, and so it is likely essential as well in *C. glabrata*. This indicates that a direct *BDF1* knockout strain can probably not be generated. The strategy chosen was to use a strictly controlled *MET3* promoter (pMET) to generate a *BDF1* conditional knockdown strain (pMET-*BDF1* strain). The principle is shown in [Figure 20A](#). Briefly, the expression of a pMet-controlled gene is induced by the activator Met4. The presence of methionine or cysteine activate ubiquitin ligase Met30, which adds a chain of ubiquitin to Met4 and leads to the degradation of the latter via the proteasome. The absence of Met4 silences the expression of the pMet-controlled gene (Mao *et al.*, 2002). The pMET-*BDF1* strain had already been generated by two Ph.D. students in the lab, Morgane Champleboux and Cécile Garnaud, before my arrival in the lab. In this strain, the endogenous *BDF1* promoter was replaced by the *MET3* promoter, and an upstream *HIS3* gene was used as the selection marker ([Figure 20B](#)).

I attempted to verify the expression level of Bdf1 in the pMET-*BDF1* strain. In the laboratory, a specific antibody against *C. glabrata* Bdf1 (CgBdf1) was not available to perform a Western blot. Instead, we already had antibodies against *S. cerevisiae* Bdf1 (ScBdf1) and *C. albicans* Bdf1 (CaBdf1). I first tested whether these two antibodies could recognize CgBdf1. The anti-CaBdf1 antibody only recognized CaBdf1 and not CgBdf1 ([Figure 20C](#)). As for the anti-ScBdf1 antibody, it could recognize both ScBdf1 and CgBdf1 but did not recognize CaBdf1. However, the specificity of the anti-ScBdf1 antibody was much lower, as it strongly recognized proteins having a molecular weight slightly lower than Bdf1 ([Figure 20D](#)).

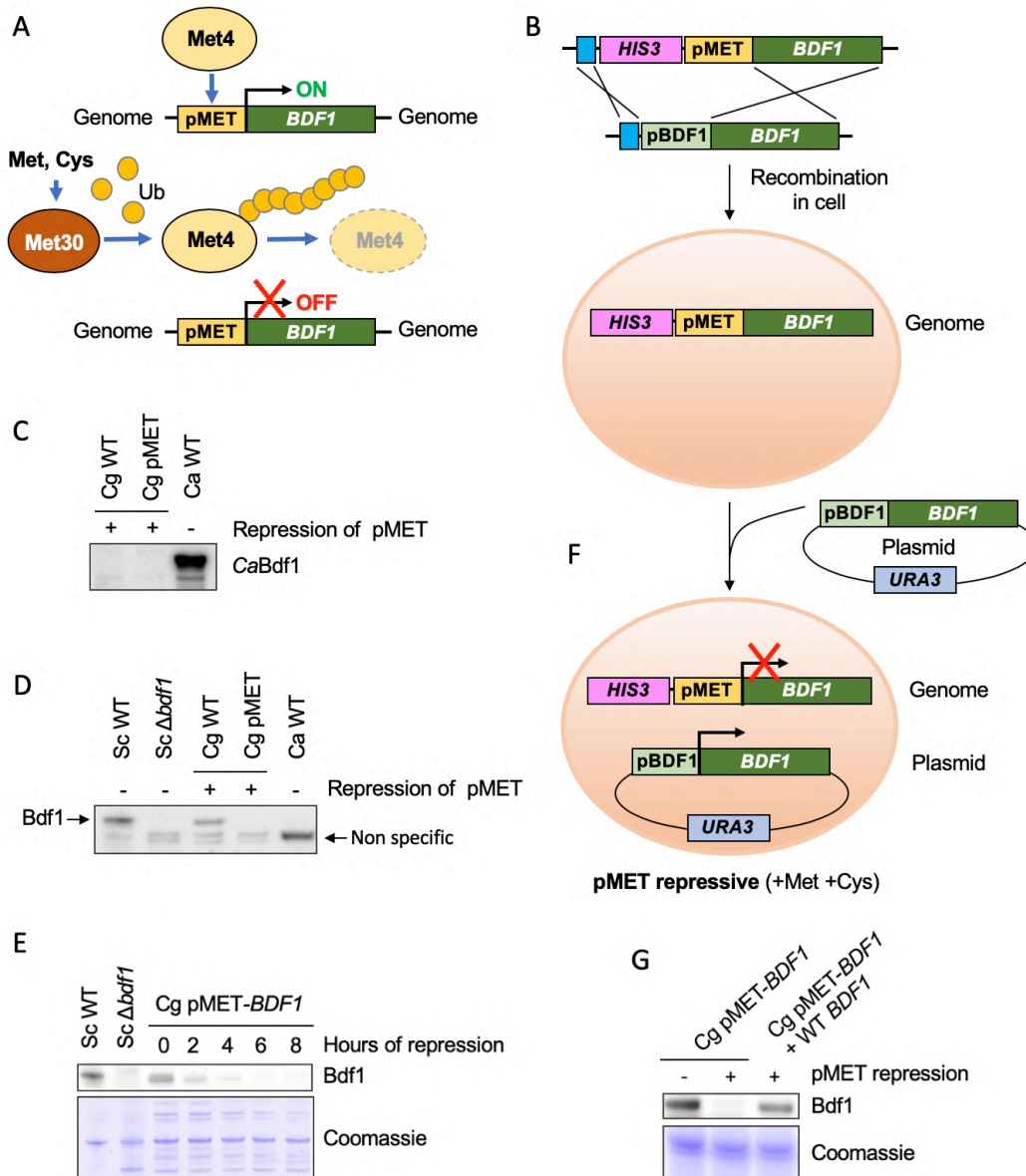


Figure 20. Construction of *BDF1* conditional knockdown and rescue strains. **A.** Conditional gene knockdown strategy using a *MET3* promoter (pMet) (Mao *et al.*, 2002). Met: methionine; Cys: cysteine; Ub: ubiquitin. **B.** Construction of *BDF1* conditional knockdown strain. *HIS3*: selection marker *HIS3* gene; pMET: *MET3* promoter; pBDF1: endogenous *BDF1* promoter; *BDF1*: *BDF1* gene ORF. **C** and **D.** Western blots verifying the specificity of anti-CaBdf1 (C) and anti-ScBdf1 (D) antibodies. Cg WT: whole cell extract (WCE) from *C. glabrata* wildtype strain (ATCC200989); Cg pMET: WCE from *C. glabrata* pMET-*BDF1* strain; Ca WT: WCE from *C. albicans* wildtype strain; Sc WT: WCE from *S. cerevisiae* wildtype strain; Sc Δ*bdf1*: WCE from *S. cerevisiae* *BDF1* deletion strain. **E.** Bdf1 expression level by Western blot. **F.** Construction of *BDF1* conditional knockdown rescue strain. Once the genomic *BDF1* is repressed by methionine and cysteine, only the *BDF1* copy in the plasmid can be expressed. *URA3*: selection marker *URA3* gene. **G.** A Bdf1-expressing plasmid rescues the expression level in the *BDF1* knockdown strain. Cg pMET-*BDF1* + WT *BDF1*: WCE from *C. glabrata* pMET-*BDF1* strain transformed with the plasmid containing wildtype *BDF1*. The repression of pMET lasted 7 hours.

Next, I used the anti-ScBdf1 antibody to verify the Bdf1 expression level. The results show that pMET activity is quickly repressed once methionine and cysteine were added to the medium. After 2 hours of incubation with methionine and cysteine, the Bdf1 level in the pMET-*BDF1* strain had visibly decreased. After 6 hours very little Bdf1 could be detected in cells of the pMET-*BDF1* strain (**Figure 20E**). The decrease of the signal detected using the anti-ScBdf1 antibody confirmed that the protein recognized by this antibody was indeed CgBdf1. In order to verify if the expression defect of Bdf1 could be rescued, I transformed a *BDF1*-containing *URA3* plasmid into the pMET-*BDF1* strain (**Figure 20F**). As shown in **Figure 20G**, the *BDF1* containing plasmid restored Bdf1 expression levels in the repressed pMET-*BDF1* strain. Taken together, the pMET-*BDF1* construction allowed us to reduce the expression of Bdf1, which can be rescued by a *BDF1* containing plasmid. The pMET-*BDF1* and rescue strains could then be used to verify the role that Bdf1 plays in *C. glabrata*.

1.1.2. Bdf1 is essential for the viability of *C. glabrata*

To verify the essential role of Bdf1 in *C. glabrata*, I tested the growth of the pMET-*BDF1* strain under conditions in which pMET was or was not repressed by methionine and cysteine. In the medium where pMET was active, the observed growth activity was the same for the wild-type (WT) and pMET-*BDF1* strains. When the activity of pMET was repressed and the Bdf1 level was low, the pMET-*BDF1* strain did not grow, whereas the growth of the WT strain was not affected (**Figure 21A**). I next verified whether restoring the Bdf1 level could rescue the growth of the pMET-*BDF1* strain. As shown in **Figure 21A**, the transformation of a *BDF1*-containing plasmid rescued the growth activity of the pMET-*BDF1* strain under conditions where pMET was repressed.

The results in **Figure 20E** showed that 6 or 8 hours of pMET repression could significantly decrease the level of Bdf1, but was not enough to totally deplete Bdf1 from cells. When we increased the duration of inhibition to 24 hours, SDS-PAGE analysis of the whole cell extract (WCE) showed that the proteins in non-rescued pMET-*BDF1* strains were highly degraded (**Figure 21B**). This might indicate that after repressing Bdf1 expression for 24 h, the cells were dead. Taken together, the above results confirmed that Bdf1 is essential for *C. glabrata* viability.

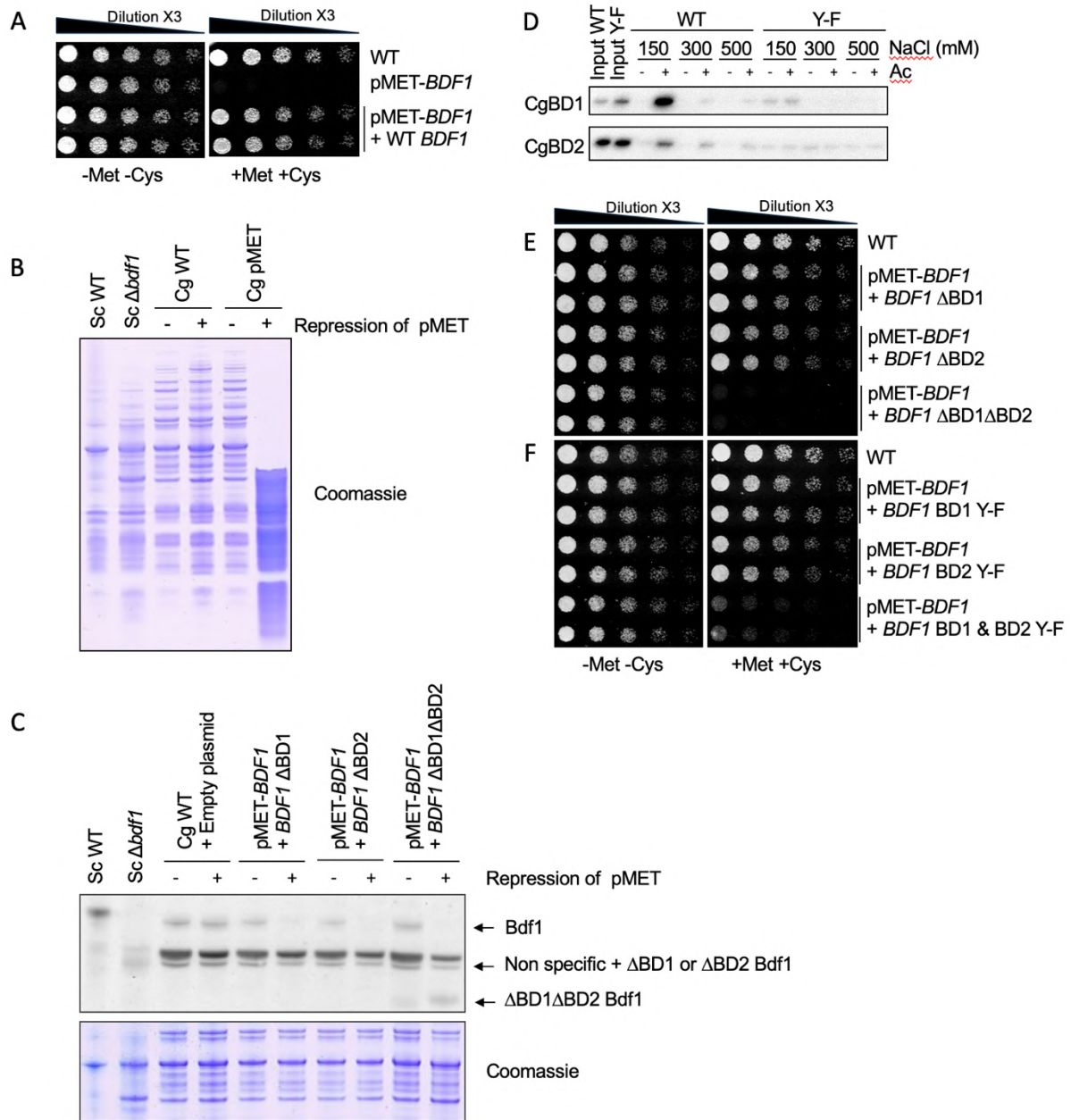


Figure 21. Bdf1 and its bromodomains are essential for *C. glabrata* growth. **A.** Growth test of pMET-*BDF1* and rescue strains in solid medium. -Met -Cys and +Met +Cys: SC media with or without methionine and cysteine, respectively. **B.** SDS-PAGE analysis of WCE from different *S. cerevisiae* and *C. glabrata* strains. **C.** Western blot analysis of Bdf1 expression using anti-ScBdf1 as the primary antibody. Sc WT: WCE from *S. cerevisiae* wildtype strain; Sc $\Delta bdf1$: WCE from *S. cerevisiae* *BDF1* deleted strain; Cg WT + Empty plasmid: WCE from *C. glabrata* wildtype strain (ATCC200989) transformed with empty plasmid; Cg pMET + *BDF1* Δ BD1: WCE from *C. glabrata* pMET-*BDF1* strain transformed with a plasmid containing *BDF1* deleted for BD1; Cg pMET + *BDF1* Δ BD2: WCE from *C. glabrata* pMET-*BDF1* strain transformed with a plasmid containing *BDF1* deleted for BD2; Cg pMET + *BDF1* Δ BD1 Δ BD2: WCE from *C. glabrata* pMET-*BDF1* strain transformed with a *BDF1* containing plasmid deleted both for BD1 and BD2. The repression of pMET lasted for 24 hours. **D.** Pull-down assay using histone H4 (Ac-) and tetra-acetylated H4 (H4K5acK8acK12acK16ac, Ac+) peptides. Y-F refers to mutations Y166F present in CgBD1 and Y343F in CgBD2. **E** and **F.** Growth test of pMET-*BDF1* strains rescued by different forms of Bdf1 in solid medium. Y-F represents Y166F in BD1 and Y343F in BD2.

1.2. Bdf1 bromodomains are essential in *C. glabrata* growth.

1.2.1. Deletion of Bdf1 bromodomains inhibit the growth of *C. glabrata*.

The two bromodomains of BET family proteins play a very important role in the function of this protein family. These two domains in mammalian BET proteins have successfully been targeted by numerous small-molecule inhibitors (Filippakopoulos and Knapp, 2014). Moreover, our teams previously demonstrated that Bdf1 bromodomains were essential for the growth of *C. albicans*. I next set out to verify the role played by Bdf1 bromodomains in *C. glabrata*. In order to generate *C. glabrata* strains expressing Bdf1 deleted for either one (Bdf1 Δ BD1 and Bdf1 Δ BD2) or both (Bdf1 Δ BD1 Δ BD2) bromodomains, the strategy was to transform plasmids encoding these mutants into the pMET-*BDF1* strain so that, once pMET is repressed, those strains would only express the modified proteins.

A Western blot showed that when pMET was inhibited, a strain transformed with plasmids encoding the three deletion mutants, only the expression of Bdf1 Δ BD1 Δ BD2 could be detected. However, because of the poor specificity of the anti-ScBdf1 antibody, we could not detect the Bdf1 Δ BD1 and Bdf1 Δ BD2 proteins because they migrated together with non-specifically recognized proteins. Coomassie staining did not reveal any global degradation of proteins, suggesting that the deletion of the bromodomains did not cause cell death in *C. glabrata* (Figure 21C).

Since the two bromodomains were not essential for the viability of the yeast, we next wanted to know whether their deletion had any impact on yeast growth. Growth assays showed that the deletion of either BD1 or BD2 did not cause significant growth defects in *C. glabrata*, but the deletion of both totally inhibited yeast growth (Figure 21E). Thus, the presence of at least Bdf1 bromodomain is essential for the growth, but not the viability, of *C. glabrata*.

1.2.2. Point mutations in Bdf1 bromodomains inhibit the growth of *C. glabrata*.

In *S. cerevisiae*, Bdf1 residues Tyr186 and Tyr353 are located in the ligand binding pockets of BD1 and BD2 respectively, forming part of a hydrogen bond network with the acetylated lysines of histones H3 and H4. Substituting these residues with phenylalanine compromised ligand binding and caused a growth defect in both *S. cerevisiae* and *C. albicans* (Ladurner *et al.*, 2003; Mietton *et al.*, 2017). Here, I wanted to verify whether the corresponding mutations had the same inhibitory effect on *C. glabrata* growth. Aligning the protein sequences of ScBdf1 and CgBdf1 showed that the CgBdf1 residues to mutate to phenylalanine were Tyr166 in BD1 and Tyr343 in BD2.

I first verified whether these two mutations could inhibit the binding of the individually expressed bromodomains to a tetra-acetylated N-terminal histone H4 peptide (H4ac4) by a pull-down assay. In this assay, the biotinylated H4ac4 peptide is bound to magnetic streptavidin-coated beads; after incubation with CgBDs, the bound proteins are precipitated with the beads and revealed by Western blot while the non-bound proteins are removed in the wash. In theory, if the mutations abolish ligand binding activity, incubation with H4ac4 or with an unacetylated H4 peptide should produce no difference in the pulled down proteins, whereas we should observe more WT protein pulled down upon incubation with H4ac4 compared to the unacetylated peptide. The results shown in [Figure 21D](#) verified perfectly these predictions, confirming that the Y166F and Y343F mutations inhibited H4ac4 binding by CgBD1 and CgBD2, respectively.

Plasmids encoding Bdf1 with mutated bromodomains were then transformed into pMET-*BDF1* strains. The results of a growth assay were similar to that performed with the bromodomain deletion mutants. Point mutations in only one bromodomain (BD1 or BD2) did not cause growth defects in *C. glabrata*, but the combined mutations in both bromodomains inhibited yeast growth ([Figure 21F](#)). This indicated that the Bdf1 functionality required for yeast growth can be inhibited by introducing only two point-mutations, one in each bromodomain. Taken together, all these results strongly support the hypothesis that the bromodomains of Bdf1 are a potential antifungal target in *C. glabrata*.

1.3. Conclusion.

As a potential therapeutic target, CgBdf1 should either be essential for the viability or the growth of the pathogenic yeast. The essential role of Bdf1 in *S. cerevisiae* and *C. albicans* suggested the impossibility of directly knocking out the *BDF1* gene. Adapting the strategy of the *MET3* promoter allowed me to conditionally knock down *BDF1* expression in *C. glabrata*. By using this strategy, I verified that Bdf1 and the functionality of its bromodomains were essential for the growth of *C. glabrata*. These results suggest that CgBdf1 could be a potential antifungal target against *C. glabrata* infections. As a project performed during my Master 2 internship, this work was mostly completed before I officially began my Ph.D.

2. Structure studies on *Candida glabrata* Bdf1 bromodomains

To be an antifungal drug target in pathogenic yeast, being essential for growth is not enough. There must be enough structural divergence between the yeast target protein and its human homolog to avoid high toxicity upon treatment with the antifungal compound. This part aimed to study the structural differences between CgBdf1 and human BET bromodomains.

2.1. Ligand binding specificity of *C. glabrata* Bdf1 bromodomains

Before structural studies, I began with the binding function study of CgBdf1 bromodomains. As mentioned in Chapter I, Bdf1 is a fungal BET protein with four homologs in human: Brd2, Brd3, Brd4 and BrdT. The phylogram shows that yeast BET proteins are relatively distant from human BETs and closer to each other ([Figure 22A](#)). Also as illustrated before, *C. glabrata* is closer to *S. cerevisiae* than to *C. albicans*, which could also be seen in Bdf1 protein and its two bromodomains ([Figure 19B and 22A](#)).

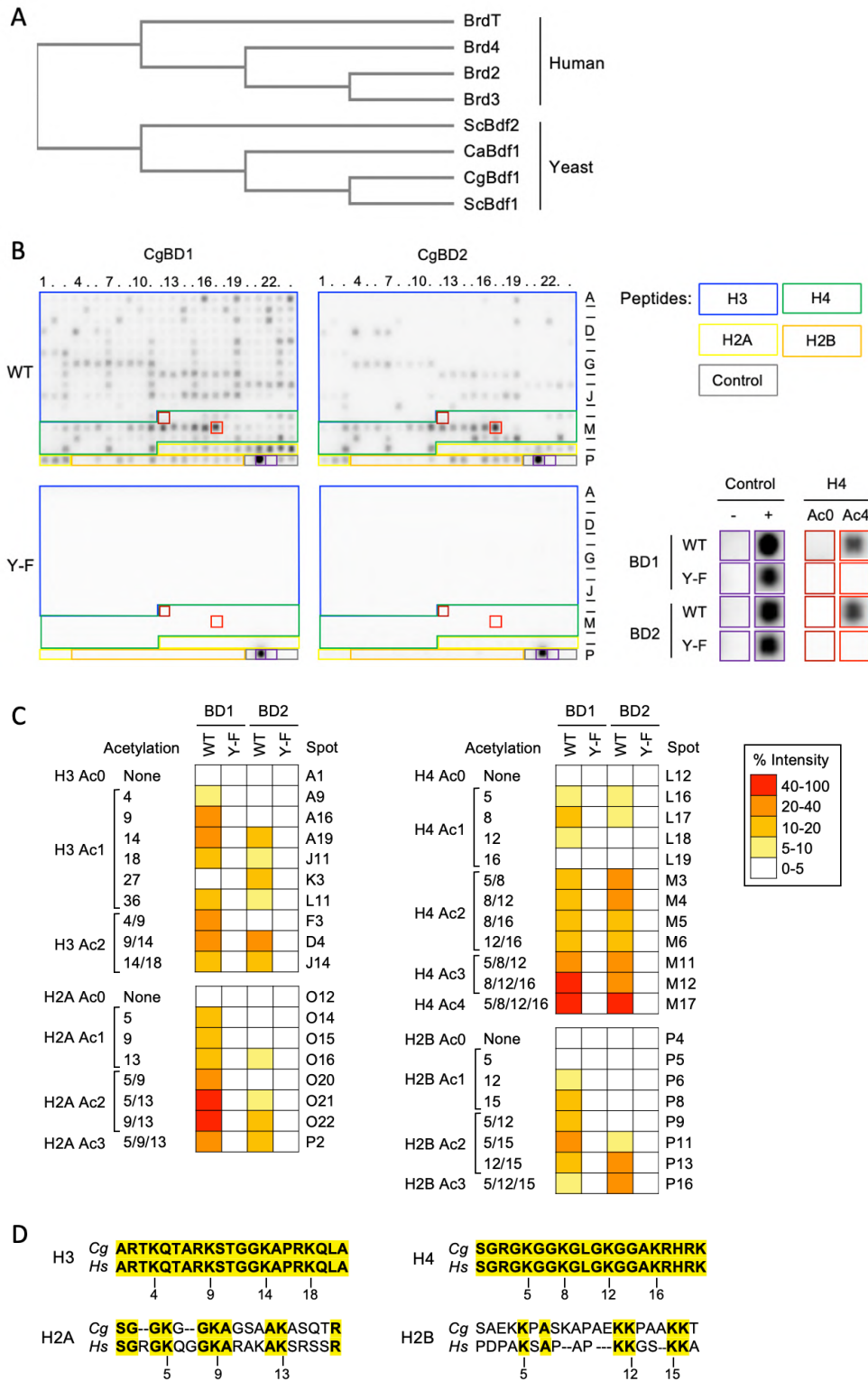


Figure 22. Histone peptide binding function of CgBdf1 bromodomains. **A.** Phylogenetic guide tree of human and yeast BET proteins. Trees were built by sequence alignment with web-based Clustal Omega. **B.** Binding of wildtype (WT) and mutant (Y-F) CgBdf1 BDs to a human histone peptide microarray. The array comprised control peptides (grey outline) or N-terminal peptides from histones H3, H4, H2A and H2B (blue, green, yellow and orange outlines, respectively). Signals for background and positive-binding controls (boxed in purple) or for H4 Ac0 and H4 Ac4 peptides (boxed in dark and light red) are shown magnified on the right of the array. **C.** Binding intensities for H3, H4, H2A and H2B peptides. **D.** Human (*Hs*) and *C. glabrata* (*Cg*) histone tail sequences.

The ligand binding specificity of CaBdf1 bromodomains had previously been studied in the lab. It was shown that both CaBdf1 BD1 and BD2 could bind to acetylated H3 and H4 peptides, and bound especially well to a tetra-acetylated H4 peptide (Mietton *et al.*, 2017). To check if the same binding specificity was shown by CgBdf1 bromodomains, I performed a binding assay using a histone peptide array from Active Motif that consisted of human histone peptides bearing various post-translational modifications. The results showed that the CgBdf1 bromodomains, especially CgBD1, recognized a broad spectrum of acetylated histone peptides (**Figure 22B**). Besides the tetra-acetylated H4 peptide, CgBD1 also showed high affinity for diacetylated H2A peptides. CgBD2 bound a narrower spectrum of histone peptides than CgBD1 and showed the highest affinity for the tetra-acetylated H4 peptides. However, its binding profile still covered the various acetylated forms from all H2A, H2B, H3 and H4 peptides (**Figure 22C**).

To check whether the binding activity of CgBDs to human histone peptides was relevant for the ability of these domains to recognize *C. glabrata* histone peptides, I performed a sequence alignment of the N-termini of histone peptides from those two species (**Figure 22D**). For H3 and H4, the human and *C. glabrata* sequences were completely identical over residues 1 to 20, and so the results concerning these histones in **Figure 22C** are biologically relevant. In contrast, for H2A and H2B the N-terminal sequences diverge significantly between human and *C. glabrata* and so the biological relevance of the results shown in **Figure 22C** for these two histones is less certain.

2.2. Purification of recombinant *C. glabrata* Bdf1 bromodomains

In order to evaluate the structural differences between CgBdf1 bromodomains (CgBDs) and its human homologs, I next tried to purify the cleavable His-tagged CgBdf1 BDs for subsequent structure determination and other biochemical tests. The design of the His-BD constructs is shown in **Figure 23A**. An N-terminal tag composed of 6 histidines was followed by a TEV protease cleavage site and the C-terminal bromodomain. The TEV site would allow me to cut the His tag during purification. Two constructs based on the sequence alignment with CaBdf1, His-CgBD 112-224 and 305-409 for BD1 and BD2 respectively, were firstly purified.

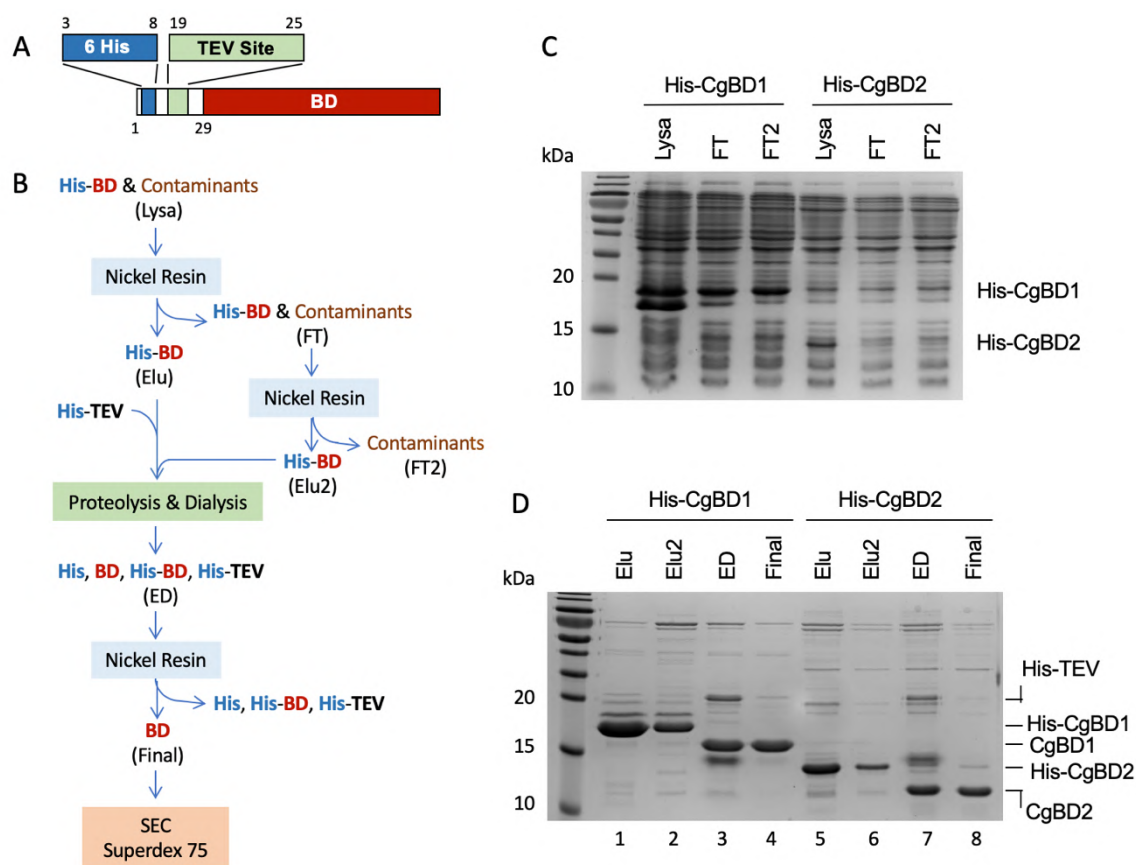


Figure 23. Nickel purification of the His tagged CgBdf1 bromodomains (His-BDs). **A.** His-tagged CgBdf1 bromodomain construct. BD: bromodomain. **B.** Diagram illustrating the purification protocol of His-BD. **C** and **D.** SDS-PAGE analysis of the nickel purification step for the two His-tagged CgBdf1 bromodomains. Lysa: bacterial cellular lysate; FT and FT2: Flow through of different purification stages; Elu and Elu2: Elution of different purification stages; ED: sample after dialysis in the presence of TEV protease.

The cell pellet from a 2 L culture of *Escherichia coli* (*E. coli*) strain BL21 induced by 1 mM IPTG overnight at 18 °C was used for the purification. As shown in **Figure 23B**, His-BDs were purified using a nickel resin which has an affinity for the His tag. A TEV proteolysis step followed in order to remove the His tag. The CgBdf1 BDs were obtained in the flow-through of a second Nickel resin purification step after the proteolysis. Here, I used a His-BD/TEV ratio of 20 (w/w), the cleavage of His tag for His-CgBD 112-224 was complete (**Figure 23D**, lines 2 and 3). It seems like the TEV worked less efficiently for His-CgBD 305-409, but the cleavage could still be considered as essentially complete (**Figure 23D**, lines 6 and 7). The final His-BD samples obtained after this nickel purification step could be considered highly pure (**Figure 23D**, lines 4 and 8).

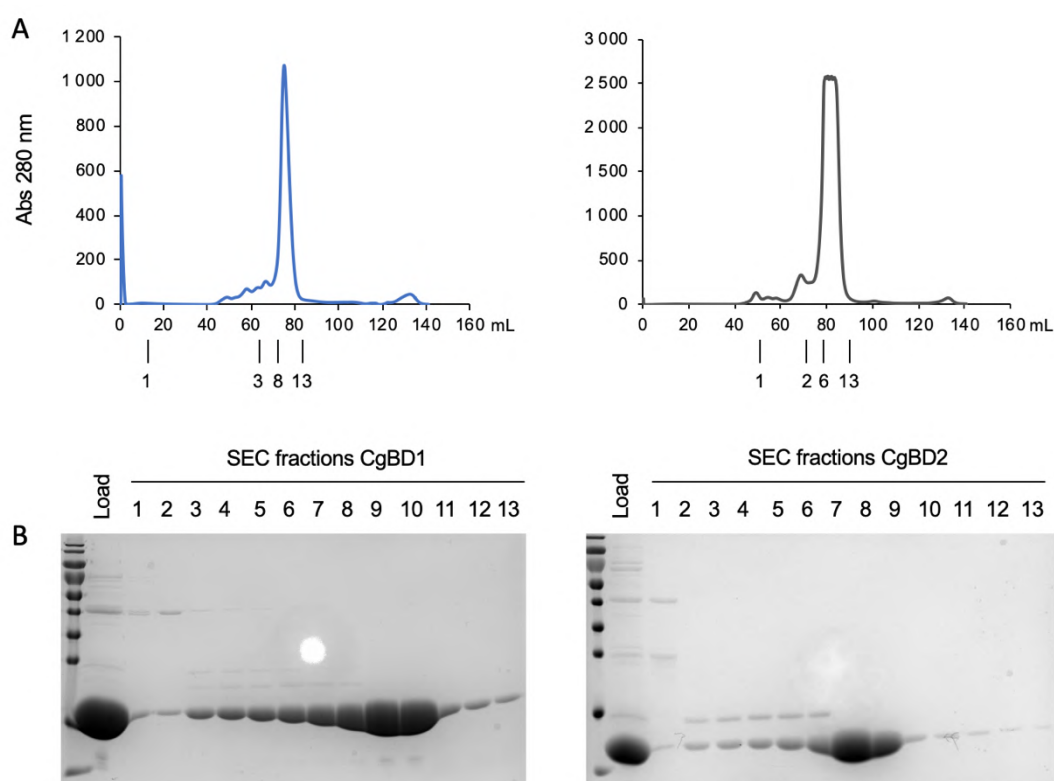


Figure 24. Size-Exclusion Chromatography (SEC) purification of the CgBdf1 bromodomains (CgBDs). **A.** SEC profile of CgBD1 (left) and CgBD2 (right). Fractions taken to analyze are indicated. **B.** SDS-PAGE analysis of the SEC elution fractions of CgBD1 (left) and CgBD2 (right). Load: concentrated sample injected onto the SEC column.

Crystallization requires a high level of protein monodispersity. A size-exclusion chromatography (SEC) purification step was therefore performed to assess sample polydispersity and remove any aggregates. Samples from the nickel purification step were concentrated and loaded onto a Hiload Superdex 75 column. The SEC fractions were collected and analyzed by SDS-PAGE. **Figure 24** shows that a single major peak is obtained for both proteins, and that these peaks can be separated from a small amount of protein eluting earlier, which may correspond to partly unfolded, multimerized or aggregated protein. Fractions corresponding to the single major peak were then pooled and concentrated to a high concentration. The yield was reasonable for both proteins but was nearly twice as high for CgBD1 as for CgBD2 (**Table 5**).

Table 5. Key purification conditions for initial constructs of CgBDs.

Constructs	Size (kDa)	<i>E. coli</i> culture (L)	His-BD/TEV	Final concentration (mg/mL)	Yield (mg)
CgBD1 112-244	15.38	2	20	22	7.04
CgBD2 304-409	12.71	2	20	12	3.28

I purified a second batch of CgBD1 112-244 using a cell pellet from 4 L of culture to have more protein. This time, 20.8 mg protein at 51 mg/mL was produced. I screened the protein for crystallization conditions using the European Molecular Biology Laboratory (EMBL) high-throughput crystallization (HTX) facility. After over one month of incubation with different crystallization conditions, no crystals appeared. This suggested that a new CgBD construct had to be tested. It should be mentioned that construct 112-244 was based on the alignment with the CaBdf1 BD1 (CaBD1) crystal structure. However, CgBD1 is more closely related to BD1 from *S. cerevisiae* (ScBD1) than to CaBD1. I then made a new CgBD1 construct (residues 128-237) based on the alignment with the ScBD1 crystal structure previously solved in the lab. This construct gave a better yield compared to the first construct: the total protein at the end of the purification was 20.4 mg at 81 mg/mL. This construct tended to precipitate a little bit during the concentration step before loading onto the SEC column. The precipitation could be removed by centrifugation at 6000 g for 5 min, and after SEC purification no more precipitation occurred even at very high concentration.

As for CgBD2, in order to have more protein, I generated three other constructs comprising residues 304-411, 304-415 and 304-418. The purification profiles of these CgBD constructs was similar, as shown in [Figure 23C](#) and [D](#). However, the yield for CgBD2 constructs 304-411 and 304-415 was still lower than the original construct 304-409. Using construct 304-418 I obtained 6.6 mg protein at 41.4 mg/mL, which was enough to perform crystallization trials at the EMBL HTX facility.

I then decided to use CgBD1 construct 128-237 and CgBD2 construct 304-418 for further purification. For CgBD2, the purification process was optimized in order to obtain a better yield: the His-BD/TEV ratio was decreased to 12 and the amount of nickel resin used for the Lysa sample was doubled. The results of the purification are summarized in [Table 6](#).

Table 6. Key purification conditions for final constructs of CgBDs.

Constructs	Size (kDa)	<i>E. coli</i> culture (L)	His-BD/TEV	Final concentration (mg/mL)	Yield (mg)
CgBD1 128-237	12.932	2	20	> 60	> 20
CgBD2 304-418	13.816	4	12	> 60	> 30

2.3. Crystal structure analysis of *C. glabrata* Bdf1 bromodomains

Purified CgBDs samples were prepared at concentrations of 40, 25 and 15 mg/mL and used to screen crystallization conditions at the EMBL HTX facility. For CgBD1, single crystals began to appear within 72 hours in 30 crystallization conditions at 4 °C. For CgBD2, many small showers of crystals began to appear in 18 crystallization conditions at 4 °C within 72 hours (Table 7).

Table 7. Positions of crystallization plate that form crystals. All the conditions can be found in Appendix I.

Plate	Plate position (protein concentration)	
	CgBD1	CgBD2
Wizard_I+II_rigaku	A1 (40 g/L), F12 (40 g/L)	F9 (15 & 25 & 40 g/L)
PEGs-I_qiagen	A12 (25 & 40 g/L), B12 (25 g/L), C10 (15 g/L), D7 (25 g/L), D8 (40 g/L), D9 (15 & 40 g/L),	H7 (25 & 40 g/L),
Salt-Grid_hampton	B4 (40 g/L), B5 (40 g/L), B6 (40 g/L), C11 (40 g/L), C12 (15 & 25 & 40 g/L), D10 (15 & 25 & 40 g/L), D11 (15 & 25 & 40 g/L), D12 (25 & 40 g/L)	F2 (15 g/L), F3 (15 g/L)
PACT_MD	B5 (25 g/L), B6 (25 g/L)	A1 (15 & 25 g/L), A7 (25 g/L), A7 (25 & 40 g/L), B1 (40 g/L), C1 (40 g/L), C2 (25 & 40 g/L), D1 (15 g/L)
JCSG_MD	A10 (40 g/L), A12 (25 g/L), C12 (40 g/L), G9 (40 g/L)	A3 (40 g/L), A4 (25 g/L), B7 (40 g/L), B8 (25 & 40 g/L)
Classics-Suite_qiagen	A5 (40 g/L), C6 (40 g/L), C8 (40 g/L), E2 (25 & 40 g/L), F10 (25 & 40 g/L), G1 (25 g/L), H5 (40 g/L), H8 (15 & 25 & 40 g/L)	A4 (15 g/L), B3 (40 g/L), D5 (40 g/L)

Some of the formed crystals are shown in **Figure 25A**. For CgBD1, some crystals obtained in the initial screen were already large enough and could be directly harvested into cryoloops by the HTX facility via their CrystalDirect technology (**Figure 25A**). For CgBD2, crystals from the screene were too small (**Figure 25B**) and needed to be reproduced and optimized using manual drops to obtain bigger crystals. The high-resolution crystal structure of ScBD2 had previously been determined in our laboratory. The crystallization conditions which gave the highest-resolution structure for ScBD2 were 13-30% 2-Methyl-2,4-Pendenediol (MPD) as the precipitant and 0.1 M sodium acetate pH 4.6 as the buffer. Similar conditions were among those which gave crystals of CaBD2. To optimize the size and shape of crystals, I therefore manually set up crystallization drops screening between 13% and 36% MPD as precipitant and 0.1 M sodium acetate pH 4.6 as buffer. Bulky, single crystals appeared readily in some drops at 4 °C and were manually harvested. All harvested CgBD1 and CgBD2 crystals were sent to the highly automated ESRF beamline ID30A1 (Massif-1) to perform X-ray diffraction tests.

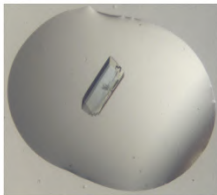
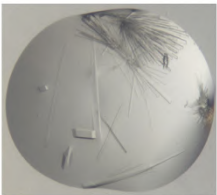


A CgBD1 (128-237)		B CgBD2 (304-418)		
				
Protein concentration	25 mg/mL	40 mg/mL	40 mg/mL	25 mg/mL
Precipitant	25% PEG1500	1.6 M (NH ₄) ₂ SO ₄	0.2M NH ₄ H ₂ PO ₄ 20% PEG 3350	33% MPD
Buffer	0.1 M MIB buffer	0.1 M Hepes	-	0.1 M CH ₃ COONa
pH	9	7	-	4.6
Resolution	-	1.2 Å	-	2.0 Å
R _{work}	-	0.151	-	0.197
R _{free}	-	0.175	-	0.224

Figure 25. Some crystals obtained of CgBD1 (A) and CgBD2 (B) and their corresponding crystallization conditions. PEG: polyethylene glycol; MIB buffer: malonic acid, imidazole and boric acid (2:3:3 molar ratio); MPD: 2-methyl-2,4-pentenediol.

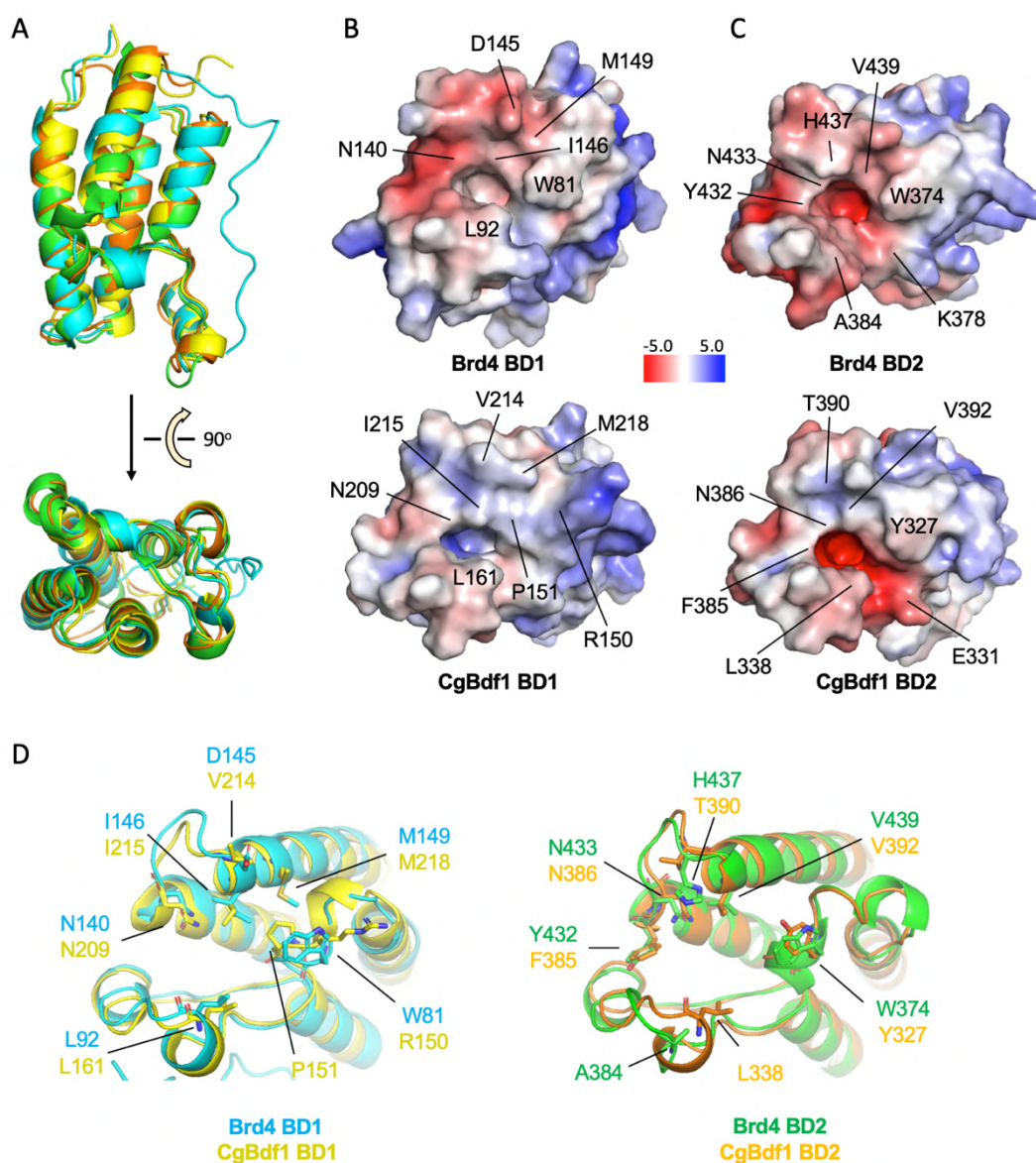


Figure 26. Structure of bromodomains from CgBdf1. **A.** Alignment of structures of human Brd4 BD1 (cyan, PDB codes 4LYI) and BD2 (green, PDB codes 2OUO) with CgBD1 (yellow) and CgBD2 (orange). **B** and **C.** Plots of electrostatic surface potential of bromodomain structures from human Brd4 (up) and CgBdf1 (down). Regions of negative and positive potential are shown in red and blue, respectively. **D.** Alignment of structures of human Brd4 BD1 (cyan) with CgBD1 (yellow) and Brd4 BD2 (green) with CgBD2 (orange) with key residues marked in B and C.

Crystals for both CgBD1 and BD2 diffracted very well with a resolution of about 2 Å and 1.6 Å, respectively (Figure 25). The structures were solved by molecular replacement and refined to high resolution. This step was performed by my supervisor Carlo Petosa and crystallographic statistics are shown in appendix II. Alignment of BD1 and BD2 structures from human Brd4 and CgBdf1 showed that the core structure of these bromodomains was very similar (Figure 26A and 26D). However, comparing electrostatic surface representations of

CgBDs and human Brd4 BDs showed that there were significant differences in the charge and shape of the binding pocket. In general, CgBdf1 bromodomains seemed to have less negative charge around the pocket compared to Brd4 bromodomains. Additional detailed differences can be observed.

As shown in **Figure 26B**, the size of the binding pocket is similar between BD1 from Brd4 and CgBdf1. However, Brd4 BD1 has different residues available for interaction compared to CgBD1. Only residues Leu92 and Asn140 in Brd4 BD1 are conserved with Leu161 and Asn209 in CgBD1, respectively. Residue Trp81 in Brd4 that forms a channel with Leu92, which is missing in CgBD1 with its corresponding residues Arg150 and Leu161, respectively. The three residues Ile146, Met149 and Asp145 form a “three-step staircase” structure around the binding pocket of Brd4 BD1. In CgBD1, Ile215, Met218 and V214 do not form the same structure.

The Brd4 BD2 binding pocket that includes Tyr432 and the conserved Asn433 appears slightly larger than that of CgBD2 that includes Phe385 and Asn386. Residue His437 provide a polar interaction site in Brd4 BD2, which is replaced by a hydrophobic Val392 in CgBD2. In contrast, the CgBD2 contains an interaction site provided by Leu338 that non available in Brd4 BD2. Residues Trp372 and Tyr327 in Brd4 and CgBD2, respectively, also lead to different forms around the binding pocket (**Figure 26C**).

2.4. Purification of *C. glabrata* Bdf1 construct containing both bromodomains and the full length Bdf1

Structural studies of single bromodomains can provide precise information concerning the binding pocket. However, information concerning the interactions between the two bromodomains and the rest of the protein is lost. To try to obtain such information, I purified a construct containing both BD1 and BD2 from CgBdf1 (CgBdf1 128-418, 33.83 kDa) as well as the full-length protein (FL CgBdf1, 75.38 kDa).

The purification protocol was the same as that used for CgBD1 and CgBD2 shown in **Figure 23B**. For each construct a cell pellet from a 2 L culture induced by 1 mM IPTG overnight at 18 °C was used. A His-BD/TEV ratio of 20 was used for proteolysis at 4 °C overnight. SDS-

PAGE analysis of samples from the nickel purification step revealed bands of the expected size, and showed that the cleavage by TEV was almost complete for both constructs (**Figure 27A**). There was clearly much less protein expressed for FL CgBdf1 compared to CgBdf1 128-418. Also, the full-length protein sample contained many more contaminants at the end of the nickel purification step.

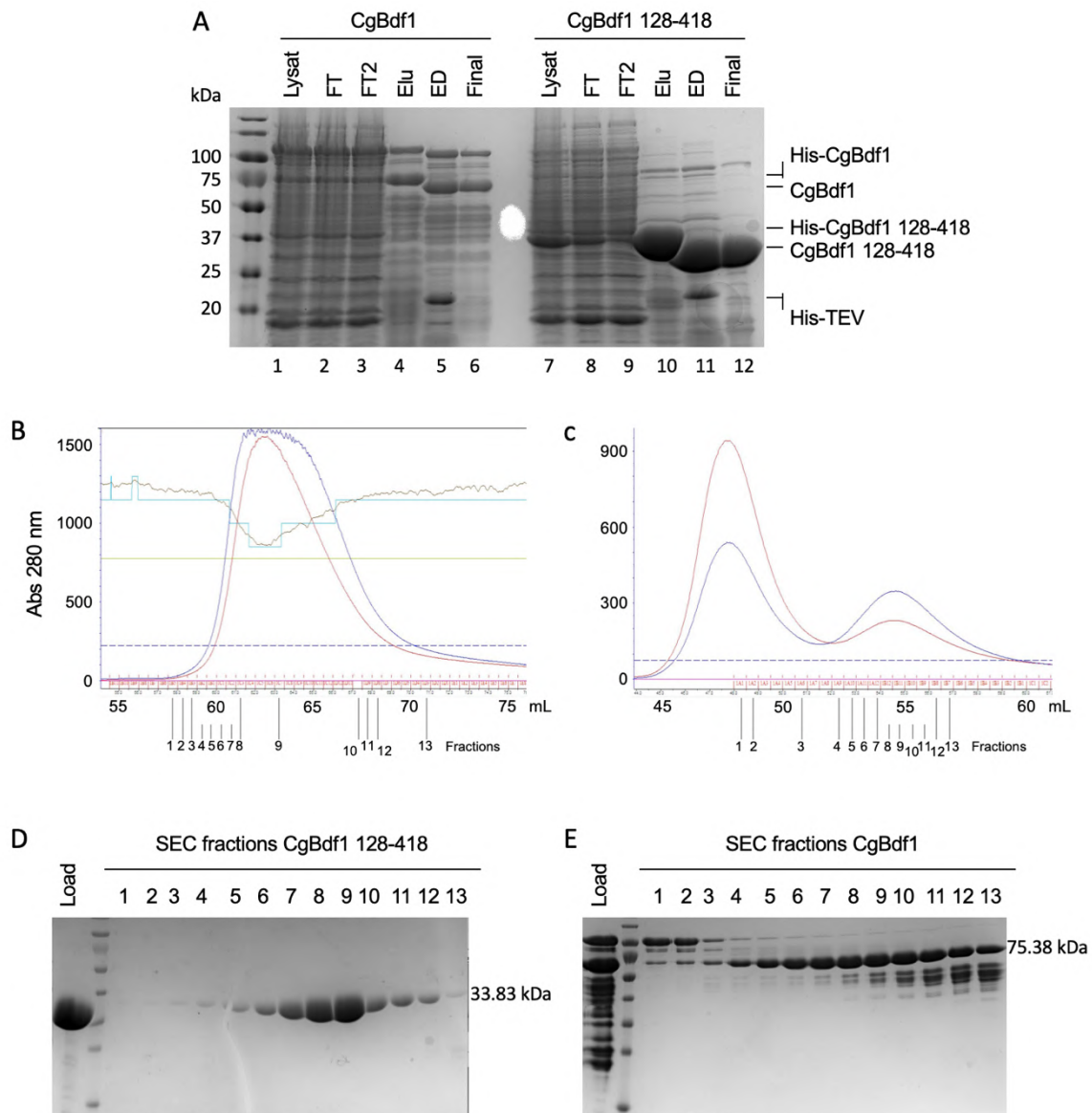


Figure 27. Nickel and SEC purification of the His tagged CgBdf1 construct containing both bromodomains (CgBdf1 128-418) and the full length Bdf1. **A.** SDS-PAGE analysis of the purification of different constructions of His tagged CgBdf1 constructs. Lysa: bacteria cellular lysate; FT and FT2: Flow through of different purification stages; Elu: Elution sample; ED: sample after dialysis overnight in the presence of TEV protease. **B** and **C.** SEC profile of CgBdf1 128-418 (**B**) and CgBdf1 (**C**) and fractions collected. The blue and red curves represent the absorbance at 280 nm and 260 nm, respectively. **D** and **E.** SDS-PAGE analysis of the SEC elution fractions of CgBdf1 128-418 (**D**) and FL CgBdf1 (**E**). Load: concentrated sample injected onto the SEC column.

A SEC purification step was then performed. Samples were concentrated and loaded onto a Hiload Superdex 75 column. The profile of CgBdf1 128-418 was very similar to that of the single CgBDs: only a single peak appeared and SDS-PAGE analysis of SEC fractions showed that very pure protein could be obtained (**Figure 27B and 27D**). Fractions with high protein concentration and few contaminants were pooled together and concentrated before being stored at -80 °C. At the end, 12.6 mg protein at 41.9 mg/mL was obtained. The purified CgBdf1 128-418 sample was then prepared at concentrations of 25 and 15 mg/mL and used to screen crystallization conditions at the EMBL HTX facility. Unfortunately, no crystals were obtained in any of the screened conditions.

However, the situation was different for the FL CgBdf1 construct. Two peaks, instead of only one like the other constructs, could be evidently separated (**Figure 27C**). SDS-PAGE analysis demonstrated that the full-length protein eluted over a wide volume range. The first SEC peak represented mainly a contaminant protein of high molecular weight (**Figure 27E**). The second peak represented mainly FL CgBdf1. However, many fractions within this peak contained proteins of smaller molecular weight compared to CgBdf1 (**Figure 27E**). I could not be sure that if they were contaminants or degraded CgBdf1. At the end, only a few fractions (4 to 8) that were considered relatively pure were collected. After the concentration step, only 0.7 mg protein at 13.9 mg/mL was obtained. I decided not to pursue this line of inquiry in order to focus my attention on other aspects of the project. Nevertheless, as a first attempt at expressing and purifying the full-length construct these results are highly promising. They suggest that by optimizing and scaling up the expression and by including additional steps in the purification protocol, such as an ion-exchange column, it should be possible to obtain pure protein at sufficient yield to perform structural and biophysical studies.

2.5. Conclusion

An ideal therapeutic target in a pathogen would lack a human homolog in order to limit the toxicity upon administration of the drug. If not the case, then significant differences in the drug binding site should exist between the target protein in the pathogen compared to its human homolog. Fungal Bdf1 belongs to the BET protein family with four human homologs. I adapted the purification protocol developed previously in the lab (Mietton *et al.*, 2017) to

obtain both Bd1 and BD2 from CgBdf1 in good yield and at high purity. I then succeeded to obtain well-diffracting crystals which yielded high-resolution crystal structures. These showed that even though the overall structure of bromodomains from Brd4 and CgBdf1 was similar, their ligand binding pockets still exhibited significant differences in electrostatic charge and shape. These differences provide evidence that the selective inhibition of CgBDs without inhibiting human BETs is feasible. Thus, taken together with their essential role for *C. glabrata* growth, CgBdf1 bromodomains seemed promising as a potential antifungal target. The project could move to the next step, concerning the discovery of inhibitors that selectively target CgBdf1 bromodomains.

3. High-throughput chemical screening *in vitro* for inhibitors of *Candida glabrata* Bdf1 bromodomains

3.1. Optimization of the Homogeneous Time-Resolved Fluorescence (HTRF) assay

A key objective of my Ph.D. project is to identify small-molecule inhibitors of CgBdf1 bromodomains. A Homogeneous Time Resolved Fluorescence (HTRF) assay had previously been developed in our laboratory to screen for compounds that disrupt the acetylpeptide binding activity of CaBdf1 BD1 and BD2, which was based on the transfer of energy from a fluorescence donor to an acceptor. I therefore needed to adapt and optimize this assay for CgBdf1 BD1 and BD2.

There are primarily four components in this HTRF assay: the bromodomain of interest tagged with glutathione S-transferase (GST-BD); a biotin labelled N-terminal histone H4 peptide tetra-acetylated on residues K5, K8, K12 and K16 (biotin-H4 K_{ac4}); an anti-GST antibody coupled to Lumi4-Terbium Cryptate, the fluorescence donor (Anti-GST-Tb); and streptavidin coupled to D2 dye, the fluorescence acceptor (SA-D2). Anti-GST-Tb associates with GST-BD through antibody-antigen interactions and SA-D2 binds to biotin-H4K_{ac4} via the streptavidin-biotin interaction. In theory, when GST-BD binds to the acetylpeptide, the

fluorescence donor is brought into close proximity of the acceptor. Following excitation of the donor at 330 nm, this proximity favors energy transfer, leading to the emission of fluorescence by the D2 dye at 665 nm (**Figure 28A**). This emitted fluorescence is then detected in a time-resolved mode by introducing a delay between the excitation pulse and a time-gated measurement window and is referred to as the HTRF signal. When the binding of GST-BD to Biotin-H4 Kac₄ is inhibited, the fluorescence donor has a lower probability of being close to the acceptor, resulting in a weaker emission from the acceptor (**Figure 28B**). This decrease of the HTRF signal will then indicate the presence of the bromodomain inhibitor.

3.1.1. Signal/Background Ratio

In the ideal situation, the signal produced by the D2 dye is induced only by the bromodomain-peptide interaction. However, even when there is no binding of GST-BD to acetyl-peptide (when GST-BD is absent for example), the fluorescence donor can still be close to the acceptor just by chance, which will generate a background signal (**Figure 28C**). To evaluate the performance quality of the assay, the Signal/Background (S/B) ratio is calculated, which indicates the HTRF signal compared to the background signal (Zhang, Chung and Oldenburg, 1999). According to our collaborators at the California Institute for Biomedical Research (Calibr) who would ultimately perform the high-throughput chemical screen, the S/B ratio of the screening assay had to exceed at least 3 in order to achieve a reliable and efficient screen.

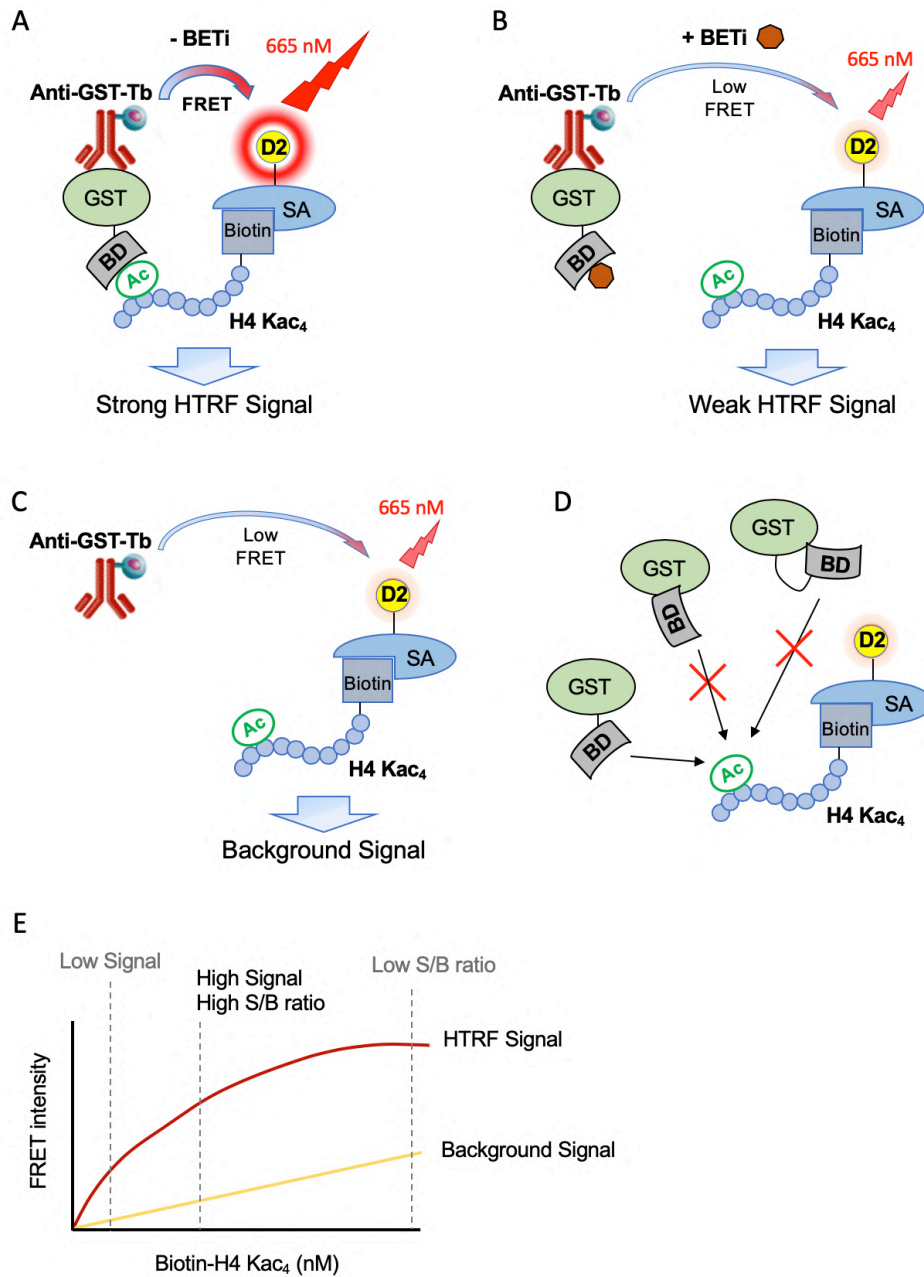


Figure 28. Homogeneous time-resolved fluorescence (HTRF) assay. **A**, **B** and **C**. Cartoons illustrating the HTRF experimental configurations. BD: bromodomain; GST: glutathione S-transferase protein; Ac: acetyl group; H4 KAc₄: K5, K8, K12 and K16 tetra-acetylated histone H4 N-terminal peptide; SA: Streptavidin; FRET: fluorescence resonance energy transfer; Anti-GST-Tb: anti-GST antibody coupled to the Lumi4-Tb Cryptate fluorescence donor, excitation at 330 nm; D2: fluorescence acceptor, emission at 665 nm. **D**. The conformation of the GST-BD fusion protein is important for its ability to bind efficiently to the acetylated peptide. Constructs in which the BD boundaries are defined either too short or too long can lead to undesired steric constraints or interactions between the GST tag and BD, respectively. Both cases will reduce the HTRF signal whereas the optimal configuration can yield high affinity binding of the BD to the H4 Kac₄ peptide. **E**. Illustration of the influence of biotin-H4 Kac₄ peptide concentration on the Signal/Background ratio (S/B ratio).

Several factors, including the concentration and ratio of components, the incubation time and temperature, and the specific GST-BD construct used, can influence the S/B ratio of the HTRF assay. The assay to be optimized in the lab used a commercial kit from Cisbio, where the protein concentration and the ratio among components have already been optimized. The incubation temperature has also been optimized in our lab before my arrival which indicated that 4 °C was better than room temperature. My primary task in this part was then to test different GST-BD constructs to identify the one giving the highest S/B ratio. The background signal depends primarily only on the concentrations of Anti-GST-Tb and of SA-D2, for which the respective relative ratios with the GST-BD and H4 Kac₄ peptide have been optimized by Cisbio. Thus, I set out to identify the constructs for BD1 and BD2 that gave the highest HTRF signal possible. These constructs should be neither too short, in order to avoid an incompletely folded bromodomain, nor too long, in order to prevent undesired interactions between the bromodomain and the GST tag which could mask the binding site (**Figure 28D**). The choice of a well-defined construct can directly decide the success of the HTRF optimization. To screen the construct, conditions of HTRF assay are summarized in **Table 8**.

Table 8. HTRF conditions for GST-BD constructs screening.

	Final concentration (nM)	Total volume (μL)	Incubation
GST-BD	5	6	Up to 24 hours at 4 °C
Biotin-H4 Kac ₄	Various	4	
Anti-GST-Tb	0.5	5	
SA-D2	Various	5	

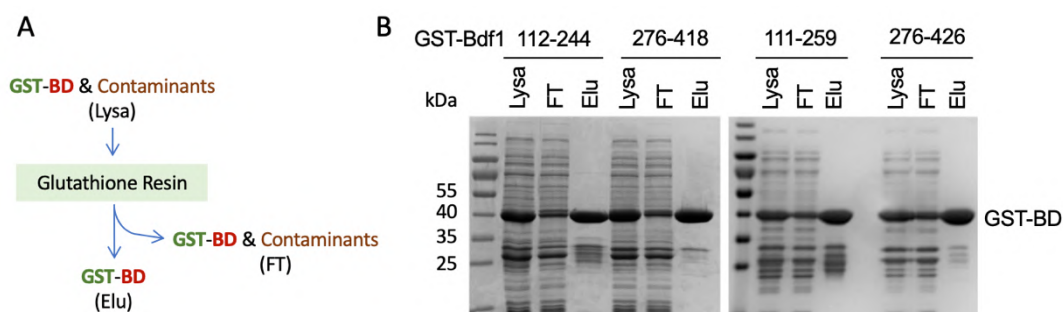


Figure 29. Purification of the GST tagged CgBdf1 bromodomains (GST-BDs) from 50 mL of culture. A. Flow chart of the purification protocol of GST-BD from 50 mL of bacterial culture. **B.** Examples of SDS-PAGE analysis of the glutathione affinity purification step for two GST-BD1 and two GST-BD2 constructs tested. Lysa: bacterial cellular lysate; FT: Flow through; Elu: Elution.

The GST-BD concentration was held fixed at 5 nM, the value recommended by Cisbio; I also verified that increasing this did not significantly increase the S/B ratio. In cooperation with that, the concentration of Anti-GST-BD was also fixed at 0.5 nM as recommended by Cisbio. On the other hand, the concentration of Biotin-peptide was varied, as well as the concentration of the SA-D2 dye. However, Cisbio recommended that the H4 Kac₄/SA-D2 ratio should be constant at eight. Obviously, the concentration of Biotin-H4 Kac₄ and SA-D2 should avoid being too low in order to prevent a low HTRF signal being produced. However, it cannot be too high either since a high concentration of SA-D2 increases its probability of being within energy transfer distance of the Anti-GST-Tb by chance, which will lead to a high background signal (**Figure 28E**).

The purification protocol for GST-CgBDs was very simple compared to that for the His-BDs (**Figure 29A**) and the purification profile was similar for all the constructs. The GST tag has a glutathione transferase activity so it naturally has an affinity for its substrate glutathione (GSH), allowing us to purify the GST-CgBDs using a GSH resin. When soluble free GSH is added to the resin it competes with the immobilized GSH and allows the bound GST-CgBDs to be eluted. SDS-PAGE analysis showed that the GST-BD proteins in the eluted fractions were relatively pure (**Figure 29B**). These fractions also contained some protein or peptides with a lower molecular weight than the GST-CgBDs, which may be contaminants or GST-BD degradation products. It cannot be excluded that these species might have a negative impact on the HTRF assay. Nevertheless, since the HTRF assay and the inhibitor screening do not need a very high purity of the protein, I pooled all the fractions with a high concentration of GST-BDs.

I next tested the purified GST-tagged constructs of CgBD1 and CgBD2 with different H4 Kac₄ concentrations in order to obtain a S/B ratio as high as possible in the HTRF assay. The 384-microwell plates were prepared in the following order: (i) The Biotin-H4 Kac₄, Anti-GST-Tb and SA-D2 were mixed in the correct concentration. Since I planned to test ten different acetylated peptide concentrations, ten master mixes were prepared here. (ii) 6 µL of the GST-BD were loaded into each well. In an additional row, 6 µL of buffer were loaded instead of the GST-BD to test the background signal. (iii) 14 µL of master mix were loaded into each well. (iv) The plate was sealed by parafilm and covered by an aluminum foil to protect from light. The plate was then incubation at 4 °C in the dark.

The microplate was read on a CLARIOstar Plus plate reader available in the lab and specific HTRF signal was calculated as the ratio of emission at 665 nm to that at 620 nm (all multiplied by 10,000 to avoid very small numbers). Emission at 665 nm is the emission peak of the fluorescence acceptor D2 dye while the emission at 620 nm is one of the emission peaks of the fluorescence donor Lumi4-Tb and used as a normalization control.

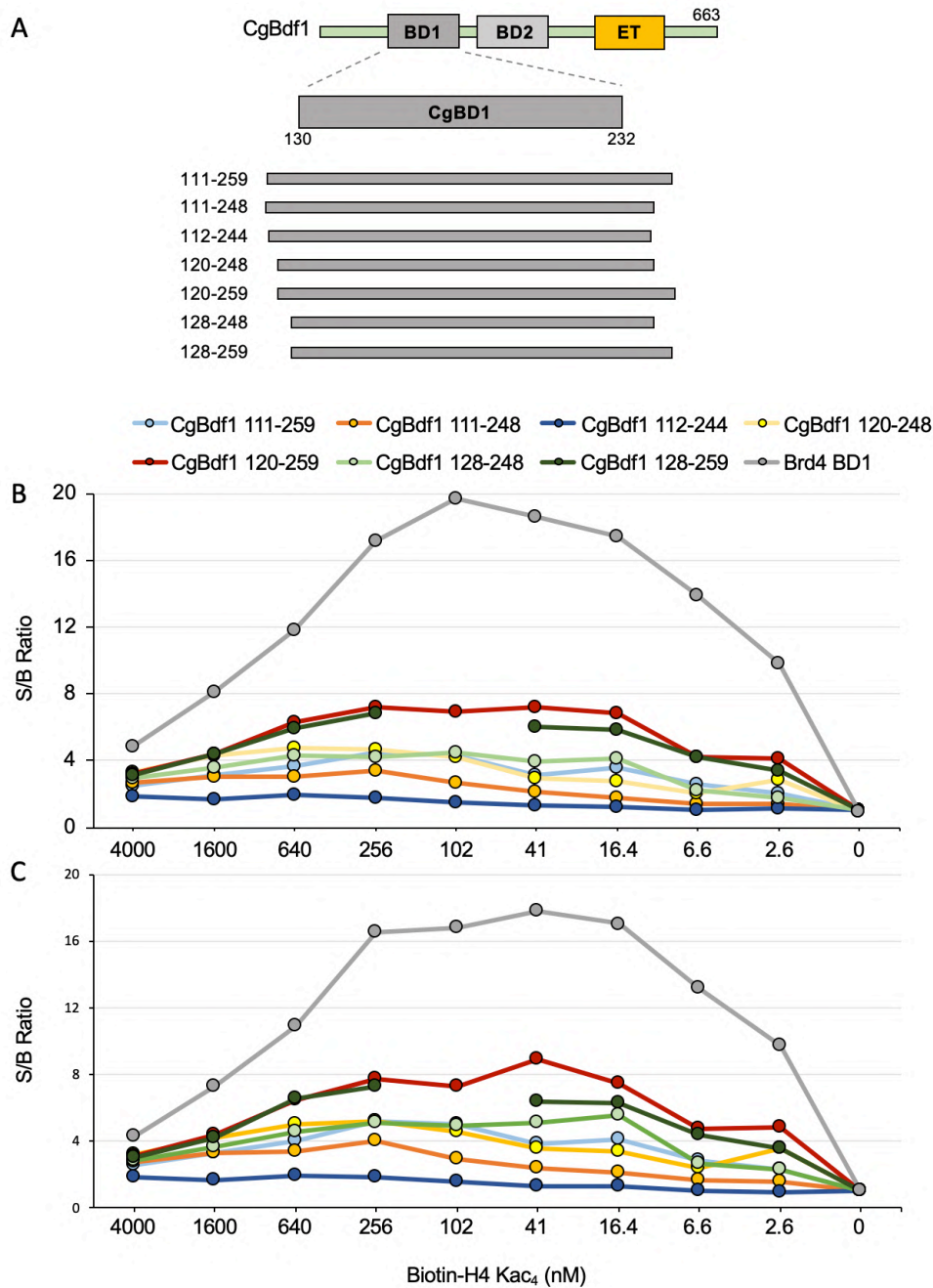


Figure 30. Comparison of seven CgBdf1 BD1 constructs and human Brd4 BD1 in an HTRF assay. A. The seven CgBD1 constructs. **B and C.** S/B ratio obtained of the CgBD1 constructs. Incubation was performed at 4°C for 1 hour (B) or 4 hours (C).

For BD1, none of the seven CgBD1 constructs tested performed better than, or even close to, the construct used as a positive control, human Brd4 BD1, which exhibited a S/B ratio above 15 in many conditions tested. The GST-CgBD1 construct spanning residues 120-259 showed the best performance among all the tested GST-CgBD1 constructs: after just 1 hour of incubation, the S/B ratio was above 7 and after 4 hours it reached about 9 (**Figure 30**). This construct was therefore chosen for further characterization to verify whether it could be used for inhibitor screening.

For BD2, the situation was similar compared to BD1: none of the seven CgBD2 constructs performed as well as the control construct, human Brd4 BD2. The two best constructs spanning residues 289-410 and 289-411 performed similarly with a S/B ratio exceeding 6 in some conditions. Construct 289-410 tended to show better performance at higher H4 Kac4 concentration conditions while 289-411 performed better at slightly lower peptide concentration (**Figure 31**). In order to save on acetylated histone peptide and SA-D2, construct 289-411 was chosen for further characterization even though it did not perform as well as the best CgBD1 construct. It should also be mentioned that for BD2, four hours of incubation did not guarantee a good performance and that 24 hours of incubation at 4 °C were necessary.

Chemical compounds used for screening are generally dissolved and stored in dimethylsulfoxide (DMSO). Since DMSO has a structure resembling the acetyl group of acetyllysine (**Figure 32A**) it is a weak ligand of bromodomains and can competitively inhibit the binding of the latter to the acetylpeptide (Philpott *et al.*, 2011). It is therefore important to optimize the HTRF assay in the presence of a DMSO concentration compatible with the screening of chemical libraries. Both best-performing constructs of CgBD1 and BD2 were tested in the HTRF system with different DMSO concentrations. Because DMSO could directly be added to the Biotin-H4 Kac₄ preparation there was no need to change the microplate loading protocol. The results showed that DMSO disturbed the performance by significantly decreasing the S/B ratio. As the concentration of DMSO was progressively increased from 0% to 1.5%, the S/B ratio of GST-CgBD1 progressively decreased, but it values above 3 could still be obtained in some conditions (**Figure 32B**).

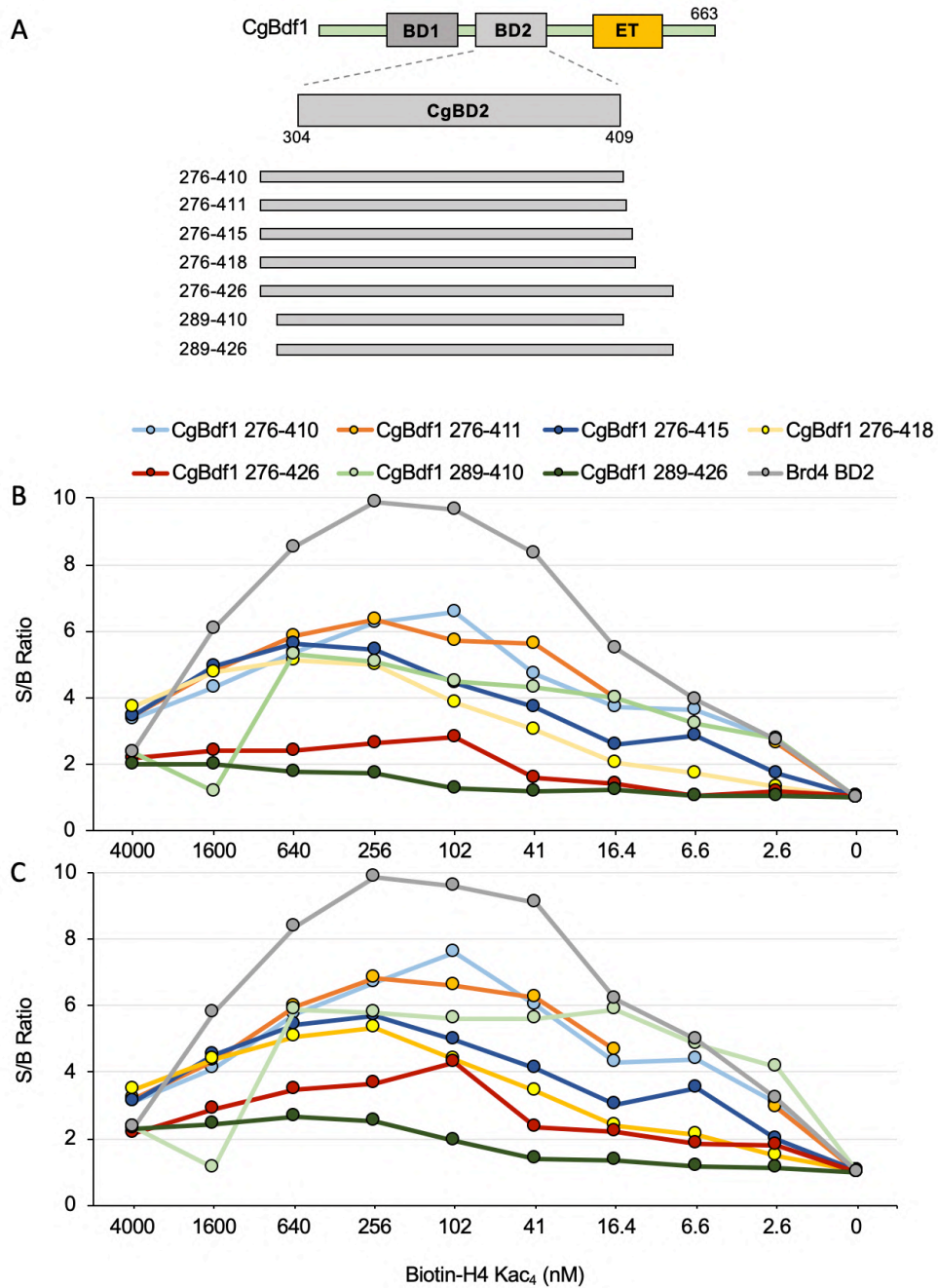


Figure 31. Comparison of seven CgBdf1 BD2 constructs and human Brd4 BD2 in an HTRF assay. A. The seven CgBD2 constructs. **B and C.** S/B ratio obtained of the CgBD2 constructs. Incubation was performed at 4°C for 4 hour (B) or 24 hours (C).

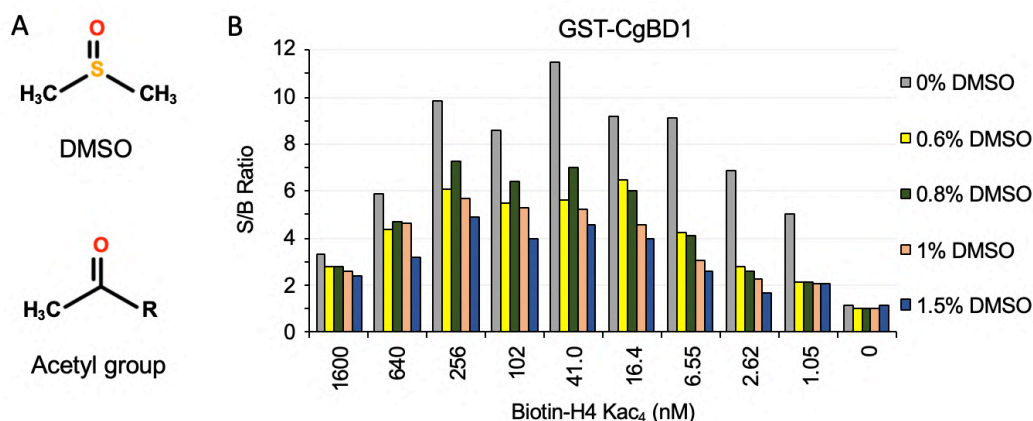


Figure 32. Effect of DMSO on HTRF assay performance. **A.** Structure of DMSO compared to that of the lysine acetyl group. **B.** S/B ratio of HTRF assay of GST-CgBD1. Incubation was performed for 4 hours at 4 °C.

Once the best constructs for CgBD1 and CgBD2 were defined, I repeated the purification based on 1 L of bacteria culture to have enough protein for chemical screening (**Figure 33A**). The results showed that the proteins or peptides with a molecular weight below that of GST-BDs were largely eliminated by including a SEC purification step using a Hiload Superdex 200 column (**Figure 33C and 33D**). At the end of each purification, I adjusted the final concentration of glycerol to 30% to allow long-term storage at -80 °C. Some sample information is shown in **Table 9**. The HTRF assay showed that the proteins obtained after SEC purification performed generally better than all others, especially when the Biotin-H4 Kac₄ concentration was low (**Figure 33E and 33F**).

I next used the SEC-purified GST-CgBD proteins for further characterization. This time, I added 1% of DMSO into the assay, since this was the concentration previously used to perform high-throughput chemical screening with bromodomain BD1 of CaBdf1 (Mietton *et al.*, 2017). In this condition, the S/B ratio of GST-CgBD1 could still reach about 8 (**Figure 34A**), significantly higher than the recommended minimum of 3. As for GST-CgBD2, the S/B ratio obtained was substantially lower than that for the CgBD1 construct. However, with 1% of DMSO, the S/B ratio could still be above 4 (**Figure 34B**). The final concentration of DMSO was then fixed at 1% for both CgBD1 and BD2 constructs. This concentration would allow the Calibr compound libraries to be tested at a final concentration of 20 µM during the screen. At this point the optimization of the S/B ratio was achieved and I could move on to the next optimization step.

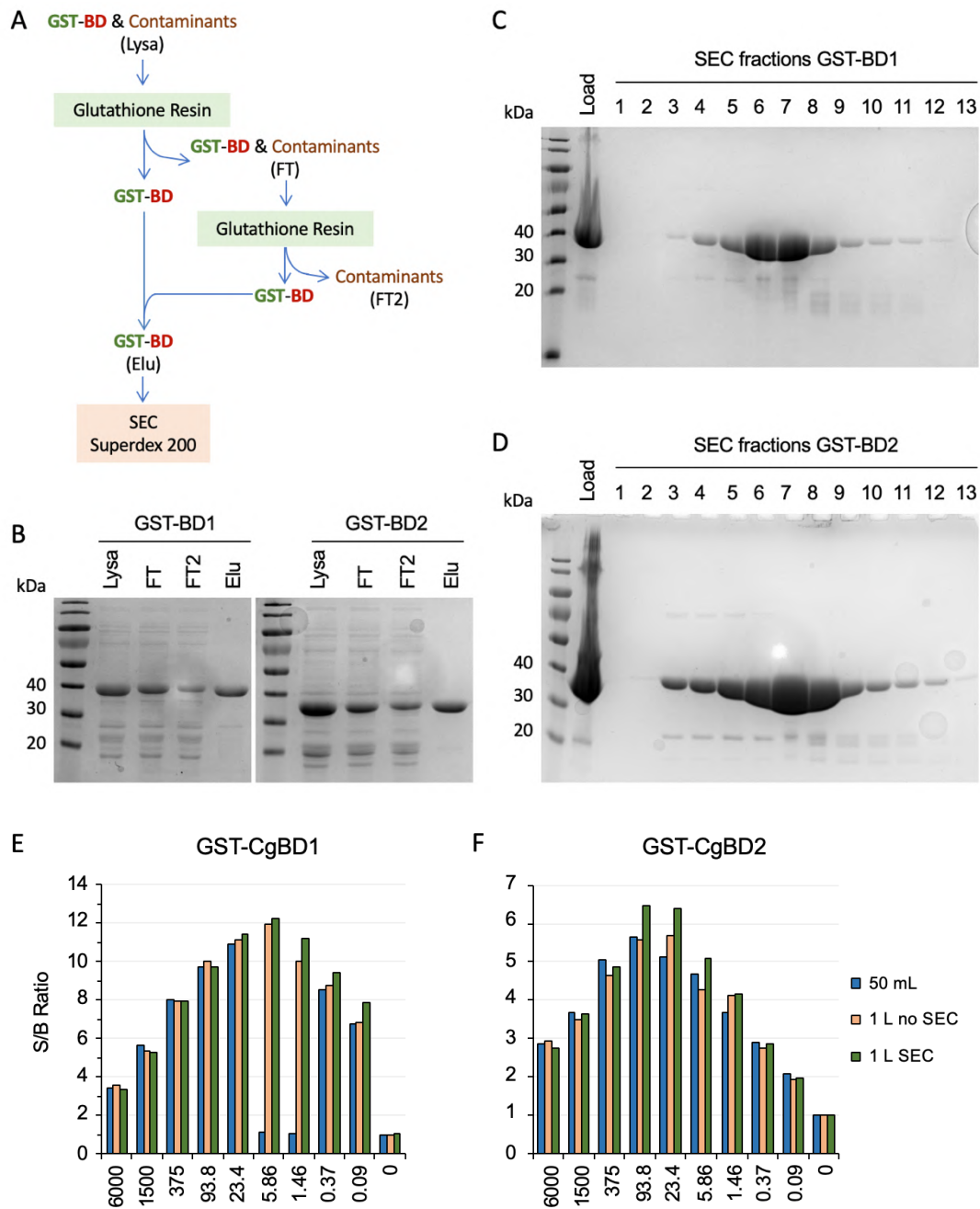


Figure 33. HTRF assays of GST-CgBDs exhibit an improved S/B ratio following size-exclusion chromatography (SEC). **A.** Flow chart summarizing the purification protocol of GST-CgBDs from 1L of bacterial culture. **B, C** and **D.** SDS-PAGE analysis of the purification of GST-CgBDs with glutathione affinity resin (**B**) and size-exclusion chromatography (**C** and **D**). Lysa: bacteria cellular lysate; FT and FT2: Flow through of different purification stages; Elu: Elution; Load: concentrated sample loaded onto the SEC column. **E** and **F.** S/B ratio of HTRF assay for different batches of GST-CgBD1 (**A**) and GST-CgBD2 (**B**). 50 mL: batch purified from 50 mL bacteria culture without the SEC step; 1 L no SEC: batch from 1 L bacteria culture without SEC purification; 1 L SEC: batch from 1 L bacteria culture with SEC purification. The incubation was performed at 4 °C for 4 hours for BD1 and 24 hours for BD2.

Table 9. Purification of GST-BDs from 1 L of bacteria culture.

Protein	Construct	Size (kDa)	Concentration (μ M)	Quantity (mg)	Aliquots
GST-CgBD1	120-259	42.095	110	35	2 μ L; 10 μ L;
GST-CgBD2	289-411	40.766	151.62	37	100 μ L

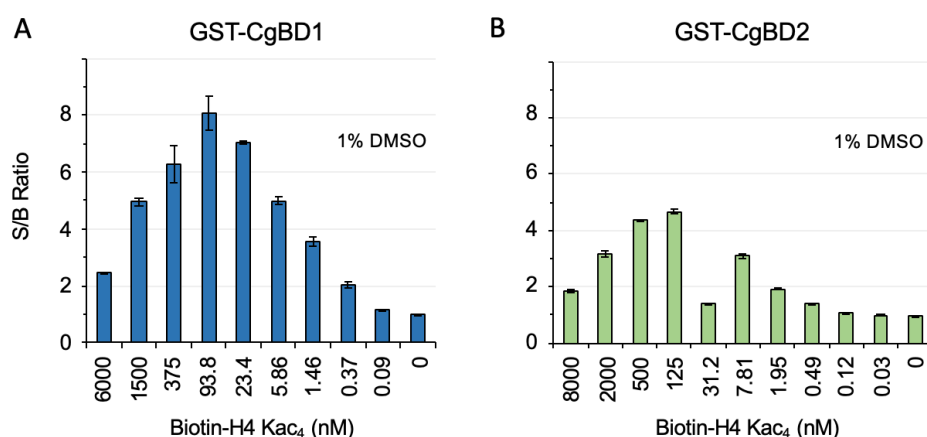


Figure 34. Final S/B ratios observed for GST-CgBD1 and CgBD2. **A** and **B.** S/B ratio of HTRF assay of GST-CgBD1 (**C**) and GST-CgBD2 (**D**) with 1% of DMSO. The incubation was performed at 4 °C for 4 hours for BD1 and 24 hours for BD2. Data are presented as means \pm SD from technical duplicates of each experiment.

3.1.2. Z' factor and final optimized HTRF conditions

The S/B ratio provides a useful criterion for evaluating the quality of a high-throughput screening assay by comparing the specific signal to the background signal. However, this ratio does not evaluate the variability of data measured in the assay or how reliably one can distinguish a true hit from a false positive. For this reason the so-called Z' factor is another critical parameter used to evaluate a high-throughput screening assay (Zhang, Chung and Oldenburg, 1999). The Z' factor is calculated as shown in [Figure 35A](#). The importance of the Z' factor is shown in [Figure 35B](#) and [35C](#). Data shown in both figures have the same mean value and variance for the background signal (negative control). For the specific signal (positive control, HTRF signal for HTRF assay), the mean is lower in [Figure 35B](#) than in [35C](#). Hence, the

calculated S/B ratio will show a higher value for the data in **Figure 35C**. However, it is hard to say that the data in **Figure 35B** are more reliable than in **35C**, because the variation level in **35C** is very high, indicating a non-stable specific signal produced. The calculated Z' factor is 5 times higher for the data in **Figure 35B** compared to **35C**, indicating that the former assay is better (more informative). In general, for efficient high-throughput screening one should use an assay with a Z' factor above 0.5.

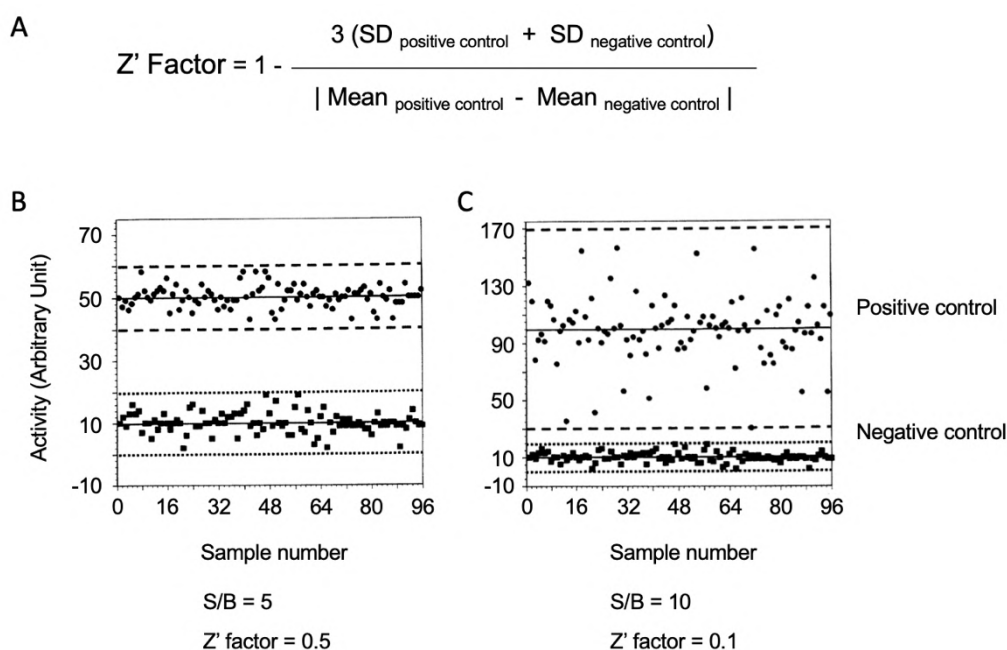


Figure 35. The use of Z' factor to evaluate a screening assay. **A.** Equation for calculating the Z' factor. **B** and **C.** Typical assay data from a single screening run using two different formats or conditions. The data measured in the negative control have a mean value of 10 and a 3(SD) value of 10 for both B and C. For the positive control, in B, the mean and 3(SD) values are 50 and 10, respectively, while they are 100 and 70 in C. The calculated S/B ratio is higher in C than in B, but the Z' factor is higher in B. (Figure adapted from J.-H. Zhang *et al.*, 1999)

In the HTRF assay, the negative control indicates the 100% inhibition level, which can be obtained using a high concentration of non-biotinylated acetylpeptide (Non biotin-H4 Kac₄). That Non biotin-H4 Kac₄ peptide competes with the biotinylated peptide for BD binding but cannot induce any energy transfer. The positive control gives 0% inhibition and represents the condition in which only the vehicle (DMSO) was additionally added.

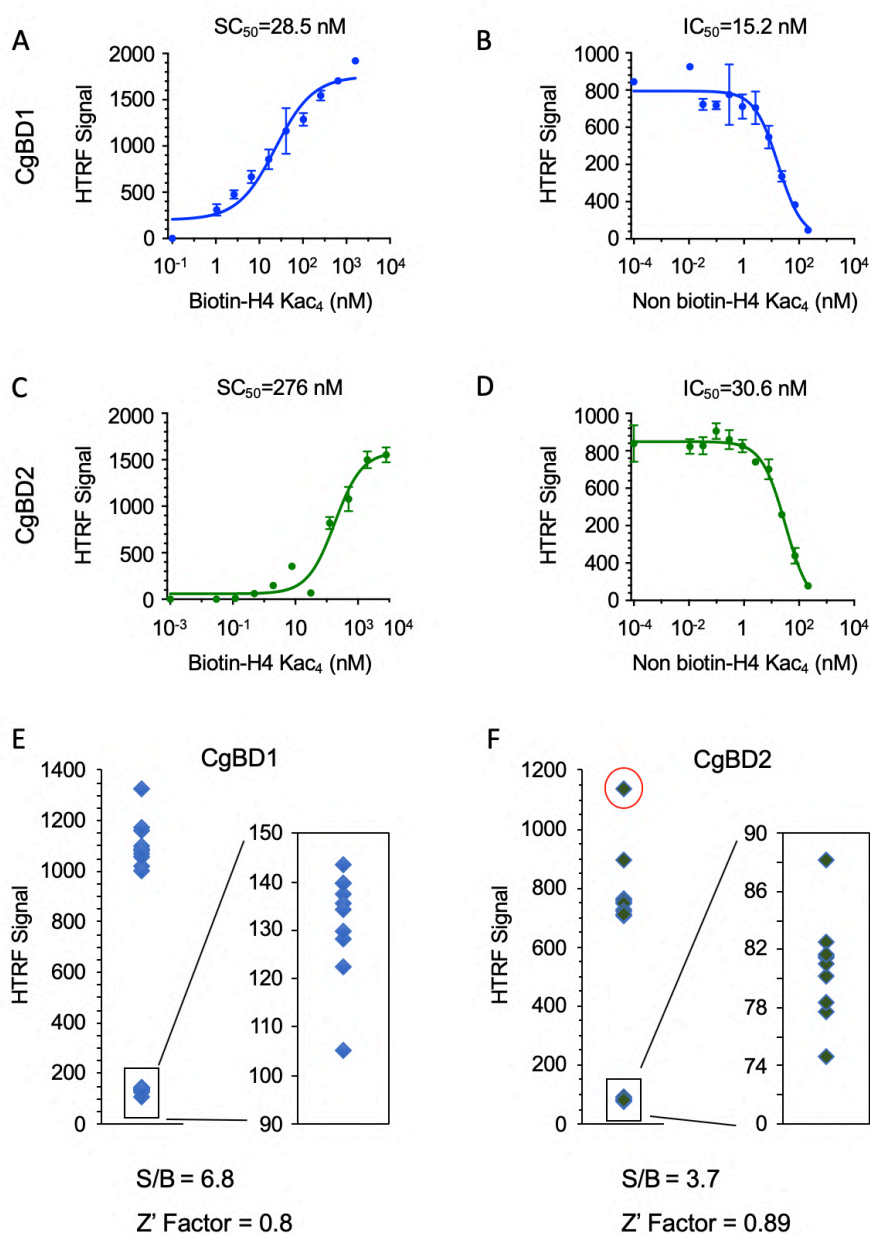


Figure 36. Characterization of GST-CgBDs by HTRF. **A** and **C**. Binding curve showing the dependence of HTRF signal on Biotin-H4 Kac₄ concentration. The half maximal stimulatory concentration (SC_{50}) of the biotin-acetylpeptide was calculated by fitting the data in GraphPad Prime 7 by using “log(agonist) vs. response (three parameters)” model. The incubation was performed at 4°C for 4 hours for BD1 and 24 hours for BD2. Data are presented as means \pm SD from technical triplicates performed for each experiment. **B** and **D**. Inhibition curves showing the decrease in HTRF signal observed for GST-CgBDs upon adding the non-biotin acetyl peptide. The incubation was performed at 4°C for 4 hours for BD1 and 24 hours for BD2. The half maximal inhibitory concentration (IC_{50}) was calculated using GraphPad Prime 7 by using “log(inhibitor) vs. response (three parameters)” model. Data are presented as means \pm SD from technical triplicates performed for each experiment. **E** and **F**. Plot of HTRF signals obtained for the positive (vehicle, upper points) and negative (non-biotinylated acetylpeptide, lower points) controls allowing calculation of the Z' factor. Z' factor tested by using 106.5 μ M or 213 μ M non-biotinylated acetylpeptide for BD1 and BD2, respectively. The concentration used of the biotin-H4 Kac₄ peptide was 30 nM for BD1 and 250 nM for BD2. The incubation was performed at 4°C for 4 hours for BD1 and 24 hours for BD2. The outlier for GST-CgBD2 is marked in red and was not used to calculate the Z' factor.

The biotin-acetylpeptide concentration was fixed during the chemical screening. Its concentration needed to be optimized so as to keep the S/B ratio as high as possible, but also be as close to the half maximal stimulatory concentration (SC_{50}) of Biotin-H4 Kac₄ as possible. The next step was therefore to determine the SC_{50} of the the Biotin-H4 Kac₄/GST-BD interaction. The results showed that the EC_{50} of the biotin-acetylpeptide was about 30 nM for GST-BD1 and 275 nM for GST-BD2 (**Figure 36A and 36C**). The concentration of the Biotin-H4 Kac₄ in HTRF screening assay was then fixed at 30 nM for the GST-BD1 construct and 250 nM for GST-BD2.

I then tested the inhibition effect in the HTRF assay by using different concentrations of Non biotin-H4 Kac₄. As one component (inhibitor) was added to the HTRF system, the conditions of HTRF assay were changed and summarized in **Table 10**. The plate loading was also changed and shown in order as follows: (i) GST-BD, Biotin-H4 Kac₄, Anti-GST-Tb, SA-D2 and DMSO were mixed in the correct concentration. Because there were only two proteins to be tested, only two master mixes were prepared. (ii) For the negative control, 2 μ L of Non biotin-H4 Kac₄ were loaded at different concentrations. (iii) For the positive control, 2 μ L of buffer (containing DMSO) were loaded. (iv) 18 μ L of master mix were loaded into each well.

Table 10. HTRF conditions for inhibition test.

	Final concentration (nM)	Total volume (μ L)	Incubation
GST-BD	5	4	4 hours (BD1) or 24 hours (BD2) at 4 °C
Biotin-H4 Kac ₄	30 (BD1) or 250 (BD2)	4	
Anti-GST-Tb	0.5	5	
SA-D2	3.75 (BD1) or 31.25 (BD2)	5	
Non biotin-H4 Kac ₄	To be determined	2	

The half maximal inhibitory concentration (IC_{50}) values of Non biotin-H4 Kac₄ determined were 15.2 μ M for GST-BD1 and 30.6 μ M for GST-BD2 (**Figure 36B and 36D**). The fact that these two values were relatively close indicated that the concentrations of Biotin-H4 Kac₄ chosen for GST-BD1 and GST-BD2 were reasonable.

To obtain 100% inhibition, a high concentration of Non biotin-H4 Kac₄ was needed. For CgBD1, the concentration of 106.5 μ M (3550 times that of the Biotin-H4 Kac₄) was finally used to perform the Z' factor test. The Z' factor obtained was about 0.8 with a S/B ratio about 6.8 (**Figure 36E**). Both these values were high enough to permit chemical screening. As for GST-BD2, I finally used a non-biotinylated peptide concentration of 213 μ M (852 times that of the biotinylated peptide) to perform the Z' factor test. The Z' factor obtained was above 0.85 when a significant outlier was removed from the statistical analysis (**Figure 36F**). With a S/B ratio of 3.7, GST-BD2 provided parameters sufficient for screening as well.

In summary, I finished optimizing the HTRF assay for both CgBD1 and CgBD2. The optimized conditions are summarized in **Table 11**. The assay was ready for further optimization by our collaborators at Calibr, who would miniaturize the assay and perform a high throughput chemical screen to identify specific inhibitors of CgBD1 and CgBD2.

Table 11. HTRF conditions for chemical screening.

	Final concentration (nM)	Total volume (μ L)	Incubation
GST-BD	5	4	4 hours (BD1) or 24 hours (BD2) at 4 °C
Biotin-H4 Kac ₄	30 (BD1) or 250 (BD2)	4	
Anti-GST-Tb	0.5	5	
SA-D2	3.75 (BD1) or 31.25 (BD2)	5	
Compound in DMSO	Up to 1% of DMSO	2	

Table 12. Comparison between the HTRF assay developed here and that developed for CaBD2 previously.

	CgBD2	CaBD2
Biotin-H4 Kac ₄ concentration	250 nM	400 nM
DMSO concentration	1%	0.4% or 0.8%
S/B Ratio	> 3.5	3.5 (0.4% DMSO) or 2.3 (0.8% DMSO)
Z' Factor	> 0.8	0.8 (0.4% DMSO) or 0.7 (0.8% DMSO)

Compared to the HTRF assay previously developed in the lab for CaBDs, the assays I developed showed advantages, especially for CgBD2 (**Table 12**). First of all, the assay for CgBDs

allows us to consume less biotin-acetylpeptide and Streptavidin-d2, which substantially decreases the cost of the assay. Secondly, the assay optimized here is adapted with a DMSO concentration of 1% for both CgBD1 and CgBD2, which will allow Calibr to screen their compound libraries at a final concentration of 20 μ M. In the former screen performed for the CaBDs, over 200 hits were identified against CaBD2, but the assay only allowed a maximum of 0.4 to 0.8% DMSO. With 1% DMSO, a higher compound concentration can be screened, which should allow one to discover a larger number of hit compounds against CgBD2.

3.2. *In vitro* effect of four human BET bromodomain inhibitors on *C. glabrata* Bdf1 bromodomains

The HTRF chemical screening assay was optimized, but I still needed to verify that this assay could identify small-molecule inhibitors of the CgBDs. In our lab, four human BET inhibitors (BETis) – JQ1, I-BET151, Bromosporine and PFI-1 – were readily available. I used the optimized assay to test the sensitivity of CgBDs to these human BET inhibitors. The conditions used for CgBDs and human Brd4 bromodomains (hBDs) (taken from Mietton et al., 2017) are shown in [Table 10](#) and [Table 13](#), respectively. The compounds were already dissolved in DMSO at 50 mM. To ensure that the DMSO concentration was the same in different concentrations of compounds, I performed a serial dilution of compounds with 100% DMSO before diluting them with buffer to a correct concentration. The final concentration of DMSO used here was 0.2%. The microplate loading protocol was very similar to that for the Non biotin-H4 Kac₄ and was as follows: (i) The GST-BD, Biotin-H4 Kac₄, Anti-GST-Tb and SA-D2 were mixed at the correct concentrations. Because only two proteins were to be tested, only two master mixed were prepared. (ii) 2 μ L of compounds were loaded at different concentrations in 2% of DMSO. (iii) 18 μ L of master mix were loaded into each well.

The results shown in [Table 14](#) demonstrate that most of the BETi compounds inhibited all four bromodomains tested. However, the inhibition of the hBDs was >100-fold more potent compared to that of the CgBDs. This finding is consistent with the crystal structures of CgBD1 and CgBD2, which revealed ligand binding pockets quite distinct from those of the human BDs (section 2.3 of this Chapter). JQ1 had a very similar effect against both hBDs, but was ~8-fold more effective at inhibiting CgBD2 compared to CgBD1. I-BET151 was comparable to JQ1 in its

ability to inhibit the CgBDs, but this compound inhibited hBD1 better than hBD2 via the HTRF assay. Bromosporine inhibited CgBD2 with a somewhat higher IC₅₀ compared to JQ1 and I-BET151 and, like JQ1, had little activity against CgBD1. PFI-1 was almost inactive against both CgBDs. Of the four compounds, I-BET151 is the most interesting, as it showed the lowest IC₅₀ for both CgBD1 and CgBD2 compared to the other inhibitors.

Table 13. HTRF conditions for human BET bromodomains. (data from Mietton et al., 2017)

	Final concentration (nM)	Total volume (μL)	Incubation
GST-BD	5	4	
Biotin-H4 Kac ₄	50 (BD1) or 600 (BD2)	4	4 hours (BD1) or
Anti-GST-Tb	0.5	5	24 hours (BD2)
SA-D2	6.25 (BD1) or 75 (BD2)	5	at 4 °C
Compound in DMSO	Up to 20 μM	2	

Table 14. Inhibition effects of human BETis.

Compound	IC ₅₀ (nM)*			
	CgBD1	CgBD2	hBD1**	hBD2**
JQ1***	23700 ± 6450	2960 ± 719	91 ± 59	48 ± 29
I-BET151***	4770 ± 956	1630 ± 429	17 ± 18	51 ± 66
Bromosporine***	17800 ± 5480	4370 ± 199	130 ± 138	51 ± 67
PFI-1****	23200 ± 707	ND	35	150

*CgBD binding inhibition IC₅₀ calculated by GraphPad Prime 7.

** hBD1 and hBD2 represent respectively BD1 and BD2 from human Brd4.

** IC₅₀ data are presented as means ± SD, n=3 independent experiments for CgBDs, n=2 independent experiments for hBDs.

*** IC₅₀ data are presented as means ± SD, n=2 independent experiments for CgBD1, n=1 experiment for all the others.

The IC₅₀ value varied a lot for the previous tests, suggesting that the compounds used might lose some activities during the performance of those tests. Learning that all those compounds had been dissolved and stored at -20 °C for a long time, I then dissolved a new batch of JQ1 and I-BET151 powder that had been stored at -80 °C. I aliquoted the new dissolved molecules and stored them all at -80 °C. By using these new prepared inhibitors, I re-performed the HTRF assay. Results showed similar tendencies compared to the previous

tests, but with a lower IC_{50} (Figure 37A and 37B). Thus, the new batch of BETis appeared more active than the old batch and were consequently used for all future tests.

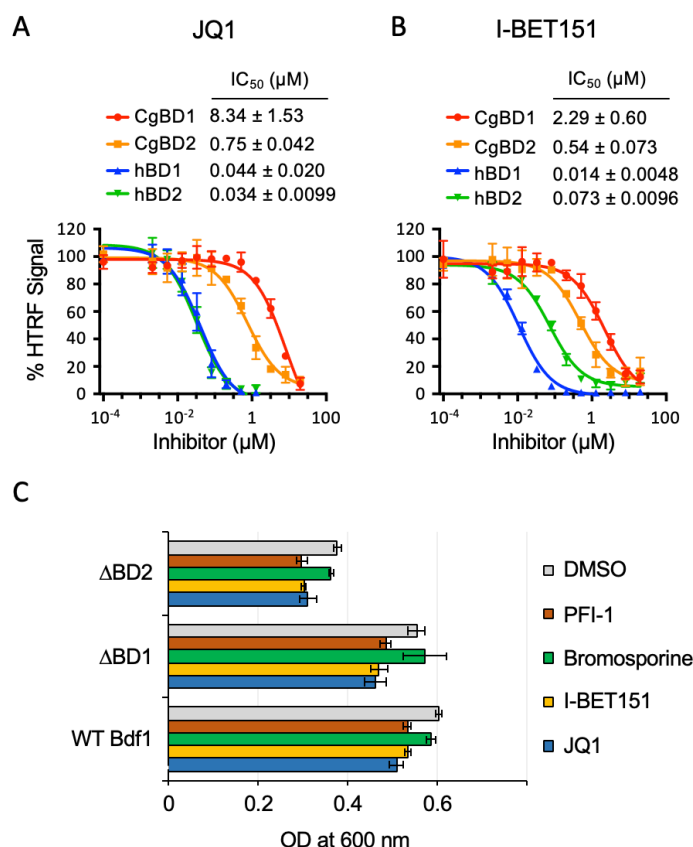


Figure 37. Four human BET inhibitors inhibit Bdf1 bromodomains in HTRF assays but not yeast viability. A and B. CgBD binding inhibition curves obtained by HTRF assays and IC_{50} values calculated by GraphPad Prime 7 by using “log(inhibitor) vs. response (three parameters)” model. Data are presented as means \pm SD, $n \geq 2$ independent experiments. hBD1 and hBD2 represent respectively BD1 and BD2 from human Brd4. C. Growth test of *C. glabrata* co-incubated with human BET inhibitors. WT Bdf1, Δ BD1 and Δ BD2 represented the strains expressing only wildtype Bdf1 or Bdf1 deleted for either BD1 or BD2, respectively. Data are presented as means \pm SD from technical triplicates performed for each experiment.

The relatively low IC_{50} suggested that some of these inhibitors might have an effect on the ability of *C. glabrata* to grow. I therefore next tested the viability of yeast in the presence of the human BET inhibitors. The *C. glabrata* strains used were those generated in section 1.2, in which the endogenous *BDF1* promoter was replaced by the *MET3* promoter. The expression of endogenous *BDF1* was suppressed by an incubation of 23 hours with methionine and cysteine and hence only the WT or mutant Bdf1 protein encoded by the plasmid was expressed. These strains were then incubated with different inhibitors for 24 hours and their

viability was assessed. None of the strains incubated with BET inhibitors showed any viability defect compared to those incubated with DMSO alone (**Figure 37C**), indicating that none of the tested compounds can inhibit the growth of *C. glabrata*.

3.3. Discovery of *C. glabrata* Bdf1 bromodomain 1 inhibitors

The conditions of HTRF assay that I optimized (shown in **Table 10**) required a final volume of 20 μL for each well. This volume was too large for the automated chemical screen to be performed at Calibr, which allowed only up to 5 μL as the final volume in each well. In order to adapt to this requirement, I re-optimized the volume of the HTRF assay, as shown in **Tables 15** and **16**.

Table 15. HTRF conditions for Z' factor determination in Calibr.

	Final concentration (nM)	Total volume (μL)	Incubation
GST-BD	5	1	
Biotin-H4 Kac ₄	30 (BD1) or 250 (BD2)	0.5	
Non biotin-H4 Kac ₄	213 000	0.5	4 hours (BD1) or 24 hours (BD2)
Anti-GST-Tb	0.5	1.25	at 4 °C
SA-D2	3.75 (BD1) or 31.25 (BD2)	1.25	
DMSO	1%	0.5	

Table 16. HTRF conditions for chemical screening in Calibr.

	Final concentration (nM)	Total volume (μL)	Incubation
GST-BD	5	1	
Biotin-H4 Kac ₄	30 (BD1) or 250 (BD2)	0.5	
Buffer	-	0.5	4 hours (BD1) or 24 hours (BD2)
Anti-GST-Tb	0.5	1.25	at 4 °C
SA-D2	3.75 (BD1) or 31.25 (BD2)	1.25	
Compound in DMSO	20 000 (1% DMSO)	0.5	

The acetylated histone peptide coupled or not with biotin, Anti-GST-Tb and SA-D2 were re-purchased and sent directly to our collaborators at the University of Southern California (USC) in Los Angeles. The purified GST-BDs divided into large aliquots (10 and 100 μ L) were also sent to the USC on dry ice. All these components were used to perform the chemical screening at Calibr by postdoc Nathan Dupper and PhD student Yingsheng Zhou, our collaborators at USC in the laboratory of Dr. Charles E. McKenna.

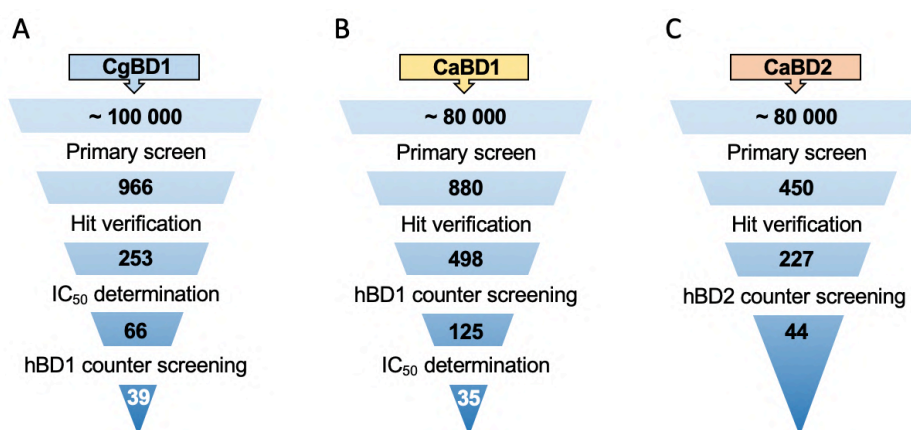


Figure 38. Screening workflow to identify selective CgBD1 (A), CaBD1 (B) and CaBD2 (C) inhibitors. (Data for B and C are from Mietton *et al.*, 2017)

Our USC collaborators chose to begin with CgBD1 because the HTRF assay with this construct provided a better S/B ratio and Z' factor. Before performing the full screen, the assay was validated once again in a small-scale pilot screen to check that the S/B ratio and Z' factor were still acceptable using the smaller volume and a totally automated liquid handling procedure. Once it was done, the full chemical screen was performed.

As shown in **Figure 38**, about 100 000 compounds were tested in the first round and 966 hits were identified. This number was comparable to that obtained in the screen performed previously for CaBD1 (880 hits) and about twice that obtained for CaBD2 (450 hits). After the primary screen, the identified hits were specifically retested to control for false positives. In this test only 253 hits were verified, indicating that more than 70% of the primary positive hits were false. This rate was significantly higher than those previously obtained for both CaBDs, which were about 50%. After that, the screening strategy was slightly modified compared to that used for the CaBDs. Instead of counter screening the hits against the hBDs

at a single concentration, our collaborators performed IC₅₀ determinations for all 253 verified hits against both CgBDs and hBD1 and then sent me the results. Using IC₅₀ < 5 µM as a selection criterion and by inspecting the shape of the inhibition curves, I defined 66 compounds as positive CgBD1 inhibitors.

It was mentioned in Chapter I and section 1.2 of this Chapter that the simultaneous inhibition of both bromodomains was necessary to inhibit the growth of both *C. albicans* and *C. glabrata*. However, during the screening for CaBDs, our lab did not find any compound that inhibited both bromodomains of CaBdf1 (Mietton *et al.*, 2017). Because of that, they needed to find strategies to combine two inhibitors targeting the separate CaBDs. Surprisingly, however, among the 66 inhibitors identified for CgBD1, several were found to also inhibit CgBD2. In fact, 17 molecules had an IC₅₀ < 10 µM against CgBD2 and were defined as dual CgBD inhibitors. On the other hand, I defined CgBD1 inhibitors having an IC₅₀ > 5 mM against hBD1 as selective CgBD1 inhibitors and there were 39 in this group. At the end, 11 compounds were identified that showed selective inhibition against both CgBDs versus hBD1.

3.4. Conclusion

As a key objective, the optimization of the HTRF assay for CgBD inhibitor screening could directly decide the success of my Ph.D. project. I tested several constructs for both CgBD1 and CgBD2 and identified the best assay conditions. The optimized HTRF assay provided a high S/B ratio and Z' factor both for manually performed assays using relatively large volumes and in highly miniaturized assays automated by liquid handling robots, which could guarantee reliable results of the chemical screening. Unlike the project previously performed in the lab concerning CaBdf1, molecules that simultaneously targeted both bromodomains of CgBdf1 were successfully identified. Moreover, some of these dual CgBD inhibitors did not inhibit human Brd4 BD1, which is very promising for potential antifungal agent development. These compounds would be further validated in manual assays to determine IC₅₀ values for both CgBDs and human BDs. Their capacity to inhibit *C. glabrata* cell growth would also be tested.

4. *In vitro* characterization of screening hits

4.1. *In vitro* hit validation

In the previous section, our collaborators at USC performed the high-throughput chemical screening for CgBD1 and identified 66 compounds as potential inhibitors against this protein. They also found that of those 66 molecules, 63 were commercially available. We then purchased these compounds from ChemDiv as a powder and dissolved them in DMSO at a final concentration of 50 mM without further purification. They were aliquoted and stored all at -80 °C. I named those compounds iCG-1 to 63, where iCG stands for “inhibitor for *C. glabrata*”. All 63 compounds would be tested in manual HTRF assays in order to validate their activity in CgBD1 inhibition.

4.1.1. High-throughput adaption for in bench HTRF assay

The HTRF assay that I previously optimized required loading the plate one well at a time. For testing a few numbers compounds, this not a problem. However, to test 63 compounds, this method was too slow. For this reason, with the help of Marjolaine Noirclerc-Savoye in our lab at the IBS, the HTRF assay was optimized once again, especially for the plate loading process, to allow me to test many compounds all in the same day.

When a reaction volume of 20 µL was loaded, the wells of the plate were almost totally filled. This was not a problem when I manually loaded wells one at a time. However, if I wanted to load several wells in parallel, it risked causing an undesired overflow of the wells. To avoid this risk, Morjolaine recommended me to decrease the total volume in each well from 20 µL to 16 µL.

Once the assay conditions were changed, the S/B ratio and Z' factor were determined against to verify if they still were sufficiently high. The conditions used are shown in [Table 17](#). For GST-CgBD1, the S/B ratio and Z' factor were still high enough, although the S/B ratio was lower than in the previous test ([Figure 39A](#)). However, for GST-CgBD2 these two factors gave a very low value: the S/B ratio was lower than 3 and the Z' factor lower than 0.5, indicating a poor quality assay. The problem might be due to the acetylated peptide used, which always

came from the same aliquot that had been subjected to freeze-thaw cycles for more than a year.

To solve this problem, I prepared a new batch of Biotin-H4 Kac₄ from the powder stored at -80 °C. The use of this new peptide rescued the HTRF assay quality. In both 20 μ L and 16 μ L conditions, the S/B ratio was higher than 3 and the Z' factor higher than 0.6 for GST-CgBD2 (**Figure 39C and 39D**). There was no significant difference between the assays with 20 μ L and 16 μ L reaction volumes, indicating that the smaller volume could be used for inhibitor validation.

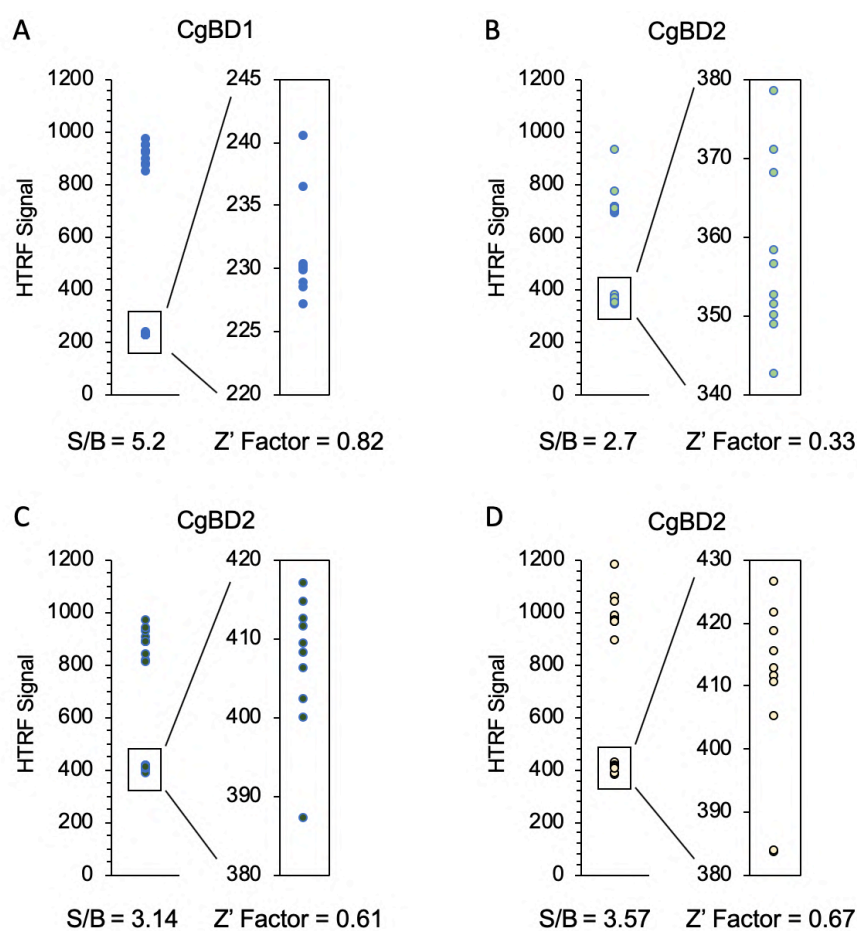


Figure 39. Z' factor and S/B ratio given by the two GST-CgBDs in different conditions. Z' factor tested using 106.5 μ M or 213 μ M non-biotinylated acetylpeptide for BD1 and BD2, respectively. The concentration used of the biotin-H4 Kac₄ peptide was 30 nM for BD1 and 250 nM for BD2. The incubation was performed at 4°C for 4 hours for BD1 and 24 hours for BD2. **A** and **B**. Z' factor and S/B ratio given by CgBD1 (A) and CgBD2 (B) with the old batch of biotin-H4 Kac₄ peptide in 16 μ L reaction volumes. **C** and **D**. Z' factor and S/B ratio given by CgBD2 with the new batch of biotin-H4 Kac₄ peptide in 20 μ L (C) and 16 μ L (D) reaction volumes.

Table 17. HTRF conditions for Z' factor test.

	Final concentration (nM)	Total volume (μL)	Incubation
GST-BD	5	2	4 hours (BD1) or 24 hours (BD2) at 4 °C
Biotin-H4 Kac ₄	30 (BD1) or 250 (BD2)	4	
Anti-GST-Tb	0.5	4	
SA-D2	3.75 (BD1) or 31.25 (BD2)	4	
DMSO	1%	0.4	
Non biotin-H4 Kac ₄	213 000	1.6	

4.1.2. Hit confirmation and IC₅₀ determination

Once the quality control of the assay was finished, hit confirmation was performed. The conditions are shown in Table 18 and the plate loading process was adapted as follows: (i) The GST-BD, Biotin-H4 Kac₄, Anti-GST-Tb and SA-D2 were mixed at the correct concentrations. Because only four proteins were to be tested, four master mixed were prepared. (ii) 14 μL of master mix were loaded into each well with an electronic multichannel pipette (Thermo Scientific™ 4671040BT). (iii) 2 μL of compounds were loaded at different concentrations in 1.6% of DMSO (the final concentration of DMSO is 0.2%). (iv) The well was mixed gently by pipetting up and down 6 times.

Table 18. HTRF conditions for inhibitor validation.

	Final concentration (nM)	Total volume (μL)	Incubation
GST-BD	5	2	4 hours (BD1) or 24 hours (BD2) at 4 °C
Biotin-H4 Kac ₄	50 (BD1) or 600 (BD2)	4	
Anti-GST-Tb	0.5	4	
SA-D2	6.25 (BD1) or 75 (BD2)	4	
Compound in DMSO	Up to 20 μM	2	

The first round of confirmation aimed to perform a quick determination of the IC₅₀ value of all 63 compounds and I performed only a single assay for each compound without performing replicates. The results are shown in Appendix III. I next defined confirmed inhibitors as those having an IC₅₀ lower than 5 μM. Unfortunately, using this definition, only

13 molecules could still be considered as CgBDs inhibitors (confirmation rate about 21%). To verify these results, I independently repeated two more times the IC₅₀ determinations for those compounds. The final IC₅₀ values are presented in [Table 19](#).

The compounds iCG-53 did not pass the confirmation step: only the first test showed an IC₅₀ lower than 5 μ M, whereas the second and third assays gave much higher values. The other 12 molecules, which reproducibly gave IC₅₀ values below 5 μ M, are shown in [Figure 40A](#). Based on their ability to inhibit different GST-BDs, they were classified into three groups.

The first group contains the selective CgBD1 inhibitors. It was the biggest group containing 6 molecules: iCG compounds 30, 32, 45, 55, 56 and 63. The compounds in this group selectively inhibited CgBD1 with little or no effect on CgBD2 and the two Brd4 bromodomains. The highest inhibition capacity was found in this group: iCG compounds 55, 56 and 63 showed IC₅₀ values of about 500 nM or lower, significantly more active compared to previously identified inhibitors against CaBDs (Mietton *et al.*, 2017).

Table 19. IC₅₀ of validated CgBDs inhibitors.

Compound ID in lab	IC ₅₀ (μ M) ⁽¹⁾			
	CgBD1	CgBD2	hBD1 ⁽²⁾	hBD2 ⁽²⁾
iCG-2	4.97 \pm 0.77	0.97 \pm 0.25	21.8 \pm 3.6	2.93 \pm 0.57
iCG-5	1.95 \pm 0.35	2.22 \pm 1.68	3.07 \pm 0.52	1.33 \pm 0.06
iCG-16	4.65 \pm 2.74	0.23 \pm 0.08	1.13 \pm 0.29	1.57 \pm 0.10
iCG-24	2.09 \pm 0.13	47.7 \pm 25.5	> 100 ⁽³⁾	> 100
iCG-29	1.81 \pm 1.14	2.06 \pm 0.23	2.73 \pm 0.34	0.52 \pm 0.20
iCG-30	0.96 \pm 0.32	ND ⁽⁴⁾	> 100	> 100
iCG-32	2.84 \pm 0.59	ND	> 100	> 100
iCG-43	2.87 \pm 0.25	~ 1.82 ⁽⁵⁾	~ 46.4 ⁽⁵⁾	ND
iCG-45	3.08 \pm 1.86	ND	> 100	ND
iCG-53	~ 32.6 ⁽⁵⁾	ND	ND	ND
iCG-55	0.10 \pm 0.03	ND	ND	ND
iCG-56	0.38 \pm 0.17	ND	ND	ND
iCG-63	0.61 \pm 0.10	ND	> 100	ND

(1) GST-BD binding inhibition IC₅₀ calculated by GraphPad Prime 7 by using “log(inhibitor) vs. response (three parameters)” model. Data are presented as means \pm SD, n \geq 2 independent experiments.

(2) hBD1 and hBD2 represent respectively BD1 and BD2 from human Brd4.

(3) > 100, IC₅₀ value calculated by GraphPad Prime 7 higher than 100 μ M (weak effect).

(4) ND, not determined (almost no effect).

(5) The IC₅₀ values varied too much, SD was at the same level or bigger than means, only the mean value was presented.

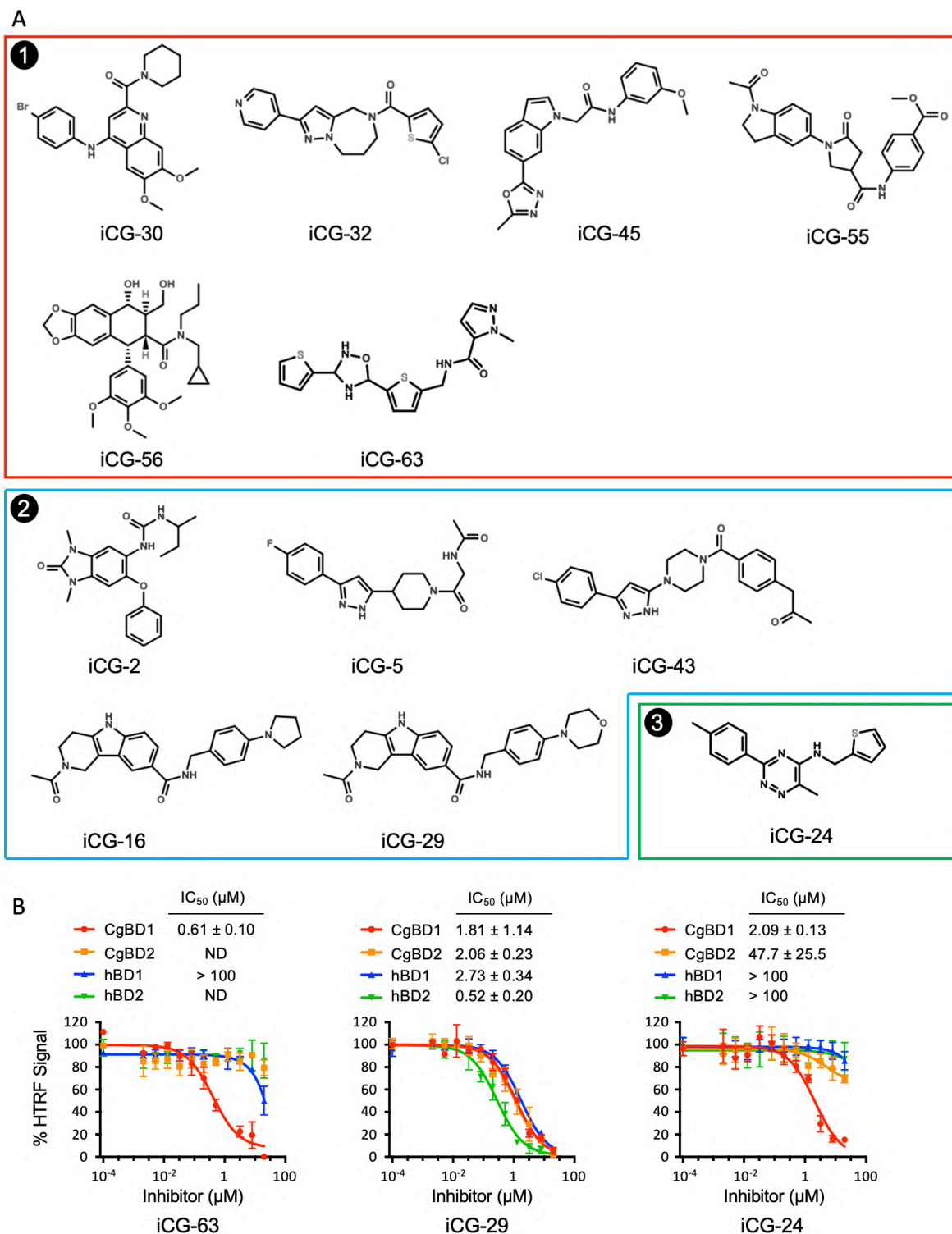


Figure 40. Confirmed hits against CgBD1. **A.** Structure of confirmed CgBD1 hit compounds. The three groups based on their inhibition ability are marked. Group 1 represents selective CgBD1 inhibitors; group 2 represents non-selective dual CgBD inhibitors; group 3 contained only one molecule as a selective dual CgBD inhibitor. **B.** Examples of inhibition curves and IC₅₀ values calculated by GraphPad Prime 7 by using “log(inhibitor) vs. response (three parameters)” model. Data are presented as means ± SD, $n \geq 2$ independent experiments. hBD1 and hBD2 represent respectively BD1 and BD2 from human Brd4.

The second group contained 5 compounds, namely iCG compounds 2, 5, 16, 29 and 43. This group of molecules showed inhibition against both CgBDs as well as the two hBDs and hence were defined as non-selective dual CgBDs inhibitors. Two compounds, iCG-2 and iCG-16 showed a higher affinity against CgBD2 than CgBD1. This group was missing in the previous study concerning CaBD inhibitors (Mietton *et al.*, 2017). Considering that yeast growth inhibition requires targeting both Bdf1 bromodomains, molecules in this group are potentially very interesting. However, it should be noted that the inhibition activity of compounds in this group is lower than those in the first group against CgBD1.

Compound iCG-24 composed the third group alone. This molecule inhibited both CgBD1 and CgBD2, even though the inhibition of the latter was quite weak compared to the former. Moreover, it showed a very weak effect on hBDs inhibition. Accordingly, compound iCG-24 was classified as a selective dual CgBD inhibitors and was the most interesting compound to pursue further.

4.2. Structural basis of CgBD inhibition

So far, the chemical screening had identified hits against CgBD1 and I confirmed 12 of these and classified them into three groups. Group 1 inhibited only CgBD1, group 2 inhibited both CgBDs and Brd4 BD2s, group 3 targeted only the two CgBDs. Next I tried to find out the mechanism to explain these different inhibition activities. I would try to co-crystallize these compounds with both CgBDs in order to determine their binding mode.

4.2.1. Structural basis of I-BET151 and JQ1 resistance by CgBDs

Before the chemical screen, I had already found out that JQ1 and I-BET151 could inhibit hBDs much more potently CgBDs (section 3.2 of this chapter). While the chemical screen was being performed in the USA, I set out to co-crystallize these two molecules with the two bromodomains of CgBdf1. All the structures in this section were solved by my supervisor Carlo Petosa. Crystallographic statistics are shown in appendix II.

4.2.1.a. Co-crystallization of CgBD1 with I-BET151

I began with I-BET151 because it had shown a lower IC_{50} against both CgBDs. I purified a new batch of the protein CgBD1 (residues 128-237) and concentrated it to 51.8 mg/mL. A 50 mM frozen aliquot of I-BET151 was diluted to 25 mM and mixed with the purified protein before being used to screen for crystallization conditions at the EMBL HTX facility. I-BET151 is soluble in DMSO but its solubility in water is low. A concentration above 25 mM in DMSO will lead to the precipitation of this compound if diluted directly in aqueous solution. Since DMSO can denature proteins, a high concentration of I-BET151 cannot be used in order to avoid a high final concentration of DMSO. I finally decided to test an iBET151/CgBD molar ratio of 1 for CgBDs at 25 mg/mL and at 15 mg/mL, and of 2 for CgBDs at 15 mg/mL (Table 20).

Table 20. Mix of CgBD1 and I-BET151 (25 mM in DMSO).

[I-BET151]/[Protein]	Final protein concentration (mg/mL)	Final I-BET151 concentration (mM)	Final DMSO concentration
1	25	1.93	7.72%
1	15	1.16	4.64%
2	15	2.32	9.28%

Table 21. Positions of crystallization plate that form co-crystals of CgBD1 with I-BET151. All the conditions can be found in Appendix I.

Plate	Plate position		
	I-BET151/CgBD1 = 1		I-BET151/CgBD1 = 2
	25 mg/mL	15 mg/mL	15 mg/mL
Salt-Grid_hampton	G9*		
PACT_MD	B10, B11, C10, C11 D11	C11, D11	
JCSG_MD			D4
Classics-Suite_qiagen	G11, H6	H6	

* Conditions are written in bold only the first time they appear in each row.

After 7 days of incubation, some crystals began to appear and by the end of 15 days, bigger crystals were observed in 9 conditions (Table 21). In contrast to the previous crystallization trials with apo CgBD1, that yielded single crystals within 72 hours in 30 crystallization conditions (Table 7), most of the drops here were observed to remain clear. This indicated that I-BET151 and DMSO might increase the solubility of this protein. Since DMSO is also a weak bromodomain ligand a high concentration might conceivably increase the solubility of CgBD1. That might also explain why crystals were only observed in one condition when the I-BET151/CgBD1 ratio was 2, since the DMSO concentration was nearly 10%.

Table 22. Crystallization conditions for manual hanging drops test of CgBD1 with I-BET151.

Precipitant	Precipitant concentration	Buffer	Protein concentration	[I-BET151]/[CgBD1]
PEG 4000	24-34%	0.1 M Tris pH 8.5 0.2 M CH ₃ COONa	10, 15, 25 and 50 g/L	2 or 1
PEG 6000	14-24%	0.1 M Tris pH 8 0.2 M CaCl ₂	" " " " "	" " "
PEG 6000	14-24%	0.1 M Hepes pH 7 0.2 M MnCl ₂	" " " " "	" " "
PEG 6000	14-24%	0.1 M Hepes pH 7 0.2 M CaCl ₂	" " " " "	" " "
PEG 2000	24-34%	0.1 M CH ₃ COONa pH4.6 0.2 M (NH ₂) ₂ SO ₄	" " " " "	" " "
PEG 8000	24-34%	0.1 M CH ₃ COONa pH4.6 0.2 M Li ₂ SO ₄	" " " " "	" " "

Manual hanging drops were then set up to try to reproduce and grow larger crystals. The crystallization conditions are shown in Table 22. In order to make a more favourable condition for crystallization, I tried to add one condition in which I mixed the protein (25 mg/mL) and I-BET151 with a volume ratio 2 to 1. In that situation, the final concentration of the protein can be concentrated to 50 mg/mL. However, even after more than one month of incubation at 4 °C, no crystal was formed. Since I already had some co-crystals of CgBD1 and iBET151 from the automated screen, these were then directly harvested and sent to the ESRF

to perform diffraction tests. However, none of these yielded analyzable diffraction. Perhaps more conditions or other solvents than DMSO needed to be tested.

4.2.1.b. Co-crystallization of CgBD2 with I-BET151

Like CgBD1, I also tried to co-crystallize CgBD2 with I-BET151. The purified protein was mixed with 25 mM of I-BET151 in DMSO (Table 23) and used to screen crystallization conditions at the EMBL HTX facility.

Table 23. Mix of CgBD2 and I-BET151 (25 mM in DMSO).

I-BET151/Protein	Final protein concentration (mg/mL)	Final I-BET151 concentration (mM)	Final DMSO concentration
1	25	1.81	7.24%
1	15	1.09	4.36%
2	15	2.18	8.72%

Unlike CgBD1, within about 120 hours of incubation, small showers of crystals of CgBD2 with I-BET151 began to appear in more than 50 crystallization conditions at 4 °C (Table 24). Those conditions varied greatly in precipitant type, buffer and pH. The greater number and variety of crystallization conditions compared to those observed for unbound CgBD2 indicated that the presence of I-BET151 facilitates CgBD2 crystal formation. Tests by native mass spectrometry showed that I-BET151 itself can form dimers (data not shown), which might be the reason why its presence facilitates protein crystal formation. Manual crystallization drops were set up (Table 25) and, as for unbound CgBD2, yielded bulky, single crystals. The harvested crystals were then sent for X-ray diffraction tests at the ESRF beamline.

Table 24. Positions of crystallization plate that form co-crystals of CgBD2 with I-BET151. All the crystallization conditions can be found in Appendix I.

Plate	Plate position		
	[I-BET151]/[CgBD2] = 1		[I-BET151]/[CgBD2] = 2
	25 mg/mL	15 mg/mL	15 mg/mL
Wizard_I+II_rigaku	B1*, B2, B8, C3, D11, F7, H2, H9	A8, F7, G7, H2, H9	
PEGs-I_qiagen	E3, F7, H3, H7	E3, F7, F11	
Salt-Grid_hampton	B2, B3, B4, B5, B6, C8, D7, D8, D9, E8, F2, F8, G2, G3, H2, H3	H2, H3, H4, C6, C7, C9, C10, C11, D8, D9, D12, F2, F8, G3, H2, H3	B2, C6
PACT_MD	A10, B10, C3	A12	
JCSG_MD	A6, D4, E1, G11	A6, C5, C6, E1, G11, H8	A6, H6
Classics-Suite_qiagen	A1, C1, C3, C8, D10, E2, G1	C2, C3, F8	A1

* Conditions are written in bold only the first time they appear in each row.

Table 25. Crystallization conditions for manual hanging drops test of CgBD2 with I-BET151.

Precipitant	Precipitant concentration	Buffer	Protein concentration	[I-BET151]/[CgBD2]
(NH ₄) ₂ SO ₄	1.3-1.8 M	0.1 M Citric acid pH 5	10, 15 and 25 g/L	2 or 1
(NH ₄) ₂ SO ₄	2.1-2.6 M	0.1 M CAPSO pH 9	" " " " "	" " "
(NH ₄) ₂ SO ₄	1.2-1.7 M	0.1 M HEPES pH 7	" " " " "	" " "
(NH ₄) ₂ SO ₄	0.9-1.3 M	0.1 M NaO ₂ As(CH ₃) ₂ pH 6.5	" " " " "	" " "
(NH ₄) ₂ SO ₄	0.9-1.3 M	0.1 M TRIS pH 8.5	" " " " "	" " "
(NH ₄) ₂ SO ₄	1.2-1.7 M	0.1 M HEPES pH 7.5	" " " " "	" " "
		0.1 M NaCl		
PEG 6000	12-21%	0.1 M Na-Citrate-Tribasic dihydrate pH 5	" " " " "	" " "
		0.1 M (NH ₄) ₂ SO ₄		
PEG 6000	1-24%	0.1 M CH ₃ COONa pH 4.5	" " " " "	" " "
		0.2 M Li ₂ SO ₄		
PEG 8000	17-22%	0.1 M NaO ₂ As(CH ₃) ₂ pH 6.5	" " " " "	" " "
		0.2 M Mg(CH ₃ COO) ₂		
PEG 8000	22-32%	0.1 M CH ₃ COONa pH 4.5	" " " " "	" " "
		0.2 M Li ₂ SO ₄		
PEG 10000	14-24%	0.1 M Citric acid pH 5	" " " " "	" " "
Malonate	1-1.5 M	-	" " " " "	" " "

The results showed that the co-crystal of CgBD2 with I-BET151 diffracted very well and yielded a structure refined at a resolution better than 2 Å (solved by my supervisor Carlo Petosa). Other crystallization conditions and statistics are shown in [Figure 41A](#). The co-crystal structure showed that the human BET inhibitor can fit well in the binding site of CgBD2 in approximately the same orientation as in Brd2 BD1 and Brd4 BD1. Several residues, including the conserved Asn382, as well as Leu338, Cys340 and Val392 can interact with I-BET151 ([Figure 41B and 41C](#)).

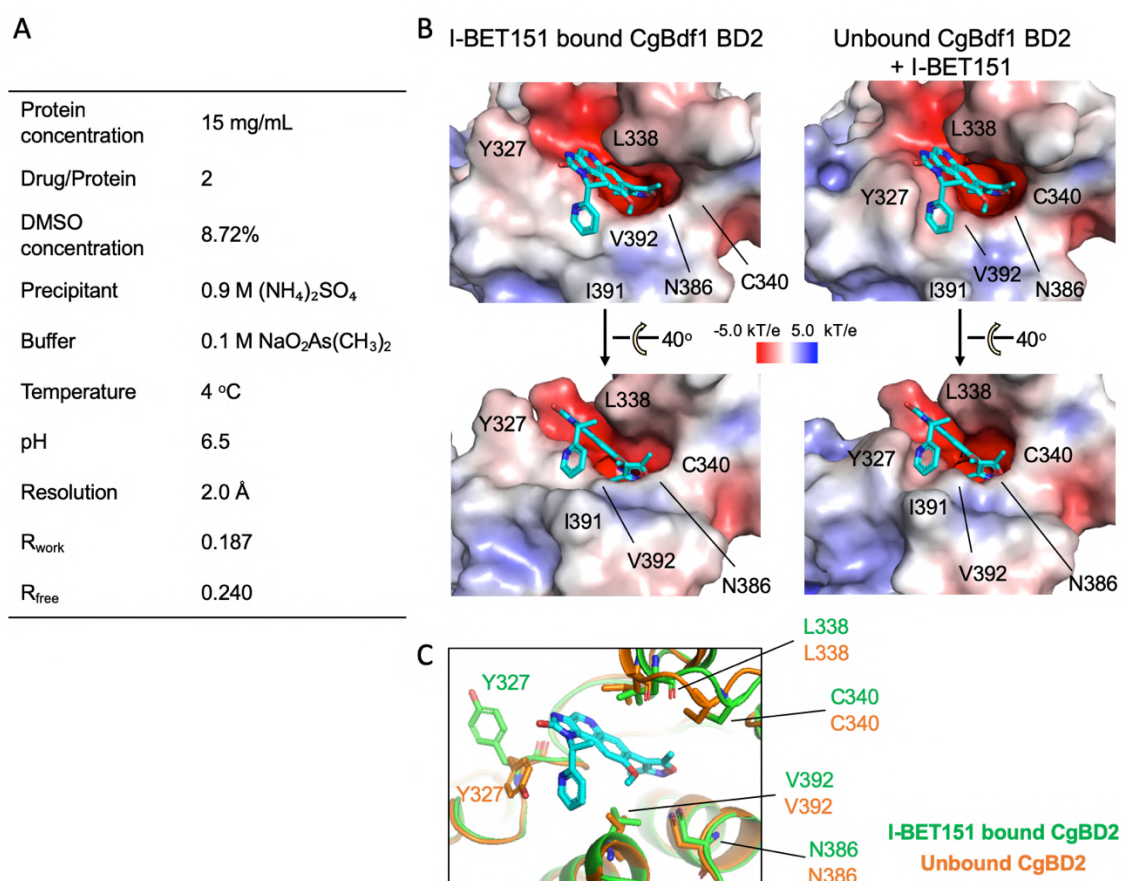


Figure 41. Binding feature of I-BET151 to CgBD2. **A.** Crystallization conditions and diffraction data analysis of co-crystals of CgBD2 with I-BET151. **B.** Comparison of the ligand-binding pocket of ligand bound CgBdf1 BD2 (left) with that of unbound CgBdf1 BD2 (right), the molecule I-BET151 bound to CgBD2 is shown in cyan. I-BET151 was superimposed on the unbound CgBD2 via a structural alignment with the ligand bound CgBD2, the root-mean square distance of the alignment was 1.38. **C.** Alignment of structures of I-BET151 bound CgBD2 (green) with unbound CgBD2 (orange) with some key residues marked in B.

The co-crystal structure of CgBD2 bound to I-BET151 was then aligned with the unbound CgBdf1 BD2 structure. The comparison of these two structures showed that upon binding I-BET151, some residues change their position to adapt the binding. The position of residues Ile391 and Val392 changed slightly to fit the form of I-BET151. The most evident change occurred with residue Tyr327. Upon binding, this residue flipped its side chain orientation toward the outside of the binding site in order to avoid the steric clash between its original orientation and the ligand (**Figure 41B and 41C**). This probably explain the weaker inhibitory effect of I-BET151 against CgBD2 compared to Brd4 BD2 (**Figure 37B**): because the preferred conformation of Tyr blocks binding and I-BET151 can only bind to CgBD2 with certain conformations.

4.2.1.c. Alignment of CgBD1 crystal model with co-crystal of Brd2 BD1 with JQ1

Since I had not obtained any co-crystals of CgBD1 with I-BET151 offering good diffraction data, I aligned the unbound CgBD1 crystal model with the JQ1-bound Brd4 BD1 structure (PDB code 3MXF) to align the JQ1 molecule into the CgBD1 binding pocket.

The results shown in **Figure 42** demonstrate that differences between the binding pockets of CgBD1 and Brd4 BD1 are probably responsible for the weaker inhibition effect of JQ1 against the former compared to the latter. In Brd4 BD1, residue Trp81 forms two channels on the binding pocket surface with residue Leu72 and residue Asp415, respectively. Two moieties of the JQ1 molecule fit perfectly into those channels (**Figure 42A**). In CgBD1, the corresponding residues – Arg150, Leu161 and Met 218 – hardly form any channel, resulting in a loss of important contacts with JQ1. More importantly, a steric clash was formed with residue Ile215, which could hinder the binding of the ligand (**Figure 42B**).

Taken together, the alignment model of CgBD1 with JQ1 showed that differences around the bromodomain binding pocket could lead either to the loss of important ligand interactions or the introduction of a steric clash, or both, which could explain the observed difference in activity of JQ1 towards the human and fungal BD.

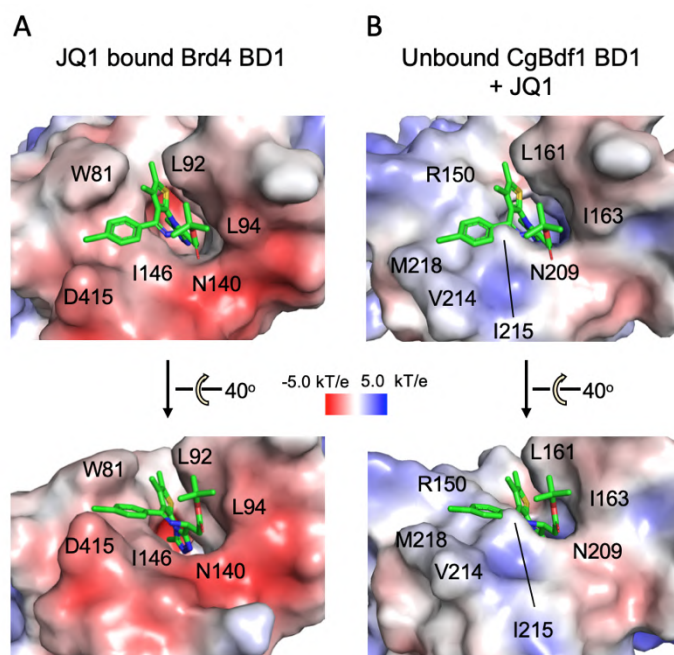


Figure 42. Comparison of the ligand-binding pockets of CgBD1 (B) with that of Brd4 BD1 (A, PDB code 3MXF). the molecule JQ1 bound to Brd4 BD1 is shown in green. JQ1 was superimposed on the CgBD1 via a structural alignment with Brd4 BD1. The root-mean square distance of the alignment was 1.46.

4.2.2. Binding features of CgBD1 inhibitors

Once the binding mode for JQ1 and I-BET151 was established or modelled, the next task was to perform the same analysis for the CgBD1 inhibitors identified by chemical screening. iCG compounds 55, 56 and 63 from the first group, 5, 16 and 29 from the second group (which showed the lowest IC_{50}) and compound 24 constituting the third group were tested for co-crystallization with CgBD1.

In order to screen as many compounds as possible for the co-crystallization conditions using a minimal number of crystallization plates, I chose to fix the protein concentration and the drug/protein ratio. 18.7 mg/mL (1.45 mM for CgBD1 and 1.35 mM for CgBD2) of each recently purified CgBD protein was incubated with 1.50 mM of each corresponding inhibitor, with a final DMSO concentration was 6.61%. For iCG compounds 24, 29 and 56, I also screened using 30.0 mg/mL CgBDs (2.32 mM for CgBD1 and 2.17 mM for CgBD2) with 4.58 mM inhibitors and a final concentration of DMSO at 9.17%. Incubation was performed at 4 °C

overnight and on the next day any precipitated material was removed by centrifugation at about 8000 g for 5 minutes before being sent to the EMBL HTX facility.

The screening results showed the same tendency as to I-BET151 co-crystallization: for a given compound, a lot more co-crystallization conditions were identified for CgBD2 than for CgBD1 (Table 26 and 27). Compounds iCG-29 and iCG-55 did not give any co-crystal with CgBD1 during this screening. However, most of the crystals formed during the screening were very small, manual crystallization drops were then set up (Table 28-32).

Table 26. Positions of crystallization plate that yielded co-crystals of CgBD1 with different inhibitors. All the crystallization conditions can be found in Appendix I.

Plate	Plate position					
	iCG-5*	iCG-16	iCG-24	iCG-56		iCG-63
	18.7 g/L**	18.7 g/L	18.7 g/L	18.7 g/L	30.0 g/L	18.7 g/L
Classics-Suite_qiagen		H6	B10, D2, E2, E4, F1, F2, F4, H9	G1	G1, G11	F10, G11, H1, H8
PACT_MD			G7			
PEGs-I_qiagen	G8		F6, G3, H7, H12		A2	
Salt-Grid_hampton			A2, A3, A12, E10, F12, H1			B1, G8
Wizard_I+II_rigaku			G5, H9, H10			A8, B4, H5
JCSG_MD			D12, F10, F11, G7, G11, H6		A12, B11, H7, H11	B9, C1, C2, C11, D4

* Different CgBD1 inhibitors.

** CgBD1 protein concentrations. When 18.7 g/L protein was used the final concentrations of inhibitors and DMSO were 1.50 mM and 6.61%, respectively; when 30.0 g/L protein was used, these concentrations were 4.68 mM and 9.17%, respectively.

Table 27. Positions of crystallization plate that yielded co-crystals of CgBD2 with different inhibitors. All the crystallization conditions can be found in Appendix I.

Plate	Plate position			
	iCG-5*	iCG-16	iCG-24	iCG-29
Classics-Suite_qiagen	B2, C1, C3, C7, C10, D10, D11, F5, F11, H3, H6, H8, H11, H12	D10, E9, G1, H2	A5, B3, B10, C1, C3, C6, C7, C9, D1, D2, D4, D5, D9-11, E2, E5, E11, F1, F4, F7-10, G1, G12, H2-4, H6, H8, H11, H12	H2
PACT_MD	A3, A10, A11, B1, B2, B7-10, C3, C4, C7, C9, C11, D2, D4, D5, E1-5, E7, E9, E10, F3, F5, F6, F8, F10	A1, A3, A7-10, B1-4, B7-9, D2, D4, E1, E2, E5, E6, E9	A2-7, B1-5, B10, B11, C5-11, D3-5, D7-11, E1, E2, E6-8, E9-12, F1-12, G1-12, H1, H2, H6, H7, H10	A2, A7, B2, B7-9, C2, C3, D2, D3, E1, E6
PEGs-I_qiagen	A2, A3, A9-12, B4, B5, C7-12, D1-6, E1-11, F1-6, F12, G3, G5, G9, G12, H1, H6	C7-10, C12, D1-5, E1, E2, E4, E6, E8, F3, F5, F6, F9, F11, H3, H5	A11, A12, B5, B6, B12, C6-12, D1-11, E1-9, E12, F3-12, G1, G3-8, G11, G12, H1-3, H5, H7-10, H12	E1, E2, F9, F10
Salt-Grid_hampton	B2, D7, E8, F1, F8, G1, G2	B2, F3	A1, A2, B2-7, C4-12, D7-10, D12, E8, E10, F2, F3, F4, F8, G1-3, G8, G9, H1, H2, H9, H10	
Wizard_I+II_rigaku	A6, A8, B8, C4, G7, G12	A6, B4, E11	A6, A12, B1, B2, B6, B8, B11, C3, C4, C9, C12, D4, D10, E3, E6, E8, E9, F4, F6, F7, F11, G3, G4, G7, G11, H1, H2, H5, H8, H12	
JCSG_MD	A2, A3, A6, B7, B9, C1, C3, C5, D12, G6, G7, G8, G11, H7, H10	A2, A3, A9, B9, C12, H8	A2, A3, A6, A10, A12, B4, B8, B12, C3, C4, D6, D12, E11, F7, F10, F11, G1, G2, G6-11, H1, H6-11	B9, C6, C12, D12, G10, H3

* Different CgBD2 inhibitors. The final compound concentration was 1.50 mM, which corresponds to a final concentration of protein and DMSO of 119.0 g/L and 6.61%, respectively.

Table 28. Crystallization conditions for manual hanging drops test of CgBD1 with iCG-24.

Precipitant	Precipitant concentration	Buffer	Protein concentration	[iCG-24]/[CgBD1]
(NH ₄) ₂ SO ₄	0.4-1.0 M	0.1 M MES pH 6	20 and 40 g/L	2 or 1
(NH ₄) ₂ HPO ₄	0.4-1.0 M	0.1 M CH ₃ COONa pH 4.5	" " " "	" " "
(CH ₂) ₂ (CO ₂ H) ₂	0.5-1.0 M	0.1 M HEPES pH 7	" " " "	" " "
PEG 2000 MME	1%			
MgSO ₄	1.0-1.8 M	0.1 M MES pH 6.5	" " " "	" " "
Mg(HCO ₂) ₂	0.14-0.24 M	-	" " " "	" " "
PEG 3350	10-19%	0.1 M (CH ₂) ₂ (CO ₂ H) ₂ pH 7	" " " "	" " "
PEG 3350	14-24%	0.1 M Mg(CHCOO) ₂	" " " "	" " "
PEG 3350	14-24%	0.1 M Tris pH 7.5 0.2 M CH ₃ COONa	" " " "	" " "
PEG 6000	6-14%	0.1 M HEPES pH 7.5	" " " "	" " "
MPD	5%			
PEG 8000	10-20%	0.04 M KH ₂ PO ₄	" " " "	" " "
Glycerol	20%			
Malonate pH 7	0.7-1.4 M	-	" " " "	" " "

Table 29. Crystallization conditions for manual hanging drops test of CgBD1 with iCG-56.

Precipitant	Precipitant concentration	Buffer	Protein concentration	[iCG-56]/[CgBD1]
(NH ₄) ₂ SO ₄	1.7 to 2.2 M	0.1 M HEPES pH 7.2	20 and 40 g/L	2 or 1
" "	" "	0.1 M HEPES pH 7.4	" " " "	" " "
" "	" "	0.1 M HEPES pH 7.6	" " " "	" " "
" "	" "	0.1 M HEPES pH 7.8	" " " "	" " "

Table 30. Crystallization conditions for manual hanging drops test of CgBD1 with iCG-63.

Precipitant	Precipitant concentration	Buffer	Protein concentration	[iCG-63]/[CgBD1]
(NH ₄) ₂ SO ₄	1.4-3.0 M	0.1 M CH ₃ COONa pH 4.6	20 and 40 g/L	2 or 1
(NH ₄) ₂ SO ₄	1.4-3.0 M	0.1 M Trisodium citrate pH 5.4	" " " "	" " "
PEG 2000	20-30%	0.1 M CH ₃ COONa pH 4.6 0.2 M (NH ₄) ₂ SO ₄	" " " "	" " "
PEG 3350	14-22%	0.1 M Trisodium citrate pH 5.4	" " " "	" " "
PEG 4000	20-30%	0.1 M CH ₃ COONa pH 4.5 0.2 M (NH ₄) ₂ SO ₄	" " " "	" " "
PEG 4000	20-30%	0.2 M (NH ₄) ₂ SO ₄	" " " "	" " "
PEG 5000 MME	20-30%	0.1 M MES pH 6.5 0.2 M (NH ₄) ₂ SO ₄	" " " "	" " "
PEG 10000	20-30%	0.1 M (CH ₃) ₂ AsO ₂ H pH 6.5 0.2 M (NH ₄) ₂ SO ₄	" " " "	" " "

Table 31. Crystallization conditions for manual hanging drops test of CgBD2 with iCG-24.

Precipitant	Precipitant concentration	Buffer	Protein concentration	[iCG-24]/[CgBD2]
PEG 2000 MME	0.6-1.1%	0.1 M HEPES pH 7 1 M (CH ₂) ₂ (CO ₂ H) ₂	20 and 40 g/L	2 or 1
PEG 3350	12-22%	0.2 M NH ₄ NO ₃	" " " "	" " "
PEG 3350	12-22%	0.2 M Potassium citrate tribasic	" " " "	" " "
PEG 6000	12-22%	0.1 M HEPES pH 7	" " " "	" " "
PEG 6000	12-22%	0.1 M HEPES pH 7 0.2 M NaCl	" " " "	" " "
PEG 6000	12-22%	0.2 M Potassium sodium tartrate	" " " "	" " "
PEG 6000	10-20%	0.1 M HEPES pH 7 0.2 M NaCl	" " " "	" " "
PEG 8000	10-20%	0.1 M Tris pH 8.5 0.2 M MgCl ₂	" " " "	" " "
PEG 8000	12-22%	0.1 M Tris pH 8.5 0.2 M MgCl ₂	" " " "	" " "
PEG 8000	6-12%	0.1 M Tris pH 7 0.2 M MgCl ₂	" " " "	" " "

Table 32. Crystallization conditions for manual hanging drops test of CgBD2 with iCG-29.

Precipitant	Precipitant concentration	Buffer	Protein concentration	[iCG-29]/[CgBD2]
Na ₂ HPO ₄	0.3 to 0.6 M	0.1 M HEPES pH 7.4 0.8 M Na ₂ HPO ₄	20 and 40 g/L	2 or 1
Na ₃ PO ₄	0.3 to 0.6 M	0.1 M HEPES pH 7.5 0.8 M Na ₃ PO ₄	" " " "	" " "
PEG 3350	16 to 22%	0.2 M KF	" " " "	" " "
PEG 6000	16 to 22%	0.1 M MES pH 6 0.2 M LiCl	" " " "	" " "
PEG 8000	6 to 12%	-	" " " "	" " "
PEG 10000	10%			

Formed crystals were harvested and sent to perform X-ray diffraction tests at the ESRF beamlines. Only co-crystals of CgBD1 with iCG-63 and co-crystals of CgBD2 with iCG-29 showed a good diffraction. The crystallization conditions and data analysis of these co-crystals are shown in [Table 33](#).

Table 33. Crystallization conditions and diffraction data analysis of co-crystals of CgBD1 with iCG-63 and co-crystals of CgBD2 with iCG-29.

	CgBD1 + iCG-63	CgBD2 + iCG-29
Protein concentration	40 mg/mL	20 mg/mL
Drug/Protein	2	1
DMSO concentration	8.4%	14.7%
Precipitant	26% PEG 10 000 0.2 M (NH ₄) ₂ SO ₄	0.8 M NaH ₂ PO ₄ 0.8 M KH ₂ PO ₄
Buffer	0.1 M NaO ₂ As(CH ₃) ₂	0.1 M Hepes
Temperature	4 °C	4 °C
pH	6.5	7.5
Resolution	1.9 Å	2.4 Å
R _{work}	0.196	0.2489
R _{free}	0.231	0.2839

It was mentioned that iCG-63 specifically inhibited CgBD1 with a low IC_{50} . The analysis of the co-crystal structure showed that this molecule could form tight interaction with CgBD1. Besides the conserved Asn209 in the binding pocket, several other residues outside the acetylated histone binding site, such as Lys147, Arg150, even Ile215 and Met218, interacted with the inhibitor (**Figure 43A**). The involvement of so many residues forming an extensive interface probably explains the high affinity of iCG-63 to CgBD1.

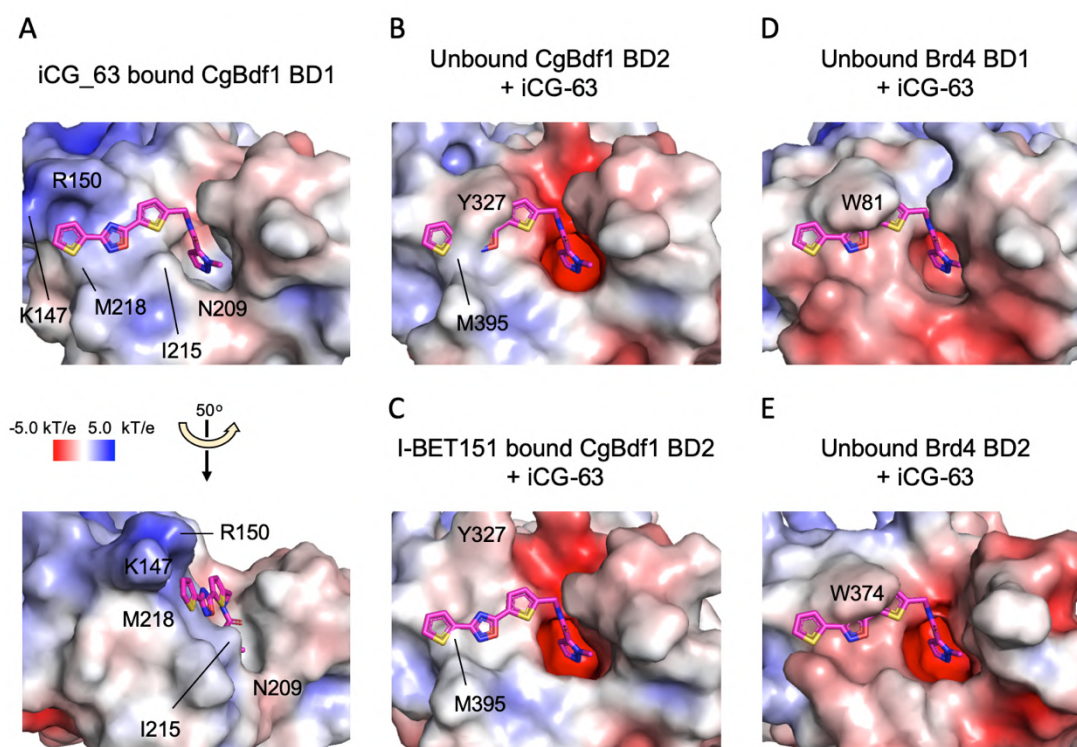


Figure 43. Binding of iCG-63 onto different bromodomains. **A.** Crystal structure of molecule iCG-63 (magentas) bound to CgBD1. **B** and **C.** Hypothetical model of compound iCG-63 aligned onto the crystal structure of CgBD2 in its unbound conformation (**B**) and its I-BET151-bound conformation (**C**). iCG-63 was superimposed on the CgBD2 models via a structural alignment with bound CgBD1. The root-mean square distances of the alignments were 1.47 (**B**) and 1.46 (**C**). **D** and **E.** Hypothetical model of molecule iCG-63 aligned onto the crystal structure of human Brd4 BD1 in the unbound conformation (**D**, PDB code 4LYI) and Brd4 BD2 (**E**, PDB code 2OUO). iCG-63 was superimposed on the Brd4 bromodomain models via a structural alignment with bound CgBD1. The root-mean square distances of the alignments were 1.68 (**D**) and 2.41 (**E**).

In order to investigate why iCG-63 efficiently inhibited CgBD1 but had only weak or no activity towards CgBD2 and the two human Brd4 bromodomains, I modeled the structure of these three bromodomains bound to iCG-63 by structurally aligning them with the CgBD1/iCG-63 complex. For CgBD2 in its unbound conformation, residues Tyr327 and Met395 formed a

very evident steric clash with the superimposed compound (**Figure 43B**). Even for CgBD2 in its I-BET151-bound conformation, in which Tyr327 adopts a different conformation, Met395 could still block the binding of iCG-63 (**Figure 43C**). The situation was similar in both Brd4 bromodomains, where BD1 residue Trp81 and and BD2 residue Trp374 were predicted to generate a steric clash blocking the inhibitor from binding (**Figure 43D and 43E**).

In summary, the large number of ligand interactions in CgBD1 explains the high affinity of iCG-63 for this bromodomain, whereas steric constraints predicted for the other bromodomains explain the selectivity of this molecule.

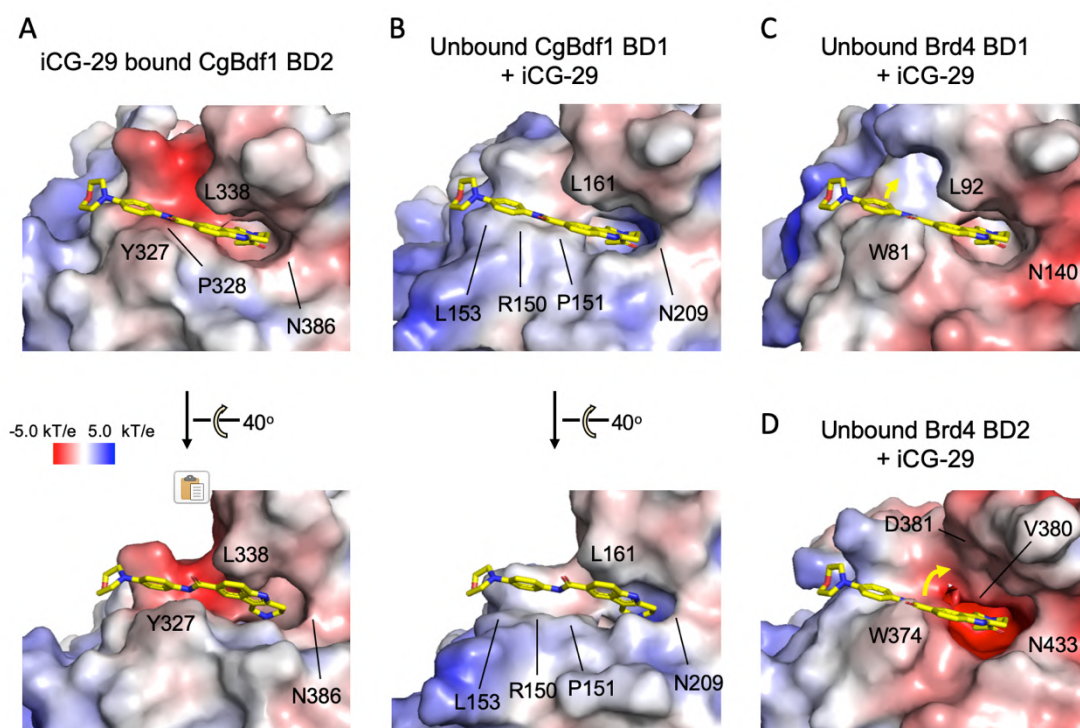


Figure 44. Binding of iCG-29 onto different bromodomains. **A.** Crystal structure of molecule iCG-29 (yellow) bound to CgBD2. **B.** Hypothetical model of compound iCG-29 aligned onto the crystal structure of CgBD1 in its unbound conformation. iCG-29 was superimposed on the CgBD1 model via a structural alignment with bound CgBD2. The root-mean square distance of the alignment was 2.33. **C and D.** Hypothetical model of molecule iCG-29 aligned onto the crystal structure of human Brd4 BD1 in its unbound conformation (**C**, PDB codes 4LYI) and Brd4 BD2 (**D**, PDB codes 2OUO). iCG-29 was superimposed on the Brd4 bromodomain models via a structural alignment with bound CgBD2. The root-mean square distances of the alignments were 1.79 (**C**) and 1.46 (**D**).

As a non-selective inhibitor, the situation for iCG-29 was totally different compared to the selective CgBD1 inhibitor iCG-63. The co-crystal structure with CgBD2 demonstrated that the acetyltetrahydropyridoindole moiety of iCG-29 went inside the acetyl group binding site

and formed a direct hydrogen bond with the conserved Asn386 while the morpholinylphenyl moiety interacted with a channel formed by residues Pro328, Tyr327 and Leu338 (**Figure 44A**). This channel is also present in CgBD1 and the two Brd4 BDs. In CgBD1, the channel formed by Arg150, Pro151, Leu153 and Leu161 could also accommodate iCG-29 very well (**Figure 44B**). In Brd4, the channel is formed by residues Trp81 and Leu92 in BD1 and by residues Val380, Asp381 and Trp374 in BD2. The orientation of iCG-29 might have to change slightly to fit into the binding site, but there is enough space to allow the molecule to bind without a steric clash (**Figure 44C and 44D**). These results reasonably account for the ability of iCG-29 to show similar inhibitory effect against the four CgBdf1 and hBrd4 bromodomains.

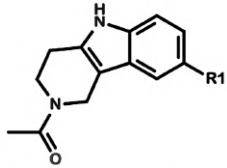
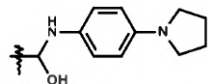
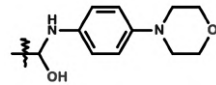
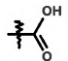
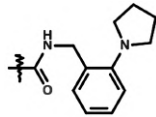
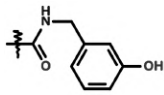
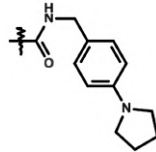
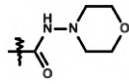
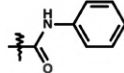
4.3. Chemical optimization of dual CgBDs inhibitor iCG-29

Given that inhibiting both CgBdf1 bromodomains is required to inhibit yeast growth and that compound iCG-29 was the only dual inhibitor for which we had a co-crystal structure, this compound was the first chosen for chemical optimization. The co-crystal structure of CgBD2 with compound iCG-29 showed that the morpholinylphenyl moiety was a little bit flexible (data not shown), indicating that it contributes less to the binding affinity compared to the acetyltetrahydropyridoindole moiety buried inside the binding pocket. For this reason, the chemical modifications concern firstly this moiety (R_1 in Table 34) in order to improve the affinity and selectivity.

Based on the co-crystal structure, our collaborators at USC designed and synthesized six analogous compounds (**Table 34**). HTRF assays showed that the modifications changed the affinity of these compounds against CgBDs and hBDs (**Table 34**). This indicated that the morpholinylphenyl moiety of iCG-29 played an important role in binding inhibition as well. Compared to the original iCG-29, compounds ND-3-70 and ND-3-77 (synthesized by postdoc Nathan Dupper) had only a very weak activity towards the two CgBDs while compound ND-3-79 had not detectable activity at all. However, the suppression of the phenyl ring in R_1 for compound ND-3-77 compared to iCG-29 might still be interesting since this compound showed enhanced selectivity for the CgBDs over the human BDs. The common structure of compounds ND-3-72, ND-3-74 and ND-3-76 was that they had a more flexible lateral moiety, by adding a carbon between the amide group and the phenyl ring, compared to the original

iCG-29 and iCG-16. This modification led to a higher selectivity towards CgBD2 over both Brd4 BDs. Of the three compounds, ND-3-76, whose structure was very similar to that of iCG-16, has the highest activity against CgBD2, which is 3-fold better than the starting compound. However, it should be pointed out that all three compounds lost affinity towards CgBD1 compared to original compound iCG-29.

Table 34. Structure and IC₅₀ values of compounds iCG-16, iCG-29 and their derived compounds.

Compound ID in lab ⁽¹⁾	 R ₁	IC ₅₀ (μM) ⁽²⁾			
		CgBD1	CgBD2	hBD1 ⁽³⁾	hBD2 ⁽³⁾
iCG-16		4.65 ± 2.74	0.23 ± 0.08	1.13 ± 0.29	1.57 ± 0.10
iCG-29		1.81 ± 1.14	2.06 ± 0.23	2.73 ± 0.34	0.52 ± 0.20
ND-3-70		49.4 ± 10.5	21.9 ± 7.6	95.9 ± 2.8	53.2 ± 7.2
ND-3-72		9.68 ± 1.30	4.73 ± 0.42	10.2 ± 3.4	12.0 ± 2.2
ND-3-74		10.5 ± 1.3	2.26 ± 0.25	4.96 ± 1.14	6.19 ± 1.19
ND-3-76		5.80 ± 0.25	0.68 ± 0.21	3.09 ± 0.68	2.07 ± 0.42
ND-3-77		24.0 ± 4.0	47.5 ± 12.6	> 100 ⁽⁴⁾	> 100
ND-3-79		ND ⁽⁵⁾	ND	> 100	5.72 ± 1.94

(1) Molecules with their ID beginning with iCG were purchased from Chemdiv. Molecules whose ID begins with ND were synthesized by our collaborators at the USC.

(2) GST-BD binding inhibition IC₅₀ calculated by GraphPad Prime 7 by using “log(inhibitor) vs. response (three parameters)” model. Data are presented as means ± SD, n ≥ 2 independent experiments.

(3) hBD1 and hBD2 represent respectively BD1 and BD2 from human Brd4.

(4) > 100, IC₅₀ value calculated by GraphPad Prime 7 higher than 100 μM (weak effect).

(5) ND, not determined (almost no effect).

4.4. Conclusion

After the high-throughput chemical screening, 66 molecules were considered to be interesting CgBD1 inhibitors. Of these, we then purchased the 63 that were commercially available in order to confirm their inhibitory activity against both CgBDs and hBDs. Among these, only 12 molecules were validated, showing an IC_{50} lower than 5 μ M against either CgBD1 or CgBD2 or both. The validation rate was less than 20%. Compounds were classified into three groups: group 1 (CgBD1-selective inhibitors) inhibited only CgBD1; group 2 (non-selective dual CgBD inhibitors) inhibited both CgBDs and hBDs; and group 3 (selective dual CgBDs inhibitors) mainly inhibited only the CgBDs. Co-crystal structures were pursued to identify the binding modes of these inhibitors. I successfully co-crystallized CgBD1 with compound iCG-63 from group 1 and CgBD2 with either I-BET151 or compound iCG-29 from group 2. I also tried to co-crystallize I-BET151 with a protein construct containing both CgBD1 and BD2 but without success. Analysis of the co-crystal structures and of hypothetical ligand-alignment models provided explanations for the different inhibitory activities of these molecules. Structure-guided chemical optimization of compound iCG-29 was also performed to obtain better inhibitors, but with only limited success. The next step was to evaluate these compounds in *C. glabrata* growth inhibition assays in order to identify inhibitors that were active against the yeast.

5. Characterization of bioactive inhibitors

5.1. Discovery of a bioactive dual *C. glabrata* Bdf1 bromodomain inhibitor

5.1.1. iCG-24: an inhibitor active against *C. glabrata* mutant strains

The 12 validated CgBD1 inhibitors were then tested for their ability to inhibit the growth of *C. glabrata*. I also added three iCG compounds 27, 39 and 42 whose IC₅₀ was only slightly above 5 μ M (Table 18) in order to increase the chances of identifying bioactive inhibitors.

The results showed that of the assayed compounds, nearly all failed to inhibit the growth of any tested strain. The only growth inhibition observed was that of the strain expressing Bdf1 Δ BD2 by the compound iCG-24 (Figure 45A), indicating that iCG-24 was the only molecule having yeast inhibitory activity. The other compounds might have had difficulty entering the yeast cell or were not stable inside the cell, possibly explaining why there were not active in this assay.

Compound iCG-24 was then further characterized. During the previous growth assay, I had sometimes observed that the strain expressed Bdf1 Δ BD2 grew too slowly without any inhibitor in the culture medium. That might be because of the presence of DMSO, which also inhibits bromodomains. For this reason, before the further characterization, I decided to check whether it was possible to optimize the solvent.

I prepared 10 different solvent by mixing DMSO and ethanol in different proportions, from 100% DMSO with no ethanol to 100% ethanol with no DMSO. These solvents were next diluted in a yeast containing culture to a final concentration of 1%. The results demonstrated that after 22 hours of incubation, the strain expressed Bdf1 Δ BD2 grew progressively more slowly as the proportion of DMSO increased (Figure 45B), suggesting that the concentration of DMSO should be decreased as much as possible.

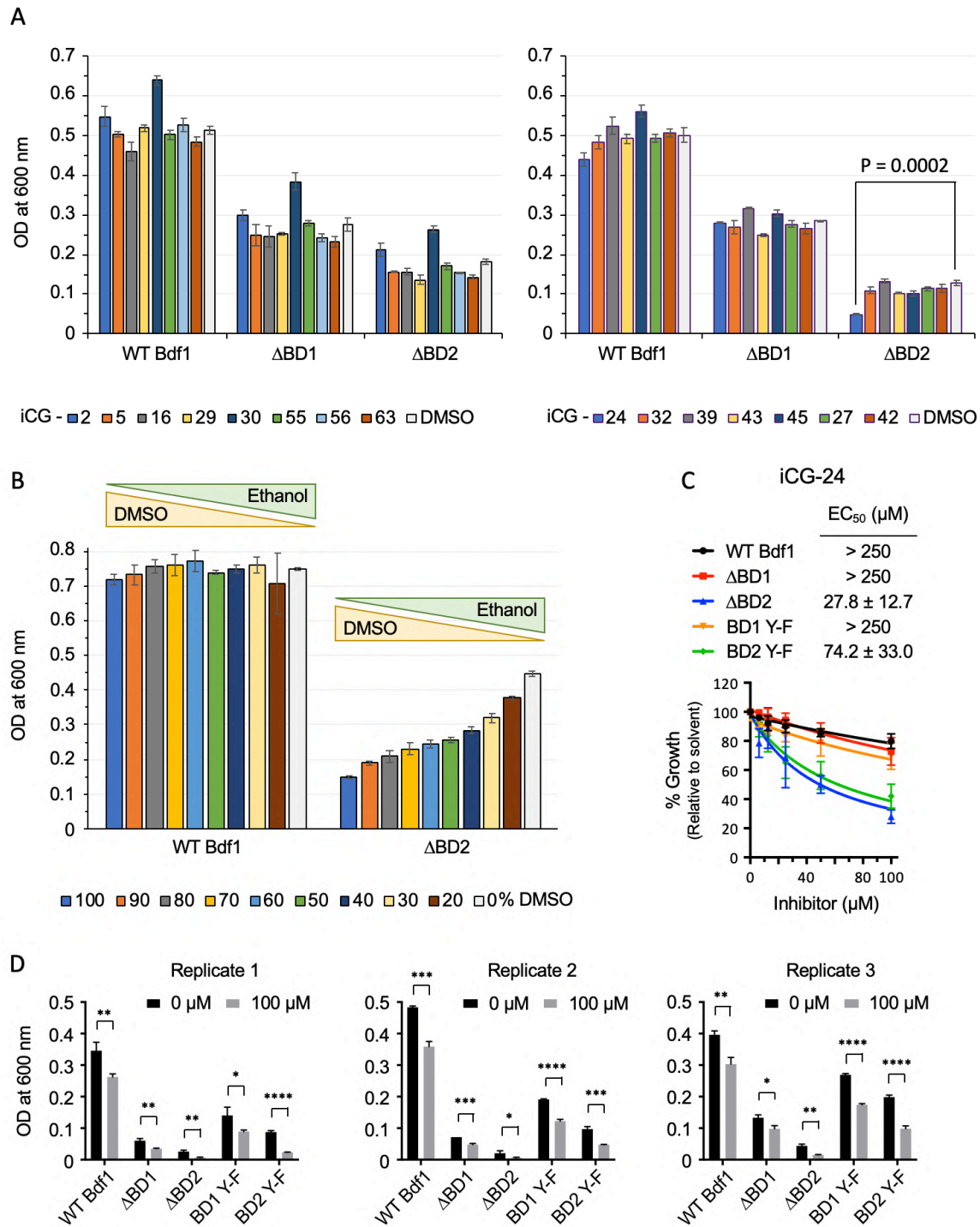


Figure 45. Identification of iCG-24 as active *C. glabrata* growth inhibitor. **A.** Yeast growth inhibition assays using confirmed CgBD1 inhibitors. Yeast strains were grown in the presence of methionine and cysteine to repress expression of the WT genomic *BDF1*. Only the *BDF1* present in the plasmid was expressed. Incubation was at 30 °C for 20 hours. WT Bdf1, ΔBD1 and ΔBD2 represented strains expressing only wildtype Bdf1 or Bdf1 deleted for either BD1 or BD2, respectively. 10 mM compounds in DMSO were diluted directly into the medium to a final concentration of 50 μM and a final DMSO concentration of 0.5%. Data are presented as the mean ± SD for technical triplicates of each experiment. Statistical significance was determined using the Holm-Sidak method in GraphPad Prime 7. **B.** Solvent test. Solvents consisted of different proportions of DMSO and ethanol. Incubation was at 30 °C for 22 hours. Data are presented as the mean ± SD for technical triplicates of each experiment. **C.** Yeast growth inhibition dose–response curves of compound iCG-24. BD1 Y-F and BD2 Y-F represent the strains expressing only Bdf1 with the Y166F and Y343F mutations, respectively. Incubation was at 30 °C for 20, 22 and

24 hours for WT Bdf1, Δ BD1/ Δ BD2 and BD1/BD2 Y-F strains, respectively. The inhibition curves were fitted and EC₅₀ values were calculated by GraphPad Prime 7 by using the “[inhibitor] vs. response (three parameters)” model. Data are presented as means \pm SD, n = 3 independent experiments. **D.** Three independent experiments of yeast growth inhibition by iCG-24. Incubation was at 30 °C for 20 hours. Data are presented as means \pm SD from technical triplicates of each experiment. Statistical significance was determined using the Holm-Sidak method in GraphPad Prime 7; * P \leq 0.05; ** P \leq 0.01; *** P \leq 0.001; **** P \leq 0.0001.

However, all the compounds were prepared and stored at 50 mM in DMSO because many compounds became insoluble at higher concentration. Moreover, these 50 mM solutions had to be diluted at least five-fold in the organic solvent before being diluted into aqueous solution to avoid precipitation. However, the concentration of inhibitors should not be below 10 mM before aqueous dilution in order to achieve a high final compound concentration (100 μ M) in the plate while simultaneously limiting the final solvent concentration to no more than 1%. For these reasons, all compounds in subsequent growth assays were prepared from the 50 mM compounds stored in DMSO by diluting these to 10 mM in ethanol before further dilution in yeast culture. In this way, the final solvent concentration was 0.2% DMSO and 0.8% ethanol.

I next used this optimized solvent in the *C. glabrata* growth inhibition assay to determine the half maximal effective concentration (EC₅₀) of compound iCG-24. As in the HTRF assay, to ensure a constant solvent proportion and concentration across all the compound concentrations tested, I performed a serial dilution of iCG-24 with 100% DMSO before diluting the resulting solutions five times in ethanol and then in the yeast culture. The growth curves showed that iCG-24 inhibited the growth of *C. glabrata* strains in which only a functional Bdf1 BD1 was present, with an EC₅₀ of about 30 μ M and 75 μ M for strains expressing Bdf1 Δ BD2 and Bdf1 Y343F, respectively. For all others strains expressing Bdf1 with a functional BD2, the inhibition by iCG-24 was very weak (**Figure 45C**). These results correlated well with the in vitro HRTF inhibition assays, where iCG-24 primarily inhibited CgBD1 (**Figure 40B**).

5.1.2. Analogue compounds of iCG-24

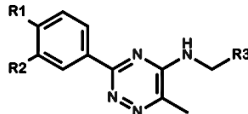
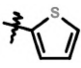
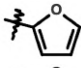
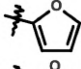
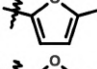
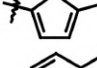
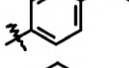
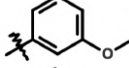
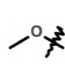
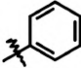
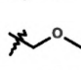
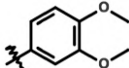
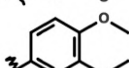
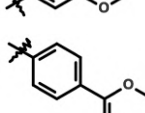
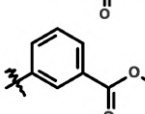
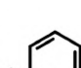
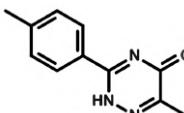
Until this point, compound iCG-24 was the only chemical screening hit that showed an effect on yeast growth. Even though it mainly inhibited CgBD1 and showed very weak

inhibition against strains expressing Bdf1 with a functional BD2, it was still a very good beginning. However, a major drawback of this molecule that hampered extensive further characterization was its very poor solubility in aqueous solution. As mentioned in section 4.2.2 of this chapter, I had already tried to co-crystallize this molecule with CgBD1 and CgBD2. Some large crystals were obtained in manually prepared drops, but the diffraction data showed that these were crystals of the compound alone, which had precipitated out of solution (Data not shown).

In order to study the inhibition mechanism of the iCG-24 scaffold, our collaborators at USC proposed a series of molecules (either commercially available or synthesized in-house) with similar structures predicted to have higher solubility (Table 35). If at least one of these more soluble compounds had bromodomain inhibition activity like that of iCG-24, then perhaps its co-crystal structure with a CgBD could be determined.

All the derived compounds were first verified for their ability to inhibit CgBDs *in vitro* using the HTRF assay. The results in Table 35 showed that small modifications could in fact significantly alter the inhibition activity observed. Generally, a methyl group at the R₁ position and a hydrogen at R₂ showed better inhibition than the opposite combination (iCG-24-334 vs iCG-24-601 and iCG-24-409 vs iCG-24-676). On the other hand, hydrogens at both the R₁ and R₂ positions also yielded a good *in vitro* activity (iCG-24-040). However, the identity of the R₃ group appeared to have the greatest impact on activity. Some compounds shared the same R₁ and R₂ with the original iCG-24, but their *in vitro* activity was almost totally lost when the R₃ group was altered (iCG-24-376, JMO-i-64 and JMO-i-68).

Table 35. Structure and IC₅₀ of iCG-24 and its derived compounds.

Compound ID in lab ⁽¹⁾				IC ₅₀ (μM) ⁽²⁾			
	R ₁	R ₂	R ₃	CgBD1	CgBD2	hBD1 ⁽³⁾	hBD2 ⁽³⁾
iCG-24	CH ₃	H		2.09 ± 0.13	47.7 ± 25.5	> 100 ⁽⁴⁾	> 100
iCG-24-334	CH ₃	H		6.99 ± 0.96	ND ⁽⁵⁾	ND	ND
iCG-24-601	H	CH ₃		16.5 ± 5.1	52.1 ± 32.0	> 100	> 100
iCG-24-409	CH ₃	H		8.28 ± 0.98	11.8 ± 2.2	> 100	> 100
iCG-24-676	H	CH ₃		12.6 ± 1.4	18.9 ± 2.6	> 100	> 100
iCG-24-040	H	H		2.24 ± 0.36	> 100	> 100	> 100
iCG-24-381	CH ₃	H		2.92 ± 0.89	> 100	> 100	> 100
iCG-24-1485		H		0.81 ± 0.17	> 100	> 100	> 100
iCG-24-376	CH ₃	H		ND	ND	ND	ND
iCG-24-533	CH ₃	H		2.59 ± 0.05	43.5 ± 18.1	> 100	> 100
iCG-24-800	H	CH ₃		4.91 ± 0.86	65.9 ± 14.3	> 100	> 100
JMO-i-64	CH ₃	H		> 100	> 100	> 100	> 100
JMO-i-66	CH ₃	H		69.7 ± 26.6	> 100	> 100	> 100
JMO-i-68	CH ₃	H		ND	ND	ND	ND
JMO-i-62				22.9 ± 0.6	71.8 ± 26.5	> 100	> 100

(1) Molecules with their ID beginning with iCG were purchased from Chemdiv. Molecules whose ID begins with JMO were synthesized by our collaborators at the USC.

(2) GST-BD binding inhibition IC₅₀ calculated by GraphPad Prime 7 by using “log(inhibitor) vs. response (three parameters)” model. Data are presented as means ± SD, n ≥ 2 independent experiments.

(3) hBD1 and hBD2 represent respectively BD1 and BD2 from human Brd4.

(4) > 100, IC₅₀ value calculated by GraphPad Prime 7 higher than 100 μM (weak effect). Data are from more than two independent experiments.

(5) ND, not determined (almost no effect). Data are from more than two independent experiments.

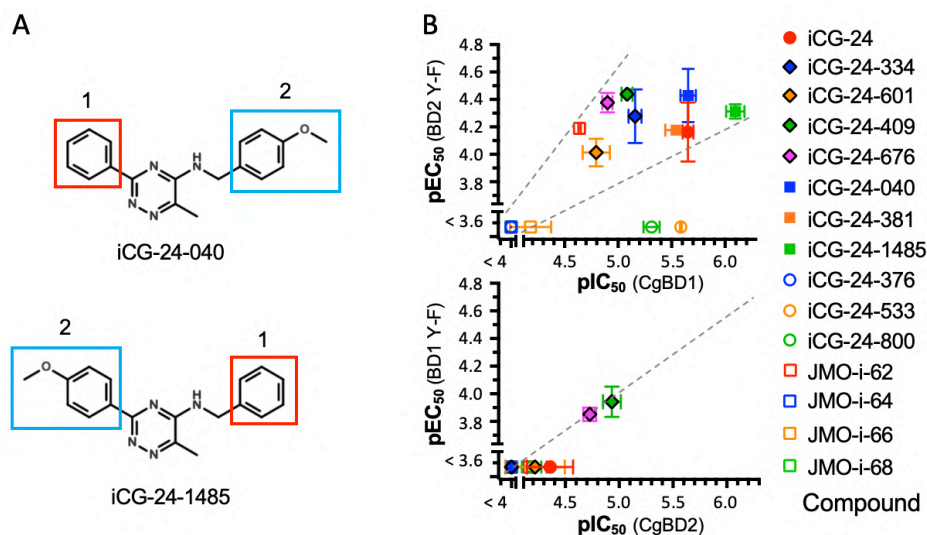


Figure 46. Comparison of two iCG-24 derived compounds. (A) Chemical structures. (B) Comparison of the CgBD inhibition activity *in vitro* with yeast growth inhibition activity. pIC_{50} and pEC_{50} values are plotted for the indicated iCG-24 analogs. $pIC_{50} = -\log_{10}(IC_{50})$, $pEC_{50} = -\log_{10}(EC_{50})$, where IC_{50} and EC_{50} are expressed in molar. Data are from Table 37 and 38, with compounds listed in the same order. BD1 Y-F and BD2 Y-F represent strains expressing only Bdf1 with either Y166F mutation or Y343F mutation, respectively.

Upon comparing the *in vitro* activity with the chemical structures, I noticed an interesting result concerning the pair of compounds iCG-24-040 and iCG-24-1485. Their structures, illustrated in [Figure 46A](#), show that the left and right substituents (group 1 and group 2) are exchanged in these two molecules. Neither of these two compounds lost significant activity compared to the starting compound iCG-24 ([Table 35](#)), suggesting that the binding orientations of these two molecules might be mutually flipped. This raises the possibility that the common scaffold of this series of compounds might have more than one binding mode to optimize interactions between the binding pocket and the different lateral groups. However, compound iCG-24-1485 had the highest inhibitory capacity among all iCG-24 derived compounds, which was almost three-fold that of iCG-24-040 ([Table 35](#)), suggesting that the configuration of iCG-24-1485 provides a better spatial arrangement compared to iCG-24-040. For further chemical optimization, it might be interesting to modify the R_3 group of iCG-24-1485 to try to obtain improved potency against CgBD2.

Next I tested all the derived compounds in yeast growth inhibition assays. Strictly, all the compounds presenting yeast growth inhibition activity also were active in the HTRF assay ([Table 35 and 36](#)). Furthermore, plotting the yeast growth inhibition activity (EC_{50}) against the *in vitro* activity (IC_{50}) showed that these activities were reasonably well correlated for most of

the compounds (**Figure 46B**). These results supported the hypothesis that iCG-24 and its derived compounds inhibited *C. glabrata* growth by directly targeting the CgBdf1 bromodomains.

Table 36. EC₅₀ against *C. glabrata* growth of iCG-24 and its derived compounds.

Compound ID in lab	EC ₅₀ (μM) ⁽¹⁾		
	WT BDF1 ⁽²⁾	BD1 Y-F ⁽²⁾	BD2 Y-F ⁽²⁾
iCG-24	> 250 ⁽³⁾	229 ± 37	74.2 ± 33.0
iCG-24-334	235 ± 25	> 250	56.0 ± 21.8
iCG-24-601	> 250	> 250	98.6 ± 21.8
iCG-24-409	93.0 ± 6.6	117 ± 30	36.6 ± 3.6
iCG-24-676	204 ± 65	141 ± 16	42.3 ± 6.7
iCG-24-040	216 ± 22	216 ± 59	40.0 ± 19.5
iCG-24-381	> 250	> 250	66.6 ± 2.4
iCG-24-1485	> 250	> 250	49.0 ± 5.8
iCG-24-376	ND ⁽⁴⁾	ND	ND
iCG-24-533	ND	ND	ND
iCG-24-800	ND	ND	ND
JMO-i-62	177 ± 39	> 250	64.7 ± 3.8
JMO-i-64	ND	ND	ND
JMO-i-66	ND	ND	ND
JMO-i-68	ND	ND	ND

(1) Yeast growth inhibition EC₅₀ calculated by GraphPad Prime 7 using the “[inhibitor] vs. response (three parameters)” model. Data are presented as means ± SD, n=3 independent experiments.

(2) WT Bdf1, BD1 Y-F and BD2 Y-F represent strains expressing only wildtype Bdf1, Bdf1 with the Y166F mutation, or Bdf1 with the Y343F mutation, respectively.

(3) > 250, EC₅₀ value calculated by GraphPad Prime 7 was higher than 250 μM (weak effect). Data are from three independent experiments.

(4) ND, not determined. No inhibitory effect was detected at 100 μM. Data are from three independent experiments.

5.1.3. iCG-24-409: a dual Bdf1 BD inhibitor active against *C. glabrata*

The initial reason for studying iCG-24 analogs was to identify a compound that retained the CgBD inhibition activity of iCG-24 but had higher solubility to allow the binding mode to be determined by co-crystallography. Surprisingly, during the characterization of the analogs, I discovered two molecules, iCG-24-409 and iCG-24-676, with more potent CgBD2 inhibition activity than all the other compounds including the original one. As already mentioned, iCG-24 did not significantly inhibit the growth of *C. glabrata* strains in which the CgBdf1 BD2 was functional (**Figure 45C**) because of its low inhibitory activity towards CgBD2 (**Table 37**). iCG-24-409 and iCG-24-676, on the other hand, showed inhibition against strains in which CgBD2 was functional (**Table 38**). Between these two molecules, iCG-24-409 was the more potent inhibitor in both the HTRF and growth inhibition assays.

The structure of iCG-24-409 is very similar to that of iCG-24 (**Figure 47A**). The IC₅₀ value towards CgBdf1 bromodomains determined by HTRF assays showed that iCG-24-409 had 4-fold weaker activity against CgBD1 than iCG-24. However, its inhibition activity towards CgBD2 was the strongest among all compounds sharing the same scaffold (**Figure 47B** and **Table 37**). iCG-24-409 also retained good selectivity towards the fungal bromodomains, as it only poorly inhibited Brd4 bromodomains BD1 and BD2. This molecule was also the most potent at inhibiting the growth of all the tested *C. glabrata* strains, including that expressing wildtype Bdf1 (**Figure 47C** and **Table 38**).

In summary, by this point I had discovered a compound, iCG-24-409, that could be described as a dual *C. glabrata* Bdf1 bromodomain inhibitor with interesting bioactivity. The next step would be to further characterize this compound.

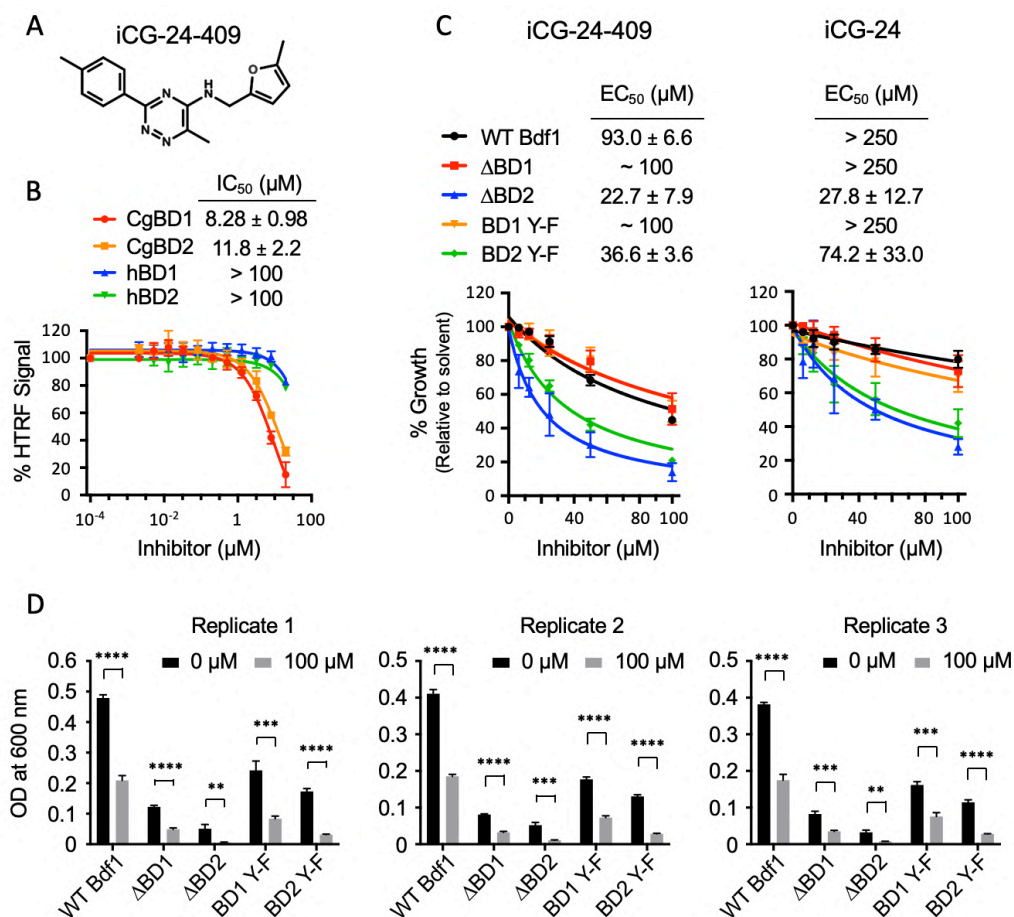


Figure 47. iCG-24-409 is a selective dual CgBD inhibitor with interesting bioactivity. **A.** Chemical structure of iCG-24-409. **B.** *In vitro* inhibition activity of iCG-24-409 towards fungal and human bromodomains determined by HTRF. The CgBD binding inhibition curves were fitted and IC_{50} values determined in GraphPad Prime 7 using the “log(inhibitor) vs. response (three parameters)” model. Data are presented as means \pm SD, $n \geq 2$ independent experiments. hBD1 and hBD2 represent BD1 and BD2 from human Brd4, respectively. **C.** Yeast growth inhibition dose–response curves of iCG-24-409 and iCG-24. Strains were pre-grown in the presence of methionine/cysteine to repress expression of the WT genomic *BDF1*. Only the *BDF1* copy present in the plasmid was expressed. Incubation was at 30 °C for 20, 22 and 24 hours for WT Bdf1, Δ BD1/ Δ BD2 and BD1/BD2 Y-F strains, respectively. The inhibition curves were fitted and EC_{50} values calculated in GraphPad Prime 7 using the “[inhibitor] vs. response (three parameters)” model. Data are presented as means \pm SD, $n = 3$ independent experiments. **D.** The three independent experiments showing yeast growth inhibition by iCG-24-409. Incubation was at 30 °C for 20 hours. Data are presented as means \pm SD from a technical triplicate of the same experiment. Statistical significance was determined using the Holm-Sidak method in GraphPad Prime 7; * $P \leq 0.05$; ** $P \leq 0.01$; *** $P \leq 0.001$; **** $P \leq 0.0001$.

5.2. Target verification of iCG-24-409

So far, I identified a molecule, iCG-24-409, which showed an inhibitory effect both against *in vitro* Bdf1 bromodomain binding activity and *C. glabrata* growth. However, the obtained results did not ensure that the yeast growth inhibition was due to CgBD inhibition, since there may be an off-target effect of the compound. In this section, I set out to verify the correlation between *in vitro* CgBD inhibition and the yeast growth inhibitory effect caused by iCG-24-409.

5.2.1. Cellular Thermal Shift Assay

To verify that CgBDs were the cellular targets of iCG-24-409, one option was to use a Cellular Thermal Shift Assay (CETSA) (Molina *et al.*, 2013). Globular proteins generally have a well-folded structure at physiological temperature or lower. When the environmental temperature increases above the melting temperature (T_m), proteins begin to unfold and have a greater tendency to precipitate. When the cell or lysate is gradually heated, cellular proteins will precipitate at their characteristic T_m . The binding of a small-molecule ligand can stabilize the folded state of the target protein at a higher temperature. Incubation with a specific inhibitor should then yield a shift in solubility of the target protein towards higher temperature compared to the condition without inhibitor (**Figure 48**) (Molina *et al.*, 2013). With this technique, one can demonstrate that a given small molecule binds to the target protein in a cellular context.

I tried to adapt this method to my project. I began with the yeast cellular lysate since it was easier to have promising results. I first tested the melt curve of CgBdf1 without any inhibitor. *C. glabrata* cellular lysate was incubated with a final concentration of 1% of solvent (18% DMSO + 82% ethanol) at room temperature for 20 minutes. The following steps were in order as follows: (i) The cell lysate was aliquoted into multiple PCR tubes on ice (50 μ L per tube). (ii) The tubes were heated at different temperatures spanning a defined range for 3 min in a PCR machine then cooled on ice. (iii) The precipitated protein was pelleted. (iv) The soluble protein was detected by Western blotting.

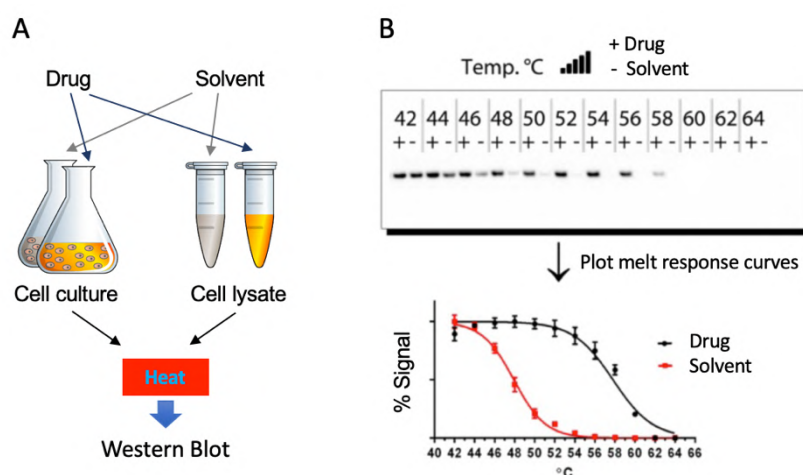


Figure 48. Schematic illustration of the CETSA procedure. **A.** A cell culture or cellular lysate is incubated with a drug or the vehicle as a control. Samples are heated at different temperatures spanning a defined range. After removing the precipitated fraction, the soluble fraction is analyzed by a Western blot. **B.** The soluble fraction from samples heated at different temperatures with or without drug show different levels of soluble target protein detected by a specific antibody. The intensity of bands obtained in the Western blot are plotted against the temperature. (adapted from Molina et al., 2013)

The results showed that the melting curve for CgBdf1 could be successfully made as the negative control. The amount of soluble CgBdf1 began to decrease at 48 °C and the T_m was about 50 °C (**Figure 49B and 49D**). I next tried to establish a positive control. So far, the small molecule that showed the highest inhibitory effect against CgBDs was I-BET151, with IC_{50} of about 2.3 μ M and 0.5 μ M for CgBD1 and CgBD2, respectively. This compound was tested to see whether it could stabilize CgBdf1 in yeast cellular lysate at a higher temperature. 90 μ M I-BET151 was incubated with cellular lysate containing 4 mg/mL whole protein at room temperature for 20 minutes before performing the CETSA. The melting curves showed that I-BET151 did indeed stabilize CgBdf1 in the cellular lysate: a shift in T_m of almost 2 °C could be observed (**Figure 49C and 49E**). Thus, a CETSA appeared useful for checking whether a given small molecule actually bound to CgBdf1 in a *C. glabrata* cellular lysate.

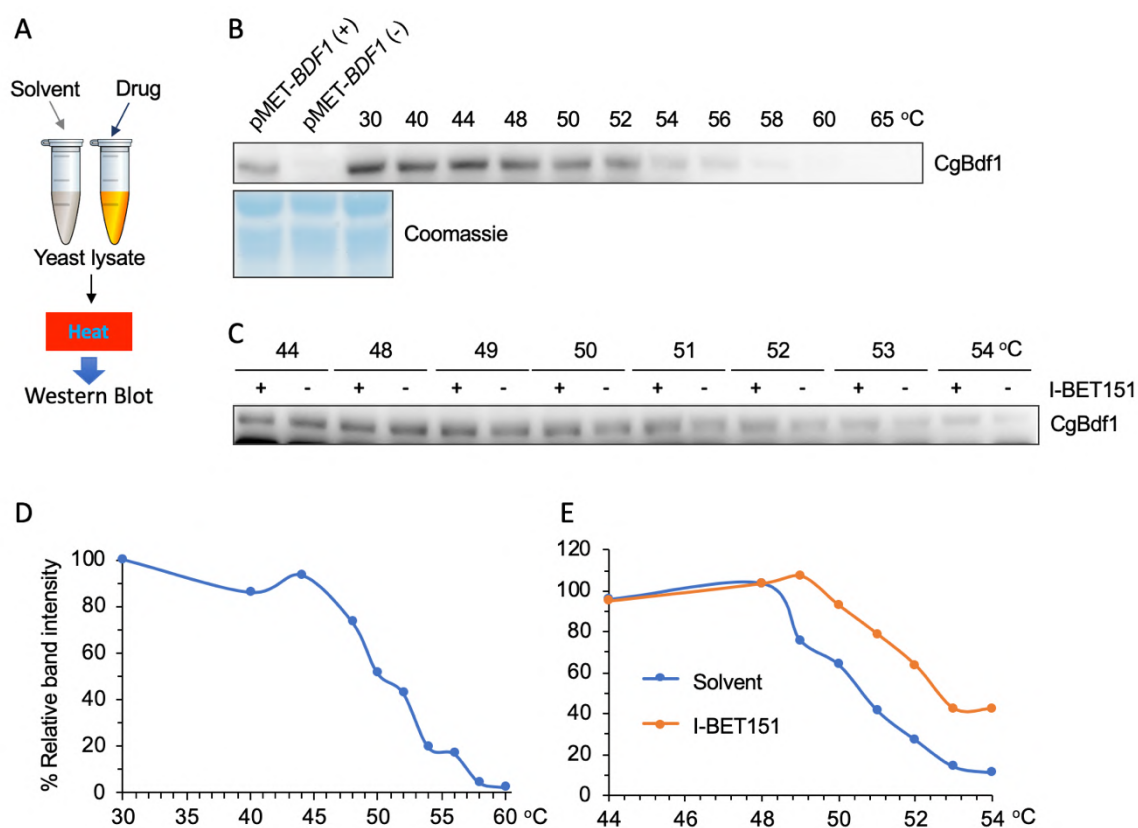


Figure 49. I-BET151 protected CgBdf1 from heat. **A.** CETSA procedure for yeast cellular lysate. **B.** Western blot of *C. glabrata* cellular lysate heated at different temperatures. Anti-ScBdf1 antibody was used as the primary antibody. pMET-BDF1 (+): whole cell extract (WCE) from *C. glabrata* pMET-BDF1 strain without pMET repression; pMET-BDF1 (-): WCE from *C. glabrata* pMET-BDF1 strain with pMET repression. The repression of pMET lasted 8 hours. **C.** Western blot of *C. glabrata* cellular lysate incubated with 90 μ M I-BET151 and heated at different temperatures. Incubation was at room temperature for 20 minutes. Anti-ScBdf1 antibody was used as the primary antibody. **D.** Melting curve from data shown in panel B. **E.** CETSA curve from data shown in panel C.

I then tried to apply this method to validate the binding of iCG-24-409 to CgBdf1 in a cellular lysate. iCG-24-409 was incubated with cellular lysate using the same conditions as previously used for I-BET151. The Western blot results did not show a clear stabilizing effect of CgBdf1 by iCG-24-409. At 50 °C, there was indeed more soluble CgBdf1 when the inhibitor was present. However, at 54 and 56 °C, it seemed like less soluble protein was detected than in conditions without the inhibitor (**Figure 50A and 50C**). Next, I also tried to perform a dose response assay. Different concentrations of iCG-24-409 were incubated with the cellular lysate for 20 minutes or one hour before being heated. The results showed that the tendency was the same for both incubation times. With increasing inhibitor concentration, the soluble CgBdf1 in the lysate seemed to increase (**Figure 50B and 50D**). Overall, however, the results were not as convincing as the results obtained with I-BET151.

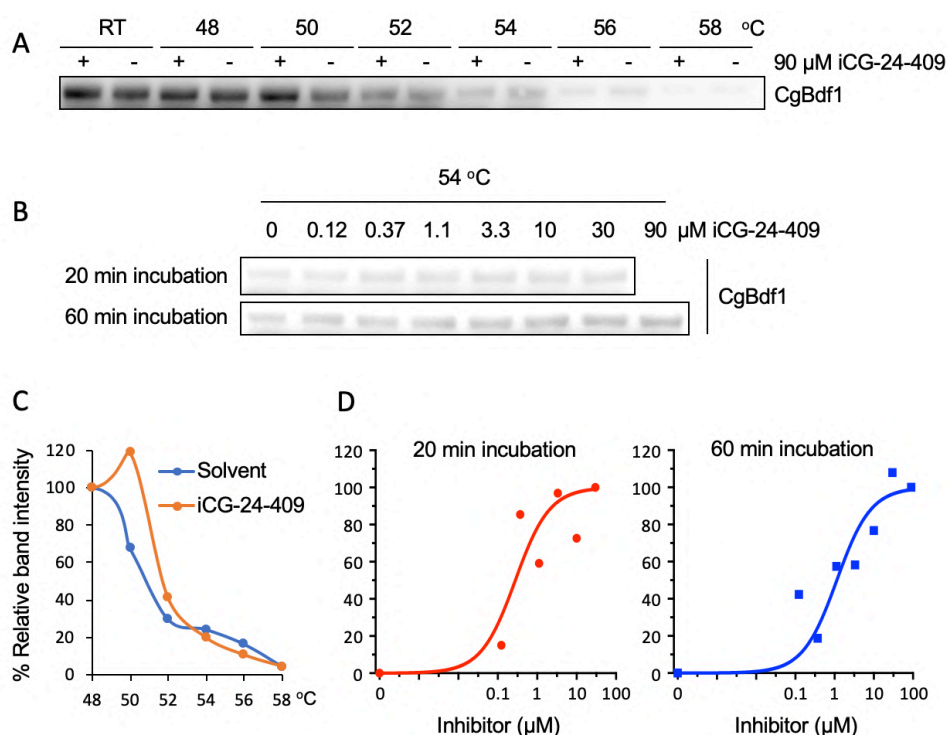


Figure 50. CETSA assay to verify the binding of iCG-24-409 to CgBdf1. Western blot of *C. glabrata* cellular lysate in TENG150 buffer. **A.** Lysate was incubated with 90 μM iCG-24-409 and heated at different temperatures. Incubation was at room temperature for 20 minutes. An anti-ScBdf1 antibody was used as the primary antibody. **B.** Lysate was incubated with different iCG-24-409 concentrations and heated at 54 °C. Incubation was at room temperature for 20 minutes. An anti-ScBdf1 antibody was used as the primary antibody. **C.** Melting curves from data shown in panel A. **D.** CETSA curve from data shown in panel B.

I showed in section 1.1.1. of this chapter that the sensitivity and specificity of the anti-ScBdf1 antibody were low when used to detect CgBdf1. This might limit its usefulness for demonstrating small differences in CgBdf1 levels. To resolve this problem, I constructed a *C. glabrata* strain in which the expressed CgBdf1 was C-terminally tagged by a FLAG octapeptide, which could be detected with high sensitivity by the monoclonal anti-FLAG M2 antibody from Sigma-Aldrich (F1804) (**Figure 51A**). A CETSA was then performed using the cellular lysate from this strain. The results did not show any stabilizing effect of iCG-24-409 on CgBdf1-FLAG regardless of whether the lysate was in TENG150 (containing Tris, EDTA, 150 mM NaCl, Glycerol) buffer or PBS (**Figure 51B and 51C**).

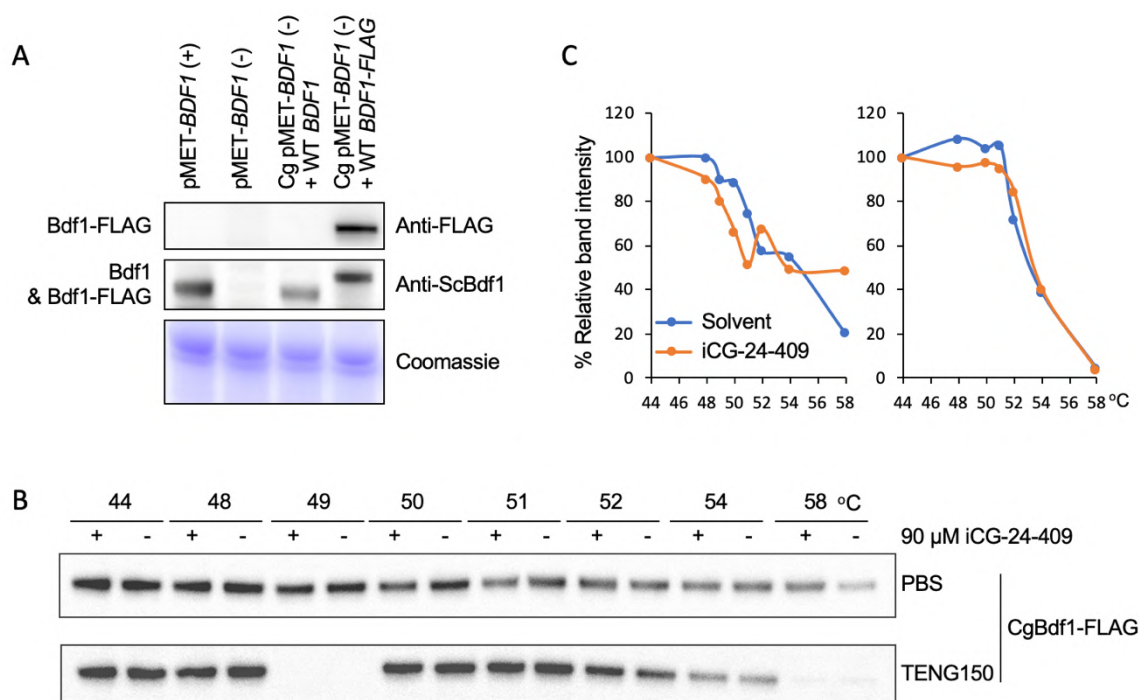


Figure 51. iCG-24-409 did not enhance the thermal stability of a FLAG tagged CgBdf1 protein in a CETSA. **A.** Verification of FLAG-tagged Bdf1 expression by Western blot. pMET-*BDF1* (+): whole cell extract (WCE) from *C. glabrata* pMET-*BDF1* strain without pMET repression; pMET-*BDF1* (-): WCE from *C. glabrata* pMET-*BDF1* strain with pMET repression; Cg pMET-*BDF1* (-) + WT *BDF1*: WCE from *C. glabrata* pMET-*BDF1* strain transformed with plasmid containing wildtype *BDF1* gene; Cg pMET-*BDF1* (-) + WT *BDF1*-FLAG: WCE from *C. glabrata* pMET-*BDF1* strain transformed with plasmid containing wildtype *BDF1*-FLAG gene. The repression of pMET lasted 8 hours. **B.** Western blot of cellular lysate in PBS or TENG150 buffer incubated with 90 μ M iCG-24-409 and heated at different temperatures. Incubation was at room temperature for 20 minutes. An anti-FLAG antibody was used as the primary antibody. **C.** Melting curves from data shown in panel B.

The IC₅₀ of I-BET151 was 2.3 μ M for CgBD1 and 0.5 μ M for CgBD2. These values are considerably lower than those of iCG-24-409, which are about 7 and 12 μ M against CgBD1 and CgBD2, respectively. The T_m change obtained with I-BET151 was less than 2 °C, and so the affinity of iCG-24-409 might be too low to yield a detectable shift in the thermal stability of CgBdf1. Thus, CETSA might not be a good technique to verify the target of an inhibitor with a low affinity, such as iCG-24-409.

5.2.2. Bromodomain replacement

Since I did not successfully validate Bdf1 as the cellular target of iCG-24-409 by the CETSA approach, another approach was needed. The observation that iCG-24-409 showed

higher inhibitory activity against CgBDs than human Brd4 bromodomains (**Figure 47B**) inspired in me the idea to replace the two BDs in CgBdf1 by the corresponding human Brd4 BDs in *C. glabrata*. If the yeast strain expressing the humanized Bdf1 could still grow and if the growth inhibition activity of the inhibitor was reduced against the humanized, but not the WT strain, then the target would be validated.

I aligned the crystal structures of CgBD1 in its iCG-24-409 bound conformation and human Brd4 BD1 in its JQ1 bound conformation (PDB code: 3MXF). Guided by this alignment I decided to replace residues 128-233 in CgBD1 by residues 58-164 in Brd4 BD1. For BD2, I aligned the crystal structures of CgBD2 and Brd4 BD2 both in their unbound conformation and chose to replace residues 302-410 of the former by residues 347-457 of the latter. I then constructed the plasmid in which the *C. glabrata BDF1* gene encoded the CgBdf1 protein containing hBD1 (Brd4 residues 58-164) and hBD2 (Brd4 residues 347-457) instead of the original CgBDs (**Figure 52A**). Since a FLAG octapeptide coding sequence was also added to the 3' of the gene sequence, I named this humanized *BDF1* gene as *BDF1*-hBD-FLAG and the strain expressing this gene the *BDF1*-hBD-FLAG strain.

At the same time, I also generated a strain that expressed a humanized form of CgBdf1 whose residues 128-410 were replaced by residues 58-457 of Brd4 (i.e., spanning both BDs). However, that strain grew too slowly with the doubling time exceeding eight hours (Data not shown) as opposed to about 1.5 hours for the wildtype strain. Considering that the distance between the two bromodomains in Brd4 is larger than in CgBdf1 (**Figure 19A**), this result suggested that the linker region between the two bromodomains might play an important functional or structural role, such as properly orientating the two bromodomains or recruiting a binding partner.

Once the *BDF1*-hBD-FLAG strain was generated, I first verified the expression level of Bdf1. Compared to the strain expressing the wildtype FLAG-tagged CgBdf1 (WT *BDF1*-FLAG strain), the *BDF1*-hBD-FLAG strain expressed a higher level of Bdf1 (**Figure 52B**). This indicated that the humanized CgBdf1 might not function as well as wildtype Bdf1 and that the cell needed to express more to compensate for the functional defect. The growth curves of the two strains demonstrated that even though more Bdf1 was present in the cell, the humanized yeast strain grew more slowly than the wildtype (**Figure 52C**).

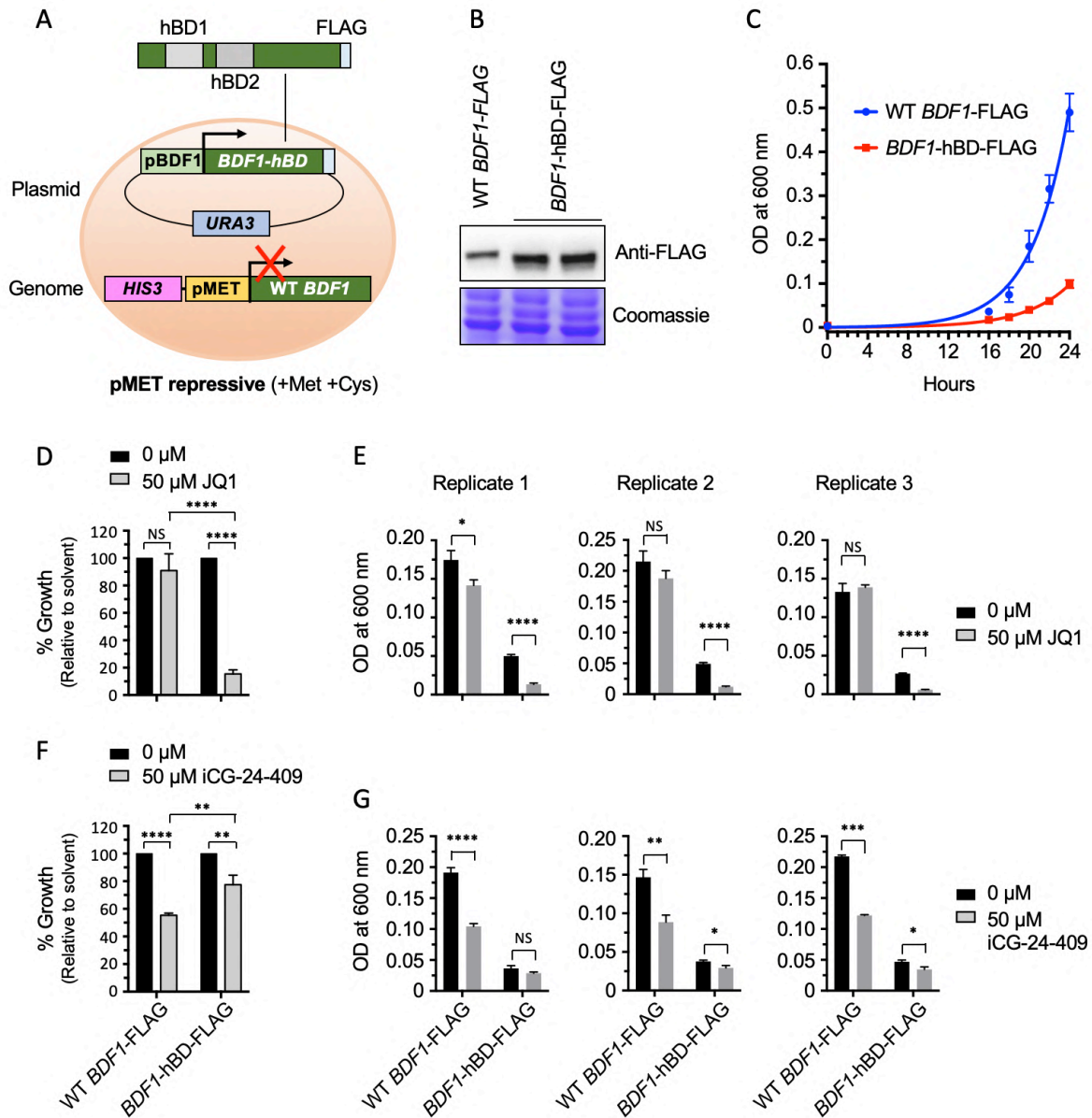


Figure 52. Bromodomain replacement strategy showing that iCG-24-409 inhibits *C. glabrata* growth by targeting CgBdf1 BDs. **A.** Construction of the humanized *C. glabrata* strain. *BDF1*-hBD: CgBDF1 in which the BD-encoding DNA sequences were replaced by sequences encoding BD1 and BD2 from human Brd4; hBD1 and hBD2: DNA sequences encoding BD1 (residues 58-164) and BD2 (residues 347-457) from human Brd4; FLAG: FLAG tag. **B.** Western blot showing the expression level of FLAG-tagged Bdf1 in whole cell extracts of different strains. Strains were grown in the presence of methionine/cysteine to repress expression of the WT genomic *BDF1* for 24 hours. Only the *BDF1* present in the plasmid was expressed. WT *BDF1*-FLAG: wildtype *BDF1*-FLAG in the plasmid; *BDF1*-hBD-FLAG: *BDF1*-FLAG gene in the plasmid containing both BD1 and BD2 from *BRD4*. **C.** Growth curves of WT *BDF1*-FLAG strain and *BDF1*-hBD-FLAG strain. Strains were pre-grown in the presence of methionine/cysteine to repress expression of the WT genomic *BDF1* for 24 hours at 30 °C. DMSO and ethanol were present at a final concentration of 0.2% and 0.8%, respectively. **D** and **F.** Relative growth rate of different strains in the presence of 50 μM JQ1 (**D**) or iCG-24-409 (**F**) compared to solvent. Strains were pre-grown in the presence of methionine/cysteine to repress expression of the WT genomic *BDF1* for 24 hours. Incubation was at 30 °C for 20 and 24 hours for WT-*BDF1*-FLAG strain and *BDF1*-hBD-FLAG strain, respectively. Data are presented as means ± SD, n = 3 independent experiments; Statistical significance was measured using the Holm-Sidak method in GraphPad Prime 7; * P ≤ 0.05; ** P ≤ 0.01; *** P ≤ 0.001; **** P ≤ 0.0001. **E** and **G.** Three

independent experiments showing optical density values at 600 nm which used to generate panels (D) and (F), respectively.

Although the humanized strain grew more slowly than the wildtype strain, after 24 hours of growth the optical density at 600 nm could still reach 0.1. Next, the effect of inhibitors was tested against the *BDF1*-hBD-FLAG and WT *BDF1*-FLAG strains. I first tested JQ1, which has a very strong selectivity for hBDs over CgBDs (**Figure 37A**). Previous test had already shown that JQ1 had almost no inhibitory effect on *C. glabrata* growth (**Figure 37C**), which was once more confirmed here (**Figure 52D and 52E**). However, on the strain expressing CgBdf1 containing the two human Brd4 bromodomains, JQ1 showed a strong inhibitory effect on yeast growth (**Figure 52D and 52E**). This result confirmed that the *BDF1*-hBD-FLAG strain was well constructed and that the bromodomain functionality of Bdf1 is essential for growth.

Finally, the effect of iCG-24-409 was tested. The results in **Figure 52F and G** showed that the inhibitory effect on yeast growth was significantly lower for the humanized *C. glabrata* strain than for the WT *BDF1*-FLAG strain. That directly demonstrated that the yeast growth inhibition shown by iCG-24-409 was at least partly due to its ability to inhibit CgBDs.

In summary, so far, I had identified a selective dual CgBD inhibitor and showed that its ability to inhibit yeast growth *in vitro* was an on-target effect.

5.3. Further characterization of iCG-24-409

5.3.1. Characterization of CgBdf1 bromodomain binding activity of iCG-24-409

The ability of iCG-24-409 to inhibit CgBdf1 bromodomains from binding an acetylated histone peptide had been established and the IC₅₀ values determined using HTRF assays. However, a direct binding assay allowing binding affinities to be determined had not yet been established. This section describes my attempts to do so.

5.3.1.a. Thermal shift assay

The thermal shift assay (TSA) is widely used to show the binding activity of a small molecule onto a protein. In this assay, the protein is labeled with a fluorescent dye (Sypro-Orange) that specifically binds to hydrophobic residues, which are usually buried inside a well folded protein. As the temperature increases, the protein unfolds and exposes its hydrophobic residues, increasing the amount of bound dye. During this initial stage, the fluorescence signal increases with temperature until reaching a maximum at a certain temperature. After that, the fluorescence decreases with further increasing temperature because of protein aggregation and dye dissociation. The melting temperature (T_m) in TSA represents the temperature at which half the maximal fluorescence signal is reached (**Figure 53A**).

As for CETSA, the binding by a small ligand stabilizes the protein and results in an increased T_m . In principle, the higher is the binding affinity of the small ligand, the larger is the shift of T_m observed. I therefore performed TSAs to assess the binding of iCG-24-409 on purified CgBD1 and CgBD2. I tried two different buffers, the buffer used for SEC purification (150 mM NaCl, 25 mM Hepes pH7.5 and 0.5 mM DTT) and a buffer derived from the HTRF assay (an equivolume mixture of the Cisbio EPlgeneous Binding Domain Diluent Buffer and Domain Detection Buffer #2). All the tests were performed with the help of Philippe Mas, who runs the ISBG (Integrated Structural Biology Grenoble) ESPRIT platform in Darren Hart's team at the IBS.

The assay was unsuccessful for CgBD1. In both buffers tested with or without inhibitor the fluorescence signal steadily kept decreasing as the temperature rose (data not shown). More buffers might need to be tested for this protein. The same result was observed for CgBD2 when the HTRF buffer was used (data not shown). This buffer contains a detergent which probably interfered with the ability of Sypro-Orange to bind to the unfolding protein. Fortunately, a proper melting curve could be obtained for CgBD2 in SEC buffer (**Figure 53B and C**). I tested the effect of iCG-24-409 on the stability of CgBD2 using two compound concentrations (160 and 200 μ M) and three protein concentrations (5, 10 and 20 μ M). With 5 μ M protein, the thermal shift was not very clear, but with 10 and 20 μ M protein, the shift was more evident, yielding ΔT_m values of 0.9 $^{\circ}$ C and 1.4 $^{\circ}$ C with 160 μ M compound and 1.8 $^{\circ}$ C and 1.4 $^{\circ}$ C at 200 μ M compound, respectively (**Figure 53B**).

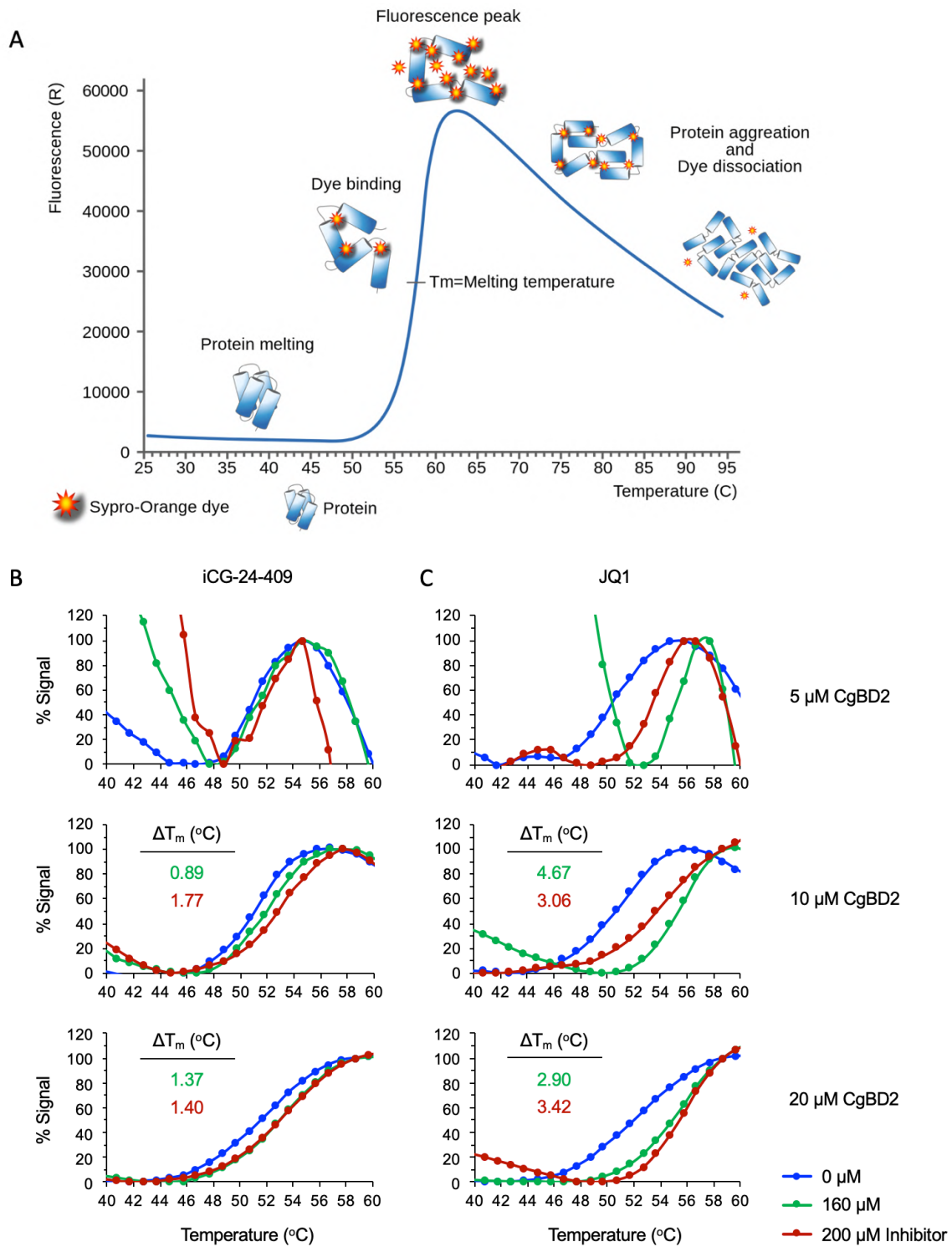


Figure 53. iCG-24-409 binding to CgBD2 shown by TSA. A. The principle of TSA. **B** and **C.** Melting curves of CgBD2 tested at different protein concentrations in the presence of 0, 160 or 200 μM iCG-24-409 (**B**) or JQ1 (**C**).

To verify that these T_m shifts were reasonable, we performed the same assay with JQ1. In the HTRF assay the IC_{50} towards CgBD2 of JQ1 (0.75 μ M) was significantly lower than that of iCG-24-409 (11.8 μ M), and so a larger ΔT_m should be observed for JQ1. This was indeed the case in all conditions tested, with ΔT_m values ranging between 2.89 °C and 4.67 °C (**Figure 53C**).

Taken together, these TSA results demonstrated the direct binding of iCG-24-409 to CgBD2. However, a more suitable assay was needed to measure the binding affinity.

5.3.1.b. Isothermal titration calorimetry

Isothermal titration calorimetry (ITC) is a commonly used method to study macromolecular interactions. Chemical reactions, including binding events, generally are accompanied by either the release or the absorption of heat. Based on this principle and by measuring and analyzing the temperature change of a binding reaction, ITC allows us to directly obtain important thermodynamic parameters characterizing a molecular interaction, including the binding constant (K_d) and the reaction stoichiometry (N).

The principle of ITC is described in **Figure 54**. When studying the interaction between a macromolecule (protein for example) and a small molecule (peptide, chemical compound), the syringe is generally used for the latter and the cell sample for the former in order to minimize the temperature change due to the dilution of the macromolecule. However, the solubility of compound iCG-24-409 was too low in aqueous solution to achieve the high concentration required for the injected sample. Accordingly, I adopted the method commonly used for BET inhibitors in ITC experiments, in which the bromodomain is placed in the syringe and the chemical inhibitor is placed in the sample cell (Filippakopoulos *et al.*, 2010; Mietton *et al.*, 2017).

We have performed initial preliminary experiments with CgBD1, which compared to CgBD2 has a higher affinity for iCG-24-409 according to the HTRF assay. All the ITC experiments for this project were performed by Caroline Mas, who runs the ISBG ITC platform in Darren Hart's team at the IBS.

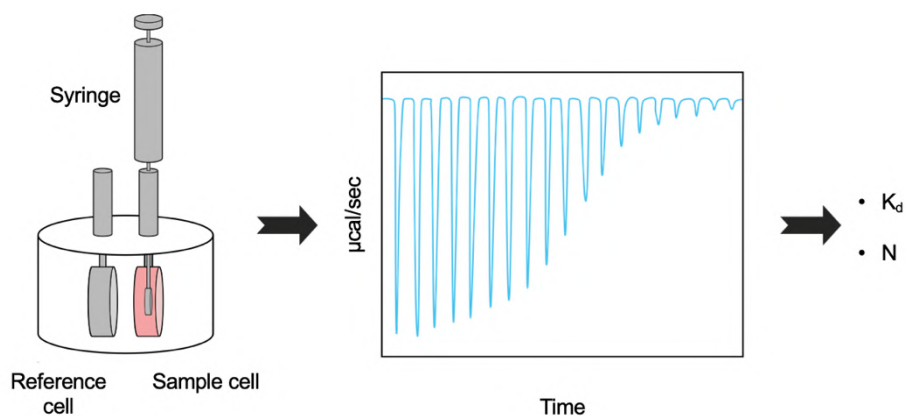


Figure 54. The principle of isothermal titration calorimetry (ITC). There are three major spaces in an ITC instrument: the syringe, sample cell and reference cell. The two cells are in an isothermal environment. The reference cell is generally filled with water, whose temperature is considered to be constant and used as reference to determine temperature changes in the sample cell. The two molecules that interact with each other are placed separately in the syringe and sample cell. During the experiment, the molecule in the syringe is injected little by little but constantly into the sample cell and interacts with the molecule inside the latter. Each injection gives rise to a temperature change if there is an interaction between the two molecules. The temperature change of each injection is then represented as the heat released or absorbed (expressed in microcalories, μcal) and plotted with time. Based on the plotted figure and data, the thermodynamic parameters of the molecular interaction, such as the binding constant (K_d) and reaction stoichiometry (N), can be calculated.

Caroline began with control experiments by titrating either the protein into the buffer or the buffer into the chemical compound. Both titrations showed a strong signal for each injection (**Figure 55A and B**). A possible reason for that could be the mismatch of DMSO concentration among the buffer, protein and chemical compound samples. We nevertheless proceeded with testing the titration of CgBD1 into the inhibitor even with some potential DMSO mismatch. The ITC profile showed increasing positive signal peaks during the course of the titration that initially rose rapidly and eventually resembled the profile seen with the compound dilution experiment (**Figure 55C**). After applying a correction using the control titration, a K_d of about $16 \mu\text{M}$ was obtained. This was in good agreement with the IC_{50} value of $8.5 \mu\text{M}$ obtained by HTRF.

To confirm this result, we performed a second ITC experiment (on a separate day), taking greater care to match the DMSO concentrations. This time, the control titration of buffer into compound gave much smaller peaks (**Figure 55E**), while the titration of CgBD1 into iCG-24-409 showed negative peaks whose size became smaller as the titration proceeded, with the final peaks corresponding to those from the control (**Figure 55D**). The calculated K_d

was about 54 μM , much higher than that obtained in the first experiment and almost 7-fold higher than the IC_{50} value.

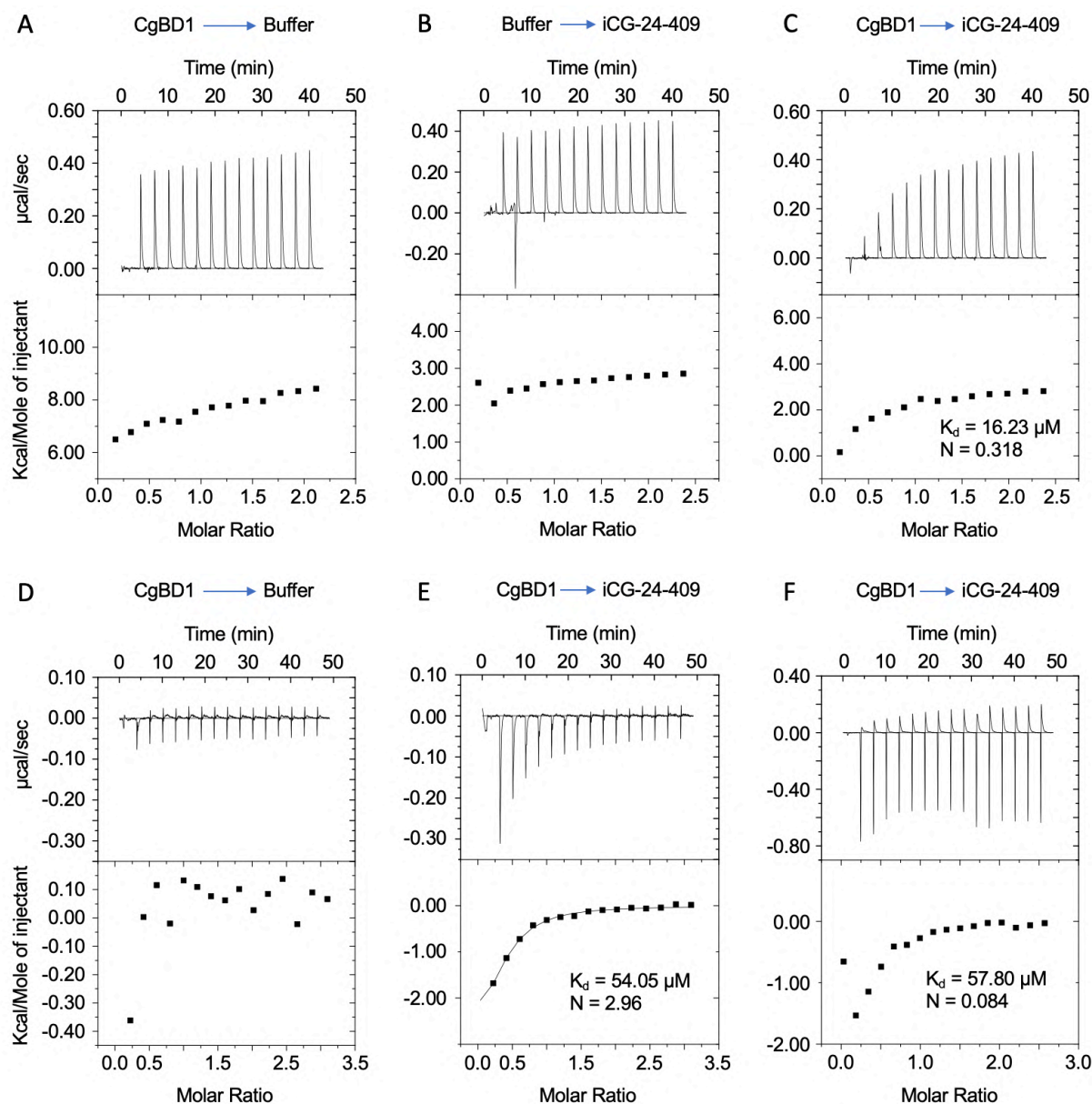


Figure 55. Preliminary ITC experiments for the interaction between CgBD1 and iCG-24-409. A, B and D. Control titrations. CgBD1 protein was titrated into the buffer (A and D) or the buffer was titrated into the compound iCG-24-409 (B). C, E and F. Different titrations of CgBD1 into iCG-24-409. A and B were the control titrations for C. D was the control titration for E. All titrations were performed at 25 $^{\circ}\text{C}$. Protein concentrations were 885 μM (A and C) or 1200 μM (D, E and F). The compound concentration was 79 μM (B, C, E and F). The final DMSO concentration was 0.99%. Data were analyzed with software provided by the manufacturer using a single binding site model.

To verify this result, a third measurement was performed on the same day using the same samples as for the second experiment. This time the ITC profile appeared highly aberrant (**Figure 55F**). Although a similar K_d value ($58\ \mu\text{M}$) was obtained, the reaction stoichiometry (N) was decreased from 2.9 to 0.084, indicating that the values were not at all reliable. The two radically different profiles suggest that either the CgBD1 protein or the chemical inhibitor iCG-24-409, might not be not very stable. Indeed, I had previously observed that this compound loses activity in the HTRF assay over extended periods of time, suggesting that it might spontaneously undergo some chemical modification. Additional experiments are needed to sort this out.

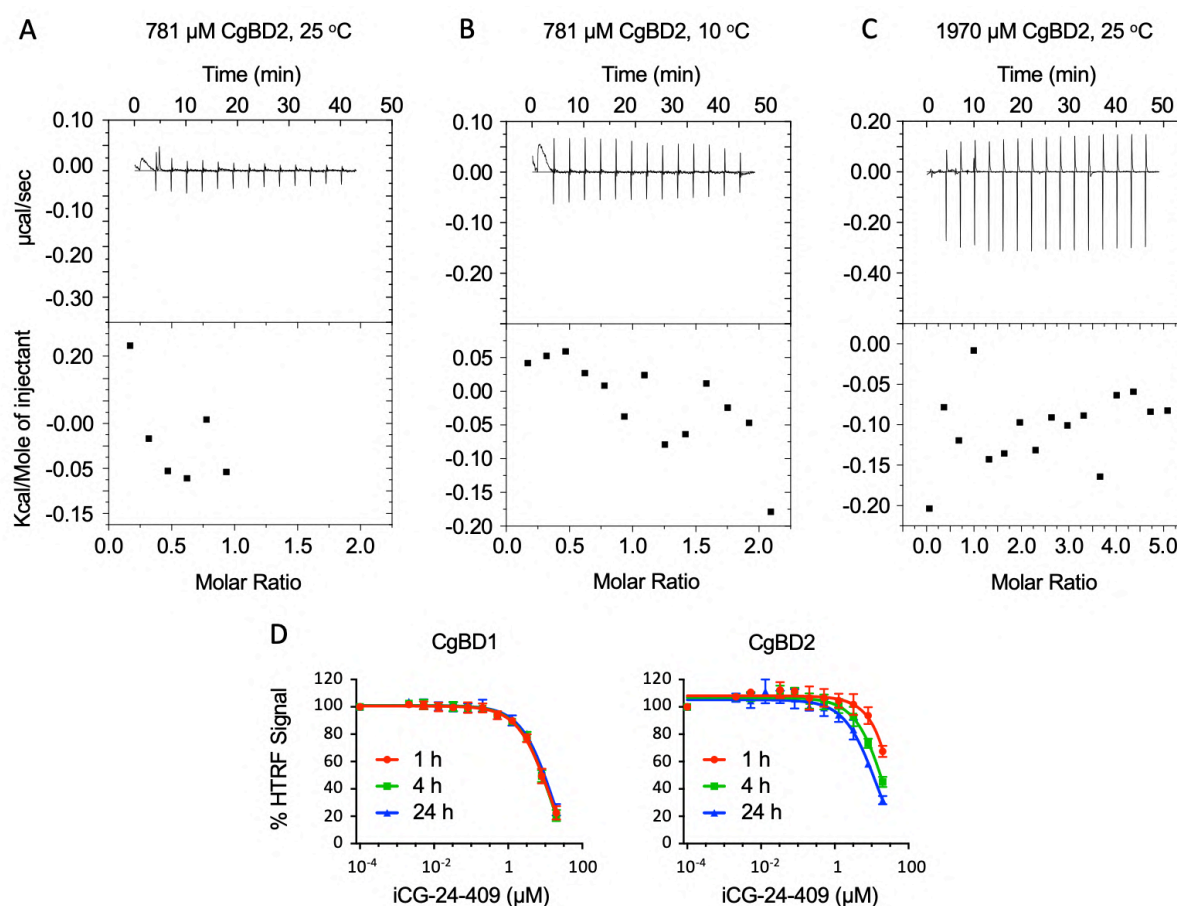


Figure 56. Primary ITC tests for the interaction between CgBD2 and iCG-24-409. A, B and C. Titrations were performed at 25 °C (A and C) or 10 °C (B). Protein concentrations were 781 μM (A and B) or 1970 μM (C). The compound concentration was 79 μM . The final DMSO concentration was 0.99%. Data were analyzed with software provided by the manufacturer using a single binding site model. D. *In vitro* inhibition activity of iCG-24-409 towards CgBdf1 bromodomains determined by HTRF with different incubation time. The CgBD binding inhibition curves were fitted in GraphPad Prime 7 using the “log(inhibitor) vs. response (three parameters)” model. Data are presented as means \pm SD, $n \geq 2$ independent experiments.

According to the HTRF assay, compared to CgBD1 iCG-24-409 had a smaller affinity for CgBD2 with an IC_{50} about 12 μ M. However, the TSA test had shown the thermostabilizing effect of iCG-24-409 on CgBD2. That encouraged us to try to titrate CgBD2 into the inhibitor. For the first experiment, the ITC profile showed very tiny peaks, just like there was no interaction at all (**Figure 56A**). Changing the temperature from 25 °C to 10 °C did not significantly improve the profile (**Figure 56B**), nor did using a much higher CgBD2 concentration (**Figure 56C**).

During the HTRF assay to determine the IC_{50} of iCG-24-409, I noticed that this compound showed little inhibitory effect against CgBD2 after 1 or 4 hours of incubation, and required 24 hours before an IC_{50} could be determined, whereas its inhibitory effect against CgBD1 could be easily obtained after only 1 hour (**Figure 56D**). This suggests that the binding of iCG-24-409 to CgBD2 might be a slow reaction. If so, ITC might not be a good method to study this interaction. In any case, more tests should be tried, maybe with other buffers at different temperatures, or another solvent for the compound.

In summary, these preliminary ITC results demonstrated the direct binding of iCG-24-409 to CgBD1. However, these experiments need to be optimized to measure binding affinities more reliably.

5.3.2. Binding mode of iCG-24-409 by co-crystallography

Previously, I did not successfully obtain co-crystals of CgBDs with the original iCG-24 compound due to the low solubility of inhibitor in aqueous buffer. A useful indicator of the solubility of a compound is the partition coefficient P , defined as the ratio of concentrations of a solute in a mixture of two immiscible solvents (often expressed in its logarithmic form, $\log P$). When one of the solvents is water and the other is a non-polar solvent (usually octanol), then $\log P$ equals $\log ([\text{solute}]_{\text{oct}}/[\text{solute}]_{\text{water}})$ and is a measure of lipophilicity or hydrophobicity. A low $\log P$ indicates a high solubility in aqueous solution of the given molecule. An estimate for the value of $\log P$ for a given compound can be calculated from its chemical structure. Our collaborator Nathan Dupper at USC used the ChemAxon software

Marvin to calculate values of $\log P$ for iCG-24 and iCG-24-409, which were 3.139 and 2.953, respectively, indicating that the latter compound should be more soluble in aqueous solution.

A technician in our lab at the IBS, Amédé Larabi, tried to co-crystallize iCG-24-409 with both CgBDs while I was performing the experiments described in section 5.2 of this chapter. Crystals were obtained with both BDs and tested for diffraction at SOLEIL, the synchrotron facility near Paris. One of the co-crystals of CgBD1 with iCG-24-409 diffracted well, yielding a dataset at a resolution of 2.22 Å. The structure could be solved by my supervisor Carlo Petosa. Crystallization conditions and final R-factor statistics are shown in **Figure 57A**. The complete crystallographic statistics are shown in appendix II.

The co-crystal structure shows that nitrogens of the triazine and amine moieties of iCG-24-409 form direct hydrogen bonds with the conserved Asn209 side chain and the Pro151 backbone carbonyl, respectively. There is also a water-mediated hydrogen bond with the conserved Tyr166 residue and several van der Waals contacts between the inhibitor and hydrophobic residues of the bromodomain (**Figure 57B**).

Diffraction data sets were also collected at Soleil for CgBD2 co-crystallized with iCG-24-409. Unfortunately, data analysis showed that there was no ligand bound to CgBD2 in these crystals, probably because of the lower binding affinity for this domain. Consequently, in order to visualize how this compound might interact with CgBD2, I aligned the CgBD1/iCG-24-409 crystal structure with that of CgBD2 in both its unbound and I-BET151 bound conformations. A steric clash between CgBD2 residue Tyr327 and the methylfuran moiety of iCG-24-409 was observed when the alignment was performed with the unbound conformation of CgBD2 (**Figure 57D**). This bromodomain changes conformation to accommodate the binding of I-BET151, forming a slightly larger binding pocket and re-orientating the Tyr327 side chain. These changes would also allow a much better fit of iCG-24-409 to CgBD2 (**Figure 57E**). Finally, when I aligned the inhibitor onto the Brd4 BDs, BD1 residue Trp81 and BD2 residue Trp374 formed very evident steric clashes with the methylfuran moiety of the ligand (**Figure 57F and G**). This is probably the reason that iCG-24-409 showed such high selectivity towards CgBDs compared to Brd4 bromodomains.

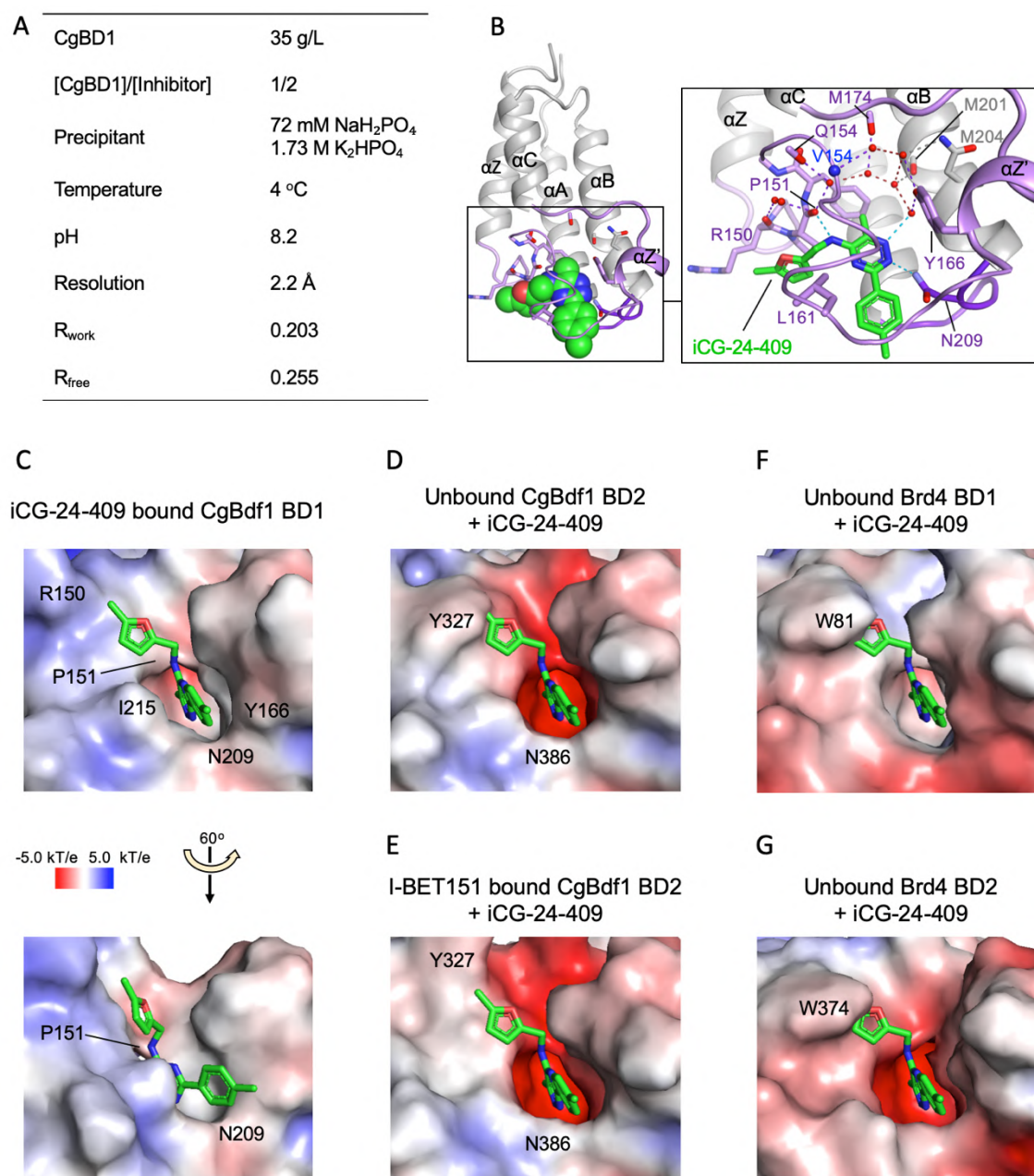


Figure 57. Structure of CgBD1 bound to iCG-24-409 and predicted interactions for different bromodomains. **A.** Co-crystallization conditions of CgBD1 with iCG-24-409 and final R-factor statistics. **B.** Crystal structure of CgBD1 bound to iCG-24-409. Inset. Details of the binding site. Residues interacting with iCG-24-409 through direct and water-mediated hydrogen bonds (dashed lines) are shown in stick representation. **C.** Surface representation showing the binding pocket of CgBD1 bound by iCG-24-409. **D** and **E** Hypothetical models of iCG-24-409 aligned onto the crystal structure of CgBD2 in its unbound conformation (**D**) and its I-BET151-bound conformation (**E**). The models were made by aligning the CgBD2 structures with that of the ligand-bound CgBD1. The root-mean square distances of the alignments were 1.60 (**D**) and 1.58 (**E**). **F** and **G.** Hypothetical model of iCG-24-409 aligned onto the crystal structure of (**F**) human Brd4 BD1 in its unbound conformation (PDB code 4LYI) and (**G**) Brd4 BD2 (PDB code 2OUO). The models were made by aligning the Brd4 bromodomain structures with that of ligand-bound CgBD1. The root-mean square distances of the alignments were 1.78 (**F**) and 2.39 (**G**).

5.3.3. Cytotoxicity of iCG-24-409 towards human cell lines

Next, we set out to test the toxicity of compound iCG-49_409 on human cell lines. To that aim, I perform an MTT colorimetric assay (using the Cell Proliferation Kit I from Roche), which had previously been used in the lab. This assay is based on the transformation of the small-molecule compound MTT in living cells. MTT is a yellow tetrazole that is reduced to formazan, a soluble purple compound (absorbance peak at 570 nm), by mitochondrial reductase in living cells (**Figure 58A**). Cell viability in this test is assessed by the rate of reduction of MTT: a high rate indicates a high percentage of living cells, whereas dead cells give a low rate. However, MTT reduction is NAD(P)H independent, and so the cellular level of metabolism (especially that of NAD(P)H) and mitochondrial function can have a great influence on the MTT reduction rate (Berridge, Herst and Tan, 2005).

All the tests described below were performed with the help of Dimitrios Skoufias in our lab. We began with HeLa cells (epithelial cancer cells, ATCC number CCL-2). We chose two commonly used antifungal agents, amphotericin B and fluconazole, as positive and negative controls, respectively. As mentioned in section 1.3 of Chapter I, amphotericin B has a high cytotoxicity level against mammalian cells since it can bind to cholesterol in the cell membrane and lead to cell death. In contrast, fluconazole targets the fungal ergosterol synthesis pathway which is absent in mammalian cells and consequently has very low cytotoxicity for human cells. Indeed, in three independent experiments, fluconazole did not show any cytotoxicity against HeLa cells while amphotericin B showed a Half-maximal Cytotoxicity Concentration (CC_{50}) below 20 μ M (**Figure 58B**). For iCG-24-409, the CC_{50} values obtained varied in the three experiments. In the first experiment, a cytotoxicity effect was observed only at 100 μ M of iCG-24-409 but not lower concentrations, while in the second experiment the CC_{50} of this compound was about 70 μ M, which was lower than the EC_{50} (about 90 μ M) against the *C. glabrata* strain expressing wildtype Bdf1. For the third test, iCG-24-409 showed no detectable cytotoxicity even at 100 μ M (**Figure 58B**). It should be noted that we used three independent passages of HeLa cells for the three tests and that their ability to resist toxic chemical agents probably differed. Indeed, in the experiment in which a higher cytotoxicity of iCG-24-409 was observed, a higher cytotoxicity was also observed for amphotericin B. Compound instability might also have contributed to variability. In any event, merging the data from all three experiments and fitting the resulting curve yielded a CC_{50} of about 100 μ M for iCG-24-409,

which was much higher than for amphotericin B (**Figure 58C**). The similarity of this value to the EC_{50} against *C. glabrata* indicates that the compound is equally toxic to HeLa and fungal cells.

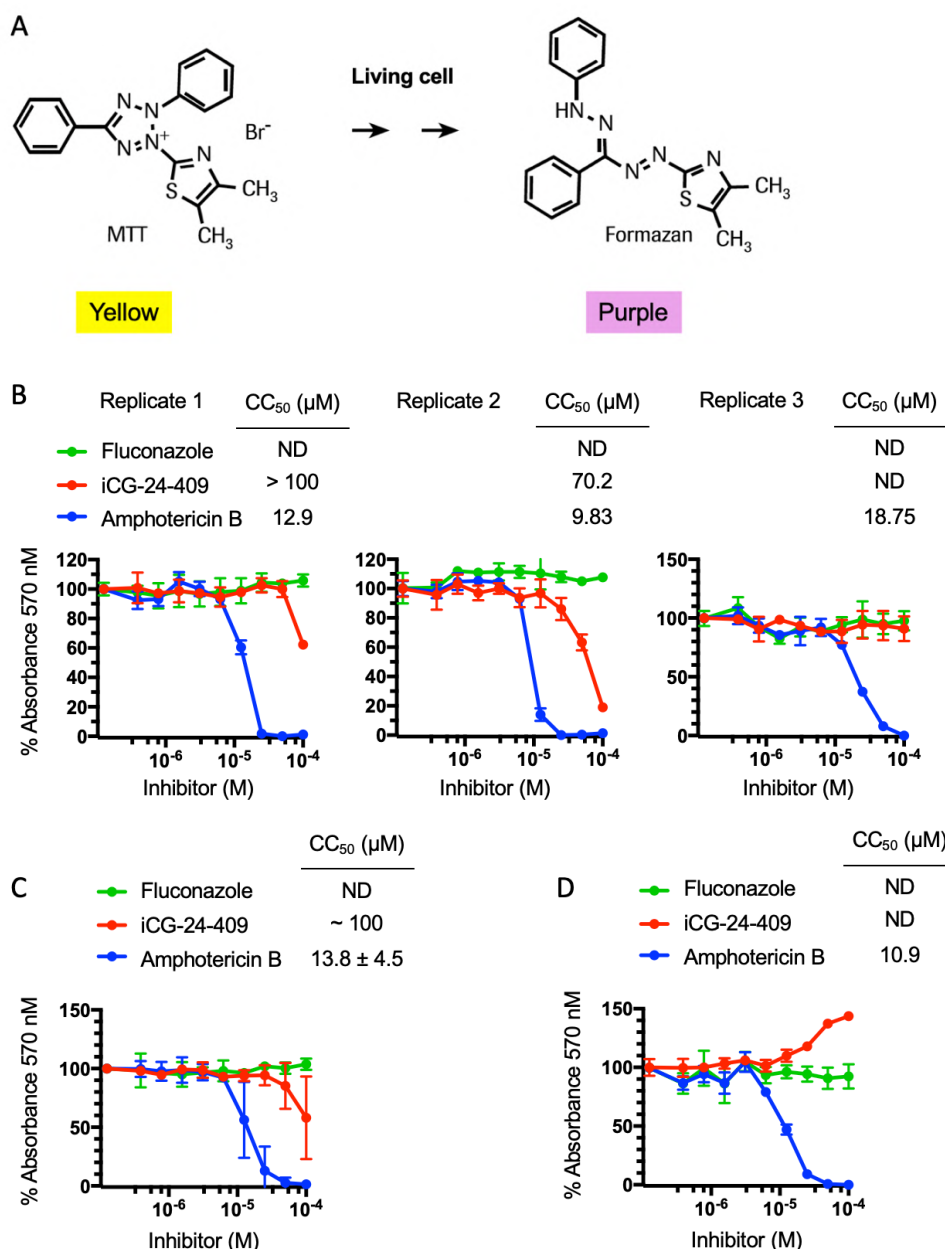


Figure 58. iCG-24-409 shows low cytotoxicity against human cells. **A.** The biochemical reaction used in the MTT colorimetric assay (Cell Proliferation Kit I, Roche). **B.** The three independent experiments of MTT cytotoxicity assays performed on HeLa cells. ND: not determined. The inhibition curves and CC_{50} value were calculated by GraphPad Prime 7 using “[inhibitor] vs. response (three parameters)” model. Data are presented as means from a technical triplicate of the same experiment. **C.** MTT cytotoxicity assays on HeLa cell line based on merged data from the replicates shown in panel B. Data are presented as means \pm SD, $n = 3$ independent experiments. **D.** MTT cytotoxicity assays on primary fibroblast cell line IMR90. The inhibition curves and the CC_{50} value were calculated as in C. Data are presented as means from a technical triplicate of the same experiment.

HeLa cells are a cancer cell line that generally exhibits different drug resistance compared to normal cells. For this reason, we also tested the toxicity of iCG-24-409 on IMR90 cells, a primary human fibroblast cell line (ATCC number CCL-186). The results showed that iCG-24-409 did not cause any decrease in the rate of MTT reduction. On the contrary, a high concentration of this compound even caused an increase in the MTT reduction rate (**Figure 58D**). Since iCG-24-409 can also inhibit human BET bromodomains at high concentration, such inhibition might contribute to an increase of NAD(P)H metabolism and/or a change in mitochondrial function that would explain the enhanced MTT reduction rate. Unfortunately, so far we have only been able to perform the assay once with this cell line. More independent measurements need to be repeated to verify these results.

5.3.4. Yeast growth inhibitory activity of iCG-24-409 against other pathogenic *Candida* species

Finally, in order to check if the discovered CgBD inhibitors can inhibit the growth of other pathogenic *Candida* species, a research engineer in our lab at the IAB, Marie Arlotto, incubated the four most promising iCG-24 analogs with clinical strains of various *Candida* species. The results she obtained showed that iCG-24-409 and its close analog iCG-24-676 inhibited the growth of almost all tested species, although at different levels. The inhibitory effect of these two compounds was similar for *C. parapsilosis* and *C. glabrata*, yielding about 50% inhibition when incubated at 100 μ M concentration for ~1 day. Their inhibitory activity was weaker on *C. albicans* and *C. krusei* and there was almost no effect on *C. tropicalis* (**Figure 59A**). Very surprisingly, both inhibitors showed very high inhibition activity against the growth of *C. auris* (**Figure 59A and 59B**), a recently identified “fungal superbug” that can develop multidrug resistance against all the currently available antifungal drug families (Spivak and Hanson, 2018).

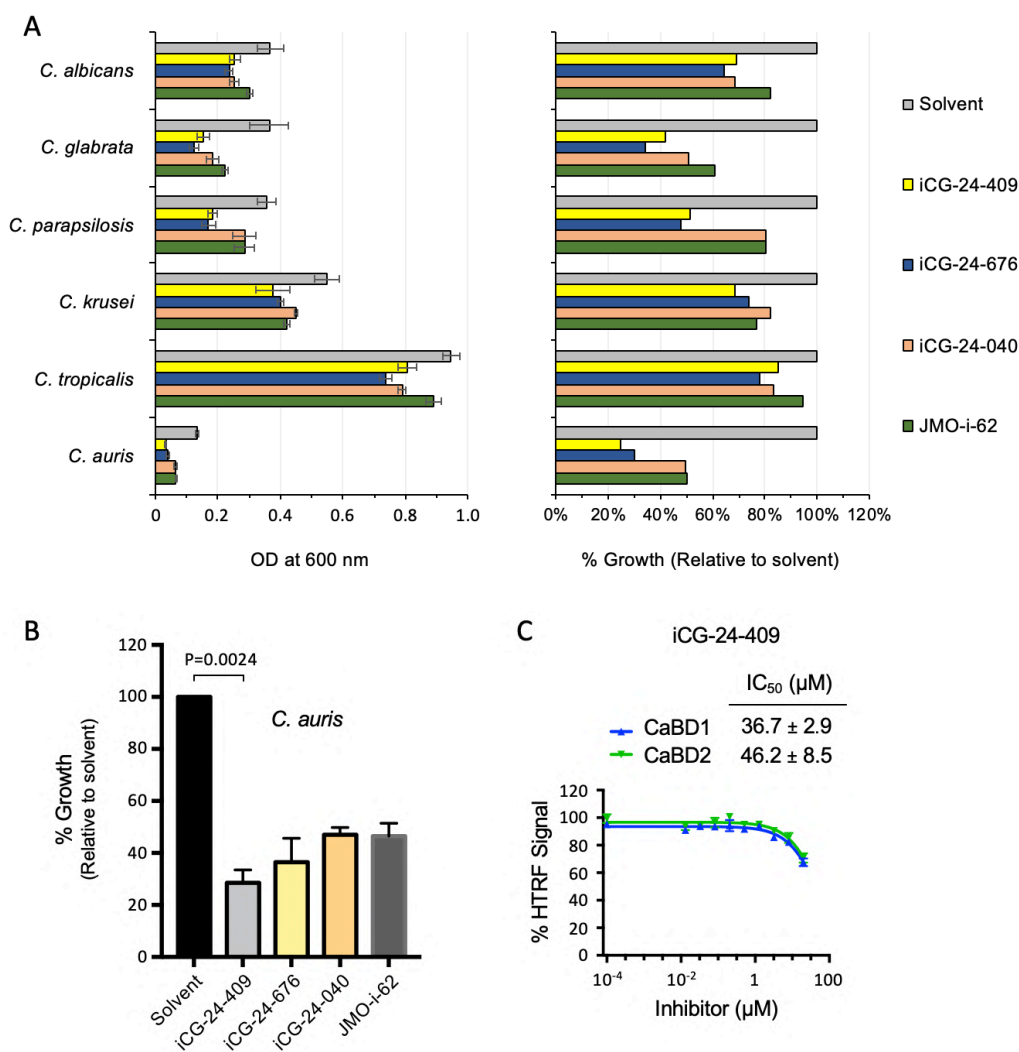


Figure 59. iCG-24-409 and other iCG-24 derived inhibitors inhibited the growth of pathogenic *Candida* species other than *C. glabrata*. **A.** Clinical strains were grown in the presence of methionine/cysteine. Incubation was at 30 °C for 16 hours for *C. glabrata*, *C. albicans*, *C. krusei* and *C. tropicalis* and 22 hours for *C. parapsilosis* and *C. auris* with 100 μM of inhibitors. Solvent consisted of a mixture of DMSO and ethanol, present at a final concentration of 0.2% and 0.8%, respectively. Data are presented as means ± SD from the triplicate of the same experiment. **B.** Growth rate of *C. auris* in the presence of 100 μM different inhibitors compared to that in the presence of solvent. Strains were grown in the presence of methionine/cysteine. Incubation was at 30 °C for 22 hours. DMSO and ethanol were present at a final concentration of 0.2% and 0.8%, respectively. Data are presented as means ± SD, n = 2 independent experiments; Statistical significance was determined using the Holm-Sidak method by GraphPad Prime 7. **C.** HTRF assays showing the inhibitory effect of iCG-24-409 against CaBdf1 BDs. The CaBD binding inhibition curves and IC₅₀ were determined calculated in GraphPad Prime 7 using the “log(inhibitor) vs. response (three parameters)” model. Data are presented as means ± SD, n = 2 independent experiments.

I next tried to verify the ability of iCG-24-409 to inhibit *C. albicans* Bdf1 bromodomains in an HTRF assay. This inhibitor showed weak CaBD inhibitory activity (Figure 59C). To compare the acetyllysine binding pockets of CgBdf1 and CaBdf1 bromodomains, I aligned the CaBD1 and CaBD2 crystal structures with those of unbound CgBD1 and CgBD2, respectively. The

results showed that most residues in the binding pockets of the corresponding bromodomains overlapped well, including the conserved Asn291 and Asn209 in CaBD1 and CgBD1, respectively. However, it also revealed a difference in the position of the ZA loop, leading to a major shift in position of a leucine residue (Leu243 in CaBD1 and Leu161 in CgBD1) that made the acetyllysine binding pocket of CaBD1 narrower than that of CgBD1 (**Figure 60A and B**). This shifted position of the leucine residue was observed in BD2 as well (Leu420 in CaBD2 and Leu338 in CgBD2), which also made the binding pocket of CaBD2 narrower than that of CgBD2 (**Figure 60C and D**). Moreover, there were slight differences in the electrostatic surface potential around the binding pocket, which was more positive in CaBD1 than in CgBD1 and more negative in CaBD2 than in CgBD2 (**Figure 60A and C**).

In order to verify whether the inhibitor binding mode could be feasibly conserved, I aligned both CaBD crystal structures with that of iCG-24-409-bound CgBD1 to align compound iCG-24-409 onto both CaBD crystal structures. This inhibitor generally fit well into the binding site of CaBD1. A steric clash was observed with residue Leu243, but a minor conformational change of the iCG-24-409 methylphenyl group would relieve this clash (**Figure 60E**). As for CaBD2, the situation was more complicated. An evident steric clash formed by residue Leu420 with the methylphenyl moiety could also be observed here. At the same time, another residue Phe409 formed another clash with the methylfuran moiety. However, in theory, both steric clashes could also be overcome by conformational changes of the inhibitor (**Figure 60F**). These results could explain the weak inhibitory effect observed for iCG-24-409 against both CaBDs in the HTRF assay and against *C. albicans* in the growth inhibition assay.

In summary, iCG-24-409 was able to inhibit the growth of several pathogenic *Candida* species. This indicates that it may be possible to develop bromodomain inhibitors as antifungal agents against a broad spectrum of pathogenic species.

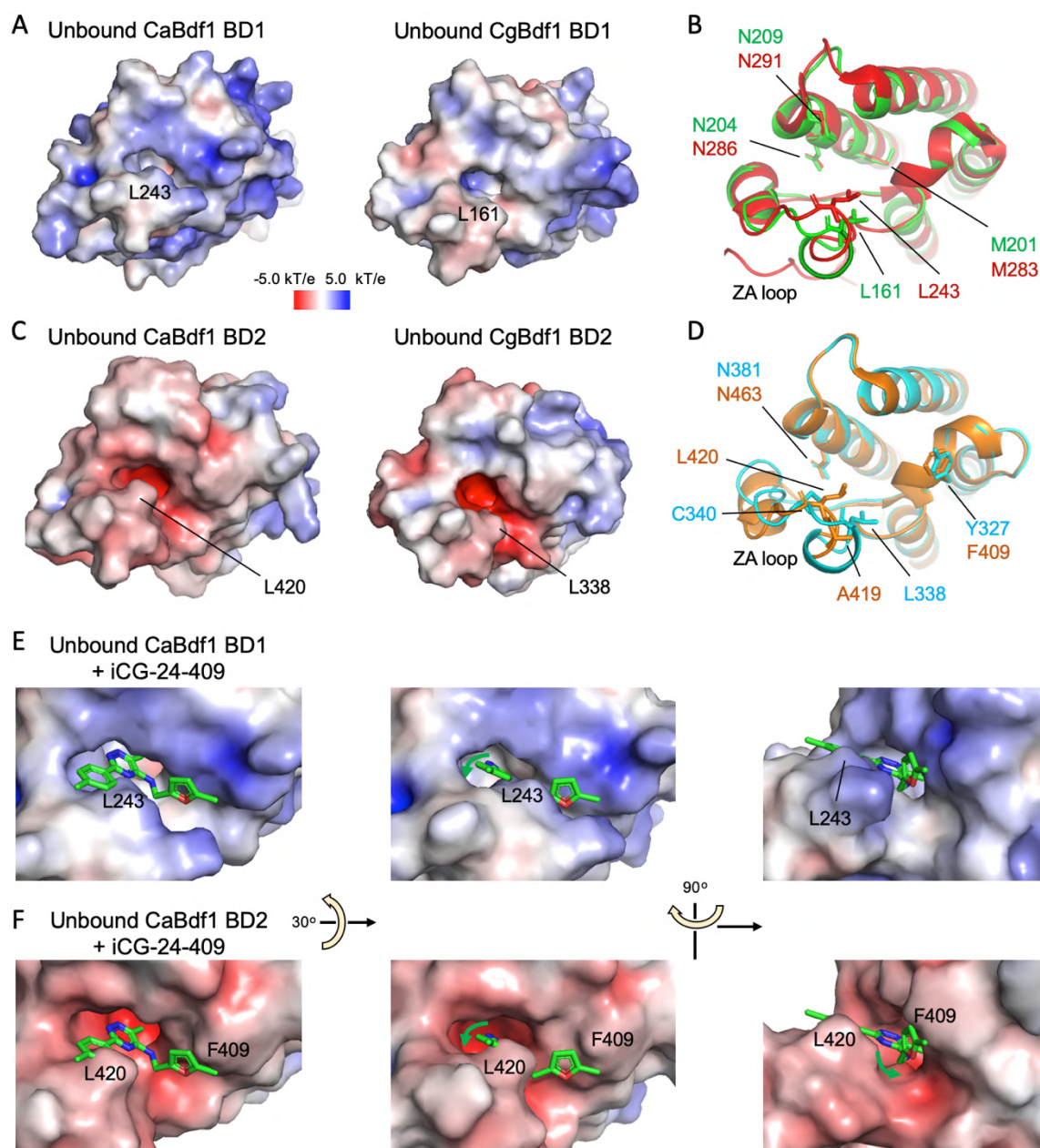


Figure 60. Alignment model of iCG-24-409 onto CaBdf1 bromodomains. **A.** Plots of electrostatic surface potential of BD1 structures from CaBdf1 (left, PDB 5N15) and CgBdf1 (right). Regions of negative and positive potential are shown in red and blue, respectively. **B.** Alignment of structures of CaBD1 (red) and CgBD1 (green) showing the shift in the ZA loop. The root-mean square distance of the alignment was 0.62. **C.** Plots of electrostatic surface potential of BD2 structures from CaBdf1 (left, PDB 5N13) and CgBdf1 (right). **D.** Alignment of structures of CaBD2 (orange) and CgBD2 (cyan) showing the shift in the ZA loop. The root-mean square distance of the alignment was 0.34. **E** and **F.** Hypothetical model of molecule iCG-24-409 aligned onto the crystal structure of CaBD1 (C, PDB 5N15) and CaBD2 (D, PDB 5N13) in their unbound conformation. iCG-24-409 was superimposed on the CaBD models via a structural alignment with bound CgBD1. The root-mean square distances of the alignments were 0.64 (E) and 1.32 (F).

5.4. Conclusion

Among all the CgBD1 inhibitors identified by high-throughput screening, iCG-24 was the only compound that showed a yeast growth inhibitory effect. However, this compound had poor water solubility and only a weak inhibitory effect against CgBD2. In order to solve these problems, our collaborators at USC proposed a series of structural analogs of iCG-24 that were predicted to be more soluble. Among these analogs, iCG-24-409 was the most promising. This compound selectively inhibited both CgBD1 and CgBD2 and showed the highest CgBD2 inhibitory effect among the compounds. iCG-24-409 had the capacity to inhibit all the tested *C. glabrata* strains, including that expressing WT Bdf1, with an EC₅₀ less than 100 μ M. I successfully confirmed that the yeast growth inhibitory effect of iCG-24-409 was due to its Bdf1 bromodomain inhibition activity by generating a *C. glabrata* strain in which the bromodomains of Bdf1 were replaced by those of human Brd4. This inhibitor showed significantly less inhibitory effect against the humanized strain compared to the WT strain. The co-crystal structure showed that iCG-24-409 could fit well into the binding pockets of both CgBD1 and CgBD2 but those of human Brd4 bromodomains. I also performed preliminary experiments to determine the binding affinity of this molecule towards both CgBdf1 bromodomains and to assess its human cytotoxicity, which appears to be low. Finally, I showed that iCG-24-409 inhibits the bromodomains of CaBdf1 *in vitro* and inhibits the growth of *C. albicans* and other *Candida* species. Although more experiments are needed to finish characterizing this inhibitor, iCG-24-409 appears to be a highly promising compound that merits being pursued further.

Chapter III – Discussion

1. Project summary

In this project, we used genetic methods to successfully construct a *BDF1* conditional knock-down strain of *C. glabrata*. By using this strain, we confirmed that Bdf1 and its two bromodomains are required for *C. glabrata* growth. We also verified that growth can be inhibited by introducing point mutations affecting only one amino acid in each Bdf1 bromodomain. These results strongly support the hypothesis that Bdf1 is a valid antifungal target in *C. glabrata*. The structure determination of the two bromodomains of CgBdf1 was also performed. The high-resolution crystal structures of unbound CgBD1 and CgBD2, as well as the co-crystal structure of CgBD2 with I-BET151, revealed significant differences between the yeast and human bromodomains. These differences further validate Bdf1 as a potential antifungal target in *C. glabrata*.

In parallel we optimized an HTRF bromodomain inhibition assay. A high-throughput chemical screen against CgBD1 was performed with this assay by our collaborators at Calibr and specific inhibitors were identified. The IC₅₀ values of these hits were determined *in vitro* against human and fungal bromodomains. Structural studies were performed and different binding modes were identified for the different inhibitors.

Besides the IC₅₀ values for bromodomain inhibition, the EC₅₀ values of hits were also determined in *in vitro* yeast growth inhibition assays. The CgBD1 inhibitor iCG-24 was identified as the only high-throughput screening hit that inhibited yeast growth. Our USC collaborators analyzed the structure of this compound and proposed a series of related molecules. These analogs showed a correlation between their bromodomain and yeast growth inhibition activities. Among them, the molecule iCG-24-409 showed improved CgBD2 and yeast growth inhibition activities compared to the original iCG-24. This derivative compound had low inhibitory activity against human Brd4 bromodomains and did not efficiently inhibit the growth of a *C. glabrata* strain expressing a Bdf1 protein modified to contain the Brd4 bromodomains. These results confirmed that iCG-24-409 inhibited yeast growth by targeting the CgBdf1 bromodomains. Further chemical optimization is ongoing to identify additional molecules showing more potent and selective CgBdf1 bromodomain inhibition.

2. Effect of iCG-24-409 on the expression of genes regulated by CgBdf1

At the time that I was looking for ways to confirm that the ability of iCG-24-409 to inhibit yeast growth was an on-target effect (section 5.2 in Chapter II), I also considered performing Chromatin Immunoprecipitation (ChIP) experiments as an alternative to the CETSA and humanized CgBdf1 strategies. Performing ChIP targeting CgBdf1 would allow us to identify the regions of chromatin interacting with Bdf1 ([Figure 61A](#)). Since Bdf1 bromodomains interact directly with DNA-associated histones, their inhibition should change the levels of specific DNA sequences that co-immunoprecipitate with Bdf1. Even though I have now already validated the target of iCG-24-409 using humanized CgBdf1 strains, it would nevertheless still be interesting to investigate the functional effects of this inhibitor to confirm its mode of action.

I have already begun looking into how such an experiment might be performed. Using published data concerning the RNA Sequencing (RNA seq) based analysis of the transcriptomic landscape of *C. glabrata* (Linde *et al.*, 2015), I plotted the expression level of genes in two growth conditions (YPD and M199 pH8 media) and observed that most investigated transcripts were present at a similar level between the two growth conditions ([Figure 61B](#)). In the absence of experimental evidence indicating which genes are regulated by Bdf1, I divided the initial range of this plot into ten intervals. In each interval, I chose three genes ([Figure 61C](#)) for which the interaction with CgBdf1 would be further characterized by Real-time PCR (qPCR). The genes in each interval were chosen according to criteria that they are single copy, lack introns and their function is known or has at least been characterized for an ortholog. The selected genes are shown in Appendix IV. The qPCR primers for these genes have already been purchased. The *C. glabrata* strains expressing C-terminally FLAG-tagged Bdf1 ([Figure 51A](#)) would be used for the ChIP experiments by adapting the experimental method previously developed in the lab (García-Oliver *et al.*, 2017). If the ChIP results for the WT strain with inhibitor were similar to those for strains harbouring bromodomain Y-F mutations, then this would strongly confirm the Bdf1 bromodomains to be the target of the inhibitor ([Figure 61D](#)).

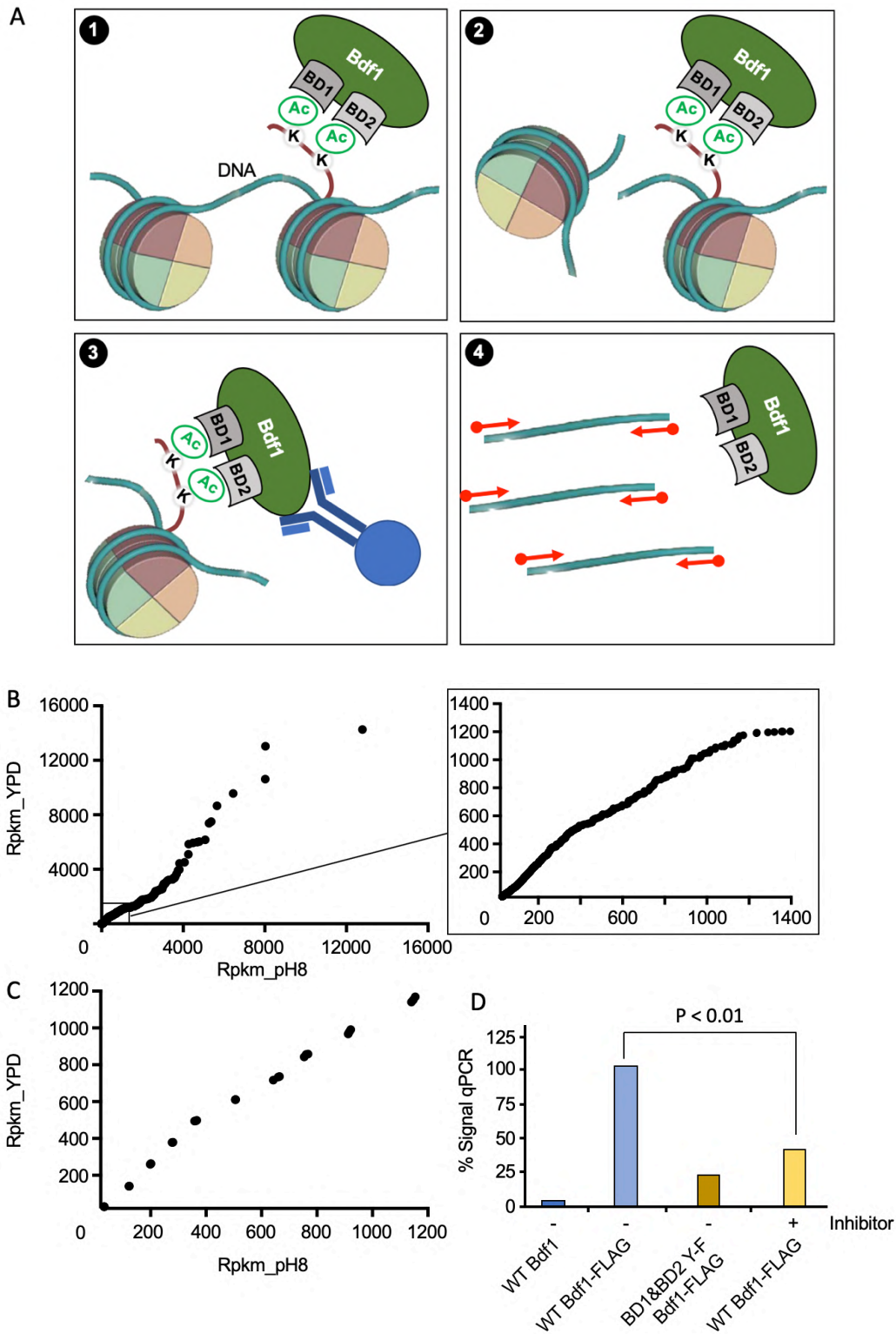


Figure 61. Proposed ChIP experiment to verify effects of iCG-24-409 on the function of CgBdf1. **A.** Principle of ChIP experiment. Step 1. Crosslinking and cell lysis. The interaction between Bdf1 and acetylated histone and associated DNA becomes covalent. Step 2. Fragmentation of chromatin. Step 3. Immunoprecipitation of Bdf1 and its associated histones and DNA fragments. Step 4. Reversal of the crosslink and determination of DNA fragments by Real-time PCR. **B.** Plot of expression level of *C. glabrata* genes in different conditions from RNA seq data. Rpkms: reads per kilobase of exon region per million mapped reads; YPD: yeast grown in YPD medium; pH8: yeast grown in pH = 8 M199 medium. **C.** The 30 genes representing different expression levels selected as target genes. The range from 0 to 1200 of reads per kilobase of exon region per million mapped reads (rpkms) of

transcripts was divided into ten intervals: 29-30, 142-147, 259-264, 376-381, 493-498, 610-615, 710-750, 840-860, 940-990 and 1100-1200. The selected genes are listed in Appendix IV. The qPCR primers for each gene were designed with Integrated DNA Technologies using the sequences centered +60 bp of Transcriptional Start Site as a template. **D.** The expected results of ChIP for a gene whose expression is regulated by Bdf1 in *C. glabrata*.

Once the ChIP experiments were completed and showed that the expression of some genes controlled by Bdf1 are inhibited by iCG-24-409, we could also perform RNA-seq to study the change of the whole transcriptome under the stress of CgBdf1 bromodomain inhibition. That experiment would allow us to have a clearer idea concerning the number of genes whose expression is regulated by CgBdf1 bromodomains. Moreover, if we could successfully show that iCG-24-409 mimics the effects produced by Y-F mutations on both CgBDs, even though this molecule is not sufficiently potent to be an antifungal agent, it could still be useful as a tool compound to study the function of CgBdf1 in the cell.

3. Validation of the Bdf1 inhibition strategy *in vivo*

3.1. pTet promoter strategy

The strategy used to conditionally knock down *BDF1* in section 1.1 of Chapter II involved the use of a pMET promoter. This promoter is generally active and can be silenced by the addition of methionine and cysteine to the culture. Since methionine and cysteine are constitutively present in animal models, the pMET construction is not suitable for tests *in vivo*. To verify the essential role of Bdf1 for the virulence of *C. glabrata in vivo*, a good option is to generate strains in which the *BDF1* gene is under control of a pTet promoter. The pTet promoter can be repressed by the tetracycline analog doxycycline and is adapted to animal models (**Figure 62A**) (Nakayama *et al.*, 1998). The *C. glabrata* strain ATCC2001 HTL (deletion of genes *HIS3*, *TRP1* and *LEU2*) could be used to construct the pTet strains, because the three deleted three genes does not influence the virulence of *C. glabrata* (Jacobsen *et al.*, 2010).

The strategy which I propose here to construct a pTet *BDF1* conditional knock-down strain is based on the research of Nakayama *et al.* (Nakayama *et al.*, 1998). A plasmid

containing the fusion structure *GAL4AD-tetR* and the *C. glabrata TRP1* gene as a selection marker would be used. A homologous recombination step could then be performed between the linearized plasmid and the genomic DNA in the upstream region of the *TRP1* gene. To replace the endogenous *BDF1* promoter, a plasmid containing the pTet promoter regulated by the Gal4AD-TetR system and the *C. glabrata HIS3* gene as a selection marker would be used. After being linearized, the plasmid would be transformed into the yeast to replace the endogenous promoter by the pTet promoter (**Figure 62A**).

Another copy of WT *BDF1* could also be introduced in another locus of the genome apart from the endogenous *BDF1* locus. The expression of this *BDF1* copy would be used to rescue the expression level of *BDF1* once the endogenous *BDF1* is silenced by doxycycline. The second copy could also be a *BDF1* gene harboring a bromodomain deletion or point mutation. Since only the mutated *BDF1* can be expressed once the WT *BDF1* is repressed by doxycycline, those strains could be used to verify the importance of the bromodomains for the virulence of *C. glabrata*.

3.2. *C. glabrata* strain constitutively expressing humanized Bdf1

Another strategy to verify the importance of Bdf1 and its two bromodomains for *C. glabrata* virulence is to create a strain in which Bdf1 can easily be inhibited. To verify the target of iCG-24-409 in yeast cells, I generated a strain in which the expressed Bdf1 was humanized by replacing its two bromodomains by those from human Brd4 (**Figure 52**). The growth of that strain was efficiently inhibited by JQ1, suggesting the possibility to improving the health of mice infected with the humanized *C. glabrata* i by administrating JQ1 or other human BET inhibitors. If that experiment could be done, Bdf1 bromodomain inhibition could be presented as a validated antifungal strategy both *in vitro* and *in vivo*, at least for the treatment of *C. glabrata* infections.

As described in section 5.2.2 of Chapter II, I have already generated strains expressing humanized Bdf1. However, that copy of humanized Bdf1 is in a plasmid with *URA3* as the selection marker. This construction is not suitable for use in animal infection models because of the possible loss of the plasmid. To address this problem, I recently tried to integrate the

humanized *BDF1* gene into the yeast genome to replace the endogenous *BDF1*. As mentioned above, the *C. glabrata* strain ATCC2001 HTL is used here. I adapted the strategy used by Morgane Champleboux and Cécile Garnaud to construct the pMET *BDF1* conditional knock-down strain and used the *HIS3* gene as a selection marker (Figure 62B). The strains have already been generated and are currently being characterized. Once the characterization is complete, our collaborators in the Muriel Cornet's laboratory at the CHU Grenoble will try to use them to systemically infect mouse models and see whether mice respond to treatment with JQ1 or other human BETi.

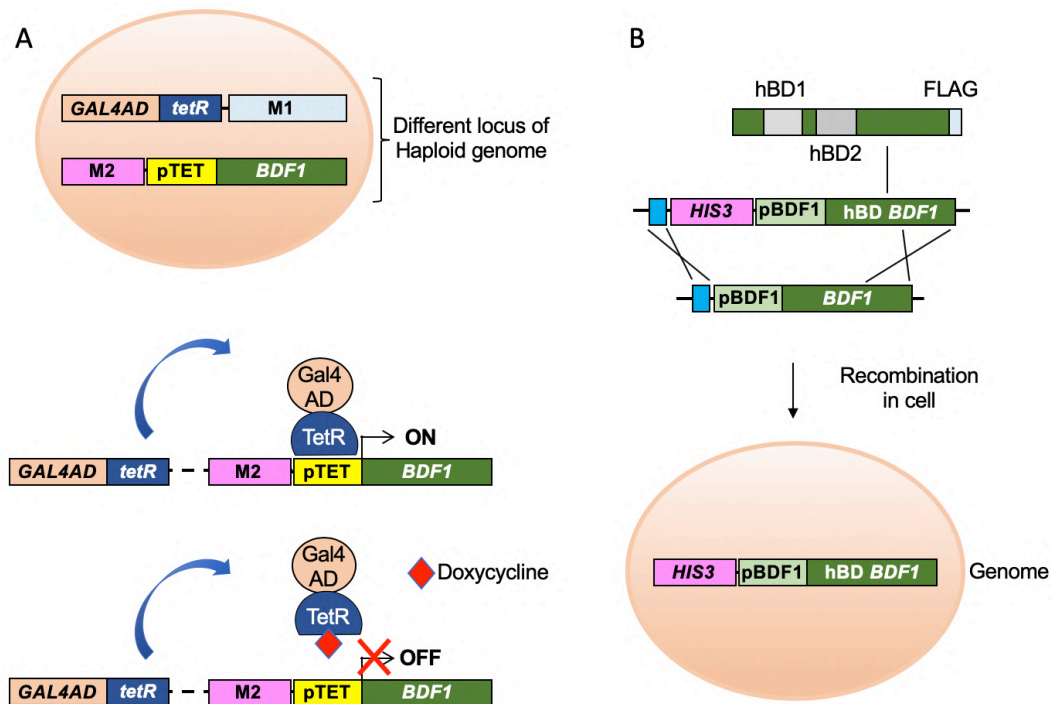


Figure 62. Construction of strains to validate the role of Bdf1 in *C. glabrata* virulence. **A.** The pTet promoter strategy. The pTet approach involves the constitutive expression of the *E. coli* tetracycline repressor (TetR) protein fused to Gal4 activation domain (Gal4AD). In the absence of doxycycline, TetR binds to pTet, inducing expression. The addition of doxycycline releases TetR from the promoter, thereby repressing expression. BDF1: BDF1 gene; M1-2: selection markers. **B.** Strategy of the construction of strains expressing humanized Bdf1. pBDF1: endogenous BDF1 promoter; hBD1: BD1 from *BRD4*, consisted residues 58-164 of Brd4; hBD2: BD2 from *BRD4*, consisted residues 347-457 of Brd4; hBD BDF1: CgBDF1 containing BD1 and BD2 from *BRD4*; FLAG: FLAG tag.

4. Inhibitor optimization

4.1. Development of more potent and selective CgBD inhibitors

The discovery of compound iCG-24-409 marks the possibility of targeting both bromodomains of a fungal BET protein, which had not been achieved in the previous study in the lab (Mietton *et al.*, 2017). It also established for the first time that the growth of WT pathogenic yeast can be inhibited by Bdf1 bromodomain inhibitors. These findings support the hypothesis that targeting Bdf1 bromodomains is a potential novel antifungal strategy.

However, compared to human BET protein inhibitors, which can have *in vitro* IC₅₀ values below 10 nM, the inhibitory activity of iCG-24-409, both *in vitro* and in yeast, is still very weak (IC₅₀ above 5 μ M for *in vitro* bromodomain inhibition and about 100 μ M for *C. glabrata* WT strain growth inhibition). More CgBdf1 bromodomains inhibitors need to be discovered or generated by medicinal chemistry optimization. More high-resolution co-crystal structures of CgBDs bound to different inhibitors should be determined in order to obtain valuable information that would facilitate the design of improved inhibitors. The ideal inhibitor should have very high affinity for both Bdf1 bromodomains (high potency), while at the same time having the lowest possible affinity for human BET (and any other human) proteins (high selectivity).

4.2. Development of drug carriers

Of the 13 validated hits from our high-throughput chemical screen, iCG-24 is the only one that showed yeast growth inhibitory activity. Some other compounds, such as iCG-16, 29, 55 and 63, were more potent inhibitors against CgBD1 alone or even against both CgBDs, compared to iCG-24. Their inability to inhibit yeast growth suggests that those molecules were either unable to enter the yeast cell or they were rapidly extruded or metabolized by the yeast cell.

To facilitate the transport of molecules into the yeast cell, drug carrier systems can be developed. In all the yeast growth assays that I performed, I used 80% ethanol and 20% DMSO as a solvent system. This was an easy way to avoid the toxicity of DMSO but it did not

significantly improve the solubility. Moreover, this solvent still showed some toxicity for the yeast, especially for the mutants (**Figure 45B**). Hence, it would be worthwhile to develop a better solvent or drug carrier system. Studies concerning drug solvent and assistant components have a long history with the development of a discipline named pharmaceutics. Most research in pharmaceutics aims to optimize drug delivery into the human body in order to improve the absorption, distribution and bioavailability of currently available drugs and to decrease their toxicity. However, advances made in this field can also serve for fundamental drug discovery research, by providing better solvent system and molecule transporters.

One proposed class of drug carriers are the cyclodextrins. Cyclodextrins are cyclic oligosaccharides of glucopyranose. In aqueous solution, these molecules form detergent-like structures with an outer hydrophilic surface and an inner hydrophobic central cavity (**Figure 63A**). The main advantage of this structure is that it improves the solubility of hydrophobic molecules. Cyclodextrins can entrap a wide range of hydrophobic molecules. Depending on the size of the central cavity, a single cyclodextrin can carry more than one guest molecule, and more than one guest molecule can bind to more than one cyclodextrin. Since the small guest molecules are entrapped by cyclodextrins, they are also protected from contact with reactants in solution, leading to the improved stability of guest molecules (Laza-Knoerr, Gref and Couvreur, 2010; Tiwari, Tiwari and Rai, 2010). The use of cyclodextrins has already been successfully implemented in the antifungal field. In a study published in 2015, Shishido *et al.* showed that the antifungal activity of anabaenolysins, lipopeptides produced by *Anabaena*, was significantly improved when used together with cyclodextrins compared to when used alone (Shishido *et al.*, 2015).

The development of nanotechnologies, defined as the design and manufacture of objects in the range of 1-1000 nm, have found many applications in the medical field in recent years. In drug delivery, nanotechnologies have been used to accumulate and distribute drugs in specific compartments, to help drugs cross certain barriers and to improve oral bioavailability (Li *et al.*, 2017; Lakkireddy and Bazile, 2019). One family of well-developed nanocarriers are the liposomes. After their first discovery in the 1960s, liposomes have developed as an almost perfect drug-carrier system. Their use can be found in the treatment of various disease, especially in cancer, to target the special distribution of a drug. Liposomes have a morphology similar to that of a cell membrane, in which each phospholipid molecule

has a hydrophilic head group and a hydrophobic chain. In aqueous solution, these molecules tend to form membrane structures with the polar head groups exposed and the hydrophobic chains interacting with each other and sequestered from solvent. This leads to the formation of either a micelle or a liposome structure (**Figure 63B**) (Bozzuto and Molinari, 2015). Both structures can be developed into drug delivery vehicles. On one hand, hydrophobic molecules can be efficiently entrapped in the hydrophobic cavity of micelles to increase their solubility in aqueous solution. On the other hand, polar drugs can be captured by liposomes and their distribution in the human body can be improved and targeted.

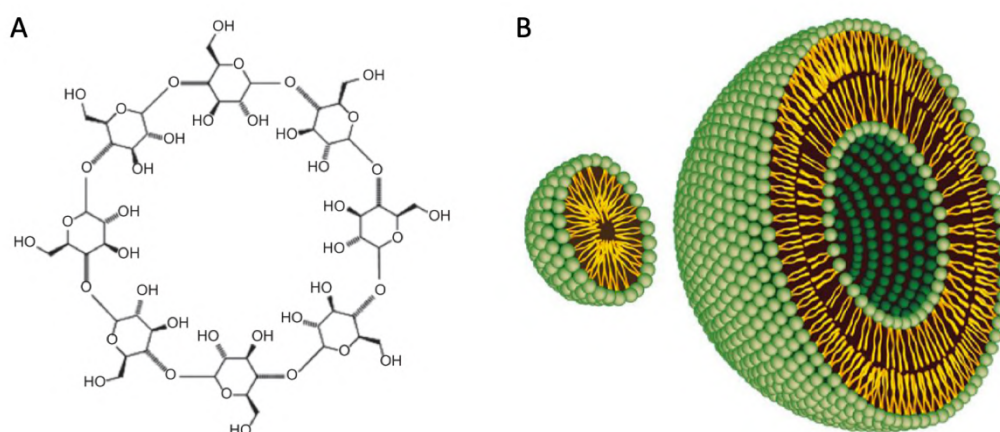


Figure 63. Examples of drug carrier systems. A. A cyclodextrin. **B.** Steric organization of micelle (left) and liposome (right). (Laza-Knoerr, Gref and Couvreur, 2010; Bozzuto and Molinari, 2015)

In this thesis project, the barriers blocking the entry of CgBD inhibitors into the yeast cell are the fungal cell membrane and the cell wall. It is not sure whether cyclodextrins could cross both two barriers but if they could, they might be ideal carriers since they could help deliver inhibitors into the yeast cell and improve their stability inside the cell. Even if they were unable to cross both barriers, cyclodextrins could still help expose yeast to a higher drug concentration by improving drug solubility and protecting drugs from reactive agents outside the fungal cell. As for micelles and liposomes, they would not have any problem crossing the cell membrane thanks to their physicochemical properties. If they could also cross the yeast cell wall, then their capacity to delivery drugs into yeast cells would be huge compared to cyclodextrins and could lead to a large accumulation of the inhibitor in the cells. However, if

they cannot cross the fungal cell wall, then the entrapped inhibitors would have little chance to get inside the yeast cell.

4.3. Development of prodrugs and proteolysis-targeted chimera system

4.3.1. Prodrugs

Besides drug carriers, the design of prodrugs can also be a good strategy. Prodrug is a term which was first introduced in 1958 (Albert, 1958). The common model of a prodrug is an active parent drug linked to a nontoxic promoiety (**Figure 64A**). After chemical and/or enzymatic transformation, the promoiety is removed and the active parent drug is released. The purpose of prodrug design was to address the high failure rate of drug candidates during development because of suboptimal pharmacokinetic properties, such as poor solubility, low bioavailability and low stability. Today, the prodrug strategy can also be used to increase permeability, improve distribution and reduce toxicity of a drug candidate (Karaman, 2014).

The use of a prodrug in the antifungal field is not a recent event either. Flucytosine is a successful prodrug whose antifungal activity was discovered during the 1960s (Groll, Piscitelli and Walsh, 1998; Perfect, 2017). The active parent drug is 5-fluorouracil, which cannot be taken up by fungal cells. Flucytosine perfectly solves this problem. This prodrug is taken up by the yeast cell and once in the cytoplasm it is converted by cytosine deaminase converts into the active 5-fluorouracil (Groll, Piscitelli and Walsh, 1998; Perfect, 2017).

Adapting the prodrug strategy to this thesis project could potentially help us discover more CgBD inhibitors that show a yeast growth inhibitory effect. Compounds like iCG-16 and iCG-29 had higher affinity towards the two CgBDs compared to iCG-24 and all its derivative compounds. Their inability to inhibit yeast growth might be due to their poor uptake by the yeast cell, just like 5-fluorouracil. The design of prodrug versions of these compounds, either by linking a carrier promoiety to the active molecules or by directly designing their bioprecursors, might help to obtain new antifungal molecules.

Whereas the discovery of flucytosine as an antifungal prodrug was an accident, most prodrugs on the market are intentionally designed (Karaman, 2014). Chemical and targeted approaches are the two methods used for prodrug design. In the chemical approach, a series of functional groups can be added to the parent drug. Among these chemical groups, phosphonate and amide can improve the aqueous solubility while carbonates and carbamates are used to improve the stability of the prodrugs (Karaman, 2014). Targeted approaches require a better understanding of the structure and function of specific transporters and concern the direct design of moieties targeting specific and well investigated transporters and/or enzymes (Karaman, 2014). To be applied to this project, the specific carriers of the pathogenic yeast cells would first need to be identified and their structure and function well investigated. Moieties attached to the parent drugs could then be designed to specifically target those carriers to guide the transport of the whole prodrug into the fungal cell. Because such a targeted approach would require a major research effort, it would be more feasible in the short term to use a chemical approach to try to improve the solubility or stability of Bdf1 inhibitors.

4.3.2. Proteolysis-targeted chimeras (PROTACs)

Another chemical modification strategy is the use of a proteolysis-targeted chimera (PROTAC), which results in the degradation of the target protein after specific binding by the inhibitor, as mentioned in section 2.2.4. of Chapter I ([Figure 64B and 64C](#)). Compared to prodrugs, the PROTAC strategy is a relatively recent development. However, the use of this strategy is already well established in the BET inhibition field. As described in section 2.2.4. of Chapter I, PROTAC molecules have shown advantages compared to classic human BET inhibitors. They can target cancer-related genes more precisely and produce a long-term effect (Zengerle, Chan and Ciulli, 2015). To adapt this strategy to our project, or more broadly to the antifungal field, there should be some differences concerning the design of the BET (Bdf1 in this case) inhibitor.

In an infected patient, the levels of human BET proteins are likely to be much higher than that of fungal Bdf1. Even in fungally infected cells, the former can still be quite high compared to the latter. It is therefore critical to ensure that the PROTAC will not lead to human

BET degradation in order to reduce the toxicity. One solution is to develop specific ubiquitin E3 ligase ligands that only recruit fungal E3. Another is to develop highly selective Bdf1 inhibitors that do not bind to human proteins (**Figure 64D**).

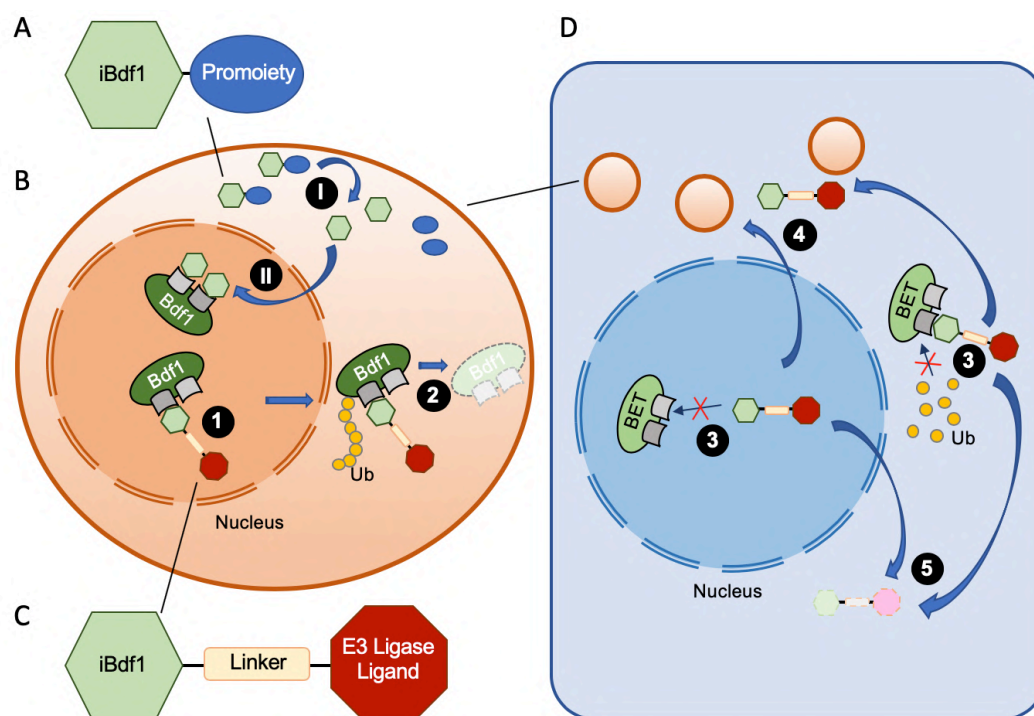


Figure 64. Use of prodrug and proteolysis-targeted chimera (PROTAC) strategies with Bdf1 inhibitors as a potential antifungal therapy. A and C. Schematic representation of a prodrug (A) and PROTAC (C) for Bdf1 inhibition. B. Functional mechanism of prodrugs and PROTACs in yeast cells. iBdf1: Bdf1 inhibitor. Step I. The non-active prodrug of Bdf1 inhibitor is taken up by the yeast cell with the help of the linked promoiety. Enzymes in the yeast cell then cleave the promoiety from the prodrug and free the active Bdf1 inhibitor. Step II. The active Bdf1 inhibitor inhibits yeast Bdf1 protein. Step 1. The PROTAC molecule is taken up by the yeast cell and binds to the yeast Bdf1. Step 2. The E3 ligase ligand of the PROTAC molecule triggers the proteolysis of Bdf1. Ub: ubiquitin D. Ideal effects of PROTACs in human cells. Step 3. the PROTAC molecule should be highly selective and not bind human BET proteins or recruit human ubiquitin ligases. Step 4. The free PROTAC molecule in the cytoplasm is taken up by the infecting yeast cells. Step 5. Other free PROTAC molecule will be degraded in the human cells.

Ubiquitin ligases are a very large family in eukaryotic cells. The two E3 ligases targeted for the development of human BET PROTACs are VHL and CRBN, which both belong to the Cullin-RING Ligases (CRLs). This group of E3 ligases contain the scaffolding protein Cullin which connects a substrate recognition domain to the RING domain that catalyzes ubiquitin ligation (Cromm and Crews, 2017). This structure makes them relatively easy to be adapted for PROTAC strategies. In *S. cerevisiae*, the CRLs share the common subunit components with

those in human (Finley *et al.*, 2012). The key challenge for developing a PROTAC for this project or for any other antifungal strategy, is to identify specific CRLs that have only fungal specific ligands. In this way, the Bdf1 PROTAC would only drive the degradation of fungal Bdf1 but not human BET or other proteins. In the ideal scenario, such CRLs would also be shared by many other pathogenic fungi, which would increase the possibility of developing a broad-spectrum agent.

Besides identifying and developing a fungal specific E3 ligase, another solution is to develop compounds whose bromodomain inhibitory activity is extremely selective for fungal Bdf1 and does not target any human proteins. The binding affinity of such inhibitors does not need to be very high to achieve antifungal activity once constructed as a PROTAC because they do not have to remain stably bound to the protein to elicit a proteolysis effect.

5. Toward a broader antifungal spectrum

A broad spectrum is always a golden goal for drug development, no matter whether it is for anticancer, antibiotic, antiviral or antifungal therapies. A broad-spectrum therapy generally allows one to treat the target diseases with fewer drugs. Moreover, for infectious diseases, broad-spectrum drugs can be administered to prevent the progress of infection before a precise diagnosis can be made reliably.

5.1. Bdf1 bromodomains inhibition in *C. albicans* and *C. glabrata*

Even though the proportion of invasive candidiasis caused by *C. albicans* relative to other species has greatly decreased over the last decades, especially in the USA and northern Europe, this species is still the most prevalent today (Kullberg and Arendrup, 2016). Together with *C. glabrata*, these two species may cause more than 60% of invasive candidiasis in many countries (Guinea, 2014). In this case, if one compound efficiently inhibited both *C. albicans* and *C. glabrata*, it could already help more than half of the patients suffering from invasive candidiasis in the world. We now have two Bdf1 bromodomain inhibitors, iCG-24-409 and iCG-

24-676, that inhibit the growth of both these species (**Figure 59A**), indicating that Bdf1 bromodomain inhibition might be a good anti-*Candida* strategy for further development. However, the yeast growth inhibitory activity of iCG-24-409 (as well as iCG-24-676) is very low against both *C. albicans* and *C. glabrata*, and so significant compound optimization would be needed.

When performing chemical optimization to obtain better CgBD inhibitors, it is also worthwhile to take into account inhibitory activity towards CaBDs and to develop inhibitors effective against the bromodomains in both species. To facilitate these efforts, it would be useful to determine the co-crystal structures of iCG-24-409 with CaBD1 and CaBD2. Moreover, one should also validate that the *C. albicans* growth inhibitory activity of iCG-24-409 is an on-target effect (due to CaBD inhibition), by using a strain expressing a humanized Bdf1 like the one I used in *C. glabrata*. However, considering the divergence between CgBDs and CaBDs, developing inhibitors that efficiently target the four bromodomains from the two species might not be an easy job.

5.2. Adaptation on potential therapy against *Candida auris*

As mentioned in section 5.3.4 of Chapter II, iCG-24-409 showed yeast growth inhibitory activity against *C. auris* which was greater than that against *C. glabrata* (**Figure 59A and 59B**), indicating that this inhibitor would also be interesting to optimize for the development of a potential drug against *C. auris* infections.

C. auris is a recently identified pathogenic yeast. After the first isolation and identification of this species in Japan and South Korea in 2009, invasive infections caused by *C. auris* were reported in South Korea only two years later (Kim *et al.*, 2009; Satoh *et al.*, 2009; Lee *et al.*, 2011). By the beginning of 2018, cases had already been reported in more than 15 countries covering five continents (Spivak and Hanson, 2018).

As for *C. albicans*, the genome of *C. auris* is diploid with about 6600 to 8300 gene coding sequences. However, whole genome alignment showed that this species is highly divergent from other major *Candida* species because most of its genomic reads did not align with previously sequenced *C. albicans*, *C. glabrata* and *S. cerevisiae* strains (Chatterjee *et al.*, 2015). Another notable point is that *C. auris* can be grouped into four distinct geographic-

specific clades, namely, South Asian, South African, South American and East Asian clades. These clades are separated by thousands of single nucleotide polymorphisms while isolates within one clade are clonal (Lockhart *et al.*, 2016).

Like *C. glabrata*, *C. auris* does not form hypha or pseudohypha either *in vitro* or in insect infection models. A specific characteristic of *C. auris* is that some cells bud without releasing the daughter cells. This leads to the formation of aggregates which are less pathogenic than nonaggregating isolates in insect models. Such cell aggregates were also observed in murine models of invasive candidiasis (Spivak and Hanson, 2018).

The mortality rate caused by *C. auris* candidemia is not higher than by other pathogenic *Candida* species, ranging from 28 to 66% depending on the healthcare setting and patient populations (Sears and Schwartz, 2017). The reason why *C. auris* has raised such a great alarm is its capacity to spread among patients in a nosocomial setting and its ability to exhibit or to develop multidrug resistance. Some isolates even show low susceptibility to all currently available antifungal classes. Susceptibility data from 54 isolates in a study from 2011 showed that more than 90% were resistant to fluconazole (≥ 32 mg/L) and more than half to voriconazole (≥ 2 mg/L). Even for amphotericin B (≥ 2 mg/L), the rate of resistance was still 35%. For echinocandins (≥ 8 mg/L), the resistant rate was 7% which was still low (Lee *et al.*, 2011). The resistance mechanisms in *C. auris* are similar to those in *C. glabrata*, including up-regulation and modification of target genes and proteins and the high activity of efflux pumps, which have already been described in section 1.3.6 of Chapter I. Notably, the rate of ABC efflux activity is significantly higher in *C. auris* than in *C. glabrata* (Chatterjee *et al.*, 2015; Ben-Ami *et al.*, 2017; Sears and Schwartz, 2017; Spivak and Hanson, 2018; Warris, 2018).

Considering the limited options for antifungal treatment, multidrug-resistant *C. auris* strains could be enormously challenging. Hence, additional antifungal agents against different targets need to be developed as soon as possible. A significant inhibitory effect by a CgBD inhibitor against *C. auris* growth suggests that Bdf1 bromodomain inhibition could be worth pursuing as an antifungal strategy against *C. auris*. Recently, I have made expression constructs for *C. auris* Bdf1 BD1 (CauBD1) and BD2 (CauBD2) and the purification of both bromodomains has been successfully carried out. A Master's student in our lab, Yordan Hayat, has been optimizing the HTRF assay in order to test whether iCG-24-409 directly inhibits either CauBD and to screen for other potential inhibitors against the CauBDs. Further work includes

structural studies of CauBDs, in the unbound state and in complex with any confirmed inhibitors. At the present time, given that *C. auris* has already developed resistance against azoles and even amphotericin B, an antifungal agent against a new target, such as Bdf1 bromodomains for example, is more urgently needed for *C. auris* than for other *Candida* species. In this case, broad-spectrum activity might be a less important priority.

5.3. Bdf1 bromodomain inhibition, narrow or broad spectrum

To date, all the available antifungal agents can be considered as broad-spectrum drugs in chemotherapies. Amphotericin B and azoles target ergosterol of the fungal cell membrane, echinocandins target β -1,3-glucan of the fungal cell wall. Both these targets are essential for fungi and without evident diversity among different fungal species.

Ergosterol is the essential sterol component of fungal cell membrane. Compared to proteins, ergosterol is simple and shared with almost all fungal, but not mammalian, cells and has very little chance of being structurally modified without any functional consequences. An antifungal agent that directly targets ergosterol, like amphotericin B, will certainly be effective against a broad spectrum of fungal species and is less likely to induce resistance because changing the main membrane sterol component is a risky event for the pathogenic microbe.

Azole and echinocandin agents do not directly bind cell wall or cell membrane components but indirectly target them via enzymatic proteins in their biosynthetic pathways. Compared to a simple molecule like ergosterol, proteins present more diversity among different species, sometimes even among different strains of the same species. Moreover, proteins are also more easily modified without serious functional consequences. For these reasons most drugs in these two antifungal families have a narrower spectrum of activity and more easily induce resistance compared to amphotericin B (Lewis, 2011).

Bdf1, unfortunately, is not a simple essential organic compound but a protein. The hypothesis that Bdf1 proteins diverge significantly among different pathogenic fungi and cannot be inhibited by a single compound can directly be asserted. Indeed, the previous study in our lab has already shown that inhibitors targeting CaBdf1 cannot inhibit CgBdf1 (data not shown). I have also demonstrated that differences in the ligand binding pocket exist between

the bromodomains of these two proteins. Considering that *C. albicans* and *C. glabrata* are relatively closely related, this problem is expected to be greater for other pathogenic fungi, such as *Aspergillus* and *Cryptococcus*. Even higher diversity concerning Bdf1 proteins can be expected among all pathogenic fungi, not to mention the differences between the two bromodomains in the same Bdf1 molecule of a given species. For these reasons, the development of a broad-spectrum antifungal agent targeting Bdf1 bromodomains is an extremely challenging, if not impossible, mission.

However, a narrow spectrum of activity is not necessarily a bad thing. It only means that certain special requirements should be considered during drug development. In general, the interest in developing narrow-spectrum drugs comes from their potentially higher efficacy against the specifically targeted pathogen compared to broad-spectrum agents. If that's not the case, then these compounds should at least be able to overcome the drug resistance developed by the target pathogen against the administered broad-spectrum drug. In these cases, a narrow-spectrum chemical therapy agent can also be highly valuable. The ideal fungal Bdf1 inhibitors should have very high inhibitory activity against both Bdf1 bromodomains (K_d less than 10 nM) and potentially inhibit the growth of yeast (similar IC_{50} as amphotericin B). Such inhibitors could be administered when resistance is developed by the fungal pathogen against the broad-spectrum antifungal agent (**Figure 65A**). Another possibility is to develop a PROTAC strategy which efficiently drives the proteolysis of the fungal Bdf1. The ability of the antifungal compound to enter the yeast cell efficiently and its high selectivity for the fungal versus the human BET target are the two specific challenges that must be met for this strategy to work as an antifungal therapy.

Cancers, including solid organ tumors and hematologic malignant disease, are part of the high-risk factors for invasive candidiasis (Kullberg and Arendrup, 2016). As mentioned in section 2.2.3 and 2.2.4 of Chapter I, some cancers are tightly associated with the deregulation of BET proteins and BET bromodomain inhibition is a therapeutic strategy for this type of cancer. Patients suffering from BET-linked cancers and invasive candidiasis at the same time comprise a very special group for the development of a Bdf1 inhibition antifungal strategy. In that clinical setting, a high selectivity of the Bdf1 inhibitor for the fungal versus the human BET targets may no longer be necessary. On the contrary, a high efficiency against both human BET and fungal Bdf1 bromodomains might be a better solution for such patients (**Figure 65B**).

The CgBD1 inhibitors discovered by high-throughput screening that belong to the second group of compounds shown in [Figure 40A](#), such as iCG-16 and iCG-29, showed similar inhibition activity (IC_{50} around 2 μ M) against all four bromodomains of Brd4 and CgBdf1 ([Table 19](#)). Those compounds would be interesting to develop to have high activity against both human BET and fungal Bdf1 bromodomains. The main challenge would be to improve their inhibitory activity *in vitro*, against yeast cells and *in vivo*.

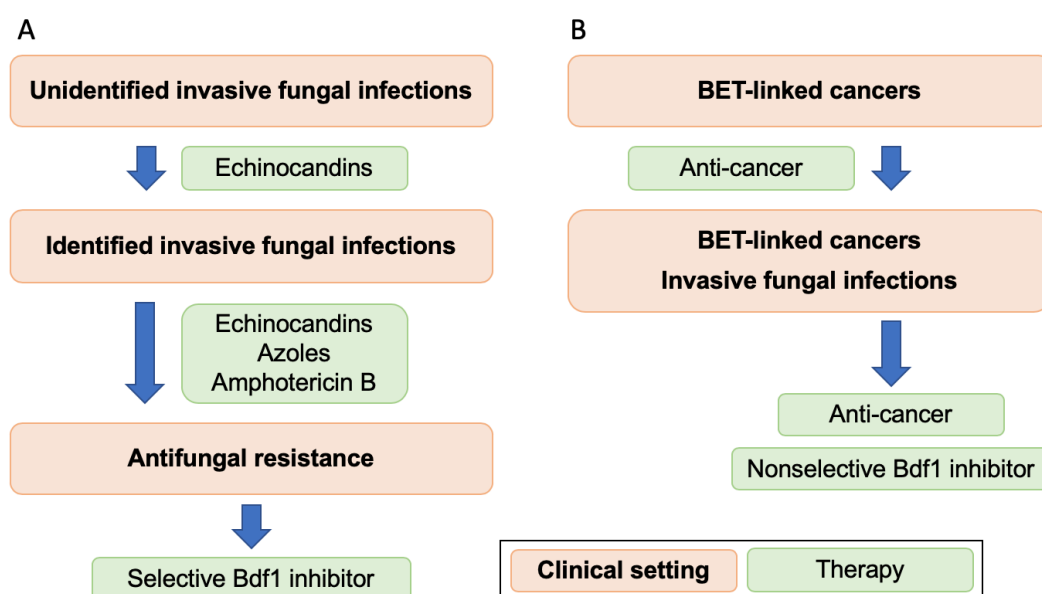


Figure 65. Possible use of a Bdf1 inhibitor in antifungal therapies. **A.** Possible therapeutic strategy for invasive fungal infections. Selective Bdf1 inhibitor: a Bdf1 inhibitor that does not target human BET proteins. **B.** Possible therapeutic strategy for invasive fungal infections of patients with BET-linked cancers. Nonselective Bdf1 inhibitor: a Bdf1 inhibitor that also targets human BET proteins.

6. Possible resistance developed against Bdf1 inhibition

In chemotherapies of modern medicine against cancer or infectious diseases, resistance is, and will always be, a war between the human and the pathogenic agent. Evolution is a process during which a given being adapts itself to its current environment. During a long period of chemotherapy, the presence of chemotherapeutic agents, including anticancer, antifungal and antiviral agents and antibiotics, generate an environment with a

strong selection pressure. It is that pressure that drives the pathogens to evolve, by genetic or epigenetic modifications, in order to survive and grow in the presence of the therapeutic agents. In the case where one cannot totally (or almost totally) eradicate the pathogen before this evolution occurs, then resistance is a sure event. It is a constant competition between modern medicine and the pathogen. What one can do is to try to ensure that the development of the therapy proceeds further and faster than the evolution of the pathogen. The intense investigation of resistance mechanisms and the constant development of novel therapeutic targets and strategies are the two ways to keep our leading position.

6.1. BET inhibition resistance in cancers

To have an idea of possible resistance mechanisms that fungi could develop against BET inhibitors it is interesting to consider what is known about the development of BETi resistance by human cells. BET protein inhibition is a recently proposed anticancer therapeutic strategy, with the discovery of JQ1 in 2010 (Filippakopoulos *et al.*, 2010). Even though there is not yet any approved BETi on the pharmaceutical market, resistance, especially that against Brd4 inhibition, has already been reported in different models. Generally, the resistance mechanisms do not involve either the mutation in BET bromodomains nor an increased level of drug efflux or metabolism (Fong *et al.*, 2015; Shu *et al.*, 2016; Pawar *et al.*, 2018). Here, I will give some examples of the mechanisms reported to give rise to the development of BET inhibition resistance.

Some mechanisms of Brd4 inhibition resistance are classified as Brd4-dependent mechanisms. These mechanisms generally involve post-translational modifications of Brd4. In 2016, Shu *et al.* showed that in triple-negative breast cancer cells, the hyperphosphorylation of Brd4 led to a stronger binding activity to Med1, a factor that coimmunoprecipitated with Brd4. That binding led to the facilitation of a bromodomain-independent chromatin recruitment mechanism and to the resistance against Brd4 bromodomain inhibition (Shu *et al.*, 2016). Later, Dai *et al.* demonstrated that the E3 ubiquitin ligase SPOP was responsible for earmarking BET proteins, including Brd4, for ubiquitination-mediated proteasome degradation. Prostate cancer cells expressing mutated SPOP had a Brd4 up-regulated phenotype at the protein level and those cells were more resistant to BETi-induced cell growth

arrest and apoptosis (Dai *et al.*, 2017). The following year, Jin *et al.* discovered the capacity of the deubiquitinase Dub3, often anomalously expressed in castration-resistant prostate cancer, to deubiquitinate and stabilize Brd4 in prostate cancer cells. That effect led to the up-regulation of Brd4 and to JQ1 resistance, which could be diminished by Dub3 inhibitors (Jin *et al.*, 2018).

In addition to Brd4-dependent mechanisms, resistance can also arise through Brd4-independent mechanisms. These generally involve the modification of different signaling pathways and are less susceptible to the genetic deletion of Brd4 (Fong *et al.*, 2015). In castration-resistant prostate cancer, Pawar *et al.* found that the phosphorylation of androgen receptor by CDK9 reactivated the signaling pathway induced by this receptor that had been inhibited by Brd4 inhibition, and that this reactivation resulted in the resistance to BET inhibitors (Pawar *et al.*, 2018). In acute myeloid leukaemia, BET inhibition resistance was found to be mediated by the activation of Wnt signaling, which could compensate for the loss of Brd4 activity (Fong *et al.*, 2015; Rathert *et al.*, 2015). In 2014, Ember *et al.* demonstrated that Brd4 BD1 was the target of diverse kinase inhibitors (Ember *et al.*, 2014). Together with the capacity of Brd4 to phosphorylate RNA pol II (Devaiah *et al.*, 2012), these results indicated that the kinase activity was an important function of Brd4. Based on that, in 2016, Kurimchak *et al.* discovered a BET inhibitor resistance mechanism involving the activation of compensatory kinase networks to overcome the inhibited Brd4 kinase activity in Brd4-dependent ovarian carcinoma (Kurimchak *et al.*, 2016). Also in 2016, the enhancement of TGF- β receptor signaling was shown to be another mechanism that allowed the development of BET inhibitor resistance (Shi *et al.*, 2016).

6.2. Studies to investigated possible Bdf1 inhibition resistance in antifungal therapies

Compared to BET inhibition in cancer therapy, Bdf1 inhibition as a novel potential antifungal therapeutic strategy has only very recently been proposed by our laboratories in 2017 (Mietton *et al.*, 2017). After that, no other studies have been published concerning Bdf1 bromodomain inhibition in fungi. Moreover, the function of fungal Bdf1 has not been investigated as extensively as that of human Brd4. For these reasons, there is not yet any

reported example of Bdf1 inhibition resistance and it is hard to guess the possible resistance mechanism. Here, I would like to propose some possible studies to investigate resistance to Bdf1 inhibition that could be developed by pathogenic yeasts.

As mentioned above, the Brd4 inhibition resistance can be induced by both Brd4 dependent and independent mechanisms. In yeast, it will be difficult to check the Bdf1 inhibition resistance mechanisms in a Bdf1 dependent manner. All the active inhibitors we have to date can only inefficiently slow down yeast growth. In order to force the yeasts to possibly post-transcriptionally modify Bdf1 to overcome the inhibition, more potent Bdf1 bromodomain inhibitors are needed. For this reason, at this moment it is more interesting to check if the pathogenic yeasts have the capacity to modify their signaling pathways to compensate the inhibited Bdf1 pathways.

The first question to answer would be whether the pathogenic yeasts can evolve a phenotype which is independent of Bdf1 or of its two bromodomains. My project and the previous project in the lab have shown that the growth of *C. glabrata* and *C. albicans* was dependent on Bdf1 and on its bromodomains (Figure 19D, 21A and 21E). However, those results were based on an assay of relatively short duration (3 days maximum) and epigenetic or genetic modifications may need more time to become established. It is possible that some yeast cells lacking Bdf1 or both of its bromodomains survive and persist until enough metabolic modifications have accumulated to allow them to overcome the missing Bdf1 pathways and restart to grow. To verify this hypothesis, one could simply seed the yeasts in conditions where Bdf1 expression is inhibited or its two bromodomains are inactivated for a week or even longer. If the yeasts begin to regrow, this would indicate their ability to live in a Bdf1 bromodomain independent manner and to develop resistance to Bdf1 inhibition. With the Bdf1 conditional knockdown strains of *C. glabrata* and *C. albicans* generated in the lab, this experiment could be easily performed.

Before proceeding further, it would be important to check by quantitative reverse transcription PCR (RT-qPCR) and/or Western blot that there is no expression of wildtype Bdf1 in the Bdf1 conditional knockdown strains growing in the knockdown conditions. This would exclude the possibility that genetic modifications may occur in those strains allowing them to express the wildtype Bdf1 even in the knockdown conditions. Once the existence of a genuine Bdf1 bromodomain independent strain is verified in *C. albicans* or *C. glabrata*, the next step

would be to identify the signaling pathways compensating Bdf1 signaling. The ChIP experiments that I proposed in section 2 of this Chapter would allow one to identify genes whose expression is controlled by Bdf1. RT-qPCR and Western blot analysis could then be performed to check if the expression of those Bdf1 target genes is downregulated in the Bdf1 bromodomain independent strain compared to the wildtype strain. If not, it would strongly suggest the existence of a distinct compensatory mechanism in the Bdf1 bromodomain independent strain. In this case, a global transcriptome analysis could be performed to look for the upregulated genes and to map them into different signaling pathways. These upregulated pathways would probably be the compensatory ones that allow the yeasts to continue their growth independently of the Bdf1 bromodomains. Subsequently, one would need to validate and investigate the roles of those signaling pathways in the development of resistance to Bdf1 inhibition.

7. Project conclusion

C. glabrata is a pathogenic yeast associated with a high rate of morbidity and mortality in immunocompromised patients. The limited number of currently available antifungal agents and the alarming rise in drug-resistant strains indicates an urgent need for novel antifungal drugs against this yeast. The objective of my Ph.D. project was to verify that chemical inhibition of the chromatin-associated protein Bdf1, a member of the BET protein family, is a valid anti-fungal therapeutic strategy in *C. glabrata*. This project was performed mainly in the laboratories of Dr. Carlo Petosa at the IBS and Dr. Jérôme Govin at the IAB, and conducted in collaboration with the laboratory of Dr. Charles E. McKenna at USC, with the company Calibr in La Jolla, California, and with the laboratory of Muriel Cornet at the TIMC-IMAG ([Figure 66](#)).

During this project, we confirmed that Bdf1 and its bromodomains are required for *C. glabrata* growth. We also verified that Bdf1 can be inhibited by introducing single point mutations in each bromodomain. The crystal structures showed that there were significant differences between bromodomains from CgBdf1 and human BET proteins. By using the HTRF assay that I optimized, a high-throughput chemical screening was performed by our collaborators in the lab of Dr. Charles E. McKenna, leading to the discovery of several diverse

CgBD inhibitors. Among these inhibitors, we successfully identified the most promising one, iCG-24-409, which harbored selective inhibition activity against both CgBDs but not human Brd4 bromodomains. We also demonstrated that this compound inhibited the growth of *C. glabrata* by inhibiting the bromodomains of Bdf1. Further characterization and chemical optimization are on-going.

The work of this multidisciplinary project involves yeast genetics, chemical screening, biochemical/biophysical and cell-based assays, and crystallography. It forms a bridge between my training in pharmacy during my bachelor's degree and in biology during my master's degree. By finishing this Ph. D. project and together with my bachelor and master, I complete my formation from basic biology research to preclinical animal model tests, which prepares me to pursue further work in the field of modern drug discovery.

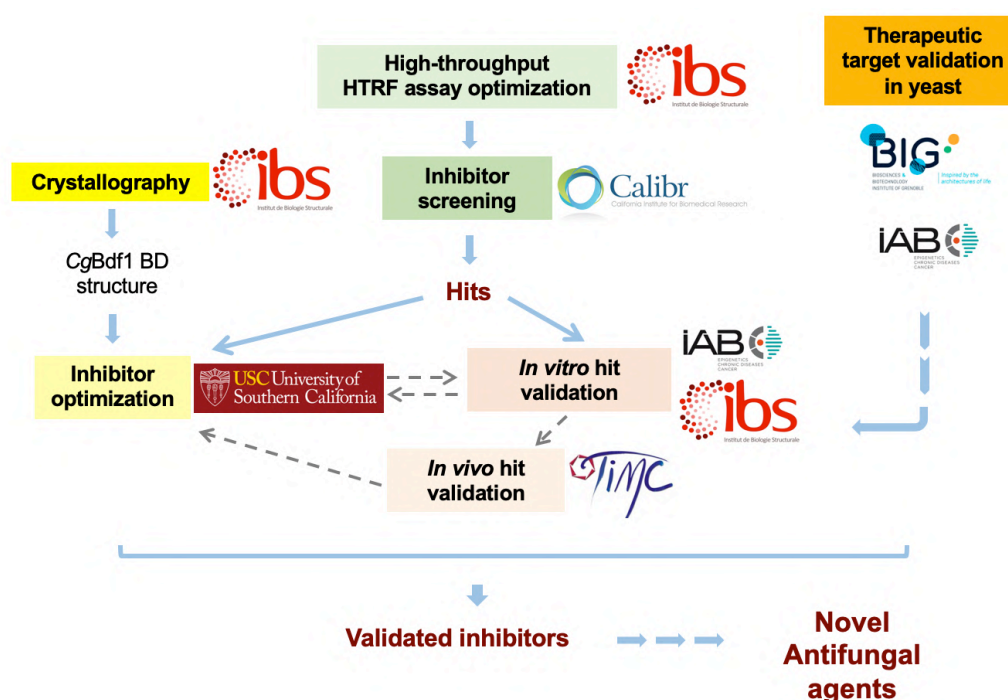


Figure 66. General tasks of the project. The optimization of the HTRF assay for the high-throughput chemical screening and structural studies of CgBDs were performed in the Petosa lab at the IBS. Therapeutic target validation was performed in the Govin lab when it was still located at the Institute of Biosciences and Biotechnologies of Grenoble (BIG). Chemical inhibitor screening was performed at the non-profit company Calibr by our collaborators from USC. The chemical optimization of hits was also performed by our USC collaborators. The characterization of the screening hits and of the derived analogs was performed at both the IBS and the IAB. The TIMC-IMAG will validate the most promising hits in animal models.

Finally, regarding the antifungal strategy targeting fungal Bdf1, there is still a long way to go. The function of Bdf1 is not yet very clear even in *S. cerevisiae*, not to mention in other fungal species. The Bdf1 inhibitors discovered to date are all much less efficient compared to human BET inhibitors. So far, the species we have investigated are only *C. albicans* and *C. glabrata*, the number of pathogenic fungi not yet investigated is huge. Considering that the sequence divergence of Bdf1 might be large across all pathogenic fungi, the development of narrow spectrum Bdf1 inhibitors might be a more reasonable course. In this case, the priority of species to be investigated should be decided, which could also be a problem: on the one hand pharmaceutical groups are generally mainly interested in diseases touching as many patients as possible; on the other hand, patients infected by uncommon pathogenic fungi should have the equal right to be treated.

陆止于此、海始于斯

Onde a terra se acaba e o mar começa

Chapter IV – Methods

1. Chemicals

BET inhibitor IBET-151 was purchased from Sigma while JQ1 was from Clinisciences (Nanterre, France). Screening validation and derived compounds were purchased from ChemDiv as powder and dissolved in DMSO without further purification. Derivative JMO-i-62, JMO-i-64, JMO-i-66 and JMO-i-68 were synthesized by our collaborators at USC.

2. Protein expression and purification

Protein expression and purification were performed as described (Mietton *et al.*, 2017) with minor changes.

2.1. Proteins used for crystallization, TSA and ITC

A DNA fragment encoding CgBdf1 residues 128–237 representing BD1 was PCR amplified from genomic *C. glabrata* DNA using the primer group:

1. CTTTATTTTCAGGGCGCCATGGGAATACCACAGCACCAGCAGAAGCACG
2. CACAGAGGGTCTCTCTGTGGCTAATCCTTTCAGGCATGTAA

A DNA fragment encoding CgBdf1 residues 304–444 representing a long version of BD2 was PCR amplified from genomic *C. glabrata* DNA using the primer group:

1. GCGCCATGGGACAACGCGCTATGAAGTTCTG
2. CTCGAATTCAGTTAGTGATGGAGGTCTCATCGATC

The above two fragments were cloned into a pETM11 vector as fusion constructs bearing an N-terminal His tag followed by a tobacco etch virus (TEV) protease cleavage site.

To construct the plasmid encoding CgBdf1 residues 304–418 representing BD2, mutagenesis was performed to put a stop codon at the correct position using the primer group:

1. GTACTCAGACGTCGAATCCTAGGAAGAGGCCGAGTCCGC
2. GCGGACTCGGCCTCTTCCTAGGATTCGACGTCTGAGTAC

The plasmids encoding His tagged CgBD1 and CgBD2 were transformed in *E. coli* strain BL21(DE3) (New England Biolabs, ref. C2527I). Cells were grown in LB medium containing kanamycin (50 µg/mL) at 37 °C until reaching an OD600 of about 0.5, induced with 1 mM IPTG and further incubated at 18 °C for 12–20 h before being collected. Cells were resuspended in buffer A (50 mM Tris-HCl pH 7.5, 300 mM NaCl, 10% glycerol, 25 mM imidazole, 5 mM β-mercaptoethanol and protease inhibitors) and lysed by sonication for 2.5 min, at 50% of amplitude, with pulses of 10 s on, 10 s off, on ice. The cleared lysate was incubated with Ni-NTA resin (Protino Ni-NTA Agarose, MACHEREY-NAGEL, ref. 745400) and washed with buffer A containing 500 mM NaCl. Proteins were eluted with 250 mM imidazole, dialysed overnight in the presence of His-tagged TEV protease against buffer A containing no imidazole and incubated with Ni-NTA resin to remove His-tagged species. Proteins were further purified on a Superdex 75 10/300 (GE Healthcare) column in 50 mM Hepes pH 7.5, 150 mM NaCl, 0.5 mM dithiothreitol (DTT). Proteins were concentrated to >20 mg/mL on a Centricon device (Millipore, 10 kDa cutoff) and stored at -80 °C for further uses in TSA, ITC and crystallization experiments.

2.2. Proteins used for HTRF, pull-down and histone peptide array

A DNA fragment encoding CgBdf1 residues 120–248 representing BD1 was PCR amplified from genomic *C. glabrata* DNA by using the primer group:

1. CGTGGATCCATGGACAACCTGCCAGCTAACC

2. CCGCTCGAGTTATTTAGTACCTGGCAGAGGGTCTCTC

A DNA fragment encoding CgBdf1 residues 289–426 representing a long version of BD2 was PCR amplified from genomic *C. glabrata* DNA using the primer group:

1. GGATCTGGTTCCGCGTGGATCCATATACCCTTACGAGATGAACAGTAAG
2. CGATGCGGCCGCTCGAGTTAGTCGTAAGCGGACTCGGC

The above two fragments were cloned into a pGEX4t1 vector as GST-tagged fusion proteins.

To construct the plasmid encoding CgBdf1 residues 289–411 representing BD2, a mutagenesis was performed to put a stop codon at the correct position by using the primer group:

1. CAAAATGGGCCGACAGACCATAGTACTCAGACGTCTGAATCCG
2. CGGATTCGACGTCTGAGTACTATGGTCTGTCTGGCCCATTTTG

Expression in *E. coli* strain BL21(DE3) cells was performed as for His-tagged constructs. Collected cells were resuspended in 50 mM Tris-HCl pH 7.5, 150 mM NaCl and protease inhibitors. Cell pellets from 50 mL cultures were lysed by sonication for 20 s, 80% of power, 10s on, about 1 min off, on ice. Cell pellets from 1 L cultures were lysed by sonication for 1 min, 40% of power, 10 s on, 10 s off, on ice. The clarified lysate was incubated with glutathione sepharose (Glutathione Sepharose 4B, GE Healthcare, ref. GE17-0756-04) and then washed with 50 mM Tris-HCl pH 7.5, 500 mM NaCl and 1% NP-40. Proteins were eluted with 10 mM glutathione and further purified on a Superdex 200 10/300 (GE Healthcare) column in 50 mM Hepes pH 7.5, 150 mM NaCl, 0.5 mM DTT. Glycerol was added to a final concentration of 30%. GST-tagged human Brd4 BD2 (residues 349–460) was purchased from Reaction Biology Corp. Human Brd4 BD1 (residues 22–204) was from the previous study in the lab (Mietton *et al.*, 2017). All proteins were stored at -80 °C for further use.

3. Pull-down and histone peptide array assay

3.1. Pull-down assay

Pull-down assays were performed as described (Mietton *et al.*, 2017). Biotinylated peptides corresponding to non-acetylated (H4Ac0) and tetra-acetylated (H4K5acK8acK12acK16ac) histone H4 tails were synthesized by Covalab (Villeurbanne, France) and immobilized on Streptavidin-coated magnetic beads (Dynabeads MyOne Streptavidin C1; Thermo Fisher) according to the manufacturer's instructions. Beads were incubated with 1.25 mg of GST-tagged CgBdf1 BD1 or BD2 in binding buffer (50mM Tris pH 7.4, 150mM NaCl, 0.1%, NP-40, 10% glycerol 10%, 1mM DTT) in a volume of 250 ml for 2h at 4 °C and subsequently washed in binding buffer containing 500mM NaCl. Bound proteins were eluted by boiling in SDS-PAGE sample loading buffer and analyzed by Western blot using an anti-GST antibody (GE Healthcare).

3.2. Histone peptide array assay

MODified Histone Peptide Array Kit was from Active motif (Ref. 13005). Array preparation was described in the manufacturer's instructions. 1 µM proteins in binding buffer (50mM Tris pH 7.4, 150mM NaCl, 0.1%, NP-40, 10% glycerol 10%, 1mM DTT) were incubated with the array at 4 °C for two hours and the array was washed three times with binding buffer. Anti-GST antibody (GE Healthcare) was used for GST-tagged bromodomains detection.

4. ITC and TSA

For ITC, calorimetric experiments were performed on an ITC200 calorimeter at 10 or 25 °C while stirring at 750 r.p.m. All proteins were buffer exchanged by dialysis into 25mM Hepes pH 7.5, 150mM NaCl, 0.5mM TCEP. The same buffer was used to prepared chemical compound samples. The protein samples contained the same DMSO concentration as the compound samples. Typically, about 80 mM compound and about 900 mM protein was placed

in the cell and syringe, respectively. Titrations consisted of an initial injection of 0.5 μ l followed by 12 identical injections of 3 μ l made at time intervals of 3 min. ITC data were corrected for the heat of dilution of injectant into buffer and analyzed with software provided by the manufacturer using a single binding site model. The first data point was excluded from the analysis. This work was performed by Caroline Mas and used the platforms of the Grenoble Instruct center (ISBG; UMS 3518 CNRS-CEA-UJF-EMBL) with support from FRISBI (ANR-10-INSB-05-02) and GRAL (ANR-10-LABX-49-01) within the Grenoble Partnership for Structural Biology (PSB).

For TSA, CgBD1 and CgBD2 were diluted first in SEC buffer (150 mM NaCl, 25 mM Hepes pH7.5, 0.5 mM DTT) to 2 mM before being diluted to proper concentration in SEC buffer or HTRF buffer (50% Eplgeneous Binding Domain Diluent Buffer and 50% Eplgeneous Binding Domain Detection Buffer #2 from Cisbio). Chemical compounds were diluted in the same buffers for CgBDs. SYPRO Orange from Invitrogen (ref. S6615) was diluted first in Standard HEPES screening buffer (100 mM HEPES, 150 mM NaCl, pH 7.5) 50X before being diluted 100X in the same buffers for CgBDs to the final concentration. The heating procedure was performed by Philippe Mas with an RT-PCR instrument (Mx3005P Q-PCR, Stratagene).

5. HTRF assay

HTRF assays were performed as described (Mietton *et al.*, 2017) with minor changes. Biotinylated and non-biotinylated tetra-acetylated H4 peptides (H4K5acK8acK12acK16ac; denoted H4ac4) were synthesized by Covalab (Villeurbanne, France). HTRF reagents and buffers were purchased from Cisbio Bioassays and the assay performed according to the manufacturer's instructions. The assay used a terbium (III) cryptate donor reagent conjugated to an anti-GST antibody (MAb anti-GST-Tb; ref. 61GSTTLA), a streptavidin-conjugated acceptor reagent (streptavidin-d2; ref. 610SADLA) and Cisbio proprietary buffers (Eplgeneous Binding Domain Diluent and Detection buffer; refs. 62DLBDDF and 62DB2FDG, respectively).

Incubation with GST-tagged bromodomains and biotinylated H4Ac4 brings the donor and acceptor into close proximity and allows FRET. The non-biotinylated H4ac4 peptide competes for binding and was used as a positive control for inhibition. GST-tagged proteins in

25mM Hepes pH 7.5, 150mM NaCl, 0.5mM DTT were diluted in EPIgeneous Binding Domain Diluent buffer from Cisbio and assayed at 5 nM final concentration. Biotinylated H4Ac4 peptides were diluted in EPIgeneous Binding Domain Diluent buffer and used at a final concentration of 50, 600, 30 or 250nM in assays involving Brd4 BD1, Brd4 BD2, CgBdf1 BD1 and CgBdf1 BD2, respectively. The antibody-conjugated donor was diluted in EPIgeneous Binding Domain Detection buffer and used at 0.5nM. The streptavidin-conjugated acceptor was diluted in EPIgeneous Binding Domain Detection buffer #2 from Cisbio and used at 1/8 of the H4Ac4 peptide concentration.

Inhibitors were tested by performing an eleven-point dilution series with a maximal final concentration of 20 mM. The final DMSO concentration was 0.2%. Components were incubated at 4 °C for 4 h (CgBdf1 BD1 and Brd4 BD1) or for 24 h (CgBdf1 BD2 and Brd4 BD2). Experiments were performed in 384-well white plates (Greiner 781080) in a volume of 16 µl and analyzed in a ClarioStar plate reader (BMG LABTECH). Excitation was at 330 nm and emission intensities were measured at 620 and 665 nm (corresponding to the donor and acceptor emission peaks, respectively; the 665/620 ratio is used to calculate the specific HTRF signal) with an integration delay of 60 µs, an integration time of 400 µs, a number of flashes of 200 and a gain of 2400.

6. High-throughput chemical screening

The screening was performed by Nathan Dupper and Yingsheng Zhou, our collaborators at the USC. The HTRF assay described above was miniaturized for performance in a 5 µl reaction volume in 1,536-well black plates. Approximately 100,000 compounds comprising the soluble diversity (ChemDiv), targeted diversity (ChemDiv) and 30K diversity (LifeChem) collections were dispensed into wells by an Echo acoustic liquid dispenser. A master mix comprising MAb anti-GST-Tb donor, streptavidin-d2 acceptor, GST-tagged CgBD protein, biotinylated H4Ac4 peptide was then added and the plates incubated for 4 h prior to reading. The primary screen was performed with compounds at a final concentration of 20 mM, corresponding to a final DMSO concentration of 1%. Hits were initially confirmed by

repeating the assay at a single concentration in triplicate, and subsequently by dose–response curves constructed using eight-point dilutions between 0 and 20 mM.

7. Generation of *C. glabrata* mutant strains

7.1. Strains and plasmids

All *C. glabrata* strains were derived from a wild-type laboratory strain (ATCC200989, *ura3-trp1-his1*). *Escherichia coli* strain DH5 α was used for all plasmid maintenance and construction. Plasmid URA3-pGRB2.0 was generated from the plasmid pGRB2.0 by inserting the URA3 gene. All the generated strains and plasmids are shown in Supplementary Table 1 and 2.

Supplementary Table 1. Plasmids used in this study.

Name	Number	Description	Cassette to transform	
URA3-pGRB2.0	pJG244	pGRB2.0 containing URA3 marker	Whole plasmid	
BDF1-URA3	pJG245/267	pGRB2.0 containing BDF1 ORF fused to URA3 marker	"	"
Δ BD1 BDF1	pJG269	pGRB2.0 containing BDF1-BD1 del sequence fused to URA3 marker	"	"
Δ BD2 BDF1	pJG271	pGRB2.0 containing BDF1-BD2 del sequence fused to URA3 marker	"	"
Δ BD1 Δ BD2 BDF1	pJG272	pGRB2.0 containing BDF1-BD1 del-BD2 del sequence fused to URA3 marker	"	"
Y166F BDF1	pJG277	pGRB2.0 containing BDF1-BD1Y166F sequence fused to URA3 marker	"	"
Y343F BDF1	pJG275	pGRB2.0 containing BDF1-BD2Y343F sequence fused to URA3 marker	"	"
Y166F-Y343F BDF1	pJG278	pGRB2.0 containing BDF1-BD1Y166F-BD2Y343F sequence fused to URA3 marker	"	"
BDF1-FLAG	pJG413	pGRB2.0 containing BDF1-FLAG sequence fused to URA3 marker	"	"
hBD-BDF1-FLAG	pJG483	pGRB2.0 containing BDF1-hBD1-hBD2-FLAG sequence fused to URA3 marker	"	"

Supplementary Table 2. Strains used in this study.

Name	Number	Parent	Genotype	Containing plasmid
WT (ATCC200989)	CgJG1		<i>ura3::trp1::his3</i>	-
WT + <i>URA3</i> -pGRB2.0	CgJG26	CgJG1	<i>ura3::trp1::his3</i>	pJG244
pMET- <i>BDF1</i>	CgJG12	CgJG1	pMET- <i>BDF1::ura3::trp1::his3</i>	-
pMET- <i>BDF1</i> + <i>URA3</i> -pGRB2.0	CgJG30	CgJG12	pMET- <i>BDF1::ura3::trp1::his3</i>	pJG244
pMET- <i>BDF1</i> + WT <i>BDF1</i>	CgJG19/20	CgJG12	pMET- <i>BDF1::ura3::trp1::his3</i>	pJG245
pMET- <i>BDF1</i> + Δ BD1 <i>BDF1</i>	CgJG35/36	CgJG12	pMET- <i>BDF1::ura3::trp1::his3</i>	pJG269
pMET- <i>BDF1</i> + Δ BD2 <i>BDF1</i>	CgJG39/40	CgJG12	pMET- <i>BDF1::ura3::trp1::his3</i>	pJG271
pMET- <i>BDF1</i> + Δ BD1 Δ BD2 <i>BDF1</i>	CgJG43/44	CgJG12	pMET- <i>BDF1::ura3::trp1::his3</i>	pJG272
pMET- <i>BDF1</i> + BD1 Y-F <i>BDF1</i>	CgBD51/52	CgJG12	pMET- <i>BDF1::ura3::trp1::his3</i>	pJG277
pMET- <i>BDF1</i> + BD2 Y-F <i>BDF1</i>	CgBD47/49	CgJG12	pMET- <i>BDF1::ura3::trp1::his3</i>	pJG275
pMET- <i>BDF1</i> + BD1 & BD2 Y-F <i>BDF1</i>	CgJG55/56	CgJG12	pMET- <i>BDF1::ura3::trp1::his3</i>	pJG278
pMET- <i>BDF1</i> + WT <i>BDF1</i> -FLAG	CgJG80	CgJG12	pMET- <i>BDF1::ura3::trp1::his3</i>	pJG413
pMET- <i>BDF1</i> + hBD <i>BDF1</i> -FLAG	CgJG88	CgJG12	pMET- <i>BDF1::ura3::trp1::his3</i>	pJG483

7.2. Media and growth condition

All bacteria were routinely grown in Luria-Bertani broth medium (LB medium) containing required antibiotics. For culturing *C. glabrata*, synthetic complete (SC) media (1.7 g/L Yeast Nitrogen Base, 5 g/L ammonium sulfate, 20 g/L glucose and 2 g/L mixture of amino acids) were used. The SC media without methionine and cysteine and with (SC-M-C) or without uracil (SC-M-C-Ura) were the non-repressive media for the *MET3* promoter; the media containing 5 mM methionine and 0.25 mM cysteine (SC+M+C) with or without uracil (SC+M+C-Ura) were the repressive media for *MET3* promoter. All yeast cultures were incubated at 30 °C (Thakur *et al.*, 2008). Liquid yeast cultures were incubated at 180 rpm.

7.3. Plasmids construction

Gibson Assembly Cloning Kit (NEB) was used to generate the bromodomain deleted BDF1 containing plasmids. A QuikChangeII Site-Directed Mutagenesis Kit (Agilent) was used to generate point mutations in *BDF1* containing plasmids. Primers used are shown in Supplementary Table 3.

Supplementary Table 3. Primers used to generate *C. glabrata* mutant strains.

Plasmid type	Plasmids	Fragments	Primers (5'-3')
URA3-pGRB2.0	pJG245/267	1	CGATAAGCTTGATATCGAATTCCTGCAGCTTTCTTTTCATGCCTGCCCCCT GGCCGCTCTAGAACTAGTGGATCTAGTTAAGCCTAATCCTTCAAACCTGC
	pJG269	1	CGATAAGCTTGATATCGAATTCCTGCAGCTTTCTTTTCATGCCTGCCCCCT TTGCAGGCATGTTAAGCATGTGCTTCTCTTTCAACCTCTTGACAGCCTTG
		2	GCTATCAAGGCTGTCAAGAGGTTGAAAGAGAAGCACATGCTTAACATGCC GGCCGCTCTAGAACTAGTGGATCTAGTTAAGCCTAATCCTTCAAACCTGC
	pJG271	1	CGATAAGCTTGATATCGAATTCCTGCAGCTTTCTTTTCATGCCTGCCCCCT TACAATGGTCTGTGCGGCCCATTTTGTGTTTCGAGGCGTACTTCTTGCTCAT
		2	AGAGAGTTGATGAGCAAGAAGTACGCCTCGAACACAAAATGGGCCGACAG GGCCGCTCTAGAACTAGTGGATCTAGTTAAGCCTAATCCTTCAAACCTGC
	pJG272	1	CGATAAGCTTGATATCGAATTCCTGCAGCTTTCTTTTCATGCCTGCCCCCT TTGCAGGCATGTTAAGCATGTGCTTCTCTTTCAACCTCTTGACAGCCTTG
		2	AGAGAGTTGATGAGCAAGAAGTACGCCTCGAACACAAAATGGGCCGACAG GGCCGCTCTAGAACTAGTGGATCTAGTTAAGCCTAATCCTTCAAACCTGC
		3	GCTATCAAGGCTGTCAAGAGGTTGAAAGAGAAGCACATGCTTAACATGCC TACAATGGTCTGTGCGGCCCATTTTGTGTTTCGAGGCGTACTTCTTGCTCAT
	pJG277	-	GTTGCCCTGAACATCCCCTTATTCTTCAACTTCATCAAGAGACC GGTCTCTTGATGAAGTTGAAGAATAAGGGGATGTTCAAGGGCAAC
	pJG275	-	CGCATTGAAGTACCAACATTCTTCGACTACGTCAAAG CTTTGACGTAGTCGAAGAATGTTGGGCAGTTCAATGCG
	pJG483	1	CGACGGTATCGATAAGCTTGATATC GCAGTTGGTTGGTCTGCCTAGGGTTAGCTGGCAAGTTG
		2	CAACTTGCCAGCTAACCCCTAGGCAGACCAACCAACTGC TGGCAGATCCTTTCAGGTTAGCTCATTTATTTTTCGAAGAAGAGC
		3	CTCTTCTTGCAAAAAATAAATGAGCTACCTGCAAAGGATCTGCCAC TCCGAGACCTTGCTGCTCTTCGACTTTGGCTTACTGTTTCATC
		4	ACAGTAAGCCAAAGTCAAGAGCAGCAAGGTCTCGGAG ACGTCTGAGTACAATGGCATCTTGGCAAAGCGCATTTTC
		5	AATGCGCTTTGCCAAGATGCCATTGTACTCAGACGTGCAATC CCTCACTAAAGGGAACAAAAGCTG

7.4. *C. glabrata* genomic DNA extraction

C. glabrata colonies from solid media were suspended in 300 µL lysis buffer (2% Triton 100X, 1% SDS, 100 mM NaCl, 10 mM Tris pH8, 1 mM EDTA). 300 µL beads were used to lyse cells by FastPrep-24 system (MP Biomedicals) for 1 min at 6.5 m/s in order to destroy the cell wall of the yeast. 300 µL Phenol:Chloroform:Isoamyl Alcohol (25:24:1) was added. The mixture was well mixed and centrifuged for 5 min at 15000 g to suppress the cellular debris. 10% volume of Sodium Acetate (3M, pH5.2) and 5X volume of ethanol (100%) were added to the supernatant. The DNA was pelleted by 10 min of centrifugation at 10000 g and washed by ethanol (70%). The dry DNA pellet was suspended in Tris-EDTA and quantified by measuring optical density at 260 nm on a Nanodrop spectrophotometer.

7.5. *C. glabrata* transformation

The transformation in *C. glabrata* was by a lithium acetate procedure, as previously described (Walther and Wendland, 2003) with minor changes. Yeast was incubated in SC-M-C medium overnight. The next day the cultures were diluted in the same medium to an optical density at 595 nm (OD₅₉₅) of 0.1 and grown for another 6 hours to reach an OD₅₉₅ of 0.8 in exponential phase. 5 mL culture of each strain was pelleted by centrifuging for 3 min at 1000 g. Each pellet was washed with 900 µL LiOAc Mix (0.1 M LiOAc; 1 m M EDTA; 10 mM Tris-HCl, pH 7.5) three times then suspended in 200 µL LiOAc Mix. In a separate micro-centrifuge tube, the following components were mixed in order: 50 µL of 20 mg/mL denatured Salmon Sperm DNA prepared by boiling for 2 min then snap cooling in ice water; 4 µg whole plasmid; 200 µL washed cells in LiOAc Mix; 1 mL PEG Mix (40% PEG-3350; 0.1 M LiOAc; 1 m M EDTA; 10 mM Tris-HCl, pH 7.5). The total mixture was incubated for 30 min at 30 °C before 15 min of heat shock at 42 °C. The cells were pelleted and washed three times with 1 mL sterile water then suspended in 150 µL sterile water. Yeast was plated in SC-M-C-Ura solid medium for 2 days.

8. Yeast growth assays

Growth assays were performed as described (Mietton *et al.*, 2017) with minor changes.

8.1. Growth on solid media

C. glabrata strains were grown in SC or SC-U (SC medium without uracil) media to an OD₆₀₀ of 0.5–0.8, pelleted and resuspended in sterile water at a final OD₆₀₀ of 0.13. Cells were spotted on solid media in a threefold dilution series starting at an OD₆₀₀ of 0.13. Plates were incubated at 30 °C for 1 day before imaging.

8.2. Growth on liquid media

C. glabrata strains were grown at 30 °C in SC+M+C-U medium (SC medium with 5 mM methionine and 0.25 mM cysteine without uracil) to an OD600 of 0.5–0.8. For the evaluation of growth defects related to Bdf1 mutations, log-phase growing cells were counted using a Neubauer chamber and diluted in liquid media to a final concentration of 13500 cells per ml per well in a sterile 96-well plate. Plates were incubated at 30 °C and OD600 was measured using a Multiskan FC Microplate Photometer (Thermo Fisher).

For the evaluation of chemical compounds, *C. glabrata* pMET strains were grown in SC+M+C-U medium 24 h at 30 °C. The next day, the cultures were diluted again in the same medium to an OD600 lower than 0.1. The new cultures were then incubated at 30 °C to an OD600 of about 0.5. Cell number was counted and 10 mL cultures of SC+M+C-U medium with a final cell concentration of 135000 cells/mL were prepared. To prepare the inhibitor containing medium, 10 mM of each compound in the solvent was diluted in SC+M+C-U medium to a final concentration of 111.11 µM. To make a control, solvent was also diluted in SC+M+C-U medium to 0.556% as a final concentration. The 96 well plate loading and OD600 measuring process was shown as follow:

1. 180 µL inhibitor containing medium were loaded to each well.
2. 20 µL yeast containing medium were mixing with the inhibitor containing medium in each well.
3. An incubation of overnight at 30 °C was followed.
4. After 16 hours of incubation, the culture of each well was mixing by pipetting up and down before OD600 was measured every two hours.

9. Analysis of whole-cell extracts and antibodies

C. glabrata cultures in repressive or non-repressive media were grown for different durations and a final OD600 of 1 was obtained to ensure that the yeast was in exponential phase. Cells were pelleted and washed three times with 1 mL fresh phosphate-buffered saline (PBS), and conserved at -80 °C. The next day, cell pellets were suspended in 400 µL TENG-300

(Tris – EDTA – NaCl (300 mM) – Glycerol) buffer containing 1 mM dithiothreitol (DTT), phosphatase inhibitor (1 complete 10 mL), 1 mM trichostatin A (TSA), 1 mg/L phenylmethylsulfonyl fluoride (PMSF) and 1 unit of Protease Inhibitor Cocktail (PIC-3). Cells were lysed by FastPrep-24 system for 1 min at 6.5 m/s with dry ice. The supernatants were taken by centrifuging 2 min at 2000 rpm. Cells debris were removed by centrifugation at 15000 g for 10 min at 4°C. The supernatant was obtained as the whole cell extract (WCE) and the amount of protein was quantified in a Bradford assay. FLAG antibody was purchased from Sigma-Aldrich (ref. F3165) and the ScBdf1 antibody was recycled from the lab (García-Oliver *et al.*, 2017).

10. Cellular thermal shift assays (CETSAs)

CETSAs assays were performed as described (Molina *et al.*, 2013) with minor changes. *C. glabrata* cellular lysate in TENG150 (Tris - EDTA - NaCl (150 mM) - Glycerol) buffer or PBS containing 1 unit of Protease Inhibitor Cocktail (PIC-3) was adjusted to 4 mg/mL of whole protein. The lysate was incubated with 90 µM inhibitors at room temperature for 20 minutes. The lysate was then divided into PCR tubes, 50 µL per tube. Heating was performed in a PCR machine for 3 min at the selected temperature. All tubes were cooled on ice after being heated for more than 3 min. All the liquid in the PCR tubes was transferred into 1.5 mL Eppendorf tubes. The precipitated protein was pelleted by centrifuging at 15000 g for 20 min at 4°C. The supernatant of each tube was taken and the whole protein concentration was adjusted to 2 mg/mL. Supernatants containing 24 µg whole protein were loaded per well on an SDS gel before being analysed by Western blotting.

The protocol for the dose-response assay was similar. *C. glabrata* cellular lysate with 4 mg/mL of whole protein was incubated with different concentrations of inhibitors at room temperature for 20 or 60 minutes. Heating was performed in a PCR machine for 3 min at 45 °C.

11. Cytotoxicity assays on human cells

Cytotoxicity assays were performed as described (Mietton *et al.*, 2017) with minor changes. Proliferation of human cells was assessed using an MTT colorimetric assay (Cell Proliferation Kit I, Roche). HeLa (epithelial cells, ATCC number CCL-2) and IMR90 (primary fibroblasts cells, ATCC number CCL-186) cells were cultured in a humidified atmosphere (37 °C and 5% CO₂) in DMEM medium containing 10% heat inactivated foetal calf serum and 2mM glutamine. Cells were seeded at a concentration of 5,000 HeLa cells per well or 15,000 IMR90 cells per well in 100 ml culture medium containing the test compound (iCG-24-409, amphotericin B or fluconazole) into 96 wells microplates (Falcon ref. 353072). Plates were incubated at 37 °C and 5% CO₂ for 24 h before adding 10 ml of MTT labelling reagent (final concentration 0.5 mg/ml) to each well. After incubating for a further 4 h, 100 ml of the solubilization solution were added in each well. Plates were allowed to stand overnight in the incubator before measuring the spectrophotometric absorbance at 570 nm and at the reference wavelength of 690 nm in a ClarioStar plate reader. The values of A₅₇₀ nm subtracted from the values of A₆₉₀ nm were normalized relative to that obtained with vehicle (0.2% DMSO, 0.8% ethanol) and plotted against compound concentration.

Chapter V - References

- Ahmad, K. M. *et al.* (2014) 'Genome structure and dynamics of the yeast pathogen *Candida glabrata*', *FEMS Yeast Research*, 14(4), pp. 529–535. doi: 10.1111/1567-1364.12145.
- Ahmad, S. *et al.* (2019) 'ERG6 and ERG2 are major targets conferring reduced susceptibility to amphotericin b in clinical *Candida glabrata* isolates in Kuwait', *Antimicrobial Agents and Chemotherapy*, 63(2), pp. 1–32. doi: 10.1128/AAC.01900-18.
- Albert, A. (1958) 'Chemical Aspects of Selective Toxicity', *Nature*, 182, pp. 421–423.
- Albulescu, L. O. *et al.* (2012) 'A quantitative, high-throughput reverse genetic screen reveals novel connections between pre-mRNA splicing and 5' and 3' end transcript determinants', *PLoS Genetics*, 8(3). doi: 10.1371/journal.pgen.1002530.
- Alexander, B. D. *et al.* (2013) 'Increasing echinocandin resistance in *Candida glabrata*: Clinical failure correlates with presence of FKS mutations and elevated minimum inhibitory concentrations', *Clinical Infectious Diseases*, 56(12), pp. 1724–1732. doi: 10.1093/cid/cit136.
- Alimehr, S. *et al.* (2015) 'Candida infection in the intensive care unit: A study of antifungal susceptibility pattern of *Candida* species in Milad hospital, Tehran, Iran', *Journal de Mycologie Medicale*. Elsevier Masson SAS, 25(4), pp. e113–e117. doi: 10.1016/j.mycmed.2015.09.005.
- Allen, D. *et al.* (2015) 'Azole antifungals: 35 years of invasive fungal infection management', *Expert Review of Anti-Infective Therapy*, 13(6), pp. 787–798. doi: 10.1586/14787210.2015.1032939.
- Anand, P. *et al.* (2013) 'BET bromodomains mediate transcriptional pause release in heart failure', *Cell*. Elsevier, 154(3), pp. 569–582. doi: 10.1016/j.cell.2013.07.013.
- Andes, D. R. *et al.* (2016) 'The epidemiology and outcomes of invasive *Candida* infections among organ transplant recipients in the United States: results of the Transplant-Associated Infection Surveillance Network (TRANSNET)', *Transplant Infectious Disease*, 18(6), pp. 921–931. doi: 10.1111/tid.12613.
- Aparicio, O. M., Billington, B. L. and Gottschling, D. E. (1991) 'Modifiers of position effect are shared between telomeric and silent mating-type loci in *S. cerevisiae*', *Cell*, 66(6), pp. 1279–1287. doi: 10.1016/0092-8674(91)90049-5.
- Arendrup, M. C. (2010) 'Epidemiology of invasive candidiasis', *Current Opinion in Critical Care*, 16(5), pp. 445–452. doi: 10.1097/MCC.0b013e32833e84d2.
- Armstrong, C. M. *et al.* (2002) 'Mutations in *Saccharomyces cerevisiae* Gene SIR2 Can Have Differential Effects on In Vivo Silencing Phenotypes and In Vitro Histone Deacetylation Activity', *Molecular biology of the cell*, 13, pp. 1427–1438. doi: 10.1091/mbc.01.
- Atanasova, R. *et al.* (2013) 'A Mouse Model for *Candida glabrata* Hematogenous

- Disseminated Infection Starting from the Gut: Evaluation of Strains with Different Adhesion Properties', *PLoS ONE*, 8(7), pp. 1–7. doi: 10.1371/journal.pone.0069664.
- Baarends, W. M. *et al.* (2003) 'Loss of HR6B Ubiquitin-Conjugating Activity Results in Damaged Synaptonemal Complex Structure and Increased Crossing-Over Frequency during the Male Meiotic Prophase', *Molecular and Cellular Biology*, 23(4), pp. 1151–1162. doi: 10.1128/mcb.23.4.1151-1162.2003.
- Bader, O. *et al.* (2012) 'Gross Karyotypic and Phenotypic Alterations among Different Progenies of the *Candida glabrata* CBS138/ATCC2001 Reference Strain', *PLoS ONE*, 7(12), pp. 1–8. doi: 10.1371/journal.pone.0052218.
- Barth, T. K. and Imhof, A. (2010) 'Fast signals and slow marks: the dynamics of histone modifications', *Trends in Biochemical Sciences*. Elsevier Ltd, 35(11), pp. 618–626. doi: 10.1016/j.tibs.2010.05.006.
- Bechter, O. and Schöffski, P. (2020) 'Make your best BET the emerging role of BET inhibitor treatment in malignant tumors', *Pharmacology and Therapeutics*. Elsevier Inc., 208, p. 107479. doi: 10.1016/j.pharmthera.2020.107479.
- Belkina, A. C., Nikolajczyk, B. S. and Denis, G. V. (2013) 'BET Protein Function Is Required for Inflammation: Brd2 Genetic Disruption and BET Inhibitor JQ1 Impair Mouse Macrophage Inflammatory Responses', *The Journal of Immunology*, 190(7), pp. 3670–3678. doi: 10.4049/jimmunol.1202838.
- Ben-Ami, R. *et al.* (2017) 'Multidrug-resistant *Candida haemulonii* and *C. Auris*, tel aviv, Israel', *Emerging Infectious Diseases*, 23(2), pp. 195–203. doi: 10.3201/eid2302.161486.
- Bennett, J. E. (2006) 'Echinocandins for candidemia in adults without neutropenia', *New England Journal of Medicine*, 355(11), pp. 1154–1159. doi: 10.1056/NEJMct060052.
- Bennett, J. E., Izumikawa, K. and Marr, K. A. (2004) 'Mechanism of Increased Fluconazole Resistance in *Candida glabrata* during Prophylaxis', *Antimicrobial Agents and Chemotherapy*, 48, pp. 1773–1777. doi: 10.1128/AAC.48.5.1773.
- Berger, S. L. (2002) 'Histone modifications in transcriptional regulation', *Current Opinion in Genetics and Development*, 12(2), pp. 142–148. doi: 10.1016/S0959-437X(02)00279-4.
- Berger, S. L. *et al.* (2009) 'An operational definition of epigenetics', *Genes and Development*, 23(7), pp. 781–783. doi: 10.1101/gad.1787609.
- Berridge, M. V., Herst, P. M. and Tan, A. S. (2005) 'Tetrazolium dyes as tools in cell biology: New insights into their cellular reduction', *Biotechnology Annual Review*, 11(SUPPL.), pp. 127–152. doi: 10.1016/S1387-2656(05)11004-7.
- Biermann, K. and Steger, K. (2007) 'Epigenetics in male germ cells', *Journal of Andrology*, 28(4), pp. 466–480. doi: 10.2164/jandrol.106.002048.
- Blazek, D. *et al.* (2005) 'Oligomerization of HEXIM1 via 7SK snRNA and coiled-coil region directs the inhibition of P-TEFb', *Nucleic Acids Research*, 33(22), pp. 7000–7010. doi: 10.1093/nar/gki997.
- Bodey, G. P. *et al.* (1999) 'The Epidemiology of *Candida glabrata* and *Candida albicans* Fungemia in', *the American Journal Ofmedicine*, 9343(01), pp. 2–7.
- Boehm, D. *et al.* (2013) 'BET bromodomain-targeting compounds reactivate HIV from latency

- via a Tat-independent mechanism', *Cell Cycle*, 12(3), pp. 452–462. doi: 10.4161/cc.23309.
- Bongomin, F. *et al.* (2017) 'Global and multi-national prevalence of fungal diseases—estimate precision', *Journal of Fungi*, 3(4). doi: 10.3390/jof3040057.
- Bönisch, C. and Hake, S. B. (2012) 'Histone H2A variants in nucleosomes and chromatin: More or less stable?', *Nucleic Acids Research*, 40(21), pp. 10719–10741. doi: 10.1093/nar/gks865.
- Bourova-Flin, E. *et al.* (2017) 'The role of bromodomain testis-specific factor, brdt, in cancer: A biomarker and a possible therapeutic target', *Cell Journal*, 19, pp. 1–8. doi: 10.22074/cellj.2017.5060.
- Bozzuto, G. and Molinari, A. (2015) 'Liposomes as nanomedical devices', *International Journal of Nanomedicine*, 10, pp. 975–999. doi: 10.2147/IJN.S68861.
- Bradbury, R. H. *et al.* (2016) 'Optimization of a Series of Bivalent Triazolopyridazine Based Bromodomain and Extraterminal Inhibitors: The Discovery of (3R)-4-[2-[4-[1-(3-Methoxy-[1,2,4]triazolo[4,3-b]pyridazin-6-yl)-4-piperidyl]phenoxy]ethyl]-1,3-dimethyl-piperazin-2-one (AZD5153)', *Journal of Medicinal Chemistry*, 59(17), pp. 7801–7817. doi: 10.1021/acs.jmedchem.6b00070.
- Brajtburg, J. *et al.* (1990) 'Amphotericin B: Current understanding of mechanisms of action', *Antimicrobial Agents and Chemotherapy*, 34(2), pp. 183–188. doi: 10.1128/AAC.34.2.183.
- Buil, J. B. *et al.* (2017) 'In vitro activity of the novel antifungal compound F901318 against difficult-to-treat *Aspergillus* isolates', *The Journal of antimicrobial chemotherapy*, 72(9), pp. 2548–2552. doi: 10.1093/jac/dkx177.
- Butler, G. *et al.* (2009) 'Evolution of pathogenicity and sexual reproduction in eight *Candida* genomes', *Nature*. Nature Publishing Group, 459(7247), pp. 657–662. doi: 10.1038/nature08064.
- Canela, H. M. S. *et al.* (2018) 'Prevalence, virulence factors and antifungal susceptibility of *Candida* spp. isolated from bloodstream infections in a tertiary care hospital in Brazil.', *Mycoses*, 61(1), pp. 11–21. doi: 10.1111/myc.12695.
- Casadevall, A. (2018) 'Fungal Diseases in the 21st Century: The Near and Far Horizons', *Pathogens and Immunity*, 3(2), p. 183. doi: 10.20411/pai.v3i2.249.
- Castanheira, M. *et al.* (2014) 'Activity of a Novel Echinocandin Biafungin (CD101) Tested against Most Common *Candida* and *Aspergillus* Species, Including Echinocandin- and Azole-resistant Strains', *Proceedings of the 54th Interscience Conference on Antimicrobial Agents and Chemotherapy*, 14, p. 1082.
- Castaño, I. *et al.* (2005) 'Telomere length control and transcriptional regulation of subtelomeric adhesins in *Candida glabrata*', *Molecular Microbiology*, 55(4), pp. 1246–1258. doi: 10.1111/j.1365-2958.2004.04465.x.
- Chapman, B. *et al.* (2017) 'Changing epidemiology of candidaemia in Australia', *The Journal of antimicrobial chemotherapy*, 72(4), pp. 1103–1108. doi: 10.1093/jac/dkw422.
- Chatterjee, S. *et al.* (2015) 'Draft genome of a commonly misdiagnosed multidrug resistant pathogen *Candida auris*', *BMC Genomics*. BMC Genomics, 16(1), pp. 1–16. doi: 10.1186/s12864-015-1863-z.

- Chen, D. *et al.* (2019) 'Discovery, structural insight, and bioactivities of BY27 as a selective inhibitor of the second bromodomains of BET proteins', *European Journal of Medicinal Chemistry*. Elsevier Masson SAS, 182, p. 111633. doi: 10.1016/j.ejmech.2019.111633.
- Cheung, K. *et al.* (2017) 'BET N-Terminal bromodomain inhibition selectively blocks Th17 cell differentiation and ameliorates colitis in mice', *Proceedings of the National Academy of Sciences of the United States of America*, 114(11), pp. 2952–2957. doi: 10.1073/pnas.1615601114.
- Chew, S. Y. *et al.* (2019) 'Glyoxylate cycle gene ICL1 is essential for the metabolic flexibility and virulence of *Candida glabrata*', *Scientific Reports*. Springer US, 9(1), pp. 1–11. doi: 10.1038/s41598-019-39117-1.
- Choi, H. W. *et al.* (2007) 'Species-specific differences in the susceptibilities of biofilms formed by *Candida* bloodstream isolates to echinocandin antifungals', *Antimicrobial Agents and Chemotherapy*, 51(4), pp. 1520–1523. doi: 10.1128/AAC.01141-06.
- Chua, P. and Roeder, G. S. (1995) 'Bdf1, a yeast chromosomal protein required for sporulation.', *Molecular and Cellular Biology*, 15(7), pp. 3685–3696. doi: 10.1128/mcb.15.7.3685.
- Clapier, C. R. *et al.* (2017) 'Mechanisms of action and regulation of ATP-dependent chromatin-remodelling complexes', *Nature Reviews Molecular Cell Biology*. Nature Publishing Group, 18(7), pp. 407–422. doi: 10.1038/nrm.2017.26.
- Coco, B. J. *et al.* (2008) 'Mixed *Candida albicans* and *Candida glabrata* populations associated with the pathogenesis of denture stomatitis', *Oral Microbiology and Immunology*, 23(5), pp. 377–383. doi: 10.1111/j.1399-302X.2008.00439.x.
- Cogliati, M. (2013) 'Global Molecular Epidemiology of *Cryptococcus neoformans* and *Cryptococcus gattii* : An Atlas of the Molecular Types ', *Scientifica*, 2013(serotype D), pp. 1–23. doi: 10.1155/2013/675213.
- Cormack, B. P. *et al.* (2016) 'An Adhesin of the Yeast Pathogen *Candida glabrata* Mediating Adherence to Human Epithelial Cells', *Science*, 285(5427), pp. 578–582.
- Cromm, P. M. and Crews, C. M. (2017) 'Targeted Protein Degradation: from Chemical Biology to Drug Discovery', *Cell Chemical Biology*. Elsevier Ltd., 24(9), pp. 1181–1190. doi: 10.1016/j.chembiol.2017.05.024.
- Csank, C. and Haynes, K. (2000) '*Candida glabrata* displays pseudohyphal growth', *FEMS Microbiology Letters*, 189(1), pp. 115–120. doi: 10.1016/S0378-1097(00)00241-X.
- Cuellar-Cruz, M. *et al.* (2008) 'High resistance to oxidative stress in the fungal pathogen *Candida glabrata* is mediated by a single catalase, Cta1p, and is controlled by the transcription factors Yap1p, Skn7p, Msn2p, and Msn4p', *Eukaryotic Cell*, 7(5), pp. 814–825. doi: 10.1128/EC.00011-08.
- Dai, X. *et al.* (2017) 'Prostate cancer-Associated SPOP mutations confer resistance to BET inhibitors through stabilization of BRD4', *Nature Medicine*. Nature Publishing Group, 23(9), pp. 1063–1071. doi: 10.1038/nm.4378.
- Davis, S. A. *et al.* (2015) 'Nontoxic antimicrobials that evade drug resistance', *Nature Chemical Biology*, 11(7), pp. 481–487. doi: 10.1038/nchembio.1821.
- Dawson, M. A. *et al.* (2011) 'Inhibition of BET recruitment to chromatin as an effective

treatment for MLL-fusion leukaemia', *Nature*. Nature Publishing Group, 478(7370), pp. 529–533. doi: 10.1038/nature10509.

Dawson, M. A., Kouzarides, T. and Huntly, B. J. P. (2012) 'Targeting epigenetic readers in cancer', *New England Journal of Medicine*, 367(7), pp. 647–657. doi: 10.1056/NEJMra1112635.

Delmore, J. E. *et al.* (2011) 'BET bromodomain inhibition as a therapeutic strategy to target c-Myc', *Cell*. Elsevier Inc., 146(6), pp. 904–917. doi: 10.1016/j.cell.2011.08.017.

Denis, G. V. *et al.* (2006) 'Identification of transcription complexes that contain the double bromodomain protein Brd2 and chromatin remodeling machines', *Journal of Proteome Research*, 5(3), pp. 502–511. doi: 10.1021/pr050430u.

Denis, J. *et al.* (2018) 'Isavuconazole: A new broad-spectrum azole. Part 1: In vitro activity', *Journal de Mycologie Medicale*. Elsevier Masson SAS, 28(1), pp. 8–14. doi: 10.1016/j.mycmed.2018.02.005.

Denning, D. W. (2003) 'Echinocandin antifungal drugs', *Lancet*, 362(9390), pp. 1142–1151. doi: 10.1016/S0140-6736(03)14472-8.

Devaiah, B. N. *et al.* (2012) 'BRD4 is an atypical kinase that phosphorylates Serine2 of the RNA Polymerase II carboxy-terminal domain', *Proceedings of the National Academy of Sciences of the United States of America*, 109(18), pp. 6927–6932. doi: 10.1073/pnas.1120422109.

Devaiah, B. N. *et al.* (2016) 'BRD4 is a histone acetyltransferase that evicts nucleosomes from chromatin', *Nature Structural and Molecular Biology*, 23(6), pp. 540–548. doi: 10.1038/nsmb.3228.

Dhalluin, C. *et al.* (1999) 'Structure and ligand of a histone acetyltransferase bromodomain', *Nature*, 399(6735), pp. 491–496. doi: 10.1038/20974.

Digan, M. E. *et al.* (1986) 'Genetic and molecular analysis of fs(1)h, a maternal effect homeotic gene in Drosophila', *Developmental Biology*, 114(1), pp. 161–169. doi: 10.1016/0012-1606(86)90392-1.

Dodgson, A. R. *et al.* (2005) 'Evidence for recombination in *Candida glabrata*', *Fungal Genetics and Biology*, 42(3), pp. 233–243. doi: 10.1016/j.fgb.2004.11.010.

Doi, A. M. *et al.* (2016) 'Epidemiology and Microbiologic Characterization of Nosocomial Candidemia from a Brazilian National Surveillance Program', *PloS one*, 11(1), p. e0146909. doi: 10.1371/journal.pone.0146909.

Domergue, R. *et al.* (2005) 'Nicotinic acid limitation regulates silencing of *Candida* adhesins during UTI', *Science*, 308(5723), pp. 866–870. doi: 10.1126/science.11101361.

Donati, B., Lorenzini, E. and Ciarrocchi, A. (2018) 'BRD4 and Cancer: Going beyond transcriptional regulation', *Molecular Cancer*. Molecular Cancer, 17(1), pp. 1–13. doi: 10.1186/s12943-018-0915-9.

Douglas, C. M. *et al.* (1997) 'Identification of the FKS1 gene of *Candida albicans* as the essential target of 1,3-β-D-glucan synthase inhibitors', *Antimicrobial Agents and Chemotherapy*, 41(11), pp. 2471–2479.

Dujon, B. *et al.* (2004) 'Genome evolution in yeasts', *Nature*, 430, pp. 35–44.

- Editorial (2017) 'Stop neglecting fungi', *Nature Microbiology*, 2(8). doi: 10.1038/nmicrobiol.2017.120.
- Ember, S. W. J. *et al.* (2014) 'Acetyl-lysine binding site of bromodomain-containing protein 4 (BRD4) interacts with diverse kinase inhibitors', *ACS Chemical Biology*, 9(5), pp. 1160–1171. doi: 10.1021/cb500072z.
- Fan, H. Y. *et al.* (2003) 'Distinct strategies to make nucleosomal DNA accessible', *Molecular Cell*, 11(5), pp. 1311–1322. doi: 10.1016/S1097-2765(03)00192-8.
- Feng, Q. *et al.* (2014) 'An epigenomic approach to therapy for tamoxifen-resistant breast cancer', *Cell Research*. Nature Publishing Group, 24(7), pp. 809–819. doi: 10.1038/cr.2014.71.
- Fernandez-Capetillo, O. *et al.* (2003) 'H2AX is required for chromatin remodeling and inactivation of sex chromosomes in male mouse meiosis', *Developmental Cell*, 4(4), pp. 497–508. doi: 10.1016/S1534-5807(03)00093-5.
- Ferri, E., Petosa, C. and McKenna, C. E. (2016) 'Bromodomains: Structure, function and pharmacology of inhibition', *Biochemical Pharmacology*. Elsevier Inc., 106, pp. 1–18. doi: 10.1016/j.bcp.2015.12.005.
- Fidel Jr, P. L., Vazquez, J. A. and Sobel, J. D. (1999) 'Candida glabrata: Review of Epidemiology, Pathogenesis, and Clinical Disease with Comparison to C. albicans', *CLINICAL MICROBIOLOGY REVIEWS*, 12(1), pp. 80–96.
- Filippakopoulos, P. *et al.* (2010) 'Selective inhibition of BET bromodomains', *Nature*. Nature Publishing Group, 468(7327), pp. 1067–1073. doi: 10.1038/nature09504.
- Filippakopoulos, P. *et al.* (2012) 'Histone recognition and large-scale structural analysis of the human bromodomain family', *Cell*, 149(1), pp. 214–231. doi: 10.1016/j.cell.2012.02.013.
- Filippakopoulos, P. and Knapp, S. (2014) 'Targeting bromodomains: Epigenetic readers of lysine acetylation', *Nature Reviews Drug Discovery*. Nature Publishing Group, 13(5), pp. 337–356. doi: 10.1038/nrd4286.
- Finley, D. *et al.* (2012) 'The ubiquitin-proteasome system of *Saccharomyces cerevisiae*', *Genetics*, 192(2), pp. 319–360. doi: 10.1534/genetics.112.140467.
- Fischle, W. *et al.* (2003) 'Molecular basis for the discrimination of repressive methyl-lysine marks in histone H3 by polycomb and HP1 chromodomains', *Genes and Development*, 17(15), pp. 1870–1881. doi: 10.1101/gad.1110503.
- Floyd, S. R. *et al.* (2013) 'The bromodomain protein Brd4 insulates chromatin from DNA damage signalling', *Nature*, 498(7453), pp. 246–250. doi: 10.1038/nature12147.
- Fong, C. Y. *et al.* (2015) 'BET inhibitor resistance emerges from leukaemia stem cells', *Nature*, 525(7570), pp. 538–542. doi: 10.1038/nature14888.
- French, C. A. *et al.* (2003) 'BRD4-NUT fusion oncogene: A novel mechanism in aggressive carcinoma', *Cancer Research*, 63(2), pp. 304–307.
- French, C. A. *et al.* (2004) 'Midline carcinoma of children and young adults with NUT rearrangement', *Journal of Clinical Oncology*, 22(20), pp. 4135–4139. doi: 10.1200/JCO.2004.02.107.
- French, C. A. *et al.* (2008) 'BRD-NUT oncoproteins: A family of closely related nuclear

- proteins that block epithelial differentiation and maintain the growth of carcinoma cells', *Oncogene*, 27(15), pp. 2237–2242. doi: 10.1038/sj.onc.1210852.
- Fu, J. *et al.* (2013) 'Interplay between BDF1 and BDF2 and their roles in regulating the yeast salt stress response', *FEBS Journal*, 280(9), pp. 1991–2001. doi: 10.1111/febs.12219.
- Fu, J. *et al.* (2015) 'The yeast BDF1 regulates endocytosis via LSP1 under salt stress', *Current Microbiology*, 70(5), pp. 671–678. doi: 10.1007/s00284-014-0773-7.
- Gabaldón, T. and Carreté, L. (2016) 'The birth of a deadly yeast: Tracing the evolutionary emergence of virulence traits in *Candida glabrata*', *FEMS Yeast Research*, pp. 1–9. doi: 10.1093/femsyr/fov110.
- Gacias, M. *et al.* (2014) 'Selective chemical modulation of gene transcription favors oligodendrocyte lineage progression', *Chemistry and Biology*. Elsevier Ltd, 21(7), pp. 841–854. doi: 10.1016/j.chembiol.2014.05.009.
- Galocha, M. *et al.* (2019) 'Divergent Approaches to Virulence in *C. albicans* and *C. glabrata*: Two Sides of the Same Coin', *International Journal of Molecular Sciences*, 20(9), p. 2345. doi: 10.3390/ijms20092345.
- Gamsjaeger, R. *et al.* (2011) 'Structural Basis and Specificity of Acetylated Transcription Factor GATA1 Recognition by BET Family Bromodomain Protein Brd3', *Molecular and Cellular Biology*, 31(13), pp. 2632–2640. doi: 10.1128/mcb.05413-11.
- García-Oliver, E. *et al.* (2017) 'Bdf1 Bromodomains Are Essential for Meiosis and the Expression of Meiotic-Specific Genes', *PLoS Genetics*, 13(1), pp. 1–26. doi: 10.1371/journal.pgen.1006541.
- Garcia-Solache, M. A. and Casadevall, A. (2010) 'Global Warming Will Bring New Fungal Diseases for Mammals', *mBio*, 1(1), pp. 1–3. doi: 10.1128/mbio.00061-10.
- Gaucher, J. *et al.* (2012) 'Bromodomain-dependent stage-specific male genome programming by Brdt', *EMBO Journal*, 31(19), pp. 3809–3820. doi: 10.1038/emboj.2012.233.
- Ghannoum, M. A. (2000) 'Potential Role of Phospholipases in Virulence and Fungal Pathogenesis', *Clinical Microbiology Reviews*, 13(1), pp. 122–143.
- Gilan, O. *et al.* (2020) 'Selective targeting of BD1 and BD2 of the BET proteins in cancer and immuno-inflammation', *Science*, 8455(March), p. eaaz8455. doi: 10.1126/science.aaz8455.
- Govin, J. *et al.* (2010) 'Systematic screen reveals new functional dynamics of histones H3 and H4 during gametogenesis', *Genes and Development*, 24(16), pp. 1772–1786. doi: 10.1101/gad.1954910.
- Goyer, M. *et al.* (2016) 'Intestinal cell tight junctions limit invasion of *Candida albicans* through active penetration and endocytosis in the early stages of the interaction of the fungus with the intestinal barrier', *PLoS ONE*, 11(3), pp. 1–19. doi: 10.1371/journal.pone.0149159.
- Groll, A. H., Piscitelli, S. C. and Walsh, T. J. (1998) 'Clinical Pharmacology of Systemic Antifungal Agents: A Comprehensive Review of Agents in Clinical Use, Current Investigational Compounds, and Putative Targets for Antifungal Drug Development', *Advances in Pharmacology*, 44(C), pp. 343–500. doi: 10.1016/S1054-3589(08)60129-5.
- De Groot, P. W. J. *et al.* (2008) 'The cell wall of the human pathogen *Candida glabrata*:

- Differential incorporation of novel adhesin-like wall proteins', *Eukaryotic Cell*, 7(11), pp. 1951–1964. doi: 10.1128/EC.00284-08.
- Guinea, J. (2014) 'Global trends in the distribution of Candida species causing candidemia', *Clinical Microbiology and Infection*. European Society of Clinical Infectious Diseases, 20, pp. 5–10. doi: 10.1111/1469-0691.12539.
- Haberland, M., Montgomery, R. L. and Olson, E. N. (2009) 'The many roles of histone deacetylases in development and physiology: Implications for disease and therapy', *Nature Reviews Genetics*, 10(1), pp. 32–42. doi: 10.1038/nrg2485.
- Hager, C. L. *et al.* (2018) 'In vitro and in vivo evaluation of the antifungal activity of APX001A/APX001 against candida auris', *Antimicrobial Agents and Chemotherapy*, 62(3), pp. 1–7. doi: 10.1128/AAC.02319-17.
- Halliwell, S. C. *et al.* (2012) 'Heterogeneous expression of the virulence-related adhesin epa1 between individual cells and strains of the pathogen candida Glabrata', *Eukaryotic Cell*, 11(2), pp. 141–150. doi: 10.1128/EC.05232-11.
- Hammad, N. M. *et al.* (2018) 'Mannose-Binding Lectin: A Potential Therapeutic Candidate against Candida Infection', *BioMed Research International*, 2018. doi: 10.1155/2018/2813737.
- Harikrishnan, K. N. *et al.* (2005) 'Brahma links the SWI/SNF chromatin-remodeling complex with MeCP2-dependent transcriptional silencing', *Nature Genetics*, 37(3), pp. 254–264. doi: 10.1038/ng1516.
- Hasenoehrl, A. *et al.* (2006) 'In vitro activity and in vivo efficacy of icofungipen (PLD-118), a novel oral antifungal agent, against the pathogenic yeast Candida albicans', *Antimicrobial Agents and Chemotherapy*, 50(9), pp. 3011–3018. doi: 10.1128/AAC.00254-06.
- Hassan, I. *et al.* (2009) 'Excess mortality, length of stay and cost attributable to candidaemia', *Journal of Infection*. Elsevier Ltd, 59(5), pp. 360–365. doi: 10.1016/j.jinf.2009.08.020.
- Hata, K. *et al.* (2011) 'Efficacy of oral E1210, a new broad-spectrum antifungal with a novel mechanism of action, in murine models of candidiasis, aspergillosis, and fusariosis', *Antimicrobial Agents and Chemotherapy*, 55(10), pp. 4543–4551. doi: 10.1128/AAC.00366-11.
- Hawksworth, D. L. and Lücking, R. (2017) '1 . Understanding the task : Writing an Essay : 2 . Plan and Prepare : 4 . Review the essay : 3 . The First Draft : Essay Structures'. doi: 10.1128/microbiolspec.FUNK-0052-2016.Correspondence.
- Healey, K. R. and Perlin, D. S. (2018) 'Fungal resistance to echinocandins and the MDR phenomenon in Candida glabrata', *Journal of Fungi*, 4(3). doi: 10.3390/jof4030105.
- Henry, K. W., Nickels, J. T. and Edlind, T. D. (2000) 'Upregulation of ERG genes in Candida species by azoles and other sterol biosynthesis inhibitors', *Antimicrobial Agents and Chemotherapy*, 44(10), pp. 2693–2700. doi: 10.1128/AAC.44.10.2693-2700.2000.
- Hesstvedt, L. *et al.* (2017) 'Differences in epidemiology of candidaemia in the Nordic countries – what is to blame?', *Mycoses*, 60(1), pp. 11–19. doi: 10.1111/myc.12535.
- Hodgetts, S. *et al.* (2008) 'Efungumab and caspofungin: Pre-clinical data supporting synergy', *Journal of Antimicrobial Chemotherapy*, 61(5), pp. 1132–1139. doi: 10.1093/jac/dkn075.

- Hsu, S. C. *et al.* (2017) 'The BET Protein BRD2 Cooperates with CTCF to Enforce Transcriptional and Architectural Boundaries', *Molecular Cell*. Elsevier Inc., 66(1), pp. 102–116.e7. doi: 10.1016/j.molcel.2017.02.027.
- Huang, B. *et al.* (2009) 'Brd4 Coactivates Transcriptional Activation of NF- B via Specific Binding to Acetylated RelA', *Molecular and Cellular Biology*, 29(5), pp. 1375–1387. doi: 10.1128/mcb.01365-08.
- Hull, C. M., Parker, J. E., *et al.* (2012) 'Facultative sterol uptake in an ergosterol-deficient clinical isolate of candida glabrata harboring a missense mutation in ERG11 and exhibiting cross-resistance to azoles and amphotericin B', *Antimicrobial Agents and Chemotherapy*, 56(8), pp. 4223–4232. doi: 10.1128/AAC.06253-11.
- Hull, C. M., Bader, O., *et al.* (2012) 'Two clinical isolates of Candida glabrata exhibiting reduced sensitivity to amphotericin B both harbor mutations in ERG2', *Antimicrobial Agents and Chemotherapy*, 56(12), pp. 6417–6421. doi: 10.1128/AAC.01145-12.
- Hussong, M. *et al.* (2017) 'The bromodomain protein BRD4 regulates splicing during heat shock', *Nucleic Acids Research*, 45(1), pp. 382–394. doi: 10.1093/nar/gkw729.
- Imai, S. I. *et al.* (2000) 'Transcriptional silencing and longevity protein Sir2 is an NAD-dependent histone deacetylase', *Nature*, 403(6771), pp. 795–800. doi: 10.1038/35001622.
- Israel, S. *et al.* (2019) 'The Epidemiology and Susceptibility of Candidemia in Jerusalem, Israel', *Frontiers in Cellular and Infection Microbiology*, 9(October), pp. 1–7. doi: 10.3389/fcimb.2019.00352.
- Jacobsen, I. D. *et al.* (2010) 'Candida glabrata persistence in mice does not depend on host immunosuppression and is unaffected by fungal amino acid auxotrophy', *Infection and Immunity*, 78(3), pp. 1066–1077. doi: 10.1128/IAI.01244-09.
- Jin, X. *et al.* (2018) 'DUB3 Promotes BET Inhibitor Resistance and Cancer Progression by Deubiquitinating BRD4', *Molecular Cell*. Elsevier Inc., 71(4), pp. 592–605.e4. doi: 10.1016/j.molcel.2018.06.036.
- Johnson, C. J. *et al.* (2016) 'The Extracellular Matrix of Candida albicans Biofilms Impairs Formation of Neutrophil Extracellular Traps', *PLoS Pathogens*, 12(9), pp. 1–23. doi: 10.1371/journal.ppat.1005884.
- Karaman, R. (2014) 'Using predrugs to optimize drug candidates', *Expert Opinion on Drug Discovery*, 9(12), pp. 1405–1419. doi: 10.1517/17460441.2014.954545.
- Kaur, R. *et al.* (2005) 'A yeast by any other name: Candida glabrata and its interaction with the host', *Current Opinion in Microbiology*, 8(4), pp. 378–384. doi: 10.1016/j.mib.2005.06.012.
- Kaur, R., Ma, B. and Cormack, B. P. (2007) 'A family of glycosylphosphatidylinositol-linked aspartyl proteases is required for virulence of Candida glabrata', *Proceedings of the National Academy of Sciences*, 104(18), pp. 7628–7633. doi: 10.1073/pnas.0611195104.
- Kedaigle, A. J. *et al.* (2020) 'Treatment with JQ1, a BET bromodomain inhibitor, is selectively detrimental to R6/2 Huntington's disease mice', *Human Molecular Genetics*, 29(2), pp. 202–215. doi: 10.1093/hmg/ddz264.
- El Kennani, S. *et al.* (2017) 'MS-HistoneDB, a manually curated resource for proteomic analysis of human and mouse histones', *Epigenetics and Chromatin*. BioMed Central, 10(1),

pp. 1–18. doi: 10.1186/s13072-016-0109-x.

El Kennani, S. *et al.* (2018) 'Proteomic analysis of histone variants and their PTMs: Strategies and pitfalls', *Proteomes*, 6(3), pp. 1–16. doi: 10.3390/proteomes6030029.

Kim, M. *et al.* (2009) 'Candida haemulonii and Closely Related Species at 5 University Hospitals in Korea: Identification, Antifungal Susceptibility, and Clinical Features', *Clinical Infectious Diseases*, 48(6), pp. e57–e61. doi: 10.1086/597108.

Ko, J. H. *et al.* (2019) 'Changing epidemiology of non-albicans candidemia in Korea', *Journal of Infection and Chemotherapy*. Elsevier Ltd, 25(5), pp. 388–391. doi: 10.1016/j.jiac.2018.09.016.

Koerber, R. T. *et al.* (2009) 'Interaction of Transcriptional Regulators with Specific Nucleosomes across the Saccharomyces Genome', *Molecular Cell*. Elsevier Ltd, 35(6), pp. 889–902. doi: 10.1016/j.molcel.2009.09.011.

Komshian, S. V. *et al.* (1989) 'Fungemia caused by candida species and torulopsis glabrata in the hospitalized patient: Frequency, characteristics, and evaluation of factors influencing outcome', *Reviews of Infectious Diseases*, 11(3), pp. 379–390. doi: 10.1093/clinids/11.3.379.

Kooistra, S. M. and Helin, K. (2012) 'Post-translational modifications: Molecular mechanisms and potential functions of histone demethylases', *Nature Reviews Molecular Cell Biology*. Nature Publishing Group, 13(5), pp. 297–311. doi: 10.1038/nrm3327.

Kramer, A., Schwebke, I. and Kampf, G. (2006) 'How long do nosocomial pathogens persist on inanimate surfaces? A systematic review', *BMC Infectious Diseases*, pp. 1–8. doi: 10.1186/1471-2334-6-130.

Kreusch, A. and Karstaedt, A. S. (2013) 'Candidemia among adults in Soweto, South Africa, 1990-2007', *International Journal of Infectious Diseases*. International Society for Infectious Diseases, 17(8), pp. e621–e623. doi: 10.1016/j.ijid.2013.02.010.

Krogan, N. J. *et al.* (2003) 'A Snf2 Family ATPase Complex Required for Recruitment of the Histone H2A Variant Htz1', *Molecular Cell*, 12(6), pp. 1565–1576. doi: 10.1016/S1097-2765(03)00497-0.

Ksiezopolska, E. and Gabaldón, T. (2018) 'Evolutionary emergence of drug resistance in candida opportunistic pathogens', *Genes*, 9(9). doi: 10.3390/genes9090461.

Kucharíková, S. *et al.* (2015) 'In vivo Candida glabrata biofilm development on foreign bodies in a rat subcutaneous model', *Journal of Antimicrobial Chemotherapy*, 70(3), pp. 846–856. doi: 10.1093/jac/dku447.

Kullberg, B. J. and Arendrup, M. C. (2016) 'Invasive Candidiasis', *Infectious Disease Clinics of North America*, 30(1), pp. 103–124. doi: 10.1016/j.idc.2015.10.013.

Kurimchak, A. M. *et al.* (2016) 'Resistance to BET Bromodomain Inhibitors Is Mediated by Kinome Reprogramming in Ovarian Cancer', *Cell Reports*. The Author(s), 16(5), pp. 1273–1286. doi: 10.1016/j.celrep.2016.06.091.

Kurtzman, C. P. and Piškur, J. (2006) 'Taxonomy and phylogenetic diversity among the yeasts', *Topics in Current Genetics*, 15(January), pp. 29–46. doi: 10.1007/b106654.

Kwok, J. *et al.* (2017) 'Jmjd6, a JmJC dioxygenase with many interaction partners and pleiotropic functions', *Frontiers in Genetics*, 8(MAR), pp. 1–19. doi:

10.3389/fgene.2017.00032.

Ladurner, A. G. *et al.* (2003) 'Bromodomains mediate an acetyl-histone encoded antisilencing function at heterochromatin boundaries', *Molecular Cell*, 11(2), pp. 365–376. doi: 10.1016/S1097-2765(03)00035-2.

Lakkireddy, H. R. and Bazile, D. V. (2019) 'Nano-carriers for drug routeing—towards a new era', *Journal of Drug Targeting*. Taylor & Francis, 27(5–6), pp. 525–541. doi: 10.1080/1061186X.2018.1561891.

Lambert, J. P. *et al.* (2019) 'Interactome Rewiring Following Pharmacological Targeting of BET Bromodomains', *Molecular Cell*, 73(3), pp. 621–638.e17. doi: 10.1016/j.molcel.2018.11.006.

Lamoth, F. *et al.* (2018) 'Changes in the epidemiological landscape of invasive candidiasis', *Journal of Antimicrobial Chemotherapy*, 73(April), pp. i4–i13. doi: 10.1093/jac/dkx444.

De Las Peñas, A. *et al.* (2003) 'Virulence-related surface glycoproteins in the yeast pathogen *Candida glabrata* are encoded in subtelomeric clusters and subject to RAP1- and SIR-dependent transcriptional silencing', *Genes and Development*, 17(18), pp. 2245–2258. doi: 10.1101/gad.1121003.

Laza-Knoerr, A. L., Gref, R. and Couvreur, P. (2010) 'Cyclodextrins for drug delivery', *Journal of Drug Targeting*, 18(9), pp. 645–656. doi: 10.3109/10611861003622552.

Lee, W. G. *et al.* (2011) 'First three reported cases of nosocomial fungemia caused by *Candida auris*', *Journal of Clinical Microbiology*, 49(9), pp. 3139–3142. doi: 10.1128/JCM.00319-11.

Lee, Y. S. *et al.* (2013) 'Runx3 Inactivation Is a Crucial Early Event in the Development of Lung Adenocarcinoma', *Cancer Cell*. Elsevier Inc., 24(5), pp. 603–616. doi: 10.1016/j.ccr.2013.10.003.

Legras, J. L. *et al.* (2007) 'Bread, beer and wine: *Saccharomyces cerevisiae* diversity reflects human history', *Molecular Ecology*, 16(10), pp. 2091–2102. doi: 10.1111/j.1365-294X.2007.03266.x.

LeRoy, G., Rickards, B. and Flint, S. J. (2008) 'The Double Bromodomain Proteins Brd2 and Brd3 Couple Histone Acetylation to Transcription', *Molecular Cell*, 30(1), pp. 51–60. doi: 10.1016/j.molcel.2008.01.018.

Lewis, R. E. (2011) 'Current concepts in antifungal pharmacology', *Mayo Clinic Proceedings*, 86(8), pp. 805–817. doi: 10.4065/mcp.2011.0247.

Li, L. and Dongari-Bagtzoglou, A. (2009) 'Epithelial GM-CSF induction by *Candida glabrata*', *Journal of Dental Research*, 88(8), pp. 746–751. doi: 10.1177/0022034509341266.

Li, X. *et al.* (2017) 'Nano carriers for drug transport across the blood–brain barrier', *Journal of Drug Targeting*, 25(1), pp. 17–28. doi: 10.1080/1061186X.2016.1184272.

Li, Y. *et al.* (2009) 'The Target of the NSD Family of Histone Lysine Methyltransferases Depends on the Nature of the Substrate', *Journal of Biological Chemistry*, 284(49), pp. 34283–34295. doi: 10.1074/jbc.

Li, Z. *et al.* (2013) 'The BET bromodomain inhibitor JQ1 activates HIV latency through antagonizing Brd4 inhibition of Tat-transactivation', *Nucleic Acids Research*, 41(1), pp. 277–287. doi: 10.1093/nar/gks976.

- Lin, S. *et al.* (2018) 'Candidemia in Adults at a Tertiary Hospital in China: Clinical Characteristics, Species Distribution, Resistance, and Outcomes', *Mycopathologia*, 183(4), pp. 679–689. doi: 10.1007/s11046-018-0258-5.
- Lindberg, E. *et al.* (2019) 'Species distribution and antifungal drug susceptibilities of yeasts isolated from the blood samples of patients with candidemia', *Scientific Reports*, 9(1), pp. 12–17. doi: 10.1038/s41598-019-40280-8.
- Linde, J. *et al.* (2015) 'Defining the transcriptomic landscape of *Candida glabrata* by RNA-Seq', *Nucleic Acids Research*, 43(3), pp. 1392–1406. doi: 10.1093/nar/gku1357.
- Liu, X. *et al.* (2007) 'Genetic and comparative transcriptome analysis of bromodomain factor 1 in the salt stress response of *Saccharomyces cerevisiae*', *Current Microbiology*, 54(4), pp. 325–330. doi: 10.1007/s00284-006-0525-4.
- Liu, X. *et al.* (2009) 'Bdf1p deletion affects mitochondrial function and causes apoptotic cell death under salt stress', *FEMS Yeast Research*, 9(2), pp. 240–246. doi: 10.1111/j.1567-1364.2008.00469.x.
- Lockhart, S. R. *et al.* (2012) 'Species identification and antifungal susceptibility testing of *Candida* bloodstream isolates from population-based surveillance studies in two U.S. cities from 2008 to 2011', *Journal of Clinical Microbiology*, 50(11), pp. 3435–3442. doi: 10.1128/JCM.01283-12.
- Lockhart, S. R. *et al.* (2016) 'Clinical Infectious Diseases Advance Access published October 20, 2016', pp. 1–24.
- Lortholary, O. *et al.* (2011) 'Recent Exposure to Caspofungin or Fluconazole Influences the Epidemiology of Candidemia: a Prospective Multicenter Study Involving 2,441 Patients', *Antimicrobial Agents and Chemotherapy*, 55(2), pp. 532–538. doi: 10.1128/aac.01128-10.
- Lortholary, O. *et al.* (2014) 'Worrisome trends in incidence and mortality of candidemia in intensive care units (Paris area, 2002-2010)', *Intensive Care Medicine*, 40(9), pp. 1303–1312. doi: 10.1007/s00134-014-3408-3.
- Lu, J. *et al.* (2015) 'Hijacking the E3 Ubiquitin Ligase Cereblon to Efficiently Target BRD4', *Chemistry and Biology*. Elsevier, 22(6), pp. 755–763. doi: 10.1016/j.chembiol.2015.05.009.
- Luger, K. *et al.* (1997) 'Crystal structure of the nucleosome core particle at 2.8 Å resolution', *Nature*, 389(6648), pp. 251–260. doi: 10.1038/38444.
- Lygerou, Z. *et al.* (1994) 'The yeast BDF1 gene encodes a transcription factor involved in the expression of a broad class of genes including snRNAs', *Nucleic Acids Research*, 22(24), pp. 5332–5340. doi: 10.1093/nar/22.24.5332.
- Mahdi, H. *et al.* (2009) 'Specific interaction between genotype, smoking and autoimmunity to citrullinated α -enolase in the etiology of rheumatoid arthritis', *Nature Genetics*. Nature Publishing Group, 41(12), pp. 1319–1324. doi: 10.1038/ng.480.
- Majithiya, J. *et al.* (2009) 'Efficacy of isavuconazole, voriconazole and fluconazole in temporarily neutropenic murine models of disseminated *Candida tropicalis* and *Candida krusei*', *Journal of Antimicrobial Chemotherapy*, 63(1), pp. 161–166. doi: 10.1093/jac/dkn431.
- Manterola, M. *et al.* (2018) 'BRDT is an essential epigenetic regulator for proper chromatin organization, silencing of sex chromosomes and crossover formation in male meiosis', *PLoS*

- Genetics*, 14(3), pp. 1–30. doi: 10.1371/journal.pgen.1007209.
- Mao, X. *et al.* (2002) 'MET3 promoter: A tightly regulated promoter and its application in construction of conditional lethal strain', *Current Microbiology*, 45(1), pp. 37–40. doi: 10.1007/s00284-001-0046-0.
- Masselink, H. and Bernards, R. (2000) 'The adenovirus E1A binding protein BS69 is a corepressor of transcription through recruitment of N-CoR', *Oncogene*, 19(12), pp. 1538–1546. doi: 10.1038/sj.onc.1203421.
- Matangkasombut, O. *et al.* (2000) 'Bromodomain factor 1 corresponds to a missing piece of yeast TFIID', *Genes and Development*, 14(8), pp. 951–962. doi: 10.1101/gad.14.8.951.
- Matangkasombut, O. and Buratowski, S. (2003) 'Different sensitivities of bromodomain factors 1 and 2 to histone H4 acetylation', *Molecular Cell*, 11(2), pp. 353–363. doi: 10.1016/S1097-2765(03)00033-9.
- Matsumoto, E. *et al.* (2014) 'Candidemia surveillance in Iowa: Emergence of echinocandin resistance', *Diagnostic Microbiology and Infectious Disease*. Elsevier Inc., 79(2), pp. 205–208. doi: 10.1016/j.diagmicrobio.2014.02.016.
- Mencarini, J. *et al.* (2018) 'Evaluation of candidemia and antifungal consumption in a large tertiary care Italian hospital over a 12-year period', *Infection*. Springer Berlin Heidelberg, 46(4), pp. 469–476. doi: 10.1007/s15010-018-1139-z.
- Mietton, F. *et al.* (2017) 'Selective BET bromodomain inhibition as an antifungal therapeutic strategy', *Nature Communications*, 8(May). doi: 10.1038/ncomms15482.
- Miller, T. C. R. *et al.* (2016) 'A bromodomain-DNA interaction facilitates acetylation-dependent bivalent nucleosome recognition by the BET protein BRDT', *Nature Communications*, 7. doi: 10.1038/ncomms13855.
- Minematsu, A. *et al.* (2019) 'Vacuolar proton-translocating ATPase is required for antifungal resistance and virulence of *Candida glabrata*', *PLoS ONE*, 14(1), pp. 1–10. doi: 10.1371/journal.pone.0210883.
- Mitsuyama, J. *et al.* (2008) 'In vitro and in vivo antifungal activities of T-2307, a novel arylamidine', *Antimicrobial Agents and Chemotherapy*, 52(4), pp. 1318–1324. doi: 10.1128/AAC.01159-07.
- Miyazaki, M. *et al.* (2011) 'In vitro activity of E1210, a novel antifungal, against clinically important yeasts and molds', *Antimicrobial Agents and Chemotherapy*, 55(10), pp. 4652–4658. doi: 10.1128/AAC.00291-11.
- Miyazaki, T. *et al.* (2010) 'Roles of calcineurin and Crz1 in antifungal susceptibility and virulence of *Candida glabrata*', *Antimicrobial Agents and Chemotherapy*, 54(4), pp. 1639–1643. doi: 10.1128/AAC.01364-09.
- Mizuguchi, G. *et al.* (2004) 'ATP-Driven Exchange of Histone H2AZ Variant Catalyzed by SWR1 Chromatin Remodeling Complex', *Science*, 303(5656), pp. 343–348. doi: 10.1126/science.1090701.
- Molina, D. M. *et al.* (2013) 'Monitoring Drug Target Engagement in Cells and Tissues Using the Cellular Thermal Shift Assay', *Science*, 341, pp. 84–87.
- Moon, K. J. *et al.* (2005) 'The bromodomain protein Brd4 is a positive regulatory component

- of P-TEFb and stimulates RNA polymerase II-dependent transcription', *Molecular Cell*, 19(4), pp. 523–534. doi: 10.1016/j.molcel.2005.06.027.
- Morinière, J. *et al.* (2009) 'Cooperative binding of two acetylation marks on a histone tail by a single bromodomain', *Nature*, 461(7264), pp. 664–668. doi: 10.1038/nature08397.
- Moros, A. *et al.* (2014) 'Synergistic antitumor activity of lenalidomide with the BET bromodomain inhibitor CPI203 in bortezomib-resistant mantle cell lymphoma', *Leukemia*, 28(10), pp. 2049–2059. doi: 10.1038/leu.2014.106.
- Morse, M. A. *et al.* (2018) 'BET bromodomain inhibitors show anti-papillomavirus activity in vitro and block CRPV wart growth in vivo', *Antiviral Research*. Elsevier, 154(March), pp. 158–165. doi: 10.1016/j.antiviral.2018.03.012.
- Muller, H. *et al.* (2008) 'The Asexual Yeast *Candida glabrata* Maintains Distinct α and α Haploid Mating Types', *Eukaryotic Cell*, 7(5), pp. 848–858. doi: 10.1128/ec.00456-07.
- Nadeem, A. *et al.* (2018) 'Inhibition of BET bromodomains restores corticosteroid responsiveness in a mixed granulocytic mouse model of asthma', *Biochemical Pharmacology*. Elsevier, 154(March), pp. 222–233. doi: 10.1016/j.bcp.2018.05.011.
- Nakayama, H. *et al.* (1998) 'A controllable gene-expression system for the pathogenic fungus *Candida glabrata*', *Microbiology*, 144(9), pp. 2407–2415. doi: 10.1099/00221287-144-9-2407.
- Narlikar, G. J., Fan, H. and Kingston, R. E. (2002) 'Cooperation between Complexes that Regulate Chromatin Structure and Transcription Chromatin structure creates barriers for each step', *Cell*, 108, pp. 475–487.
- Nguyen, U. T. T. *et al.* (2014) 'Accelerated chromatin biochemistry using dnA-barcoded nucleosome libraries', *Nature Methods*, 11(8), pp. 834–840. doi: 10.1038/nMeth.3022.
- Nicodeme, E. *et al.* (2010) 'Suppression of inflammation by a synthetic histone mimic', *Nature*, 468(7327), pp. 1119–1123. doi: 10.1038/nature09589.
- Nicola, A. M., Casadevall, A. and Goldman, D. L. (2008) 'Fungal killing by mammalian phagocytic cells', *Current Opinion in Microbiology*, pp. 313–317. doi: 10.1016/j.mib.2008.05.011.
- Nishikawa, H. *et al.* (2016) 'T-2307, a novel arylamidine, is transported into *Candida albicans* by a high-affinity spermine and spermidine carrier regulated by Agp2', *Journal of Antimicrobial Chemotherapy*, 71(7), pp. 1845–1855. doi: 10.1093/jac/dkw095.
- Nucci, M. *et al.* (2013) 'Epidemiology of Candidemia in Latin America: A Laboratory-Based Survey', *PLoS ONE*, 8(3). doi: 10.1371/journal.pone.0059373.
- Olaechea, P. M. *et al.* (2004) 'Economic impact of *Candida* colonization and *Candida* infection in the critically ill patient', *European Journal of Clinical Microbiology and Infectious Diseases*, 23(4), pp. 323–330. doi: 10.1007/s10096-004-1104-x.
- Oliver, J. D. *et al.* (2016) 'F901318 represents a novel class of antifungal drug that inhibits dihydroorotate dehydrogenase', *Proceedings of the National Academy of Sciences of the United States of America*, 113(45), pp. 12809–12814. doi: 10.1073/pnas.1608304113.
- Ong, V. *et al.* (2016) 'Preclinical Evaluation of the Stability, Safety, and Efficacy of CD101, a Novel Echinocandin Voon', *Antimicrobial Agents and Chemotherapy*, 60(11), pp. 6872–6879.

doi: 10.1128/AAC.00701-16.Address.

Ostergaard, S., Olsson, L. and Nielsen, J. (2000) 'Artigo recombinação de leveduras', 64(1), pp. 34–50.

Ott, G. (2014) 'Impact of MYC on malignant behavior', *Hematology*, 2014(1), pp. 100–106. doi: 10.1182/asheducation-2014.1.100.

Otto, S. P. and Gerstein, A. C. (2008) 'The evolution of haploidy and diploidy', *Current Biology*, 18(24), pp. 1121–1124. doi: 10.1016/j.cub.2008.09.039.

Owen, D. J. *et al.* (2000) 'The structural basis for the recognition of acetylated histone H4 by the bromodomain of histone acetyltransferase Gcn5p', *The EMBO Journal*, 19(22), pp. 6141–6149. doi: 10.1093/emboj/19.22.6141.

Pachl, J. *et al.* (2006) 'A Randomized, Blinded, Multicenter Trial of Lipid-Associated Amphotericin B Alone versus in Combination with an Antibody-Based Inhibitor of Heat Shock Protein 90 in Patients with Invasive Candidiasis', *Clinical Infectious Diseases*, 42(10), pp. 1404–1413. doi: 10.1086/503428.

Pappas, P. G. *et al.* (2015) 'Clinical Practice Guideline for the Management of Candidiasis: 2016 Update by the Infectious Diseases Society of America', *Clinical Infectious Diseases*, 62(4), pp. e1–e50. doi: 10.1093/cid/civ933.

Pappas, P. G. *et al.* (2018) 'Invasive candidiasis', *Nature Reviews Disease Primers*. Macmillan Publishers Limited, 4(May), pp. 1–20. doi: 10.1038/nrdp.2018.26.

Pasparakis, M. (2009) 'Regulation of tissue homeostasis by NF- κ B signalling: Implications for inflammatory diseases', *Nature Reviews Immunology*. Nature Publishing Group, 9(11), pp. 778–788. doi: 10.1038/nri2655.

Pawar, A. *et al.* (2018) 'Resistance to BET Inhibitor Leads to Alternative Therapeutic Vulnerabilities in Castration-Resistant Prostate Cancer', *Cell Reports*. Elsevier Company., 22(9), pp. 2236–2245. doi: 10.1016/j.celrep.2018.02.011.

Peng, J. *et al.* (2007) 'Brd2 is a TBP-associated protein and recruits TBP into E2F-1 transcriptional complex in response to serum stimulation', *Molecular and Cellular Biochemistry*, 294(1–2), pp. 45–54. doi: 10.1007/s11010-006-9223-6.

Perfect, J. R. (2017) 'The antifungal pipeline: A reality check', *Nature Reviews Drug Discovery*. Nature Publishing Group, 16(9), pp. 603–616. doi: 10.1038/nrd.2017.46.

Petratis, V. *et al.* (2004) 'Efficacy of PLD-118, a Novel Inhibitor of', *Culture*, 48(10), pp. 3959–3967. doi: 10.1128/AAC.48.10.3959.

Pfaller, M. A. *et al.* (2009) 'Activity of MGCD290, a Hos2 histone deacetylase inhibitor, in combination with azole antifungals against opportunistic fungal pathogens', *Journal of Clinical Microbiology*, 47(12), pp. 3797–3804. doi: 10.1128/JCM.00618-09.

Pfaller, M. A. *et al.* (2015) 'In vitro activity of a Hos2 deacetylase inhibitor, MGCD290, in combination with echinocandins against echinocandin-resistant *Candida* species', *Diagnostic Microbiology and Infectious Disease*. Elsevier Inc., 81(4), pp. 259–263. doi: 10.1016/j.diagmicrobio.2014.11.008.

Pfaller, M. A., Jones, R. N. and Castanheira, M. (2014) 'Regional data analysis of *Candida* non-albicans strains collected in United States medical sites over a 6-year period, 2006-2011',

- Mycoses*, 57(10), pp. 602–611. doi: 10.1111/myc.12206.
- Philpott, M. *et al.* (2011) 'Bromodomain-peptide displacement assays for interactome mapping and inhibitor discovery', *Molecular BioSystems*, 7(10), pp. 2899–2908. doi: 10.1039/c1mb05099k.
- Picaud, S., Da Costa, D., *et al.* (2013) 'PFI-1, a highly selective protein interaction inhibitor, targeting BET bromodomains', *Cancer Research*, 73(11), pp. 3336–3346. doi: 10.1158/0008-5472.CAN-12-3292.
- Picaud, S., Wells, C., *et al.* (2013) 'RVX-208, an inhibitor of BET transcriptional regulators with selectivity for the second bromodomain', *Proceedings of the National Academy of Sciences of the United States of America*, 110(49), pp. 19754–19759. doi: 10.1073/pnas.1310658110.
- Picaud, S. *et al.* (2016) 'Promiscuous targeting of bromodomains by bromosporine identifies BET proteins as master regulators of primary transcription response in leukemia', *Science Advances*, 2(10), pp. 15–20. doi: 10.1126/sciadv.1600760.
- Pradhan, M. A. *et al.* (2016) 'Kinetically defined mechanisms and positions of action of two new modulators of glucocorticoid receptor-regulated gene induction', *Journal of Biological Chemistry*, 291(1), pp. 342–354. doi: 10.1074/jbc.M115.683722.
- Puig-Asensio, M. *et al.* (2014) 'Epidemiology and predictive factors for early and late mortality in *Candida* bloodstream infections: A population-based surveillance in Spain', *Clinical Microbiology and Infection*, 20(4), pp. 245–254. doi: 10.1111/1469-0691.12380.
- Rada-Iglesias, A. *et al.* (2011) 'A unique chromatin signature uncovers early developmental enhancers in humans', *Nature*. Nature Publishing Group, 470(7333), pp. 279–285. doi: 10.1038/nature09692.
- Rahman, S. *et al.* (2011) 'The Brd4 Extraterminal Domain Confers Transcription Activation Independent of pTEFb by Recruiting Multiple Proteins, Including NSD3', *Molecular and Cellular Biology*, 31(13), pp. 2641–2652. doi: 10.1128/mcb.01341-10.
- Rai, M. N. *et al.* (2012) 'Functional Genomic Analysis of *Candida glabrata*-Macrophage Interaction: Role of Chromatin Remodeling in Virulence', *PLoS Pathogens*, 8(8). doi: 10.1371/journal.ppat.1002863.
- Rajender, S., Avery, K. and Agarwal, A. (2011) 'Epigenetics, spermatogenesis and male infertility', *Mutation Research - Reviews in Mutation Research*. Elsevier B.V., 727(3), pp. 62–71. doi: 10.1016/j.mrrev.2011.04.002.
- Rathert, P. *et al.* (2015) 'Transcriptional plasticity promotes primary and acquired resistance to BET inhibition', *Nature*, 525(7570), pp. 543–547. doi: 10.1038/nature14898.
- Ren, C. *et al.* (2018) 'Spatially constrained tandem bromodomain inhibition bolsters sustained repression of BRD4 transcriptional activity for TNBC cell growth', *Proceedings of the National Academy of Sciences of the United States of America*, 115(31), pp. 7949–7954. doi: 10.1073/pnas.1720000115.
- Richie, D. L. *et al.* (2012) 'Nonspecific effect of mycograb on amphotericin B MIC', *Antimicrobial Agents and Chemotherapy*, 56(7), pp. 3963–3964. doi: 10.1128/AAC.00435-12.
- De Rijck, J. *et al.* (2013) 'The BET Family of Proteins Targets Moloney Murine Leukemia Virus Integration near Transcription Start Sites', *Cell Reports*. The Authors, 5(4), pp. 886–894. doi: 10.1016/j.celrep.2013.09.040.

- Robert, V. A. and Casadevall, A. (2009) 'Vertebrate Endothermy Restricts Most Fungi as Potential Pathogens', *The Journal of Infectious Diseases*, 200(10), pp. 1623–1626. doi: 10.1086/644642.
- Rodrigues, C. F. *et al.* (2017) 'Candida glabrata biofilms: How far have we come?', *Journal of Fungi*, 3(1). doi: 10.3390/jof3010011.
- Rodrigues, C. F., Silva, S. and Henriques, M. (2014) 'Candida glabrata: A review of its features and resistance', *European Journal of Clinical Microbiology and Infectious Diseases*, 33(5), pp. 673–688. doi: 10.1007/s10096-013-2009-3.
- Rogers, P. D. *et al.* (1998) 'Amphotericin B Activation of Human Genes Encoding for Cytokines', *The Journal of Infectious Diseases*, 178(6), pp. 1726–1733. doi: 10.1086/314495.
- Rossoni, R. D. *et al.* (2013) 'Correlation of phospholipase and proteinase production of Candida with in vivo pathogenicity in Galleria mellonella', *Brazilian Journal of Oral Sciences*, 12(3), pp. 199–204. doi: 10.1590/S1677-32252013000300009.
- Runcie, A. C. *et al.* (2018) 'Optimization of a "bump-and-hole" approach to allele-selective BET bromodomain inhibition', *Chemical Science*. Royal Society of Chemistry, 9(9), pp. 2452–2468. doi: 10.1039/c7sc02536j.
- Ryan, P. *et al.* (2019) 'Candidaemia in an Irish intensive care unit setting between 2004 and 2018 reflects increased incidence of Candida glabrata', *Journal of Hospital Infection*. The Healthcare Infection Society. doi: 10.1016/j.jhin.2019.01.017.
- Sakagami, T. *et al.* (2019) 'Antifungal susceptibility trend and analysis of resistance mechanism for Candida species isolated from bloodstream at a Japanese university hospital', *Journal of Infection and Chemotherapy*. Elsevier Ltd, 25(1), pp. 34–40. doi: 10.1016/j.jiac.2018.10.007.
- Sakakibara, N. *et al.* (2013) 'Brd4 Is Displaced from HPV Replication Factories as They Expand and Amplify Viral DNA', *PLoS Pathogens*, 9(11). doi: 10.1371/journal.ppat.1003777.
- Sandison, T. *et al.* (2017) 'Safety and Pharmacokinetics of CD101 IV, a Novel Echinocandin, in Healthy Adults', *Antimicrobial Agents and Chemotherapy*, 61(2), pp. 1–11.
- Sanguinetti, M., Posteraro, B. and Lass-Flörl, C. (2015) 'Antifungal drug resistance among Candida species: Mechanisms and clinical impact', *Mycoses*, 58(S2), pp. 2–13. doi: 10.1111/myc.12330.
- Sansam, C. G. *et al.* (2018) 'A mechanism for epigenetic control of DNA replication', *Genes and Development*, 32(3–4), pp. 224–229. doi: 10.1101/gad.306464.117.
- Sasani, E. *et al.* (2016) 'Pseudohyphae formation in Candida glabrata due to CO₂ exposure.', *Current medical mycology*, 2(4), pp. 49–52. doi: 10.18869/acadpub.cmm.2.4.49.
- Satoh, K. *et al.* (2009) 'Candida auris sp. nov., a novel ascomycetous yeast isolated from the external ear canal of an inpatient in a Japanese hospital', *Microbiology and Immunology*, 53(1), pp. 41–44. doi: 10.1111/j.1348-0421.2008.00083.x.
- Scapaticci, M. *et al.* (2018) 'Phenotypic typing and epidemiological survey of antifungal resistance of Candida species detected in clinical samples of Italian patients in a 17 months' period', *Germs*, 8(2), pp. 58–66. doi: 10.18683/germs.2018.1132.
- Schröder, S. *et al.* (2012) 'Two-pronged binding with bromodomain-containing protein 4

- liberates positive transcription elongation factor b from inactive ribonucleoprotein complexes', *Journal of Biological Chemistry*, 287(2), pp. 1090–1099. doi: 10.1074/jbc.M111.282855.
- Sears, D. and Schwartz, B. S. (2017) 'Candida auris: An emerging multidrug-resistant pathogen', *International Journal of Infectious Diseases*. International Society for Infectious Diseases, 63, pp. 95–98. doi: 10.1016/j.ijid.2017.08.017.
- Seider, K. *et al.* (2011) 'The Facultative Intracellular Pathogen *Candida glabrata* Subverts Macrophage Cytokine Production and Phagolysosome Maturation', *The Journal of Immunology*, 187(6), pp. 3072–3086. doi: 10.4049/jimmunol.1003730.
- Seider, K. *et al.* (2014) 'Immune Evasion, Stress Resistance, and Efficient Nutrient Acquisition Are Crucial for Intracellular Survival of *Candida glabrata* within Macrophages', *Eukaryotic Cell*, 13(1), pp. 170–183. doi: 10.1128/ec.00262-13.
- Seneviratne, C. J. *et al.* (2009) 'Architectural analysis, viability assessment and growth kinetics of *Candida albicans* and *Candida glabrata* biofilms', *Archives of Oral Biology*, 54(11), pp. 1052–1060. doi: 10.1016/j.archoralbio.2009.08.002.
- Shao, Z. *et al.* (2016) 'The acetyllysine reader BRD3R promotes human nuclear reprogramming and regulates mitosis', *Nature Communications*. Nature Publishing Group, 7, pp. 1–15. doi: 10.1038/ncomms10869.
- Shi, J. and Vakoc, C. R. (2014) 'The Mechanisms behind the Therapeutic Activity of BET Bromodomain Inhibition', *Molecular Cell*. Elsevier, 54(5), pp. 728–736. doi: 10.1016/j.molcel.2014.05.016.
- Shi, X. *et al.* (2016) 'Loss of TRIM33 causes resistance to BET bromodomain inhibitors through MYC and TGF- β -dependent mechanisms', *Proceedings of the National Academy of Sciences of the United States of America*, 113(31), pp. E4558–E4566. doi: 10.1073/pnas.1608319113.
- Shibata, T. *et al.* (2012) 'T-2307 causes collapse of mitochondrial membrane potential in yeast', *Antimicrobial Agents and Chemotherapy*, 56(11), pp. 5892–5897. doi: 10.1128/AAC.05954-11.
- Shishido, T. K. *et al.* (2015) 'Antifungal activity improved by coproduction of cyclodextrins and anabaenolysins in *Cyanobacteria*', *Proceedings of the National Academy of Sciences of the United States of America*, 112(44), pp. 13669–13674. doi: 10.1073/pnas.1510432112.
- Shu, S. *et al.* (2016) 'Response and resistance to BET bromodomain inhibitors in triple-negative breast cancer', *Nature*. Nature Publishing Group, 529(7586), pp. 413–417. doi: 10.1038/nature16508.
- Silva, S. *et al.* (2009) 'Biofilms of non-*Candida albicans* *Candida* species: Quantification, structure and matrix composition', *Medical Mycology*, 47(7), pp. 681–689. doi: 10.3109/13693780802549594.
- Silva, S. *et al.* (2010) 'In vitro biofilm activity of non-*Candida albicans* *Candida* species', *Current Microbiology*, 61(6), pp. 534–540. doi: 10.1007/s00284-010-9649-7.
- Silva, S. *et al.* (2011) '*Candida glabrata* and *Candida albicans* co-infection of an in vitro oral epithelium', *Journal of Oral Pathology and Medicine*, 40(5), pp. 421–427. doi: 10.1111/j.1600-0714.2010.00981.x.

- Sims, R. J., Belotserkovskaya, R. and Reinberg, D. (2004) 'Elongation by RNA polymerase II: The short and long of it', *Genes and Development*, 18(20), pp. 2437–2468. doi: 10.1101/gad.1235904.
- Sinha, A., Faller, D. V. and Denis, G. V. (2005) 'Bromodomain analysis of Brd2-dependent transcriptional activation of cyclin A', *Biochemical Journal*, 387(1), pp. 257–269. doi: 10.1042/BJ20041793.
- Smith, S. G. and Zhou, M. M. (2016) 'The Bromodomain: A New Target in Emerging Epigenetic Medicine', *ACS Chemical Biology*, 11(3), pp. 598–608. doi: 10.1021/acscchembio.5b00831.
- Sofjan, A. K. *et al.* (2018) 'Rezafungin (CD101), a next-generation echinocandin: A systematic literature review and assessment of possible place in therapy', *Journal of Global Antimicrobial Resistance*. Taibah University, 14(2010), pp. 58–64. doi: 10.1016/j.jgar.2018.02.013.
- Spivak, E. S. and Hanson, K. E. (2018) 'Candida auris: an Emerging Fungal Pathogen', *Journal of clinical microbiology*, 56(2), pp. 1–10. doi: 10.1128/JCM.01588-17.
- Srikantha, T., Lachke, S. A. and Soll, D. R. (2003) 'Three Mating Type-Like Loci in *Candida glabrata*', *Eukaryotic Cell*, 2(2), pp. 328–340. doi: 10.1128/ec.2.2.328-340.2003.
- Sudbery, P. E. (2011) 'Growth of *Candida albicans* hyphae', *Nature Reviews Microbiology*. Nature Publishing Group, 9(10), pp. 737–748. doi: 10.1038/nrmicro2636.
- Tamkun, J. W. *et al.* (1992) 'brahma: A regulator of *Drosophila* homeotic genes structurally related to the yeast transcriptional activator SNF2 SWI2', *Cell*, 68(3), pp. 561–572. doi: 10.1016/0092-8674(92)90191-E.
- Tan, T. Y. *et al.* (2016) 'Antifungal susceptibility of invasive *Candida* bloodstream isolates from the Asia-Pacific region', *Medical Mycology*, 54(5), pp. 471–477. doi: 10.1093/mmy/myv114.
- Tanaka, M. *et al.* (2016) 'Design and characterization of bivalent BET inhibitors', *Nature Chemical Biology*, 12(12), pp. 1089–1096. doi: 10.1038/nchembio.2209.
- Taniguchi, Y. (2016) 'The bromodomain and extra-terminal domain (BET) family: Functional anatomy of BET paralogous proteins', *International Journal of Molecular Sciences*, 17(11). doi: 10.3390/ijms17111849.
- Tati, S. *et al.* (2016) 'Candida glabrata Binding to Candida albicans Hyphae Enables Its Development in Oropharyngeal Candidiasis', *PLoS Pathogens*, 12(3), pp. 1–21. doi: 10.1371/journal.ppat.1005522.
- Thakur, J. K. *et al.* (2008) 'A nuclear receptor-like pathway regulating multidrug resistance in fungi', *Nature*, 452(7187), pp. 604–609. doi: 10.1038/nature06836.
- Tiwari, G., Tiwari, R. and Rai, A. (2010) 'Cyclodextrins in delivery systems: Applications', *Journal of Pharmacy And Bioallied Sciences*, 2(2), p. 72. doi: 10.4103/0975-7406.67003.
- Trouvé, C. *et al.* (2017) 'Epidemiology and reporting of candidaemia in Belgium: a multi-centre study', *European Journal of Clinical Microbiology and Infectious Diseases*, 36(4), pp. 649–655. doi: 10.1007/s10096-016-2841-3.
- Uno, J., Shigematsu, M. L. and Arai, T. (1982) 'Primary site of action of ketoconazole on

- Candida albicans*, *Antimicrobial Agents and Chemotherapy*, 21(6), pp. 912–918. doi: 10.1128/AAC.21.6.912.
- Uppal, S. *et al.* (2019) 'The Bromodomain Protein 4 Contributes to the Regulation of Alternative Splicing', *Cell Reports*. Elsevier Company., 29(8), pp. 2450–2460.e5. doi: 10.1016/j.celrep.2019.10.066.
- Uppuluri, P. *et al.* (2010) 'Dispersion as an important step in the *Candida albicans* biofilm developmental cycle', *PLoS Pathogens*, 6(3). doi: 10.1371/journal.ppat.1000828.
- Utle, R. T. *et al.* (1998) 'Transcriptional activators direct histone acetyltransferase complexes to nucleosomes', *Nature*, 394(July), pp. 498–502.
- Vincent, J. *et al.* (2009) 'and Outcomes of Infection in Intensive Care Units', 302(21), pp. 2323–2329.
- Vitalis, E. *et al.* (2020) 'Candida biofilm production is associated with higher mortality in patients with candidaemia', *Mycoses*, (October 2019), pp. 352–360. doi: 10.1111/myc.13049.
- Wai, D. C. C. *et al.* (2018) 'The BRD3 ET domain recognizes a short peptide motif through a mechanism that is conserved across chromatin remodelers and transcriptional regulators', *Journal of Biological Chemistry*, 293(19), pp. 7160–7175. doi: 10.1074/jbc.RA117.000678.
- Walther, A. and Wendland, J. (2003) 'An improved transformation protocol for the human fungal pathogen *Candida albicans*', *Current Genetics*, 42(6), pp. 339–343. doi: 10.1007/s00294-002-0349-0.
- Wang, C. Y. and Filippakopoulos, P. (2015) 'Beating the odds: BETs in disease', *Trends in Biochemical Sciences*. Elsevier Ltd, 40(8), pp. 468–479. doi: 10.1016/j.tibs.2015.06.002.
- Wang, P. J. and Page, D. C. (2002) 'Functional substitution for TAFII250 by a retroposed homolog that is expressed in human spermatogenesis', *Human Molecular Genetics*, 11(19), pp. 2341–2346. doi: 10.1093/hmg/11.19.2341.
- Wapinski, I. *et al.* (2007) 'Natural history and evolutionary principles of gene duplication in fungi', *Nature*, 449(7158), pp. 54–61. doi: 10.1038/nature06107.
- Warris, A. (2018) 'Candida auris, what do paediatricians need to know?', *Archives of Disease in Childhood*, 103(9), pp. 891–894. doi: 10.1136/archdischild-2017-313960.
- Wassarman, D. A. and Sauer, F. (2001) 'TAF II 250 : a transcription toolbox', *Journal of Cell Science*, 114, pp. 2895–2902.
- Wiederhold, N. P. *et al.* (2016) 'The novel arylamidine T-2307 demonstrates in vitro and in vivo activity against echinocandin-resistant *Candida glabrata*', *Journal of Antimicrobial Chemotherapy*, 71(3), pp. 692–695. doi: 10.1093/jac/dkv398.
- Wiederhold, N. P. *et al.* (2018) 'The orotomide olorofim is efficacious in an experimental model of central nervous system coccidioidomycosis', *Antimicrobial Agents and Chemotherapy*, 62(9), pp. 1–7. doi: 10.1128/AAC.00999-18.
- Wiederhold, N. P. *et al.* (2020) 'The Novel Arylamidine T-2307 Demonstrates In Vitro and In Vivo Activity against *Candida auris*', *Antimicrobial Agents and Chemotherapy*, 64(3), pp. e02198-19.
- Winter, E. (2012) 'The Sum1/Ndt80 Transcriptional Switch and Commitment to Meiosis in

- Saccharomyces cerevisiae*, *Microbiology and Molecular Biology Reviews*, 76(1), pp. 1–15. doi: 10.1128/membr.05010-11.
- Wisplinghoff, H. *et al.* (2004) 'Nosocomial Bloodstream Infections in US Hospitals : Analysis of 24 , 179 Cases from a Prospective Nationwide Surveillance Study', 0019(April 2003), pp. 309–317.
- Wisplinghoff, H. *et al.* (2014) 'Nosocomial bloodstream infections due to *Candida* spp. in the USA: Species distribution, clinical features and antifungal susceptibilities', *International Journal of Antimicrobial Agents*. Elsevier B.V., 43(1), pp. 78–81. doi: 10.1016/j.ijantimicag.2013.09.005.
- Wong, C. *et al.* (2014) 'The bromodomain and extra-terminal inhibitor CPI203 enhances the antiproliferative effects of rapamycin on human neuroendocrine tumors', *Cell Death and Disease*, 5(10), pp. 1–14. doi: 10.1038/cddis.2014.396.
- Wurtele, H. *et al.* (2010) 'Modulation of histone H3 lysine 56 acetylation as an antifungal therapeutic strategy', *Nature Medicine*. Nature Publishing Group, 16(7), pp. 774–780. doi: 10.1038/nm.2175.
- Xiao, M. *et al.* (2018) 'Five-Year National Surveillance of Invasive Candidiasis: Species Distribution and Azole Susceptibility from the China Hospital Invasive Fungal Surveillance Net (CHIF-NET) Study', *Journal of Clinical Microbiology*, 56(7). doi: 10.1128/jcm.00577-18.
- Xie, Z. *et al.* (2012) 'Candida albicans biofilms do not trigger reactive oxygen species and evade neutrophil killing', *Journal of Infectious Diseases*, 206(12), pp. 1936–1945. doi: 10.1093/infdis/jis607.
- Yadav, T., Quivy, J. P. and Almouzni, G. (2018) 'Chromatin plasticity: A versatile landscape that underlies cell fate and identity', *Science*, 361(6409), pp. 1332–1336. doi: 10.1126/science.aat8950.
- Yamashita, K. *et al.* (2019) 'The novel arylamidine T-2307 selectively disrupts yeast mitochondrial function by inhibiting respiratory chain complexes', *Antimicrobial Agents and Chemotherapy*, 63(8), pp. 1–10. doi: 10.1128/AAC.00374-19.
- Yang, Z. *et al.* (2005) 'Recruitment of P-TEFb for stimulation of transcriptional elongation by the bromodomain protein Brd4', *Molecular Cell*, 19(4), pp. 535–545. doi: 10.1016/j.molcel.2005.06.029.
- Zaware, N. and Zhou, M. M. (2019) 'Bromodomain biology and drug discovery', *Nature Structural and Molecular Biology*. Springer US, 26(10), pp. 870–879. doi: 10.1038/s41594-019-0309-8.
- Zeng, L. *et al.* (2005) 'Selective small molecules blocking HIV-1 tat and coactivator PCAF association', *Journal of the American Chemical Society*, 127(8), pp. 2376–2377. doi: 10.1021/ja044885g.
- Zengerle, M., Chan, K. H. and Ciulli, A. (2015) 'Selective Small Molecule Induced Degradation of the BET Bromodomain Protein BRD4', *ACS Chemical Biology*, 10(8), pp. 1770–1777. doi: 10.1021/acscchembio.5b00216.
- Zentner, G. E. and Henikoff, S. (2013) 'Regulation of nucleosome dynamics by histone modifications', *Nature Structural and Molecular Biology*. Nature Publishing Group, 20(3), pp. 259–266. doi: 10.1038/nsmb.2470.

- Zhang, G. *et al.* (2013) 'Structure-guided design of potent diazobenzene inhibitors for the BET bromodomains', *Journal of Medicinal Chemistry*, 56(22), pp. 9251–9264. doi: 10.1021/jm401334s.
- Zhang, J.-H., Chung, T. D. Y. and Oldenburg, K. R. (1999) 'A Simple Statistical Parameter for Use in Evaluation and Validation of High Throughput Screening Assays', *Journal of biomolecular screening*, 4(2), pp. 67–73.
- Zhao, Y. *et al.* (2018) 'Significantly improved pharmacokinetics enhances in vivo efficacy of APX001 against echinocandin-and multidrug-resistant *Candida* isolates in a mouse model of invasive candidiasis', *Antimicrobial Agents and Chemotherapy*, 62(10). doi: 10.1128/AAC.00425-18.
- Zhou, Q., Li, T. and Price, D. H. (2012) 'RNA Polymerase II Elongation Control', *Annu Rev Biochem*, 81, pp. 119–143. doi: 10.1161/CIRCULATIONAHA.110.956839.
- Zhou, Y. *et al.* (2009) 'Reversible acetylation of the chromatin remodelling complex NoRC is required for non-coding RNA-dependent silencing', *Nature Cell Biology*. Nature Publishing Group, 11(8), pp. 1010–1016. doi: 10.1038/ncb1914.
- Zhu, B. *et al.* (2005) 'Monoubiquitination of human histone H2B: The factors involved and their roles in HOX gene regulation', *Molecular Cell*, 20(4), pp. 601–611. doi: 10.1016/j.molcel.2005.09.025.
- Zhu, J. *et al.* (2012) 'Reactivation of Latent HIV-1 by Inhibition of BRD4', *Cell Reports*. The Authors, 2(4), pp. 807–816. doi: 10.1016/j.celrep.2012.09.008.
- Ziegelbauer, K., Babczinski, P. and Schönfeld, W. (1998) 'Molecular mode of action of the antifungal β -amino acid BAY 10-8888', *Antimicrobial Agents and Chemotherapy*, 42(9), pp. 2197–2205. doi: 10.1128/aac.42.9.2197.

Appendices

Appendix I. Crystallization conditions at the EMBL HTX facility

Wizard_I+II_rigaku			
Position	Precipitant	Buffer (all at 0.1M)	pH
A1	20 %(w/v) PEG-8000	CHES	9.5
A2	10%(v/v) 2-propanol 0.2M sodium chloride	HEPES	7.5
A3	15%(v/v) Reagent alcohol	CHES	9.5
A4	35% (v/v) 2-methyl-2,4-pentanediol 0.2M magnesium chloride	Imidazole	8
A5	30% (v/v) PEG-400	CAPS	10.5
A6	20%(w/v) PEG-3000	Sodium citrate	5.5
A7	10%(w/v) PEG-8000 0.2M zinc acetate	MES	6
A8	2M ammonium sulfate	Sodium citrate	5.5
A9	1M ammonium phosphate dibasic	Sodium acetate	4.5
A10	20%(w/v) PEG-2000 MME	Tris base	7
A11	20%(v/v) 1,4-butanediol 0.2M lithium sulfate	MES	6
A12	20%(w/v) PEG-1000 0.2M calcium acetate	imidazole	8
B1	1.26M ammonium sulfate	Sodium cacodylate	6.5
B2	1M sodium citrate tribasic	Sodium cacodylate	6.5
B3	10%(w/v) PEG-3000 0.2M lithium sulfate	Imidazole	8
B4	2.5M sodium chloride	Potassium phosphate monobasic	6.2
B5	30%(w/v) PEG-8000 0.2M lithium sulfate	Sodium acetate	4.5
B6	1M potassium/sodium tartrate 0.2M sodium chloride	Imidazole	8
B7	20%(w/v) PEG-1000	Tris base	7
B8	1.6M potassium phosphate dibasic 0.4M sodium phosphate monobasic 0.2M sodium chloride	Imidazole	8
B9	20%(w/v) PEG-8000	HEPES	7.5
B10	10%(v/v) 2-propanol	Tris base	8.5
B11	15%(v/v) reagent alcohol 0.2M magnesium chloride	Imidazole	8
B12	35%(v/v) 2-methyl-2,4-pentanediol 0.2M sodium chloride	Tris base	7
C1	30%(v/v) PEG-400 0.2M magnesium chloride	Tris base	8.5
C2	10%(w/v) PEG-3000	CHES	9.5
C3	1.2M sodium phosphate monobasic 0.8M potassium phosphate dibasic	CAPS	10.5

Appendix

	0.2M lithium sulfate		
C4	20%(w/v) PEG-3000 0.2M sodium chloride	HEPES	7.5
C5	10%(w/v) PEG-8000 0.2M sodium chloride	CHES	9.5
C6	1.26M ammonium sulfate 0.2M sodium chloride	Sodium acetate	4.5
C7	20%(w/v) PEG-8000 0.2M sodium chloride	Sodium phosphate dibasic	4.2
C8	10%(w/v) PEG-3000	Potassium phosphate monobasic/sodium phosphate dibasic	6.2
C9	2M ammonium sulfate 0.2M lithium sulfate	CAPS	10.5
C10	1M ammonium phosphate dibasic	Imidazole	8
C11	20%(v/v) 1,4-butanediol	Sodium acetate	4.5
C12	1M sodium citrate tribasic	Imidazole	8
D1	2.5M sodium chloride	Imidazole	8
D2	1M potassium/sodium tartrate 0.2M lithium sulfate	CHES	9.5
D3	20%(w/v) PEG-1000 0.2M lithium sulfate	Sodium phosphate dibasic	4.2
D4	10%(v/v) 2-propanol 0.2M calcium acetate	MES	6
D5	30%(w/v) PEG-3000	CHES	9.5
D6	15%(v/v) reagent alcohol	Tris base	7
D7	35%(v/v) 2-methyl-2,4-pentaediol	Potassium phosphate monobasic/sodium phosphate dibasic	6.2
D8	30%(v/v) PEG-400 0.2M calcium acetate	Sodium acetate	4.5
D9	20%(w/v) PEG-3000	Sodium acetate	4.5
D10	10%(w/v) PEG-8000 0.2M calcium acetate	Imidazole	8
D11	1.26M ammonium sulfate 0.2M lithium sulfate	Tris base	8.5
D12	20%(w/v) PEG-1000 0.2M zinc acetate	Sodium acetate	4.5
E1	10%(w/v) PEG-3000 0.2M zinc acetate	Sodium acetate	4.5
E2	35%(v/v) 2-methyl-2,4-pentenediol 0.2M lithium sulfate	MES	6
E3	20%(w/v) PEG-8000 0.2M magnesium chloride	Tris base	8.5
E4	2M ammonium sulfate 0.2M sodium chloride	Sodium cacodylate	6.5
E5	20%(v/v) ammonium sulfate 0.2M sodium chloride	HEPES	7.5
E6	10%(v/v) 2-propanol 0.2M lithium sulfate	Sodium phosphate dibasic	4.2
E7	30%(w/v) PEG-3000 0.2M sodium chloride	Tris base	7
E8	10%(w/v) PEG-8000 0.2M sodium chloride	Potassium phosphate monobasic/sodium phosphate dibasic	6.2
E9	2M ammonium sulfate	Sodium phosphate	4.2
E10	2M ammonium phosphate dibasic	Tris base	8.5
E11	10%(v/v) 2-propanol 0.2M zinc acetate	Sodium cacodylate	6.5
E12	30%(v/v) PEG-400	Sodium cacodylate	6.5

Appendix

	0.2M lithium sulfate		
F1	15%(v/v) reagent alcohol 0.2M lithium sulfate	Sodium citrate	5.5
F2	20%(w/v) PEG-1000 0.2M Sodium chloride	Potassium phosphate monobasic/sodium phosphate dibasic	6.2
F3	1.26M ammonium sulfate	HEPES	7.5
F4	1M sodium citrate tribasic	CHES	9.5
F5	2.5M sodium chloride 0.2M magnesium chloride	Tris base	7
F6	20%(w/v) PEG-3000 0.2M calcium acetate	Tris base	7
F7	1.6M sodium phosphate monobasic 0.4M potassium phosphate dibasic	Sodium phosphate dibasic	4.2
F8	15%(v/v) reagent alcohol 0.2M zinc acetate	MES	6
F9	35%(v/v) 2-methyl-2,4-pentanediol	Sodium acetate	4.5
F10	10%(v/v) 2-propanol	Imidazole	8
F11	15%(v/v) reagent alcohol 0.2M magnesium chloride	HEPES	7.5
F12	30%(w/v) PEG-8000 0.2M sodium chloride	Imidazole	8
G1	35%(v/v) 2-methyl-2,4-pentanediol 0.2M sodium chloride	HEPES	7.5
G2	30%(v/v) PEG-400	CHES	9.5
G3	10%(w/v) PEG-3000 0.2M magnesium chloride	Sodium cacodylate	6.5
G4	20%(w/v) PEG-8000 0.2M calcium acetate	MES	6
G5	1.26M ammonium sulfate 0.2M sodium chloride	CHES	9.5
G6	20%(v/v) 1,4-butanediol 0.2M zinc acetate	Imidazole	8
G7	1M sodium citrate tribasic 0.2M sodium chloride	Tris base	7
G8	20%(w/v) PEG-1000	Tris base	8.5
G9	1M ammonium phosphate dibasic 0.2M sodium chloride	Sodium citrate	5.5
G10	10%(w/v) PEG-8000	Imidazole	8
G11	0.8M sodium phosphate monobasic	Sodium acetate	4.5
G12	10%(w/v) PEG-3000 0.2M sodium chloride	Sodium phosphate dibasic	4.2
H1	1M potassium/sodium tartrate 0.2M lithium sulfate	Tris base	7
H2	2.5M sodium chloride 0.2M lithium sulfate	Sodium acetate	4.5
H3	20%(w/v) PEG-8000 0.2M sodium chloride	CAPS	10.5
H4	20%(w/v) PEG-3000 0.2M zinc acetate	Imidazole	8
H5	2M ammonium sulfate 0.2M lithium sulfate	Tris base	7
H6	30%(v/v) PEG-400 0.2M sodium chloride	HEPES	7.5
H7	10%(w/v) PEG-8000 0.2M magnesium chloride	Tris base	7
H8	20%(w/v) PEG-1000 0.2M magnesium chloride	Sodium cacodylate	6.5
H9	1.26M ammonium sulfate	MES	6
H10	1M ammonium phosphate dibasic	Imidazole	8

Appendix

	0.2M sodium chloride		
H11	2.5M sodium chloride 0.2M zinc acetate	Imidazole	8
H12	1M potassium/sodium tartrate	MES	6

PEGS-I_qiagen			
Position	Precipitant	Buffer (all at 0.1M)	pH
A1	40%(v/v) PEG-200	Sodium acetate	4.6
A2	30%(v/v) PEG-300	Sodium acetate	4.6
A3	30%(v/v) PEG-400	Sodium acetate	4.6
A4	25%(v/v) PEG-500 MME	Sodium acetate	4.6
A5	25%(w/v) PEG-1000	Sodium acetate	4.6
A6	25%(w/v) PEG-2000 MME	Sodium acetate	4.6
A7	40%(v/v) PEG-200	MES	6.5
A8	30%(v/v) PEG-300	MES	6.5
A9	30%(v/v) PEG-400	MES	6.5
A10	25%(v/v) PEG-500 MME	MES	6.5
A11	25%(w/v) PEG-1000	MES	6.5
A12	25%(w/v) PEG-2000 MME	MES	6.5
B1	40%(v/v) PEG-200	HEPES	7.5
B2	30%(v/v) PEG-300	HEPES	7.5
B3	30%(v/v) PEG-400	HEPES	7.5
B4	25%(v/v) PEG-500 MME	HEPES	7.5
B5	25%(w/v) PEG-1000	HEPES	7.5
B6	25%(w/v) PEG-2000 MME	HEPES	7.5
B7	40%(v/v) PEG-200	Tris	8.5
B8	30%(v/v) PEG-300	Tris	8.5
B9	30%(v/v) PEG-400	Tris	8.5
B10	25%(v/v) PEG-500 MME	Tris	8.5
B11	25%(w/v) PEG-1000	Tris	8.5
B12	25%(w/v) PEG-2000 MME	Tris	8.5
C1	25%(w/v) PEG-3000	Sodium acetate	4.6
C2	25%(w/v) PEG-4000	Sodium acetate	4.6
C3	25%(w/v) PEG-6000	Sodium acetate	4.6
C4	25%(w/v) PEG-8000	Sodium acetate	4.6
C5	20%(w/v) PEG-10000	Sodium acetate	4.6
C6	15%(w/v) PEG-20000	Sodium acetate	4.6
C7	25%(w/v) PEG-3000	MES	6.5
C8	25%(w/v) PEG-4000	MES	6.5
C9	25%(w/v) PEG-6000	MES	6.5
C10	25%(w/v) PEG-8000	MES	6.5
C11	20%(w/v) PEG-10000	MES	6.5
C12	15%(w/v) PEG-20000	MES	6.5
D1	25%(w/v) PEG-3000	HEPES	7.5
D2	25%(w/v) PEG-4000	HEPES	7.5
D3	25%(w/v) PEG-6000	HEPES	7.5
D4	25%(w/v) PEG-8000	HEPES	7.5
D5	20%(w/v) PEG-10000	HEPES	7.5
D6	15%(w/v) PEG-20000	HEPES	7.5
D7	25%(w/v) PEG-3000	Tris	8.5
D8	25%(w/v) PEG-4000	Tris	8.5
D9	25%(w/v) PEG-6000	Tris	8.5
D10	25%(w/v) PEG-8000	Tris	8.5
D11	20%(w/v) PEG-10000	Tris	8.5
D12	15%(w/v) PEG-20000	Tris	8.5
E1	20%(w/v) PEG-3350	-	-

Appendix

	0.2M sodium fluoride		
E2	20%(w/v) PEG-3350 0.2M potassium fluoride	-	-
E3	20%(w/v) PEG-3350 0.2M ammonium fluoride	-	-
E4	20%(w/v) PEG-3350 0.2M lithium chloride	-	-
E5	20%(w/v) PEG-3350 0.2M magnesium chloride	-	-
E6	20%(w/v) PEG-3350 0.2M sodium chloride	-	-
E7	20%(w/v) PEG-3350 0.2M calcium chloride	-	-
E8	20%(w/v) PEG-3350 0.2M potassium chloride	-	-
E9	20%(w/v) PEG-3350 0.2M ammonium chloride	-	-
E10	20%(w/v) PEG-3350 0.2M sodium iodide	-	-
E11	20%(w/v) PEG-3350 0.2M potassium iodide	-	-
E12	20%(w/v) PEG-3350 0.2M ammonium iodide	-	-
F1	20%(w/v) PEG-3350 0.2M sodium thiocyanate	-	-
F2	20%(w/v) PEG-3350 0.2M potassium thiocyanate	-	-
F3	20%(w/v) PEG-3350 0.2M lithium nitrate	-	-
F4	20%(w/v) PEG-3350 0.2M magnesium nitrate	-	-
F5	20%(w/v) PEG-3350 0.2M sodium nitrate	-	-
F6	20%(w/v) PEG-3350 0.2M potassium nitrate	-	-
F7	20%(w/v) PEG-3350 0.2M ammonium nitrate	-	-
F8	20%(w/v) PEG-3350 0.2M magnesium formate	-	-
F9	20%(w/v) PEG-3350 0.2M sodium formate	-	-
F10	20%(w/v) PEG-3350 0.2M potassium formate	-	-
F11	20%(w/v) PEG-3350 0.2M ammonium formate	-	-
F12	20%(w/v) PEG-3350 0.2M lithium acetate	-	-
G1	20%(w/v) PEG-3350 0.2M magnesium acetate	-	-
G2	20%(w/v) PEG-3350 0.2M zinc acetate	-	-
G3	20%(w/v) PEG-3350 0.2M sodium acetate	-	-
G4	20%(w/v) PEG-3350 0.2M calcium acetate	-	-
G5	20%(w/v) PEG-3350 0.2M potassium acetate	-	-
G6	20%(w/v) PEG-3350 0.2M ammonium acetate	-	-
G7	20%(w/v) PEG-3350	-	-

Appendix

	0.2M lithium sulfate		
G8	20%(w/v) PEG-3350 0.2M magnesium sulfate	-	-
G9	20%(w/v) PEG-3350 0.2M sodium sulfate	-	-
G10	20%(w/v) PEG-3350 0.2M potassium sulfate	-	-
G11	20%(w/v) PEG-3350 0.2M ammonium sulfate	-	-
G12	20%(w/v) PEG-3350 0.2M di-sodium tartrate	-	-
H1	20%(w/v) PEG-3350 0.2M potassium/sodium tartrate	-	-
H2	20%(w/v) PEG-3350 0.2M di-ammonium tartrate	-	-
H3	20%(w/v) PEG-3350 0.2M sodium phosphate	-	-
H4	20%(w/v) PEG-3350 0.2M di-sodium phosphate	-	-
H5	20%(w/v) PEG-3350 0.2M potassium phosphate	-	-
H6	20%(w/v) PEG-3350 0.2M di-potassium phosphate	-	-
H7	20%(w/v) PEG-3350 0.2M ammonium phosphate	-	-
H8	20%(w/v) PEG-3350 0.2M di-ammonium phosphate	-	-
H9	20%(w/v) PEG-3350 0.2M tri-lithium citrate	-	-
H10	20%(w/v) PEG-3350 0.2M tri-sodium citrate	-	-
H11	20%(w/v) PEG-3350 0.2M tri-potassium citrate	-	-
H12	20%(w/v) PEG-3350 0.18M tri-ammonium citrate	-	-

Salt-Grid_hampton			
Position	Precipitant	Buffer (all at 0.1M)	pH
A1	0.8M ammonium sulfate	Citric acid	4
A2	0.8M ammonium sulfate	Citric acid	5
A3	0.8M ammonium sulfate	MES	6
A4	0.8M ammonium sulfate	HEPES	7
A5	0.8M ammonium sulfate	Tris	8
A6	0.8M ammonium sulfate	Bicine	9
A7	0.016M di-potassium hydrogen phosphate 0.784M sodium dihydrogen phosphate monohydrate	-	-
A8	0.08M di-potassium hydrogen phosphate 0.72M sodium dihydrogen phosphate monohydrate	-	-
A9	0.28M di-potassium hydrogen phosphate 0.52M sodium dihydrogen phosphate monohydrate	-	-
A10	0.52M di-potassium hydrogen phosphate 0.28M sodium dihydrogen phosphate monohydrate	-	-
A11	0.68M di-potassium hydrogen phosphate 0.12M sodium dihydrogen phosphate monohydrate	-	-
A12	0.768M di-potassium hydrogen phosphate 0.032M sodium dihydrogen phosphate monohydrate	-	-
B1	1.6M ammonium sulfate	Citric acid	4

Appendix

B2	1.6M ammonium sulfate	Citric acid	5
B3	1.6M ammonium sulfate	MES	6
B4	1.6M ammonium sulfate	HEPES	7
B5	1.6M ammonium sulfate	Tris	8
B6	1.6M ammonium sulfate	Bicine	9
B7	0.02M di-potassium hydrogen phosphate 0.98M sodium dihydrogen phosphate monohydrate	-	-
B8	0.1M di-potassium hydrogen phosphate 0.9M sodium dihydrogen phosphate monohydrate	-	-
B9	0.35M di-potassium hydrogen phosphate 0.65M sodium dihydrogen phosphate monohydrate	-	-
B10	0.65M di-potassium hydrogen phosphate 0.35M sodium dihydrogen phosphate monohydrate	-	-
B11	0.85M di-potassium hydrogen phosphate 0.15M sodium dihydrogen phosphate monohydrate	-	-
B12	0.96M di-potassium hydrogen phosphate 0.04M sodium dihydrogen phosphate monohydrate	-	-
C1	2.4M ammonium sulfate	Citric acid	4
C2	2.4M ammonium sulfate	Citric acid	5
C3	2.4M ammonium sulfate	MES	6
C4	2.4M ammonium sulfate	HEPES	7
C5	2.4M ammonium sulfate	Tris	8
C6	2.4M ammonium sulfate	Bicine	9
C7	0.028M di-potassium hydrogen phosphate 1.372M sodium dihydrogen phosphate monohydrate	-	-
C8	0.14M di-potassium hydrogen phosphate 1.26M sodium dihydrogen phosphate monohydrate	-	-
C9	0.49M di-potassium hydrogen phosphate 0.91M sodium dihydrogen phosphate monohydrate	-	-
C10	0.91M di-potassium hydrogen phosphate 0.49M sodium dihydrogen phosphate monohydrate	-	-
C11	1.19M di-potassium hydrogen phosphate 0.21M sodium dihydrogen phosphate monohydrate	-	-
C12	1.344M di-potassium hydrogen phosphate 0.056M sodium dihydrogen phosphate monohydrate	-	-
D1	3M ammonium sulfate	Citric acid	4
D2	3M ammonium sulfate	Citric acid	5
D3	3M ammonium sulfate	MES	6
D4	3M ammonium sulfate	HEPES	7
D5	3M ammonium sulfate	Tris	8
D6	3M ammonium sulfate	Bicine	9
D7	0.036M di-potassium hydrogen phosphate 1.764M sodium dihydrogen phosphate monohydrate	-	-
D8	0.18M di-potassium hydrogen phosphate 1.62M sodium dihydrogen phosphate monohydrate	-	-
D9	0.63M di-potassium hydrogen phosphate 1.17M sodium dihydrogen phosphate monohydrate	-	-
D10	1.17M di-potassium hydrogen phosphate 0.63M sodium dihydrogen phosphate monohydrate	-	-
D11	1.53M di-potassium hydrogen phosphate 0.27M sodium dihydrogen phosphate monohydrate	-	-
D12	1.728M di-potassium hydrogen phosphate 0.072M sodium dihydrogen phosphate monohydrate	-	-
E1	1M malonate	-	-
E2	1.5M malonate	-	-
E3	1.9M malonate	-	-
E4	2.4M malonate	-	-
E5	2.9M malonate	-	-
E6	3.4M malonate	-	-
E7	0.8M sodium formate pH4	Citric acid	4

Appendix

E8	0.8M sodium formate pH5	Citric acid	5
E9	0.8M sodium formate pH6	MES	6
E10	0.8M sodium formate pH7	HEPES	7
E11	0.8M sodium formate pH8	Tris	8
E12	0.8M sodium formate pH9	Bicine	9
F1	1M malonate	-	-
F2	1.5M malonate	-	-
F3	1.9M malonate	-	-
F4	2.4M malonate	-	-
F5	2.9M malonate	-	-
F6	3.4M malonate	-	-
F7	1.6M sodium formate pH4	Citric acid	4
F8	1.6M sodium formate pH5	Citric acid	5
F9	1.6M sodium formate pH6	MES	6
F10	1.6M sodium formate pH7	HEPES	7
F11	1.6M sodium formate pH8	Tris	8
F12	1.6M sodium formate pH9	Bicine	9
G1	1M malonate	-	-
G2	1.5M malonate	-	-
G3	1.9M malonate	-	-
G4	2.4M malonate	-	-
G5	2.9M malonate	-	-
G6	3.4M malonate	-	-
G7	2.4M sodium formate pH4	Citric acid	4
G8	2.4M sodium formate pH5	Citric acid	5
G9	2.4M sodium formate pH6	MES	6
G10	2.4M sodium formate pH7	HEPES	7
G11	2.4M sodium formate pH8	Tris	8
G12	2.4M sodium formate pH9	Bicine	9
H1	1M malonate	-	-
H2	1.5M malonate	-	-
H3	1.9M malonate	-	-
H4	2.4M malonate	-	-
H5	2.9M malonate	-	-
H6	3.4M malonate	-	-
H7	3.2M sodium formate pH4	Citric acid	4
H8	3.2M sodium formate pH5	Citric acid	5
H9	3.2M sodium formate pH6	MES	6
H10	3.2M sodium formate pH7	HEPES	7
H11	3.2M sodium formate pH8	Tris	8
H12	3.2M sodium formate pH9	Bicine	9

PACT_MD			
Position	Precipitant	Buffer (all at 0.1M)	pH
A1	25%(w/v) PEG-1500	SPG buffer	4
A2	25%(w/v) PEG-1500	SPG buffer	5
A3	25%(w/v) PEG-1500	SPG buffer	6
A4	25%(w/v) PEG-1500	SPG buffer	7
A5	25%(w/v) PEG-1500	SPG buffer	8
A6	25%(w/v) PEG-1500	SPG buffer	9
A7	20%(w/v) PEG-6000 0.2M sodium chloride	Sodium acetate trihydrate	5
A8	20%(w/v) PEG-6000 0.2M ammonium chloride	Sodium acetate trihydrate	5
A9	20%(w/v) PEG-6000 0.2M lithium chloride	Sodium acetate trihydrate	5

Appendix

A10	20%(w/v) PEG-6000 0.2M magnesium chloride hexahydrate	Sodium acetate trihydrate	5
A11	20%(w/v) PEG-6000 0.2M calcium chloride dihydrate	Sodium acetate trihydrate	5
A12	20%(w/v) PEG-6000 0.2M zinc chloride	Sodium acetate trihydrate	5
B1	25%(w/v) PEG-1500	MIB buffer	4
B2	25%(w/v) PEG-1500	MIB buffer	5
B3	25%(w/v) PEG-1500	MIB buffer	6
B4	25%(w/v) PEG-1500	MIB buffer	7
B5	25%(w/v) PEG-1500	MIB buffer	8
B6	25%(w/v) PEG-1500	MIB buffer	9
B7	20%(w/v) PEG-6000 0.2M sodium chloride	MES	6
B8	20%(w/v) PEG-6000 0.2M ammonium chloride	MES	6
B9	20%(w/v) PEG-6000 0.2M lithium chloride	MES	6
B10	20%(w/v) PEG-6000 0.2M magnesium chloride hexahydrate	MES	6
B11	20%(w/v) PEG-6000 0.2M calcium chloride dihydrate	MES	6
B12	20%(w/v) PEG-6000 0.2M zinc chloride	MES	6
C1	25%(w/v) PEG-1500	PCTP buffer	4
C2	25%(w/v) PEG-1500	PCTP buffer	5
C3	25%(w/v) PEG-1500	PCTP buffer	6
C4	25%(w/v) PEG-1500	PCTP buffer	7
C5	25%(w/v) PEG-1500	PCTP buffer	8
C6	25%(w/v) PEG-1500	PCTP buffer	9
C7	20%(w/v) PEG-6000 0.2M sodium chloride	HEPES	7
C8	20%(w/v) PEG-6000 0.2M ammonium chloride	HEPES	7
C9	20%(w/v) PEG-6000 0.2M lithium chloride	HEPES	7
C10	20%(w/v) PEG-6000 0.2M magnesium chloride hexahydrate	HEPES	7
C11	20%(w/v) PEG-6000 0.2M calcium chloride dihydrate	HEPES	7
C12	20%(w/v) PEG-6000 0.2M zinc chloride	HEPES	7
D1	25%(w/v) PEG-1500	MMT buffer	4
D2	25%(w/v) PEG-1500	MMT buffer	5
D3	25%(w/v) PEG-1500	MMT buffer	6
D4	25%(w/v) PEG-1500	MMT buffer	7
D5	25%(w/v) PEG-1500	MMT buffer	8
D6	25%(w/v) PEG-1500	MMT buffer	9
D7	20%(w/v) PEG-6000 0.2M sodium chloride	Tris	8
D8	20%(w/v) PEG-6000 0.2M ammonium chloride	Tris	8
D9	20%(w/v) PEG-6000 0.2M lithium chloride	Tris	8
D10	20%(w/v) PEG-6000 0.2M magnesium chloride hexahydrate	Tris	8
D11	20%(w/v) PEG-6000 0.2M calcium chloride dihydrate	Tris	8
D12	20%(w/v) PEG-6000 0.2M zinc chloride	Tris	8

Appendix

E1	20%(w/v) PEG-3350 0.2M sodium fluoride	-	-
E2	20%(w/v) PEG-3350 0.2M sodium bromide	-	-
E3	20%(w/v) PEG-3350 0.2M sodium iodide	-	-
E4	20%(w/v) PEG-3350 0.2M potassium thiocyanate	-	-
E5	20%(w/v) PEG-3350 0.2M sodium nitrate	-	-
E6	20%(w/v) PEG-3350 0.2M sodium formate	-	-
E7	20%(w/v) PEG-3350 0.2M sodium acetate trihydrate	-	-
E8	20%(w/v) PEG-3350 0.2M sodium sulfate	-	-
E9	20%(w/v) PEG-3350 0.2M potassium sodium tartrate tetrahydrate	-	-
E10	20%(w/v) PEG-3350 0.2M sodium/potassium phosphate	-	-
E11	20%(w/v) PEG-3350 0.2M sodium citrate tribasic dihydrate	-	-
E12	20%(w/v) PEG-3350 0.2M sodium malonate dibasic monohydrate	-	-
F1	20%(w/v) PEG-3350 0.2M sodium acetate	Bis Tris propane	6.5
F2	20%(w/v) PEG-3350 0.2M sodium bromide	Bis Tris propane	6.5
F3	20%(w/v) PEG-3350 0.2M sodium iodide	Bis Tris propane	6.5
F4	20%(w/v) PEG-3350 0.2M potassium thiocyanate	Bis Tris propane	6.5
F5	20%(w/v) PEG-3350 0.2M sodium nitrate	Bis Tris propane	6.5
F6	20%(w/v) PEG-3350 0.2M sodium formate	Bis Tris propane	6.5
F7	20%(w/v) PEG-3350 0.2M sodium acetate trihydrate	Bis Tris propane	6.5
F8	20%(w/v) PEG-3350 0.2M sodium sulfate	Bis Tris propane	6.5
F9	20%(w/v) PEG-3350 0.2M potassium sodium tartrate tetrahydrate	Bis Tris propane	6.5
F10	20%(w/v) PEG-3350 0.2M sodium/potassium phosphate	Bis Tris propane	6.5
F11	20%(w/v) PEG-3350 0.2M sodium citrate tribasic dihydrate	Bis Tris propane	6.5
F12	20%(w/v) PEG-3350 0.2M sodium malonate dibasic monohydrate	Bis Tris propane	6.5
G1	20%(w/v) PEG-3350 0.2M sodium fluoride	Bis Tris propane	7.5
G2	20%(w/v) PEG-3350 0.2M sodium bromide	Bis Tris propane	7.5
G3	20%(w/v) PEG-3350 0.2M sodium iodide	Bis Tris propane	7.5
G4	20%(w/v) PEG-3350 0.2M potassium thiocyanate	Bis Tris propane	7.5
G5	20%(w/v) PEG-3350 0.2M sodium nitrate	Bis Tris propane	7.5
G6	20%(w/v) PEG-3350 0.2M sodium formate	Bis Tris propane	7.5

Appendix

G7	20%(w/v) PEG-3350 0.2M sodium acetate trihydrate	Bis Tris propane	7.5
G8	20%(w/v) PEG-3350 0.2M sodium sulfate	Bis Tris propane	7.5
G9	20%(w/v) PEG-3350 0.2M potassium sodium tartrate tetrahydrate	Bis Tris propane	7.5
G10	20%(w/v) PEG-3350 0.2M sodium/potassium phosphate	Bis Tris propane	7.5
G11	20%(w/v) PEG-3350 0.2M sodium citrate tribasic dihydrate	Bis Tris propane	7.5
G12	20%(w/v) PEG-3350 0.2M sodium malonate dibasic monohydrate	Bis Tris propane	7.5
H1	20%(w/v) PEG-3350 0.2M sodium fluoride	Bis Tris propane	8.5
H2	20%(w/v) PEG-3350 0.2M sodium bromide	Bis Tris propane	8.5
H3	20%(w/v) PEG-3350 0.2M sodium iodide	Bis Tris propane	8.5
H4	20%(w/v) PEG-3350 0.2M potassium thiocyanate	Bis Tris propane	8.5
H5	20%(w/v) PEG-3350 0.2M sodium nitrate	Bis Tris propane	8.5
H6	20%(w/v) PEG-3350 0.2M sodium formate	Bis Tris propane	8.5
H7	20%(w/v) PEG-3350 0.2M sodium acetate trihydrate	Bis Tris propane	8.5
H8	20%(w/v) PEG-3350 0.2M sodium sulfate	Bis Tris propane	8.5
H9	20%(w/v) PEG-3350 0.2M potassium sodium tartrate tetrahydrate	Bis Tris propane	8.5
H10	20%(w/v) PEG-3350 0.2M sodium/potassium phosphate	Bis Tris propane	8.5
H11	20%(w/v) PEG-3350 0.2M sodium citrate tribasic dihydrate	Bis Tris propane	8.5
H12	20%(w/v) PEG-3350 0.2M sodium malonate dibasic monohydrate	Bis Tris propane	8.5

JCSG_MD			
Position	Precipitant	Buffer (all at 0.1M)	pH
A1	50%(v/v) PEG-400 0.2M lithium sulfate	Sodium acetate	4.5
A2	20%(w/v) PEG-3000	Sodium citrate	5.5
A3	20%(w/v) PEG-3350 0.2M Ammonium citrate dibasic	-	-
A4	30%(v/v) MPD 0.02M calcium chloride dihydrate	Sodium acetate	4.6
A5	29%(w/v) PEG-3350 0.2M magnesium formate dihydrate	-	-
A6	20%(w/v) PEG-1000 0.2M lithium sulfate	Phosphate/citrate	4.2
A7	20%(w/v) PEG-8000	CHES	9.5
A8	20%(w/v) PEG-3350 0.2M ammonium formate	-	-
A9	20%(w/v) PEG-3350 0.2M ammonium chloride	-	-
A10	20%(w/v) PEG-3350 0.2M potassium formate	-	-

Appendix

A11	50%(v/v) MPD 0.2M ammonium phosphate monobasic	Tris	8.5
A12	20%(w/v) PEG-3350 0.2M potassium nitrate	-	-
B1	0.8M ammonium sulfate	Citrate	4
B2	20%(w/v) PEG-3350 0.2M sodium thiocyanate	-	-
B3	20%(w/v) PEG-6000	Bicine	9
B4	8%(v/v) Ethylene glycol 10%(w/v) PEG-8000	HEPES	7.5
B5	5%(w/v) PEG-8000 40%(v/v) MPD	Sodium cacodylate	6.5
B6	5%(w/v) PEG-1000 40%(v/v) ethanol	Phosphate/citrate	4.2
B7	8%(w/v) PEG-4000	Sodium acetate	4.6
B8	10%(w/v) PEG-8000 0.2M magnesium chloride hexahydrate	Tris	7
B9	20%(w/v) PEG-6000	Citrate	5
B10	50%(v/v) PEG-200 0.2M magnesium chloride hexahydrate	Sodium cacodylate	6.5
B11	1.6M sodium citrate tribasic dihydrate	-	-
B12	20%(w/v) PEG-3350 0.2M potassium citrate tribasic monohydrate	-	-
C1	20%(w/v) PEG-8000 0.2M sodium chloride	Phosphate/citrate	4.2
C2	20%(w/v) PEG-6000 1M lithium chloride	Citrate	4
C3	20%(w/v) PEG-3350 0.2M ammonium nitrate	-	-
C4	10% PEG-6000	HEPES	7
C5	0.8M sodium phosphate monobasic monohydrate 0.8M potassium phosphate monobasic	Sodium HEPES	7.5
C6	40%(v/v) PEG-300	Phosphate/citrate	4.2
C7	10%(w/v) PEG-3000 0.2M zinc acetate dihydrate	Sodium acetate	4.5
C8	20%(v/v) ethanol	Tris	8.5
C9	10%(v/v) glycerol 25%(v/v) 1,2-propanediol	Sodium/potassium phosphate	6.2
C10	10%(w/v) PEG-20000 2%(v/v) 1,4-dioxane	Bicine	9
C11	2M ammonium sulfate	Sodium acetate	4.6
C12	10%(w/v) PEG-1000 10%(w/v) PEG-8000	-	-
D1	24%(w/v) PEG-1500 20%(v/v) glycerol	-	-
D2	30%(v/v) PEG-400 0.2M magnesium chloride hexahydrate	Sodium HEPES	7.5
D3	50%(v/v) PEG-200 0.2M sodium chloride	Sodium/potassium phosphate	6.2
D4	30%(w/v) PEG-8000 0.2M lithium sulfate	Sodium acetate	4.5
D5	70%(v/v) MPD	HEPES	7.5
D6	20%(w/v) PEG-8000 0.2M magnesium chloride hexahydrate	Tris	8.5
D7	40%(v/v) PEG-400 0.2M lithium sulfate	Tris	8.5
D8	40%(v/v) MPD	Tris	8
D9	25.5%(w/v) PEG-4000 15%(v/v) glycerol 0.17M ammonium sulfate	-	-

Appendix

D10	40%(v/v) PEG-300 0.2M calcium acetate hydrate	Sodium cacodylate	6.5
D11	30%(v/v) glycerol 14%(v/v) 2-propanol 0.14M calcium chloride dihydrate	0.07M sodium acetate	4.6
D12	16%(w/v) PEG-8000 20%(v/v) glycerol 0.04M potassium phosphate monobasic	-	-
E1	1M sodium citrate tribasic dihydrate	Sodium cacodylate	6.5
E2	2M ammonium sulfate 0.2M sodium chloride	Sodium cacodylate	6.5
E3	10%(v/v) 2-propanol 0.2M sodium chloride	HEPES	7.5
E4	1.26M ammonium sulfate 0.2M lithium sulfate	Tris	8.5
E5	40%(v/v) MPD	CAPS	10.5
E6	20%(w/v) PEG-3000 0.2M zinc acetate dihydrate	Imidazole	8
E7	10%(v/v) 2-propanol 0.2M zinc acetate dihydrate	Sodium cacodylate	6.5
E8	1M ammonium phosphate dibasic	Sodium acetate	4.5
E9	1.6M magnesium sulfate heptahydrate	MES	6.5
E10	10%(w/v) PEG-6000	Bicine	9
E11	14.4%(w/v) PEG-8000 20%(v/v) glycerol 0.16M calcium acetate hydrate	0.08M sodium cacodylate	6.5
E12	10%(w/v) PEG-8000	Imidazole	8
F1	30%(v/v) jeffamine M-600 0.05M cesium chloride	MES	6.5
F2	3.2M ammonium sulfate	Citrate	5
F3	20%(v/v) MPD	Tris	8
F4	20%(v/v) jeffamine M-600	HEPES	7.5
F5	50%(v/v) ethylene glycol 0.2M magnesium chloride hexahydrate	Tris	8.5
F6	10%(v/v) MPD	Bicine	9
F7	0.8M succinic acid	-	-
F8	2.1M DL-malic acid	-	-
F9	2.4M sodium malonate dibasic monohydrate	-	-
F10	0.5%(v/v) jeffamine ED-2003 1.1M sodium malonate dibasic monohydrate	HEPES	7
F11	1%(w/v) PEG-2000 MME 1M succinic acid	HEPES	7
F12	30%(v/v) jeffamine M-600	HEPES	7
G1	30%(v/v) jeffamine ED-2003	HEPES	7
G2	22%(w/v) poly(acrylic acid sodium salt) 5100 0.02M magnesium chloride hexahydrate	HEPES	7.5
G3	20%(w/v) polyvinylpyrrolidone 0.01M cobalt(II) chloride hexahydrate	Tris	8.5
G4	20%(w/v) PEG-2000 MME 0.2M TMAO	Tris	8.5
G5	12%(w/v) PEG-3350 0.005M cobalt(II) chloride hexahydrate 0.005M cadmium chloride hemi(pentahydrate) 0.005M magnesium chloride hexahydrate 0.005M nickel (II) chloride hexahydrate	HEPES	7.5
G6	20%(w/v) PEG-3350 0.2M sodium malonate dibasic monohydrate	-	-
G7	15%(w/v) PEG-3350 0.1M succinic acid	-	-
G8	20%(w/v) PEG-3350	-	-

Appendix

	0.15M DL-malic acid		
G9	30%(w/v) PEG-2000 MME 0.1M potassium thiocyanate	-	-
G10	30%(w/v) PEG-2000 MME 0.15M potassium bromide	-	-
G11	2M ammonium sulfate	Bis Tris	5.5
G12	3M sodium chloride	Bis Tris	5.5
H1	0.3M magnesium formate dihydrate	Bis Tris	5.5
H2	1%(w/v) PEG-3350 1M ammonium sulfate	Bis Tris	5.5
H3	25%(w/v) PEG-3350	Bis Tris	5.5
H4	45%(v/v) MPD 0.2M calcium chloride dihydrate	Bis Tris	5.5
H5	45%(v/v) MPD 0.2M ammonium acetate	Bis Tris	5.5
H6	17%(w/v) PEG-10000 0.1M ammonium acetate	Bis Tris	5.5
H7	25%(w/v) PEG-3350 0.2M ammonium sulfate	Bis Tris	5.5
H8	25%(w/v) PEG-3350 0.2M sodium chloride	Bis Tris	5.5
H9	25%(w/v) PEG-3350 0.2M lithium sulfate	Bis Tris	5.5
H10	25%(w/v) PEG-3350 0.2M ammonium acetate	Bis Tris	5.5
H11	25%(w/v) PEG-3350 0.2M magnesium chloride hexahydrate	Bis Tris	5.5
H12	45%(v/v) MPD 0.2M ammonium acetate	HEPES	7.5

Classics-Suite_qiagen			
Position	Precipitant	Buffer (all at 0.1M)	pH
A1	1M 1,6-hexanediol 0.01M cobalt chloride	Sodium acetate	4.6
A2	2.5M 1,6-hexanediol	Tri-sodium citrate	5.6
A3	3.4M 1,6-hexanediol 0.2M magnesium chloride	Tris	8.5
A4	5%(v/v) isopropanol 2M ammonium sulfate	-	-
A5	20%(w/v) PEG-4000 10%(v/v) isopropanol	HEPES	7.5
A6	20%(v/v) isopropanol 0.2M calcium chloride	Sodium acetate	4.6
A7	20%(w/v) PEG-4000 20%(v/v) isopropanol	Tri-sodium citrate	5.6
A8	20%(v/v) isopropanol 0.2M tri-sodium citrate	HEPES	7.5
A9	30%(v/v) isopropanol 0.2M tri-sodium citrate	Sodium cacodylate	6.5
A10	30%(v/v) isopropanol 0.2M magnesium chloride	HEPES	7.5
A11	30%(v/v) isopropanol 0.2M magnesium chloride	Tris	8.5
A12	1.5M sodium chloride 10%(v/v) ethanol	-	-
B1	20%(v/v) ethanol	Tris	8.5
B2	25%(v/v) ethylene glycol	-	-

Appendix

B3	30%(v/v) MPD 0.02M calcium chloride	Sodium acetate	4.6
B4	30%(v/v) MPD 0.2M sodium chloride	Sodium acetate	4.6
B5	30%(v/v) MPD 0.2M magnesium acetate	Tri-sodium citrate	5.6
B6	30%(v/v) MPD 0.2M magnesium acetate	Sodium cacodylate	6.5
B7	30%(v/v) MPD 0.2M tri-sodium citrate	HEPES	7.5
B8	30%(v/v) MPD 0.5M ammonium sulfate	HEPES	7.5
B9	50%(v/v) MPD 0.2M ammonium phosphate	Tris	8.5
B10	70%(v/v) MPD	HEPES	7.5
B11	25%(v/v) tert-butanol	Tris	8.5
B12	35%(v/v) tert-butanol	Tri-sodium citrate	5.6
C1	0.4M ammonium phosphate	-	-
C2	1M ammonium phosphate	Tri-sodium citrate	5.6
C3	2M ammonium phosphate	Tris	8.5
C4	2M ammonium formate	HEPES	7.5
C5	2M ammonium sulfate	Sodium acetate	4.6
C6	2M ammonium sulfate	Tris	8.5
C7	2M ammonium sulfate	-	-
C8	1.6M ammonium sulfate 0.1M sodium chloride	HEPES	7.5
C9	1.8M ammonium sulfate 0.01M cobalt chloride	MES	6.5
C10	2M ammonium sulfate 0.2M potassium/sodium tartrate	Tri-sodium citrate	5.6
C11	1M imidazole	-	-
C12	0.4M potassium/sodium tartrate	-	-
D1	0.8M potassium/sodium tartrate	HEPES	7.5
D2	1M sodium acetate	Imidazole	6.5
D3	1M sodium acetate 0.05M cadmium sulfate	HEPES	7.5
D4	1.4M sodium acetate	Sodium cacodylate	6.5
D5	2M sodium chloride	Sodium acetate	4.6
D6	2M sodium chloride 0.1M sodium phosphate 0.1M potassium phosphate	MES	6.5
D7	4.3M sodium chloride	HEPES	7.5
D8	1.4M tri-sodium citrate	HEPES	7.5
D9	1.6M tri-sodium citrate	-	7.5
D10	0.8M sodium phosphate 0.8M potassium phosphate	HEPES	7.5
D11	2M sodium formate	Sodium acetate	4.6
D12	4M sodium formate	-	-
E1	10%(w/v) PEG-20000 2%(v/v) dioxane	Bicine	9
E2	1.6M ammonium sulfate 10%(v/v) dioxane	MES	6.5
E3	35%(v/v) dioxane	-	-
E4	2%(v/v) ethylene imine polymer 0.5M sodium chloride	Tri-sodium citrate	5.6
E5	12%(v/v) glycerol 1.5M ammonium sulfate	Tris	8.5
E6	0.5M sodium chloride 0.01M magnesium chloride 0.01M CTAB	-	-

Appendix

E7	10%(v/v) jaffamine M-60 0.01M ferric chloride	Tri-sodium citrate	5.6
E8	20%(v/v) jeffamine M-60	HEPES	7.5
E9	1M lithium sulfate 0.5M ammonium sulfate	Tri-sodium citrate	5.6
E10	1M lithium sulfate 0.01M nickel chloride	Tris	8.5
E11	1.5M lithium sulfate	HEPES	7.5
E12	2M magnesium chloride	Bicine	9
F1	0.2M magnesium formate	-	-
F2	1.6M magnesium sulfate	MES	6.5
F3	8%(w/v) PEG-8000	Tris	8.5
F4	10%(w/v) PEG-8000	HEPES	7.5
F5	15%(w/v) PEG-8000 0.5M lithium sulfate	-	-
F6	18%(w/v) PEG-8000 0.2M zinc acetate	Sodium cacodylate	6.5
F7	18%(w/v) PEG-8000 0.2M calcium acetate	Sodium cacodylate	6.5
F8	20%(w/v) PEG-8000 0.2M magnesium acetate	Sodium cacodylate	6.5
F9	30%(w/v) PEG-8000 0.05M potassium	-	-
F10	30%(w/v) PEG-8000 0.2M ammonium sulfate	Sodium cacodylate	6.5
F11	30%(w/v) PEG-8000 0.2M sodium acetate	Sodium cacodylate	6.5
F12	30%(w/v) PEG-8000 0.2M ammonium sulfate	-	-
G1	2%(v/v) PEG-400 2M ammonium sulfate	HEPES	7.5
G2	28%(v/v) PEG-400 0.2M calcium chloride	HEPES	7.5
G3	30%(v/v) PEG-400 0.1M cadmium chloride	Sodium acetate	4.6
G4	30%(v/v) PEG-400 0.2M magnesium chloride	HEPES	7.5
G5	30%(v/v) PEG-400 0.2M tri-sodium citrate	Tris	8.5
G6	20%(w/v) PEG-550 MME 0.1M sodium chloride	Bicine	9
G7	25%(w/v) PEG-550 MME 0.01M zinc sulfate	MES	6.5
G8	10%(w/v) PEG-8000 10%(w/v) PEG-1000	-	-
G9	30%(w/v) PEG-1500	-	-
G10	20%(w/v) PEG-2000 MME 0.01M nickel chloride	Tris	8.5
G11	30%(w/v) PEG-2000 MME 0.2M ammonium sulfate	Sodium acetate	4.6
G12	8%(w/v) PEG-4000	Sodium acetate	4.6
H1	25%(w/v) PEG-4000 0.2M ammonium sulfate	Sodium acetate	4.6
H2	30%(w/v) PEG-4000 0.2M ammonium acetate	Sodium acetate	4.6
H3	30%(w/v) PEG-4000 0.2M ammonium acetate	Tri-sodium citrate	5.6
H4	30%(w/v) PEG-4000 0.2M magnesium chloride	Tris	8.5
H5	30%(w/v) PEG-4000	Tris	8.5

Appendix

	0.2M lithium sulfate		
H6	30%(w/v) PEG-4000 0.2M sodium acetate	Tris	8.5
H7	30%(w/v) PEG-4000 0.2M ammonium sulfate	-	-
H8	30%(w/v) PEG-5000 MME 0.2M ammonium sulfate	MES	6.5
H9	10%(w/v) PEG-6000 5%(v/v) MPD	HEPES	7.5
H10	10%(w/v) PEG-6000 2M sodium chloride	-	-
H11	20%(w/v) PEG-10000 8%(v/v) ethylene glycol	HEPES	7.5
H12	12%(w/v) PEG-20000	MES	6.5

Appendix II. Crystallographic statistics

	Unbound CgBD1	Unbound CgBD2	I-BET151 bound CgBD2
Data Collection¹			
Synchrotron beamline	ESRF ID30A-1	ESRF ID30A-1	ESRF ID30A-3
Wavelength (Å)	0.9660	0.9660	0.9677
Space group	P 1	P 2 ₁	C 2 2 2 ₁
Unit cell dimensions	$a=22.89$ Å, $b=40.59$ Å, $c=48.87$ Å, $\alpha=98.14^\circ$, $\beta=94.37^\circ$, $\gamma=94.77^\circ$	$a=80.29$ Å, $b=67.69$ Å, $c=96.62$ Å, $\beta=95.5^\circ$	$a=70.59$ Å, $b=88.43$ Å, $c=257.78$ Å
Molecules in asym. unit	2	7	4
Resolution range (Å) ²	48.2 - 1.17 (1.19-1.17)	43.0 - 1.95 (2.02 -1.95)	55.2- 1.95 (2.18 - 1.95)
No. of measured reflections	89,463 (4071)	230,301 (21,270)	207,522 (10,888)
No. of unique reflections	53,469 (2591)	75256 (7513)	28,171 (1410)
Multiplicity	1.67 (1.57)	3.1 (2.8)	7.4 (7.7)
Completeness (%)	90.5 (87.7)	99.8 (100.0)	91.7 (76.9)
Mean I/sigma(I)	10.8 (2.1)	13.4 (1.2)	6.7 (1.7)
R _{merge}	0.032 (0.318)	0.053 (0.864)	0.271 (1.918)
R _{meas}	0.045 (0.450)	0.080 (1.064)	0.292 (2.056)
R _{pim}	0.032 (0.318)	0.035 (0.611)	0.107 (0.733)
CC _{1/2}	0.999 (0.823)	0.994 (0.690)	0.990 (0.601)
Refinement			
Resolution	48.2 - 1.17	43.0 - 1.95	43.6 - 1.95
No. reflections (total/R _{free})	52,622 / 1669	74,574 / 6918	28,164 / 1407
R _{work} /R _{free}	0.1514 / 0.1747	0.1974 / 0.2242	0.1874 / 0.2395
Number of atoms/Mean B-factor (Å ²)			
Protein	1807 / 11.58	6618 / 76.9	3753 / 36.7
Water	394 / 21.8	179 / 52.9	226 / 30.4
Ligands	0	176 / 74.9	278 / 40.1
R.m.s. deviations:			
Bond distances (Å)	0.005	0.010	0.008
Bond angles (°)	0.785	0.925	0.920
Ramachandran analysis (%)			
Favored/ outliers	100.0 / 0.0	98.7 / 0.0	98.7 / 0.0
Molprobrity analysis			
Clash Score / Overall score	3.56 / 1.15	1.65 / 0.91	5.70 / 1.31

¹ A single crystal was used for the structure.

² Numbers in parentheses refer to the outer resolution shell.

Appendix

	iCG-29 bound CgBD2	iCG-63 bound CgBD1	iCG-24-409 bound CgBD1
Data Collection¹			
Synchrotron beamline	ESRF ID30A-1	ESRF ID30A-1	Soleil PROXIMA-1
Wavelength (Å)	0.9660	0.9660	1.033
Space group	I 4 ₁ 2 2	C 2 2 2 ₁	I 4 2 2
Unit cell dimensions	a=67.58 Å, b=67.58 Å, c=152.83 Å	a=32.84 Å, b=142.62 Å, c=93.55 Å	a=128.70 Å, b=128.70 Å, c=148.21 Å
Molecules in asym. unit	1	2	4
Resolution range (Å) ²	47.8 - 2.12 (2.41-2.12)	39.1- 1.82 (1.86-1.82)	64.4 - 2.19 (2.26-2.19)
No. of measured reflections	70,838 (2492)	81,767 (4264)	222,933 (19,474)
No. of unique reflections	5779 (289)	20,025 (1160)	32,208 (2779)
Multiplicity	12.3 (8.6)	4.1 (3.7)	6.9 (7.0)
Completeness (%)	93.5 (81.5)	99.1 (99.6)	100.0 (100.0)
Mean I/sigma(I)	8.3 (1.9)	7.41 (0.53)	7.3 (3.4)
R _{merge}	0.265 (1.190)	0.103 (0.894)	0.202 (0.697)
R _{meas}	0.277 (1.266)	0.116 (1.048)	0.218 (0.754)
R _{pim}	0.078 (0.423)	0.058 (0.536)	0.082 (0.283)
CC _{1/2}	0.997 (0.696)	0.996 (0.532)	0.993 (0.415)
Refinement			
Resolution	47.8 - 2.11	39.1 - 1.82	57.5 - 2.19
No. reflections (total/R _{free})	5779 / 295	20,006 / 1001	32,200 / 3143
R _{work} /R _{free}	0.2489 / 0.2839	0.1962 / 0.2312	0.2030 / 0.2549
Number of atoms/Mean B-factor (Å ²)			
Protein	950 / 42.4	1774 / 35.7	3583 / 31.6
Water	23 / 24.6	162 / 39.0	423 / 32.5
Ligands	57 / 49.3	86 / 35.7	141 / 53.3
R.m.s. deviations:			
Bond distances (Å)	0.007	0.005	0.003
Bond angles (°)	1.136	0.728	0.533
Ramachandran analysis (%)			
Favored/ outliers	97.4 / 0.88	100.0 / 0.00	99.1 / 0.00
Molprobrity analysis			
Clash Score / Overall score	8.94 / 1.60	4.39 / 1.22	6.18 / 1.34

¹ A single crystal was used for the structure.

² Numbers in parentheses refer to the outer resolution shell.

Appendix III. IC₅₀ of hits to be validated

Compound ID in lab	IC ₅₀ (μM)*			
	CgBD1	CgBD2	hBD1	hBD2
iCG-1	9.43	> 100**	ND***	> 100
iCG-2	4.40	1.12	25.90	2.81
iCG-3	19.20	22.20	> 100	55.60
iCG-4	> 100	ND	ND	ND
iCG-5	1.82	1.03	2.48	1.41
iCG-6	18.50	8.23	28.60	2.68
iCG-7	ND	ND	> 100	> 100
iCG-8	6.44	6.32	74.60	12.30
iCG-9	ND	ND	> 100	> 100
iCG-10	66.10	> 100	> 100	ND
iCG-11	> 100	ND	ND	ND
iCG-12	90.00	ND	92.40	10.00
iCG-13	ND	ND	ND	ND
iCG-14	ND	ND	> 100	> 100
iCG-15	ND	ND	ND	ND
iCG-16	1.79	0.30	1.16	1.47
iCG-17	6.95	20.90	31.40	> 100
iCG-18	24.50	25.70	16.20	> 100
iCG-19	> 100	ND	ND	> 100
iCG-20	22.59	> 100	> 100	> 100
iCG-21	> 100	> 100	> 100	3.53
iCG-22	20.90	> 100	> 100	25.38
iCG-23	> 100	ND	ND	ND
iCG-24	2.51	77.00	> 100	> 100
iCG-25	> 100	> 100	11.16	ND
iCG-26	> 100	8.37	> 100	ND
iCG-27	5.90	71.90	16.80	ND
iCG-28	ND	ND	26.20	3.49
iCG-29	1.12	2.32	2.91	0.44
iCG-30	0.64	> 100	> 100	21.80
iCG-31	6.33	> 100	ND	ND
iCG-32	2.94	> 100	> 100	> 100
iCG-33	26.70	ND	ND	ND
iCG-34	> 100	> 100	ND	ND
iCG-35	> 100	> 100	> 100	ND
iCG-36	ND	ND	ND	> 100

Appendix

Compound ID in lab	IC ₅₀ (μM)*			
	CgBD1	CgBD2	hBD1	hBD2
iCG-38	> 100	6.46	ND	> 100
iCG-39	6.70	ND	ND	ND
iCG-40	> 100	ND	ND	> 100
iCG-41	> 100	> 100	ND	> 100
iCG-42	5.94	8.78	38.30	13.50
iCG-43	2.70	3.32	> 100	> 100
iCG-44	19.10	ND	> 100	ND
iCG-45	4.21	ND	> 100	ND
iCG-46	> 100	ND	ND	ND
iCG-47	10.60	ND	> 100	ND
iCG-48	> 100	ND	> 100	55.82
iCG-49	> 100	ND	ND	ND
iCG-50	> 100	> 100	ND	ND
iCG-51	12.10	> 100	37.50	50.70
iCG-52	> 100	ND	ND	ND
iCG-53	4.77	ND	ND	ND
iCG-54	> 100	ND	ND	ND
iCG-55	0.11	ND	> 100	ND
iCG-56	0.36	ND	ND	ND
iCG-57	7.48	ND	ND	ND
iCG-58	> 100	> 100	ND	> 100
iCG-59	13.61	ND	> 100	> 100
iCG-60	> 100	ND	> 100	> 100
iCG-61	> 100	> 100	> 100	ND
iCG-62	> 100	ND	> 100	ND
iCG-63	0.62	ND	> 100	ND

* GST-BD binding inhibition IC₅₀ calculated by GraphPad Prime 7 by using “log(inhibitor) vs. response (three parameters)” model.

** > 100, IC₅₀ value calculated by GraphPad Prime 7 higher than 100 μM (weak effect).

*** ND, not determined (almost no effect).

Appendix IV. Genes selected to perform ChIP experiments

Gene name	Rpkm_YPD	Function
CAGL0k01397g	29.10	FMNAT verified Flavin mononucleotide adenylyltransferase
CAGL0L03630g	141.91	GSH1 verified Putative gamma glutamylcysteine synthetase
CAGL0K06831g	259.07	Verified Puruvate dehydrogenase activity
CAGL0K05973g	378.54	HSP60 verified Heat shock protein 60
CAGL0M01562g	494.58	Ortholog of <i>S. cerevisiae</i> YDR391C
CAGL0G00286g	611.62	GAS1 verified Putative glycoside hydrolase
CAGL0J11748g	736.68	PLB2 verified Putative phospholipase
CAGL0M08514g	858.17	PIR5 uncharacterized Pir protein family
CAGL0C05379g	977.99	SSB1 verified Heat shock protein
CAGL0I06160g	1140.73	PIR4 verified Pir protein family

All data are from (Linde *et al.*, 2015)

Appendix V. Résumé en français

Introduction et objectif

Candida est un genre de levures qui fait partie des microbes commensal au niveau de muqueuse humaine. Pour les individus immunosupprimés, *Candida* peut aussi causer les infections systémiques. Candidose systémique est la plus commune infection fongique pour les patients hospitalisés. Selon l'estimation conservative, candidose systémique touche plus de 250 000 patients dans le monde chaque année. Parmi les espèces *Candida*, *C. albicans* est encore le pathogène le plus fréquemment détecté pour les candidoses systémiques. Cependant, les infections causées par les espèces de *Candida non-albicans* augmentent rapidement. Parmi ces espèces, *C. glabrata* est le plus important qui représente la deuxième cause des candidoses. Les infections systémiques par cette espèce ont généralement un lien avec la mortalité élevée, qui peut être causé par la résistance développée par ce pathogène.

Le nombre des médicaments antifongiques pour le traitement de candidose causé par *C. glabrata* est limité. Aujourd'hui, il n'existe que trois familles de médicament qui peuvent être utilisées indépendamment contre les infections fongiques systémiques : polyène (amphotéricine B), azoles et echinocandines. Amphotéricine B tue les fungi en ciblant l'ergostérol, un composant essentiel au niveau de la membrane cellulaire fongique. Cependant, son administration est limitée par sa toxicité très élevée. Azoles ciblent aussi l'ergostérol en inhibant sa biosynthèse et ont une toxicité beaucoup plus modérée qu'amphotéricine B, mais *C. glabrata* est moins sensible sur les azoles et peut développer résistance facilement contre cette famille antifongique. Echinocandines représentent la plus nouvelle famille antifongique. Les médicaments de cette famille ciblent la synthèse de glucan de la paroi cellulaire chez les fungi. Cependant, la résistance contre echinocandines peut aussi développer vite après l'initiation de la thérapie.

Bien que beaucoup d'études aient été réalisées afin de découvrir des nouvelles familles antifongiques, le nombre limité des médicaments antifongiques actuellement disponibles et la croissance de la résistance indiquent que des nouveaux agents thérapeutiques contre *C. glabrata* sont toujours un besoin urgent. Le but de ce projet est de développer une nouvelle stratégie antifongique en ciblant une protéine essentielle chromatinique.

Dans le noyau d'une cellule eucaryote, l'unités basique et répétitive est nucléosome. Dans chaque nucléosome, un fragment d'ADN se roule autour un octamère protéique qui compose de deux copies de chaque histone de cœur (H2A, H2B, H3 et H4). Cette structure est stabilisée par l'histone H1. Pendant beaucoup de processus, comme la transcription et la réparation d'ADN, la chromatine a besoin d'être modifiée pour s'adapter à une structure plus ouverte. En effet, plein de mécanismes impliquent dans la modification de la structure de nucléosome et de chromatine.

La modification post-traduction (PTM) des histones joue un rôle très important dans la régulation de la structure chromatique et de l'expression des gènes. Parmi les différentes PTMs, l'acétylation des histones est l'un des plus importantes. Reconnu par les domaines de lecture épigénétique appelant bromodomaines, l'acétylation des histones est généralement associée avec une structure de chromatine ouverte et l'activation de la transcription. Beaucoup de protéines contiennent bromodomaines, y compris la famille appelant « Bromodomaine and Extra-Terminal » (BET). Les protéines de cette famille partagent une architecture en commun : il y a deux bromodomaines (BD1 et BD2) conservés proche de N-terminal et un domaine « extra-terminal » (ET). Des protéines BET ont un lien avec plusieurs maladies, comme des cancers et des maladies inflammatoires. Beaucoup d'inhibiteurs de bromodomaine de BET protéines ont été identifiés. Ils sont déjà investigués dans les stratégies de traitement de plusieurs maladies humaines.

Bdf1 est la protéine BET chez les levures. Chez *S. cerevisiae*, Bdf1 interagit avec le factor de transcription TFIID afin d'initier la transcription et participe également dans le remodelage de la structure chromatique. Elle est essentielle chez *S. cerevisiae* en contrôlant l'expression de plus de 500 gènes. Nos équipes ont récemment validé que l'inhibition de bromodomaines de Bdf1 par des petites molécules comme une stratégie potentielle antifongique contre la levure pathogène *C. albicans*.

L'objectif de ce projet est d'essayer de développer l'inhibition de bromodomaines de Bdf1 comme une stratégie thérapeutique potentielle contre les infections causées par *C. glabrata*.

Résultats

Pour être une cible thérapeutique potentielle, *C. glabrata* Bdf1 (CgBdf1) doit être essentielle pour soit la viabilité soit la croissance de la levure. Le rôle essentiel joué par Bdf1 chez *S. cerevisiae* suggère qu'il est impossible de délecter directement le gène *BDF1* chez *C. glabrata*. Nous utilisons le promoteur *MET3*, qui est inhibé par méthionine et cystéine, afin de conditionnellement supprimer l'expression de *BDF1* chez *C. glabrata*. En utilisant cette stratégie, nous avons vérifié que Bdf1 et la fonctionnalité de ces bromodomaines étaient essentielles pour la croissance de *C. glabrata*. Ces résultats suggèrent que CgBdf1 peut être une cible thérapeutique potentielle contre les infections par *C. glabrata*.

Une cible thérapeutique idéale chez un pathogène doit être dépourvue d'homologue humain afin de limiter la toxicité lors de l'administration du médicament. Si ce n'est pas le cas, il doit avoir des différences significatives dans le site de fixation du médicament entre la protéine cible du pathogène et son homologue humain. Bdf1 chez les fungi appartient à la famille des protéines BET avec quatre homologues humains. J'ai adapté le protocole de purification développé précédemment en laboratoire pour obtenir BD1 et BD2 de CgBdf1 (CgBD1 et CgBD2) avec un bon rendement et une pureté élevée. J'ai ensuite réussi à obtenir des cristaux qui ont donné des structures cristallines à haute résolution. Ceux-ci ont montré que même si la structure globale des bromodomaines de Brd4 et CgBdf1 était similaire, leurs poches de fixation de ligand présentaient toujours des différences significatives sur la charge électrostatique et le forme. Ces différences prouvent que l'inhibition sélective des CgBdf1 bromodomaines (CgBD) sans inhiber les BET humains est réalisable. Ainsi, pris ensemble avec leur rôle essentiel pour la croissance de *C. glabrata*, les bromodomaines CgBdf1 semblaient prometteurs comme une cible antifongique potentielle. Le projet pourrait passer à l'étape suivante, concernant la découverte d'inhibiteurs qui ciblent sélectivement les bromodomaines CgBdf1.

Comme un objectif clé, l'optimisation du test HTRF (Homogeneous Time Resolved Fluorescence) pour cribler des inhibiteurs de CgBD pourrait directement décider le succès de ce projet. J'ai testé plusieurs constructions pour CgBD1 et CgBD2 et identifié les meilleures conditions de test. Le test HTRF optimisé a fourni un rapport S/B (Signal/Background) et un facteur Z' élevés à la fois pour les tests réalisés manuellement en utilisant des volumes relativement plus importants et pour les tests à haut-débit par des robots de manipulation de

liquides. Ces données suggèrent que les résultats fiables du criblage chimique peuvent être garantis.

Après avoir réalisé le criblage à haut débit, 66 molécules ont été identifiées comme des inhibiteurs intéressants de CgBD1. Nous avons ensuite acheté 63 d'eux qui étaient disponibles dans le commerce afin de confirmer leur activité d'inhibition contre les CgBD et les bromodomaines de Brd4 humains (hBD). Parmi eux, seulement 12 molécules ont été validées, montrant une IC_{50} (la concentration correspondant à la moitié d'inhibition maximale) inférieure à 5 μ M contre CgBD1 ou CgBD2 ou les deux. Le taux de validation était inférieur à 20%. Les composés ont ensuite été classés en trois groupes : le groupe 1 (inhibiteurs sélectifs de CgBD1) inhibait uniquement CgBD1 ; le groupe 2 (inhibiteurs doubles non sélectifs de la CgBD) inhibait à la fois les CgBD et les hBD et le groupe 3 (inhibiteurs sélectifs des CgBD) inhibait principalement les CgBD. Les structures des co-cristaux ont été réalisées pour étudier les modes de fixation de ces inhibiteurs. J'ai co-cristallisé avec succès CgBD1 avec le composé iCG-63 du groupe 1 et CgBD2 avec I-BET151 ou le composé iCG-29 du groupe 2. J'ai également essayé de co-cristalliser I-BET151 avec une construction protéique contenant à la fois CgBD1 et CgBD2 mais sans succès. L'analyse des structures des co-cristaux a fourni des explications pour les différents effets d'inhibition de ces molécules. Une optimisation chimique guidée par la structure du composé iCG-29 a également été réalisée pour obtenir de meilleurs inhibiteurs, mais seulement avec un succès limité.

Parmi tous les inhibiteurs de CgBD1 identifiés par criblage à haut débit, le composé iCG-24 du groupe 3 était le seul qui a montré un effet d'inhibition contre la croissance des souches de *C. glabrata*. Cependant, ce composé avait une faible solubilité dans l'eau et montrait seulement un effet faible d'inhibition contre CgBD2. Afin de résoudre ces problèmes, notre collaborateur aux États-Unis ont proposé une série de molécules dont la structure est similaire de celle de iCG-24 et qui pouvaient être plus solubles. Parmi ces analogues, iCG-24-409 était le plus prometteur. Ce composé inhibait sélectivement CgBD1 et CgBD2 par rapport à hBD et montrait l'effet d'inhibition le plus élevé contre CgBD2 parmi les composés. iCG-24-409 avait la capacité d'inhiber la croissance de toutes les souches de *C. glabrata* testées, y compris celle exprimant WT Bdf1, avec une EC_{50} (la concentration correspondant à la moitié d'effet d'inhibition maximale) inférieure à 100 μ M. J'ai confirmé avec succès que l'effet d'inhibition de croissance des levures de iCG-24-409 était dû à son activité d'inhibition contre

les bromodomaines de Bdf1 en générant une souche de *C. glabrata* dans laquelle les bromodomaines de Bdf1 ont été remplacés par ceux de Brd4 humaine. Cet inhibiteur montrait un effet d'inhibition significativement faible contre la souche humanisée par rapport à la souche de type sauvage. La structure de co-cristal a montré que iCG-24-409 pouvait bien s'intégrer dans les poches de fixation de CgBD1 et de CgBD2 mais pas celles des bromodomaines Brd4 humaines. J'ai également effectué des expériences préliminaires pour déterminer l'affinité de fixation de cette molécule envers les deux bromodomaines de CgBdf1 et pour évaluer sa cytotoxicité humaine qui semblait faible. Enfin, j'ai montré que iCG-24-409 inhibait les bromodomaines de CaBdf1 *in vitro* et inhibe la croissance de *C. albicans* et d'autres espèces de *Candida*. Bien que d'autres expériences soient nécessaires pour terminer la caractérisation de cet inhibiteur, iCG-24-409 semble être un composé très prometteur qui mérite d'être poursuivi.

Conclusion

C. glabrata est une levure pathogène associée à un taux de morbidité et de mortalité élevé chez les patients immunodéprimés. Le nombre limité d'agents antifongiques actuellement disponibles et l'augmentation des souches pharmaco-résistantes indiquent un besoin urgent de nouveaux médicaments antifongiques contre cette levure. L'objectif de mon projet doctoral visait à vérifier que l'inhibition de la protéine Bdf1, qui associe avec la chromatine et qui est le membre de la famille des protéines BET, est une stratégie thérapeutique antifongique valide contre *C. glabrata*. Ce projet a été réalisé principalement dans les laboratoires du Dr Carlo Petosa à l'IBS et du Dr Jérôme Govin à l'IAB, et mené en collaboration avec le laboratoire du Dr Charles E. McKenna à l'USC, avec la société Calibr à La Jolla, Californie, et avec le laboratoire de Muriel Cornet au TIMC-IMAG

Au cours de ce projet, nous avons confirmé que Bdf1 et ses bromodomaines sont nécessaires pour la croissance de *C. glabrata*. Nous avons également vérifié que Bdf1 peut être inhibé en introduisant des mutations ponctuelles uniques dans chaque bromodomaine. Les structures de cristaux ont montré qu'il y avait des différences significatives entre les bromodomaines de CgBdf1 et les protéines BET humaines. En utilisant le test HTRF que j'ai optimisé, un criblage chimique à haut débit a été effectué par nos collaborateurs dans le

laboratoire du Dr Charles E. McKenna, menant à la découverte de plusieurs inhibiteurs de CgBD. Parmi ces inhibiteurs, nous avons identifié avec succès le plus prometteur, iCG-24-409, qui présentait une activité d'inhibition sélective contre les deux CgBD mais pas les bromodomaines Brd4 humaines. Nous avons également démontré que ce composé inhibait la croissance de *C. glabrata* en inhibant les bromodomaines de Bdf1. D'autres caractérisations et optimisations chimiques sont en cours.

Les travaux de ce projet multidisciplinaire portent sur la génétique des levures, le criblage chimique, les expériences biochimiques/biophysiques et cellulaires et la cristallographie. Il joue un rôle comme un pont entre ma formation en pharmacie lors de ma Licence et en biologie de mon Master. En terminant ce projet de doctorat et avec ma Licence et mon Master, je complète ma formation couvrant de la recherche fondamentale en biologie aux tests précliniques sur modèles animaux, qui me prépare à poursuivre mon projet professionnel dans le domaine de la découverte moderne de médicaments.

RESUME

Candida glabrata est une levure pathogène associée à une mortalité élevée chez les patients immunodéprimés. Une croissance importante des souches résistantes aux médicaments antifongiques au cours des derniers dix ans indique un besoin urgent de nouvelles stratégies thérapeutiques. Ce projet concerne une nouvelle stratégie antifongique potentielle qui cible la protéine Bdf1, membre de la famille BET des facteurs de transcription. Les protéines BET s'associent à la chromatine par le biais de leurs deux bromodomaines (BD1 et BD2), des modules "lecteur" épigénétiques qui reconnaissent les lysines acétylées dans les histones. L'objectif global de ce projet est de valider les bromodomaines (BDs) de Bdf1 en tant que cible antifongique chez *C. glabrata*. Les objectifs spécifiques sont de (i) vérifier la fonction essentielle des BDs de Bdf1 chez *C. glabrata* ; (ii) étudier l'activité de liaison et la structure atomique des deux BDs de Bdf1 ; et (iii) identifier des composés qui inhibent sélectivement les BDs de Bdf1.

J'ai démontré que les deux BDs de Bdf1 sont essentiels pour la croissance de *C. glabrata in vitro*. J'ai déterminé les structures cristallines à haute résolution de BD1 et BD2, qui révèlent que leurs poches de liaison sont différentes de celles des BDs BET humains. J'ai aussi optimisé un essai FRET de type « homogeneous time-resolved » (HTRF) afin d'identifier des inhibiteurs des BDs de Bdf1 et je l'ai utilisé pour cribler une chimiothèque de plus de 100 000 composés. Cela a identifié plusieurs composés qui inhibent les BDs fongiques de façon sélective par rapport aux homologues humains. De plus, quelques-uns de ces composés sont capables d'inhiber la croissance de *C. glabrata in vitro*. En final, j'ai également déterminé la structure cristalline du composé le plus prometteur en complexe avec BD1 de Bdf1 afin de faciliter l'optimisation chimique de cet inhibiteur. Nous espérons que les résultats de ces études vont ouvrir la porte sur le rôle de Bdf1 comme une cible thérapeutique antifongique chez *C. glabrata*.

Mots-clés : Infectiologie, antifongique, *Candida glabrata*, Bdf1, bromodomaine

ABSTRACT

Candida glabrata is a pathogenic yeast associated with a high rate of morbidity and mortality in immunocompromised patients. An alarming rise in drug resistant strains over the past decade has led to an urgent need for novel therapeutic strategies. This project concerns a potential new antifungal strategy that targets the protein Bdf1, a member of the BET family of transcription factors. BET proteins associate with chromatin through their two bromodomains (BD1 and BD2), epigenetic "reader" modules that recognize acetylated lysine residues in histones. The overall goal of this project is to validate Bdf1 bromodomains (BDs) as an antifungal drug target in *C. glabrata*. Specific objectives are to: (i) verify that Bdf1 BD function is essential in *C. glabrata*; (ii) investigate the ligand-binding activity and structure of *C. glabrata* Bdf1 BDs; and (iii) identify compounds that selectively inhibit *C. glabrata* Bdf1 BDs.

I have shown that the two BDs of Bdf1 are essential for the growth of *C. glabrata in vitro*. I determined crystal structures of Bdf1 BD1 and BD2, which reveal that their ligand binding pockets are stereochemically distinct from those of human BDs. I developed a homogeneous time-resolved FRET (HTRF) assay to identify Bdf1 BD inhibitors and used it to screen a library of >100,000 compounds. This identified several compounds that selectively inhibit the fungal BDs compared to the human homologs. Furthermore, a few of these compounds are active against *C. glabrata* in yeast growth inhibition assays. Finally, I also determined the crystal structure of the most promising compound in complex with Bdf1 BD1 in order to facilitate further chemical optimization. Successful completion of this work will establish proof of principle that BET inhibition is a valid antifungal therapeutic strategy in *C. glabrata*.

Keywords: Infectiology, antifungal, *Candida glabrata*, Bdf1, bromodomain